université de BORDEAUX

THÈSE PRÉSENTÉE

POUR OBTENIR LE GRADE DE

DOCTEUR DE

L'UNIVERSITÉ DE BORDEAUX

ÉCOLE DOCTORALE : SCIENCES DE LA VIE ET DE LA SANTE / LIFE SCIENCES AND HEALTH

SPÉCIALITÉ : BIOLOGIE DU CANCER / CANCER BIOLOGY

Par **Julia ROSSI**

Targeted lentiviral niche-engineering to enhance CAR T cell efficacy in pancreatic ductal adenocarcinoma

Ingénierie ciblée de la niche tumorale par vecteurs lentiviraux pour améliorer l'efficacité des cellules CAR T dans l'adénocarcinome canalaire pancréatique

Sous la direction du Professeur Sandrine DABERNAT

Soutenue le 10 Septembre 2026

Membres du jury :

Mme. Melita IRVING	PhD, Team Leader, Senior Lecturer, Maître d'Enseignement et de Recherche de type 1	University of Lausanne, Suisse (Epalinges, SUISSE)	**Rapporteure**
M. Jacob GIEHM MIKKELSEN	Professeur	University of Aarhus C, Denmark (Aarhus C, DANEMARK)	**Rapporteur**
Mme. Alice CARRIER	Directrice de recherche	Université de Marseille (Marseille)	**Examinatrice**
M. Nicolas LARMONIER	Professeur	Université de Bordeaux (Bordeaux)	**Examinateur Président du jury**
Mme. Sandrine DABERNAT	Professeur	Université de Bordeaux (Bordeaux)	**Directrice de thèse**

Membres invités :

M. Sebastian KOBOLD	Professeur	University of Munich, Germany (Munich, GERMANY)	**Invité**
Mme. Els VERHOEYEN	Directrice de recherche	Université de Nice (Nice)	**Invitée**

Acknowledgements

First of all, I would like to deeply thank the members of my thesis jury, Dr. Melita Irving and Prof. Jacob Giehm Mikkelsen, for agreeing to evaluate this PhD work as reviewers. I would also like to sincerely thank Dr. Alice Carrier and Prof. Nicolas Larmonier for taking part in this jury as examiners. I would also like to warmly thank Els, both as an invited member of this jury and as an essential collaborator in this project. Your help, support and expertise have been extremely valuable throughout this work, and I am very grateful for your involvement.

Bien sûr, je tiens à remercier très chaleureusement Sandrine, ma directrice de thèse, et bien plus que cela. Merci d'avoir accepté d'encadrer ce projet nouveau et ambitieux. Merci de m'avoir fait confiance dès le début, de m'avoir laissé une grande liberté dans la construction de ce travail, et de m'avoir permis d'apprendre, d'essayer, de me tromper et de progresser. Tu m'as appris à construire un projet, à défendre des idées, à prendre du recul sur les résultats et à garder en tête les grandes questions derrière chaque expérience. Je garderai aussi en mémoire nos longues sessions brainstorming, les congrès à l'étranger, les moments plus légers qui les accompagnaient, et toutes les étapes partagées au cours de ces quatre années. Je suis très reconnaissante d'avoir pu réaliser cette thèse sous ta direction, avec ta confiance, ton exigence et ton soutien.

Merci également à François et Aurélie, qui ont cru en ce projet et m'ont fait confiance.

Sebastian, thank you so much for giving me the opportunity to spend several research stays in your lab. I learned so much in this new environment. Discovering a new laboratory, new scientists, new scientific backgrounds and a new culture was an essential part of this PhD experience. And of course, Munich would not have been Munich without the Klinpharm spirit and Oktoberfest.

Noémie, je tiens à te remercier tout particulièrement pour cette dernière année passée à travailler avec toi sur ce projet. Merci pour ta confiance, ton investissement et ton aide précieuse. Je sais que tu feras une chercheuse formidable. Merci pour ton soutien scientifique et ton soutien moral, surtout dans la dernière ligne droite de cette aventure, lorsqu'ils étaient plus que nécessaires.

Je veux aussi remercier celles et ceux qui ont travaillé avec moi sur ce projet : Louna, Riccardo et Jimena.

Plus généralement, je veux remercier l'ensemble de l'équipe 8, ce qui représente un grand nombre de remerciements. Aux doctorantes Léana, Chloé, Julie et Camille, avec qui j'ai traversé cette aventure, merci pour tous ces moments partagés. Merci à Isa M pour ses beaux Western blots et ses magnifiques histologies. Merci à Mag et Jessica pour leur grande aide en biologie moléculaire. Merci à Isa LG pour ses conseils en cytométrie. Merci à Coco pour ses belles histologies. Merci également à toutes les autres personnes de l'équipe qui ont contribué, de près ou de loin, à ce travail.

À l'équipe Vect'UB, merci infiniment pour toutes ces fois où je suis venue vous poser des questions, demander des productions toujours plus complexes, en quantités toujours plus importantes. Jennifer, merci de m'avoir toujours écoutée et d'avoir tout fait pour que nos demandes aboutissent dans les meilleurs délais. Camille, merci également pour ton aide et pour les très nombreuses p24 réalisées. Bien sûr, Véro, merci beaucoup pour ton aide, ton soutien et ta confiance tout au long de ce projet.

Un immense merci à toute l'équipe de l'A2, et surtout à Julien et Léa. Je ne vous remercierai jamais assez pour tout ce que vous avez fait pour ce projet. Ces heures passées au bioimageur, ces heures de chirurgie, toutes ces implantations et ces injections, essentielles à la réalisation de cette thèse. Je ne pensais pas que l'*in vivo* pouvait être fun, et c'est grâce à vous que ça l'a été. Merci pour votre soutien professionnel, et surtout moral. Vous n'imaginez pas l'impact que vous avez eu sur cette thèse. Vous faites un travail formidable.

Je remercie également les nombreuses personnes du BBS qui m'ont aidée de près ou de loin. Martina, merci pour ton aide et pour tes réponses à mes nombreuses questions. Clément et Lina, merci de m'avoir fait découvrir le monde des radioéléments et de m'avoir permis de visiter le mystérieux premier étage. Aurélien, que d'heures passées à essayer d'imprimer ces lymphocytes qui mouraient instantanément. Sandrine Hamon, c'est toujours un plaisir de travailler avec toi. Merci pour ta bonne humeur à toute épreuve.

I would also like to deeply thank all the members of Klinpharm, who have been part of this journey since 2022. Most specifically, Stefanos, thank you for your guidance, your help, your precious advice and your supervision. I am extremely grateful for everything you have done for me.

Mara, Seo, Charlotte and Wendy, thank you for making my time in Munich so memorable. I made true friends there, and I know these friendships will last. Ema, Emre, David and all the PhD students, it was a pleasure working with you and sharing this life abroad. Marcel, Janina, Dona,

Bruno and all the postdocs, thank you for your help, your advice and your support throughout the project.

Mona and Hans, I am so grateful that I got to spend my time in Munich with you. I could not have done it without you. You made me feel at home while I was abroad. Thank you for your help with the German administration, for the lovely dinners we shared, for the excursions in the mountains, for being there in the evening when I came back from difficult days in the lab, and for so much more. I will never forget you, and I truly hope we will keep in touch.

À mes parents et à ma sœur, merci infiniment pour votre soutien inestimable et pour avoir toujours cru en moi. Merci de m'avoir donné l'opportunité de suivre mes rêves et mes ambitions, même lorsque le chemin était long, incertain ou difficile. Vous m'avez toujours encouragée à aller au bout des choses, à croire en mes capacités et à ne pas abandonner face aux obstacles. Votre confiance, votre présence et votre amour ont été des repères essentiels tout au long de ces années. Merci pour tous les encouragements et vos mots rassurants dans les moments où j'en avais le plus besoin. Vous êtes des exemples pour moi, par votre force, votre générosité et votre façon d'avancer dans la vie. Si j'en suis là aujourd'hui, c'est en grande partie grâce à vous. Je ne vous remercierai jamais assez.

À mes vraies amies rencontrées au cours de ces huit années d'études : Ombéline, depuis l'IUT puis la licence, Alex, Sonia et Mariana, rencontrées en master, et Sabrina, pendant la thèse. Merci d'avoir été présentes à chaque étape, dans les moments de doute comme dans les moments de joie. Merci pour les discussions, les rires, les encouragements, les messages au bon moment, qui ont rendu ces années plus légères. Ces années d'études n'auraient pas eu la même saveur sans vous. Je sais que ce n'est que le début de longues et belles années d'amitié, même si la vie nous mène parfois aux quatre coins du monde.

Joann, tu sais déjà tout, mais ces remerciements ne pouvaient pas se terminer sans quelques mots pour toi. Merci d'avoir été présent à chaque étape de cette thèse, avec patience, confiance et soutien inconditionnel. Merci d'avoir cru en moi quand je doutais, de m'avoir encouragée dans les périodes de fatigue, et de m'avoir aidée à garder le cap. Depuis le début de nos études, nous avançons côte à côte, en partageant les réussites, les incertitudes et les projets. Merci pour ta présence et pour tout ce que tu m'as apporté pendant ces années. Ce sera bientôt à ton tour, et je serai là pour toi comme tu l'as été pour moi.

Pour terminer, je voudrais remercier ma professeure de SVT de première, Mme Garrigue, qui m'a donné le goût des sciences et de la cancérologie. Votre passion et votre enthousiasme ont

beaucoup compté dans mon parcours. C’est en partie grâce à vous que cette curiosité scientifique est née, et qu’elle m’a menée jusqu’ici.

In the same spirit, I would also like to thank Prof. Matt Dun, who gave me the opportunity to discover what cancer research truly was. This experience was a turning point for me. It made me rethink my plans, follow this path, and choose to dedicate myself to cancer research. I am very grateful for the trust you placed in me, and for the inspiration and opportunity you gave me.

Table of contents

Acknowledgements 1

Table of contents 5

List of abbreviations 7

List of tables 9

List of figures 9

INTRODUCTION 11

I. Pancreatic ductal adenocarcinoma (PDAC) 11

1. Anatomy 11
2. Tumor initiation, genomic instability and molecular heterogeneity 13
3. Clinical burden and therapeutic dead-end 16
4. The PDAC tumor microenvironment: a stromal-dominant and immune-excluded niche 20
5. What has been tried, and why it failed 26

II. Adoptive cell therapy 27

1. Adoptive cell therapy and engineered lymphocytes 27
2. Why CAR T cells could work in PDAC 30
3. Why CAR T cells currently fail in solid tumors and PDAC 33

III. Thesis project: targeted lentiviral TME niche engineering for CAR T cell therapy 38

1. Chemokine-based recruitment of effector lymphocytes 39
2. Decorin-mediated stromal remodeling and tumor sensitization 40
3. Rationale for combining chemokine recruitment and stromal remodeling 42
4. Lentiviral vectors as precision delivery tools 43
5. From broad tropism to targeted pseudotyping 44
6. Target antigens for LV retargeting in PDAC and associated tumor models 59
7. scFv as modular targeting domains for lentiviral retargeting 61

OBJECTIVES OF THE THESIS 62

MATERIALS AND METHODS 64

RESULTS 76

I. Comparative evaluation of lentiviral pseudotyping platforms for tumor-targeted gene delivery 76

Comparative lentiviral pseudotyping identifies Sindbis virus glycoprotein as a versatile platform for highly specific *in vivo* tumor targeting 77
Introduction 79
Results 80
Discussion 93
Material & methods 96
References 102
Supplementary figures 106

II. Chemokine- and decorin-based tumor niche engineering to enhance T cell recruitment and antitumor activity 109

A. Preliminary evaluation of CXCL10-decorin tumor niche engineering in human mesothelin-positive PDAC models 109

Tumor-cell engineering for local decorin secretion enhances T cell therapy in pancreatic cancer by modulating matrix- and TGFβ-associated barriers 111
Abstract 111
Introduction 112
Results 116
Discussion 129
Materials and methods 133
References 138
B. *In vivo* assessment of partial tumor niche engineering in simplified and orthotopic models 149

***DISCUSSION* 156**

1. Retargeted lentiviral vectors as tools for tumor-restricted gene delivery 157

2. From targeted delivery to tumor niche engineering 159

3. A sequential payload model: recruitment, niche remodeling and effector output 159

4. Proteomic evidence for remodeling of the tumor-CAR T cell interface 161

5. *In vivo* relevance of partial tumor engineering 163

6. Relationship to *in vivo* CAR T cell generation by retargeted lentiviral vectors 164

7. Limitations of the current work 164

8. Future directions 166

***CONCLUSION* 169**

***REFERENCES* 170**

***Scientific publications* 189**

***Scientific communications* 190**

***Teaching and supervision* 191**

***French and English abstracts* 192**

List of abbreviations

ACT Adoptive cell therapy
ADM Acinar-to-ductal metaplasia
ANOVA Analysis of variance
AUC Area under the curve
BLI Bioluminescence imaging
CAF Cancer-associated fibroblast
CAR Chimeric antigen receptor
CC Cellular component
CD Cluster of differentiation
cDNA Complementary DNA
CD3ζ CD3 zeta chain
CDKN2A Cyclin-dependent kinase inhibitor 2A
CEA Carcinoembryonic antigen
CXCL10 C-X-C motif chemokine ligand 10
CXCR3 C-X-C motif chemokine receptor 3
Dcn Decorin
DNA Deoxyribonucleic acid
EDTA Ethylenediaminetetraacetic acid
ECM Extracellular matrix
EF1α Elongation factor 1 alpha
EGFR Epidermal growth factor receptor
ELISA Enzyme-linked immunosorbent assay
EpCAM Epithelial cell adhesion molecule
FACS Fluorescence-activated cell sorting
FAP Fibroblast activation protein
FDR False discovery rate
GFP Green fluorescent protein
GM-CSF Granulocyte-macrophage colony-stimulating factor
GO Gene ontology
GPI Glycosylphosphatidylinositol
H&E Hematoxylin and eosin
HER2 Human epidermal growth factor receptor 2
HEK293T Human embryonic kidney 293T cells
HEPES 4-(2-hydroxyethyl)-1-piperazineethanesulfonic acid
hFF-hTERT Human foreskin fibroblasts immortalized with human telomerase reverse transcriptase
HIV Human immunodeficiency virus
HLA Human leukocyte antigen
IFNγ Interferon gamma
IHC Immunohistochemistry
IL Interleukin
IPMN Intraductal papillary mucinous neoplasm
IRES Internal ribosome entry site
IV Intravenous
IVIS *In vivo* imaging system
KPC KrasLSL-G12D/+; Trp53LSL-R172H/+; Pdx1-Cre pancreatic cancer model
KRAS Kirsten rat sarcoma viral oncogene homolog
LC-MS/MS Liquid chromatography-tandem mass spectrometry
LV Lentiviral vector
mAb Monoclonal antibody
MAPK Mitogen-activated protein kinase
MCN Mucinous cystic neoplasm
MDSC Myeloid-derived suppressor cell
MFI Mean fluorescence intensity
MHC Major histocompatibility complex

MND Myeloproliferative sarcoma virus enhancer, negative control region-deleted,
MOI Multiplicity of infection
mRNA Messenger RNA
MSLN Mesothelin
MSI Microsatellite instability
MV Measles virus
NiV Nipah virus
NK Natural killer
NSG NOD scid gamma mouse
NT Non-transduced
OVA Ovalbumin-derived antigen
OT-I Ovalbumin-specific $CD8^+$ T cell receptor transgenic T cells
PanIN Pancreatic intraepithelial neoplasia
PanNET Pancreatic neuroendocrine tumor
PBMC Peripheral blood mononuclear cell
PBS Phosphate-buffered saline
PC3 Human prostate cancer cell line
PC3-PIP PSMA-positive PC3 cell line
PC3-WT Wild-type PC3 cell line
PCR Polymerase chain reaction
PDAC Pancreatic ductal adenocarcinoma
PD-1 Programmed cell death protein 1
PD-L1 Programmed death-ligand 1
PFA Paraformaldehyde
PGK Phosphoglycerate kinase promoter
PI3K Phosphoinositide 3-kinase
PMPA 2-(phosphonomethyl)pentanedioic acid
PSCA Prostate stem cell antigen
PSMA Prostate-specific membrane antigen
qPCR Quantitative polymerase chain reaction
recDcn Recombinant decorin
RNA Ribonucleic acid
ROI Region of interest
scFv Single-chain variable fragment
SD Standard deviation
SINV Sindbis virus
SLAM Signaling lymphocytic activation molecule
SMAD4 SMAD family member 4
STAT3 Signal transducer and activator of transcription 3
TAM Tumor-associated macrophage
TCR T cell receptor
TGFβ Transforming growth factor beta
TIL Tumor-infiltrating lymphocyte
TME Tumor microenvironment
TNFα Tumor necrosis factor alpha
Treg Regulatory T cell
TU/mL Transducing units per milliliter
VSV Vesicular stomatitis virus
WT Wild type

List of tables

TABLE 1: CLINICAL STUDIES OF CAR T CELL THERAPY INCLUDING PATIENTS WITH PANCREATIC CANCER. 38
TABLE 2: COMPARATIVE STRUCTURAL AND FUNCTIONAL CHARACTERIZATION OF RETARGETED LENTIVIRAL ENVELOPE PLATFORMS. 81

List of figures

FIGURE 1: ANATOMICAL ORGANIZATION OF THE PANCREAS AND ITS RELATIONSHIP WITH ADJACENT DIGESTIVE AND VASCULAR STRUCTURES. 12
FIGURE 2: HISTOLOGICAL PROGRESSION AND MAJOR GENETIC EVENTS INVOLVED IN PANCREATIC DUCTAL ADENOCARCINOMA DEVELOPMENT. 14
FIGURE 3: CURRENT STAGE-ADAPTED MANAGEMENT OF PDAC AND RATIONALE FOR MICROENVIRONMENT-DIRECTED THERAPEUTIC STRATEGIES. 19
FIGURE 4: HISTOLOGICAL ARCHITECTURE AND MAJOR COMPONENTS OF THE PANCREATIC DUCTAL ADENOCARCINOMA MICROENVIRONMENT. 21
FIGURE 5: STRUCTURAL EVOLUTION OF CHIMERIC ANTIGEN RECEPTORS (CARS) ACROSS SUCCESSIVE GENERATIONS. 29
FIGURE 6: CAR T CELL-MEDIATED IMMUNE ACTIVATION IN POORLY INFLAMED PDAC. 33
FIGURE 7: MAIN BARRIERS LIMITING CAR T CELL EFFICACY IN PANCREATIC DUCTAL ADENOCARCINOMA. 34
FIGURE 8: MAJOR EFFECTS OF DECORIN IN THE PDAC TUMOR MICROENVIRONMENT. 41
FIGURE 9: CHEMOKINE- AND DECORIN-BASED NICHE ENGINEERING TO IMPROVE CAR T CELL ACTIVITY IN PDAC. . 42
FIGURE 10: TUMOR-ASSOCIATED SURFACE ANTIGENS SELECTED FOR LENTIVIRAL VECTOR RETARGETING AND ASSOCIATED PRO-TUMORAL SIGNALING PATHWAYS. 59
FIGURE 11: TUMOR-TARGETED LENTIVIRAL NICHE ENGINEERING TO ENHANCE CAR T CELL ACTIVITY IN PDAC 63
FIGURE 12: COMPARATIVE PSEUDOTYPING IDENTIFIES SINV-SCFV ENVELOPES AS THE MOST EFFICIENT PLATFORM FOR ANTIGEN-DIRECTED LENTIVIRAL TRANSDUCTION. 83
FIGURE 13: SINV-SCFV PSEUDOTYPED LENTIVIRAL VECTORS MEDIATE ANTIGEN-DEPENDENT TRANSDUCTION ACROSS MULTIPLE TUMOR ANTIGENS. 86
FIGURE 14: SINV-SCFV-HMSLN PSEUDOTYPED LENTIVIRAL VECTORS MEDIATE SPATIALLY RESTRICTED AND EFFICIENT GENE TRANSFER IN 3D TUMOR MODELS. 88
FIGURE 15: MULTISPECIFIC SINV PSEUDOTYPES BROADEN ANTIGEN RECOGNITION WHILE PRESERVING TRANSDUCTION EFFICIENCY AT MATCHED VIRAL INPUT. 90
FIGURE 16: SINV-SCFV PSEUDOTYPED LENTIVIRAL VECTORS MEDIATE ANTIGEN-DEPENDENT GENE TRANSFER IN VIVO. 92
FIGURE 17: STRUCTURAL MODELING OF TARGET ANTIGEN-BINDER COMPLEXES RELATIVE TO THE PLASMA MEMBRANE. 94
FIGURE 18 SUPPLEMENTARY: CHARACTERIZATION OF TUMOR-ANTIGEN EXPRESSION AND MEMBRANE-MODULATION ASSAYS USED FOR TARGETED LENTIVIRAL TRANSDUCTION. 106
FIGURE 19 SUPPLEMENTARY: PSMA-TARGETED SINV PSEUDOTYPES SELECTIVELY TRANSDUCE PSMA-POSITIVE CELLS IN MIXED PC3 SPHEROIDS. 107
FIGURE 20 SUPPLEMENTARY: EX VIVO BIODISTRIBUTION ANALYSIS OF SYSTEMIC ANTI-PSMA SINV-SCFV LENTIVIRAL DELIVERY. 108
FIGURE 21: TUMOR-SECRETED HCXCL10 AND HDECORIN CAN BE CO-EXPRESSED IN MESOTHELIN-POSITIVE PDAC CELLS WHILE PRESERVING CAR T CELL RECRUITMENT. 117
FIGURE 22: HCXCL10-HDECORIN ENHANCES MESOTHELIN CAR T CELL CYTOTOXICITY AND RECOVERY OF VIABLE HUMAN CAR T CELLS IN 2D AND 3D COCULTURE. 119

FIGURE 23: HCXCL10-HDECORIN PRESERVES A RELATIVE CAR T CELL FUNCTIONAL ADVANTAGE UNDER TGFB EXPOSURE. 121
FIGURE 24: RECOMBINANT DECORIN PARTIALLY REMODELS THE TGFB-DRIVEN CAR T CELL PROTEOMIC STATE. . 124
FIGURE 25: DECORIN PROMOTES A BIOSYNTHETIC AND PROTEOSTATIC CAR T CELL STATE AFTER TUMOR ENGAGEMENT. 126
FIGURE 26: DECORIN-CONTAINING CONDITIONS INDUCE PARTIALLY OVERLAPPING PROTEOMIC CHANGES IN CAR T CELLS BEFORE AND AFTER TUMOR-CELL ENGAGEMENT. 127
FIGURE 27: TUMOR-CELL PROTEOMICS IDENTIFIES A COORDINATED DECORIN-ASSOCIATED REMODELING PROGRAM AT THE TUMOR CELL INTERFACE. 129
FIGURE 28 SUPPLEMENTARY: TUMOR-SECRETED HCXCL10 AND HDECORIN CAN BE CO-EXPRESSED IN TWO DIFFERENT MODELS OF MESOTHELIN-POSITIVE PDAC CELLS WHILE PRESERVING CAR T CELL RECRUITMENT. 144
FIGURE 29 SUPPLEMENTARY: ADDITIONAL FUNCTIONAL ANALYSES OF CXCL10-DECORIN ACTIVITY IN HUMAN MESOTHELIN-POSITIVE PDAC MODELS. 145
FIGURE 30 SUPPLEMENTARY: EXPERIMENTAL DESIGN OF THE COMPARTMENT-RESOLVED PROTEOMIC ANALYSES. 146
FIGURE 31 SUPPLEMENTARY: PROTEOMIC ANALYSES SUPPORTING DECORIN-ASSOCIATED REMODELING OF TUMOR CELLS AND CAR T CELLS. 147
FIGURE 32 SUPPLEMENTARY: RECOMBINANT DECORIN DOES NOT FULLY RESTORE THE PROTEOMIC STATE OF TGFB-TREATED CAR T CELLS. 148
FIGURE 33: PARTIAL CXCL10-DECORIN TUMOR ENGINEERING IMPROVES ANTIGEN-SPECIFIC T CELL-MEDIATED TUMOR CONTROL IN VIVO. 152
FIGURE 34 SUPPLEMENTARY: VALIDATION OF MURINE CXCL10 AND CXCL10-DECORIN PANC02-OVA-EPCAM CELLS. 153
FIGURE 35: EXPLORATORY ORTHOTOPIC SUIT-2-HMSLN MODEL WITH SYSTEMIC MESOTHELIN CAR T CELL TRANSFER. 155

INTRODUCTION

I. Pancreatic ductal adenocarcinoma (PDAC)

1. Anatomy

The pancreas is a vital glandular organ of the digestive system, located deep within the abdominal cavity, posterior to the stomach and anterior to the first and second lumbar vertebrae, a position that contributes to the difficulty of its clinical assessment and early disease detection. It is closely associated with several major organs, including the duodenum, spleen, and liver, and is embedded within a complex vascular and neural network. Anatomically, the pancreas is divided into four distinct regions that are highly vascularized and innervated, supporting its dual exocrine and endocrine functions. From right to left, the pancreatic head lies within the curvature of the duodenum and is intimately connected to it; it is traversed by the common bile duct, which conveys bile from the liver into the duodenum to emulsify dietary lipids and promote their absorption. The pancreatic neck, or isthmus, is positioned anterior to the portal vein and represents a key anatomical landmark. Extending obliquely toward the upper left quadrant of the abdomen, the pancreatic body lies anterior to the left kidney and adrenal gland. The tail forms the distal extremity of the gland and is located in close proximity to the spleen and its associated vessels, including the splenic artery and vein. The pancreas also contains a well-organized ductal system essential for its exocrine function. The main pancreatic duct, or duct of Wirsung, originates in the tail and runs longitudinally through the gland to empty into the duodenum, collecting digestive enzymes produced by acinar cells together with bicarbonate-rich fluid secreted by ductal cells. This secretion neutralizes gastric acidity in the duodenum and provides the alkaline pH required for efficient digestive enzyme activation and activity. In addition, the accessory pancreatic duct, known as the duct of Santorini, drains part of the pancreatic head directly into the duodenum, providing an additional pathway for pancreatic secretion **(Figure 1)**.

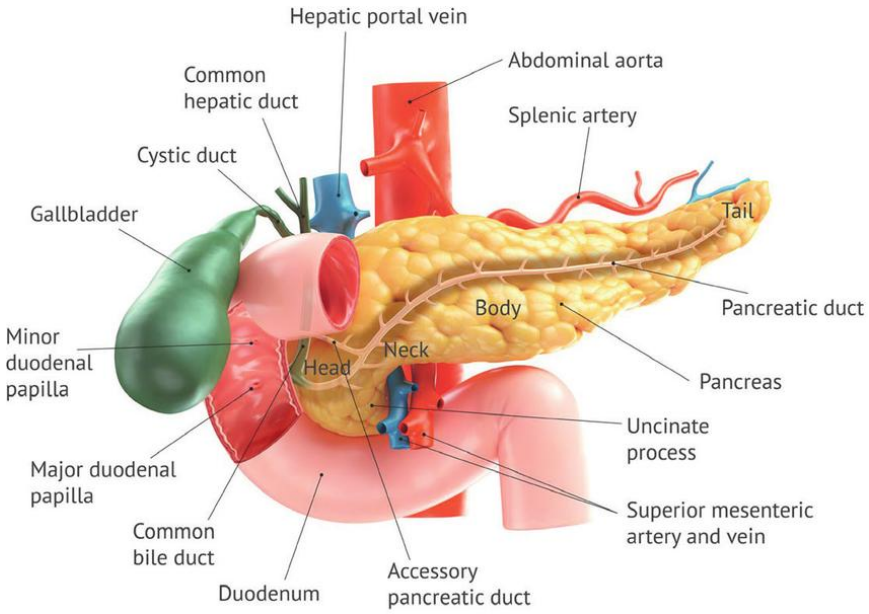


Figure 1: Anatomical organization of the pancreas and its relationship with adjacent digestive and vascular structures.

Anterior view of the pancreas showing its main anatomical regions, including the head, neck, body and tail, together with the duodenum, biliary tract, pancreatic ducts and major neighbouring vessels. The anatomical position of the pancreas, its close association with the duodenum and its proximity to major vascular structures are clinically relevant because they influence both early disease detection and surgical resectability in pancreatic ductal adenocarcinoma. Adapted from Di Dato et al., 2025[1].

In addition to its macroscopic organization, the pancreas exhibits a highly specialized cellular architecture that underlies its dual function. The exocrine compartment is composed predominantly of acinar cells responsible for enzyme production, organized around a branched ductal network lined by ductal epithelial cells. In contrast, the endocrine component consists of the islets of Langerhans, which secrete hormones directly into the bloodstream, mainly insulin, glucagon, somatostatin and pancreatic polypeptide. This close spatial integration of exocrine and endocrine elements contributes to the complex physiological regulation of pancreatic function, but also creates a heterogeneous cellular landscape from which distinct tumor types can arise.

From a clinical perspective, the anatomical proximity of the pancreas to major vascular structures, including the superior mesenteric artery and vein, the portal vein, and the celiac trunk, has important implications for surgical management. Tumor involvement of these vessels frequently determines resectability status and contributes to the classification of tumors into resectable, borderline resectable, or locally advanced categories. As a result, anatomical constraints play a central role in therapeutic decision-making and prognosis.

2. Tumor initiation, genomic instability and molecular heterogeneity

The vast majority of pancreatic cancers originate from exocrine pancreatic cells, with pancreatic ductal adenocarcinoma (PDAC) alone accounting for more than 90% of pancreatic malignancies. Other rarer neoplasms include mucinous cystic neoplasms (MCNs) and intraductal papillary mucinous neoplasms (IPMNs), as well as pancreatic neuroendocrine tumors (PanNETs), which derive from endocrine cells producing glucose-regulating hormones. PDAC typically evolves through a stepwise sequence of non-invasive precursor lesions and accumulating molecular alterations[2].

By far the most common precursor lesion is pancreatic intraepithelial neoplasia (PanIN), a microscopic, non-invasive dysplastic lesion with a ductal phenotype. Experimental models indicate that many PanINs can arise from acinar cells through acinar-to-ductal metaplasia, a process in which acinar cells lose their differentiated identity and acquire duct-like features. Ductal cells can also serve as a cell of origin under specific conditions[3]. PanINs progress through increasing grades of dysplasia and can ultimately give rise to infiltrating PDAC.

In contrast, IPMNs and MCNs are macroscopic, radiologically detectable cystic lesions; when resected at an early, non-invasive stage, these lesions are often associated with excellent outcomes, whereas PanINs, due to their small size and microscopic nature, are typically identified only incidentally or after resection of an established invasive tumor[2]. The sequential genetic and histologic changes that define this progression are summarized in **Figure 2**, which highlights PDAC as the most prevalent and clinically relevant subtype of pancreatic cancer and the central focus of the present study.

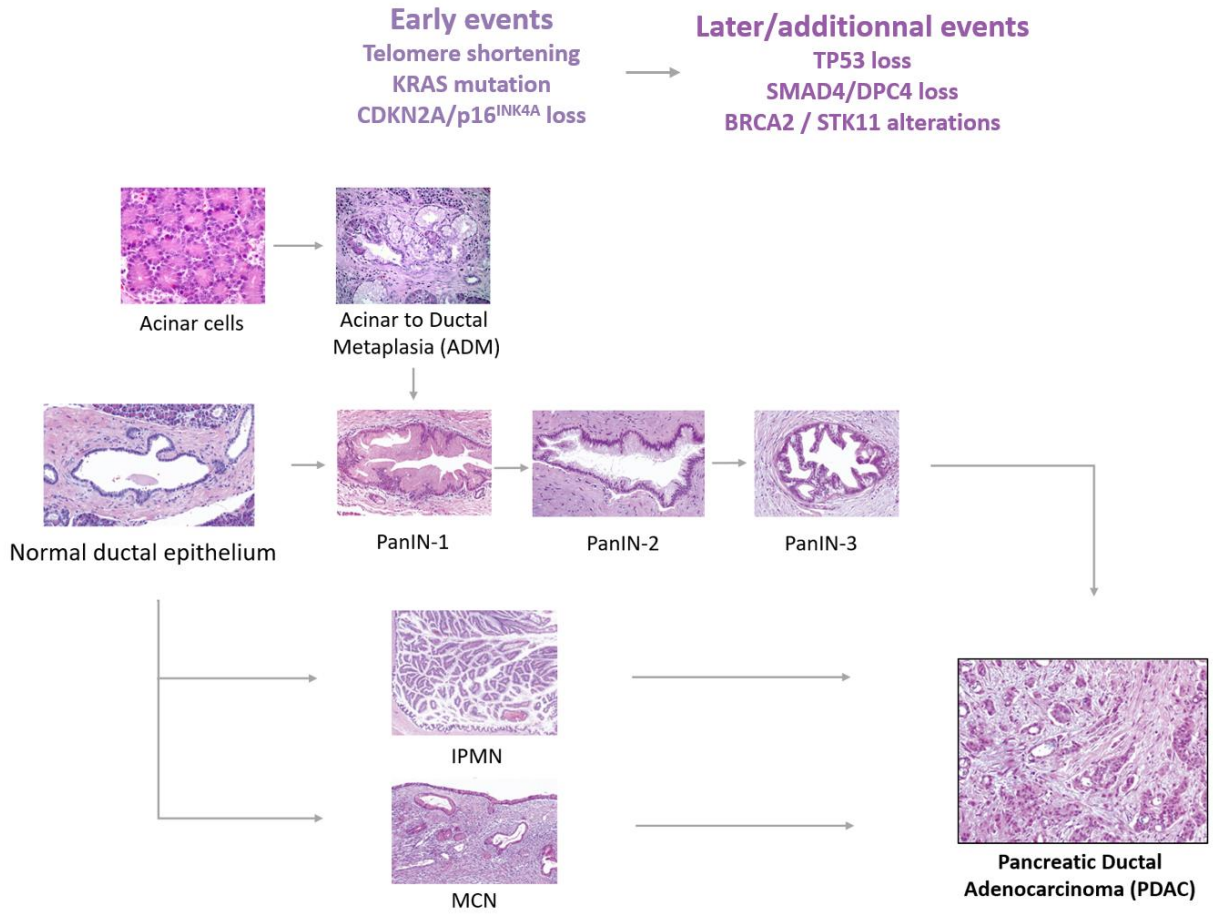


Figure 2: Histological progression and major genetic events involved in pancreatic ductal adenocarcinoma development.

Pancreatic ductal adenocarcinoma can arise through the stepwise progression of pancreatic intraepithelial neoplasia (PanIN), a microscopic, non-invasive precursor lesion with a ductal phenotype. Experimental lineage-tracing studies indicate that PanINs can originate from acinar cells following acinar-to-ductal metaplasia, while the cell of origin of human PanINs remains incompletely resolved. PanIN progression from low-grade to high-grade dysplasia and invasive carcinoma is accompanied by recurrent molecular alterations. Early events include telomere shortening, activating KRAS mutations and CDKN2A/p16INK4A loss. Later events include TP53 loss and SMAD4/DPC4 loss, with additional alterations in genes such as BRCA2 and STK11/LKB1 in selected tumors. Macroscopic precursor lesions, including intraductal papillary mucinous neoplasms and mucinous cystic neoplasms, may also progress toward invasive disease through distinct but partially overlapping molecular trajectories. Adapted from Hezel et al., 2006, with an updated representation of PanIN cell of origin.[4]*.*

This histological progression is accompanied by recurrent genetic and epigenetic changes that drive tumor initiation, invasion, metastatic dissemination, and therapeutic resistance. PDAC evolution is not strictly linear. It combines stepwise acquisition of driver mutations with punctuated genomic events, including large-scale copy-number changes and chromosomal rearrangements. Activating KRAS mutations and telomere shortening are among the earliest events detected during pancreatic tumorigenesis. CDKN2A/p16INK4A loss is frequently acquired during early to intermediate stages

of PanIN progression. Alterations in TP53 and SMAD4/DPC4 are usually associated with high-grade dysplasia, invasive progression and advanced disease. Less frequent defects in DNA damage response or tumor-suppressor pathways, including BRCA1, BRCA2, PALB2, ATM and STK11/LKB1, add further diversity to PDAC evolution in selected tumors. Recent single-cell DNA sequencing studies have shown that the clonality of these alterations can vary substantially within individual tumors, with copy-number alterations accounting for a major proportion of spatial genomic heterogeneity[4–6].

This intratumoral diversity also affects clinically relevant pathways. Subclonal variation in KRAS mutant allele dosage, loss of the mutant KRAS allele, and alternative activation of MAPK signaling may generate variable dependence on oncogenic KRAS and provide pre-existing routes of resistance to KRAS-targeted therapies[6]. Defects in DNA damage response genes, including BRCA1, BRCA2, PALB2, and ATM, add another layer of genomic instability in a subset of tumors[7–9]. In PDACs arising in patients with germline BRCA2 mutations, biallelic BRCA2 inactivation can occur at different stages of tumor evolution, leading to distinct genomic trajectories and potentially heterogeneous therapeutic responses[6]. Together, these alterations promote chromosomal instability, subclonal diversification and a high capacity to adapt under therapeutic pressure.

In addition to genetic heterogeneity, PDAC cells display marked metabolic plasticity that contributes to therapeutic resistance. Mitochondrial metabolism is increasingly recognized as a central determinant of PDAC adaptation, with oxidative phosphorylation, tricarboxylic acid cycle activity, glutamine and fatty-acid metabolism, and redox homeostasis representing potential therapeutic vulnerabilities[10]. In line with this concept, chemotherapy-treated PDAC tumors can enter a drug-tolerant persister state characterized by increased mitochondrial mass, ATP levels, mitochondrial superoxide, total reactive oxygen species and antioxidant defenses[11]. These observations suggest that treatment-induced tumor regression may leave behind metabolically adapted residual populations, making mitochondrial and redox metabolism relevant axes of PDAC resistance and relapse.

Beyond recurrent driver mutations, transcriptomic studies have identified distinct molecular subtypes of PDAC. Early classifications mainly distinguished classical or progenitor tumors from basal-like or squamous tumors[12,13]. These subtypes differ in differentiation, prognosis, and response to treatment. More recent single-cell and spatial studies have shown that these programs are not fixed categories. They can coexist within the same tumor and change during disease progression or treatment[14,15]. Additional tumor-cell states have also been described, including a neural-like progenitor program enriched after therapy[16]. These tumor-cell programs are associated with specific fibroblast and immune-cell states, showing that PDAC heterogeneity also depends on the organization of the tumor microenvironment [15–17].

However, the genetic landscape of PDAC does not fully explain its clinical aggressiveness. A central feature of the disease is that malignant epithelial cells evolve within a complex ecosystem composed of stromal, immune, vascular, neural and extracellular matrix components. In PDAC, therapeutic

resistance therefore arises from tumor-cell-intrinsic alterations and from the architecture and functional state of the surrounding niche. For this reason, the tumor microenvironment must be considered as a biological driver of disease progression and maybe also as a therapeutic target.

3. Clinical burden and therapeutic dead-end

Over the last few decades, the surgical management of pancreatic ductal adenocarcinoma (PDAC) has improved substantially. Pancreatic resections are now often performed in high-volume centers, where surgical expertise, multidisciplinary decision-making, and postoperative complication management have reduced perioperative mortality.[18,19]

Patient selection has also become more precise. High-quality imaging and the assessment of tumor involvement of major vessels remain central to the evaluation of anatomical resectability. Biological factors are now also considered. The carbohydrate antigen 19-9 (CA19-9) is the most widely used serum biomarker in PDAC, and its baseline level and evolution during systemic therapy provide information on tumor burden, prognosis, and treatment response. Its interpretation requires caution in patients with biliary obstruction and in individuals who do not secrete CA19-9[20]. Together with the response observed on imaging, CA19-9 dynamics can help identify patients with more favorable tumor biology and support surgical decision-making. This has shifted part of the therapeutic strategy from immediate surgery to staged treatment, especially in borderline-resectable disease, where neoadjuvant therapy can improve patient selection and increase the likelihood of complete tumor resection[21].

Surgical technique has also progressed. Venous resection and reconstruction of the portal or superior mesenteric vein can now be performed in selected patients to achieve complete tumor clearance when the tumor involves the mesentericoportal axis[22]. Perioperative care has improved through standardized enhanced recovery pathways, optimized analgesia, nutritional support, and earlier management of complications such as pancreatic fistula, delayed gastric emptying, and postoperative bleeding[23]. Minimally invasive and robotic approaches are also increasingly used, mainly for distal pancreatectomy and in selected expert centers for pancreaticoduodenectomy, with potential benefits on blood loss and duration of hospital stay[24]. These surgical advances are clinically relevant. They have made pancreatic surgery safer, more standardized, and applicable to selected patients with more complex disease. Systemic therapy has also moved forward, mainly with FOLFIRINOX and gemcitabine plus nab-paclitaxel in advanced disease, and modified FOLFIRINOX in the adjuvant setting after resection[25–27]. Still, the global impact remains limited. Only a minority of patients present with localized disease, relapse after surgery is frequent, and most patients eventually require systemic treatment.

Long-term survival has improved over recent decades. Older studies commonly reported 5-year survival below 5%, while recent reviews now report values around 13%[28,29]. This improvement confirms that progress in surgery, perioperative care, and chemotherapy has had a measurable

clinical impact. Still, international survival remains highly heterogeneous and globally poor, confirming that progress in surgery and chemotherapy has not solved the central therapeutic problem of PDAC.

This poor outcome is partly explained by the difficulty of detecting PDAC at an early stage. Most patients do not belong to a clearly defined high-risk group, and no simple, specific, and affordable test is currently available for population-wide screening. Early symptoms are rare or nonspecific. Consequently, many patients are diagnosed only once the disease is locally advanced or metastatic, when curative surgery is no longer feasible[30].

At present, the backbone of PDAC therapy remains multimodal, combining surgery when feasible with systemic chemotherapy and, in selected cases, radiotherapy.

For patients with good performance status, first-line systemic therapy largely relies on two regimens: FOLFIRINOX (5-fluorouracil, leucovorin, oxaliplatin, and irinotecan) and the combination of gemcitabine plus nab-paclitaxel. In metastatic disease, a phase III trial demonstrated that FOLFIRINOX improves median overall survival compared with gemcitabine alone (11.1 versus 6.8 months), establishing it as a standard first-line option in fit patients[25]. Similarly, another phase III study showed that adding nab-paclitaxel to gemcitabine significantly prolongs survival from 6.7 to 8.5 months in advanced PDAC, supporting gemcitabine plus nab-paclitaxel as an alternative first-line backbone[26]. In France, FOLFIRINOX or modified FOLFIRINOX remains the main standard for fit patients.

In localized disease, complete surgical resection is the only potentially curative modality. Recurrence still occurs in most patients after surgery, with reported rates commonly ranging around 60%. These relapses frequently involve distant sites, especially the liver, peritoneum, and lungs, indicating that micrometastatic disease is probably already present at the time of resection[31,32].

Adjuvant chemotherapy has been firmly established by a phase III trial showing that FOLFIRINOX after resection improves median overall survival and relapse-free survival compared with gemcitabine alone, making it the preferred adjuvant regimen in eligible patients[33].

In the adjuvant setting after PDAC resection, modified FOLFIRINOX, defined by omission of the 5-FU bolus and reduction of irinotecan dose, has become the preferred regimen for fit patients in France and in most Western guidelines. This recommendation is based on the PRODIGE 24/CCTG PA.6 trial, which showed significantly longer survival with modified FOLFIRINOX compared with gemcitabine after pancreatic cancer resection[27,33].

For patients who are not eligible for modified FOLFIRINOX, gemcitabine-based adjuvant strategies remain relevant, particularly gemcitabine alone or gemcitabine plus capecitabine, depending on performance status and comorbidities[34].

More recently, the therapeutic landscape of PDAC has begun to evolve with the emergence of molecularly targeted approaches directed against KRAS and RAS signaling. Although KRAS was historically considered difficult to target with drugs, allele-specific inhibitors such as sotorasib have shown clinical activity in the rare $KRAS^{G12C}$-mutated PDAC subset, while $KRAS^{G12D}$-directed

inhibitors such as MRTX1133 have recently demonstrated strong preclinical activity in pancreatic cancer models[35–37].

More broadly, direct RAS inhibition is now emerging as a clinically relevant strategy in PDAC. Daraxonrasib/RMC-6236, an oral multiselective RAS(ON) inhibitor targeting active RAS signaling, has shown antitumor activity in previously treated RAS-mutated PDAC, with responses observed across several RAS variants. In phase I/II data, objective responses were reported in 35% of patients with RAS G12-mutated PDAC treated at the 300 mg dose in the second-line setting, and in 29% of patients across a broader RAS G12/G13/Q61-mutated cohort.

These early results were followed by the phase III RASolute 302 trial, in which daraxonrasib improved median overall survival compared with chemotherapy in previously treated metastatic PDAC, increasing it from 6.7 to 13.2 months. These results position direct RAS inhibition as one of the most important recent therapeutic advances under clinical evaluation in PDAC, although regulatory approval, long-term benefit and resistance mechanisms remain to be fully defined.

Preclinical work has also explored combination strategies aimed at blocking parallel KRAS-dependent escape pathways, including EGFR, RAF1 and STAT3 signaling[38]. These studies suggest a trend toward stronger tumor control when KRAS pathway inhibition is combined with blockade of compensatory survival nodes, particularly STAT3. However, these findings remain preclinical and should be interpreted cautiously, as clinical benefit has not yet been demonstrated.

These data support direct RAS inhibition as one of the most promising recent therapeutic developments in PDAC, while resistance remains a major challenge and combination strategies are still under clinical investigation.

In parallel, local intensification strategies are also being revisited for patients with locally advanced, unresectable PDAC. One recent example is the ACAPELLA trial, initiated in Europe at CHU Grenoble Alpes, which evaluates intratumoral Alpha DaRT sources combined with capecitabine in patients with inoperable locally advanced PDAC after first-line mFOLFIRINOX. This approach relies on the endoscopic ultrasound-guided implantation of radium-224-loaded sources directly into the pancreatic tumor, with the aim of delivering highly localized alpha irradiation while limiting exposure of surrounding healthy tissues. Although still investigational and primarily designed to assess safety, this strategy illustrates the current effort to develop spatially controlled treatments that intensify local tumor control in anatomically constrained pancreatic lesions (NCT06755359).

Taken together, these observations underscore that, despite recent progress, PDAC remains a biologically aggressive disease with early systemic dissemination in a majority of patients[39]. Surgery, when feasible, is still the best option for prolonged survival, but it is only applicable to a minority of patients at diagnosis. Systemic therapy alone typically yields median overall survivals in the 12-15-month range for metastatic disease and only slightly longer for locally advanced tumors, in line with the current standard-of-care regimens outlined above[40]. Reflecting this clinical reality, current therapeutic management **(Figure 3)** emphasizes initial stratification based on anatomical and biological resectability, leading to an urgent need for deeper patient characterization, including

molecular and cellular phenotyping, to guide next-generation interventions[40]. This persistent gap between the intensity of current multimodal treatment and the limited long-term benefit justifies a shift towards therapeutic strategies that more directly address the biological determinants of PDAC lethality, including its genomic complexity and its protective tumor microenvironment[30].

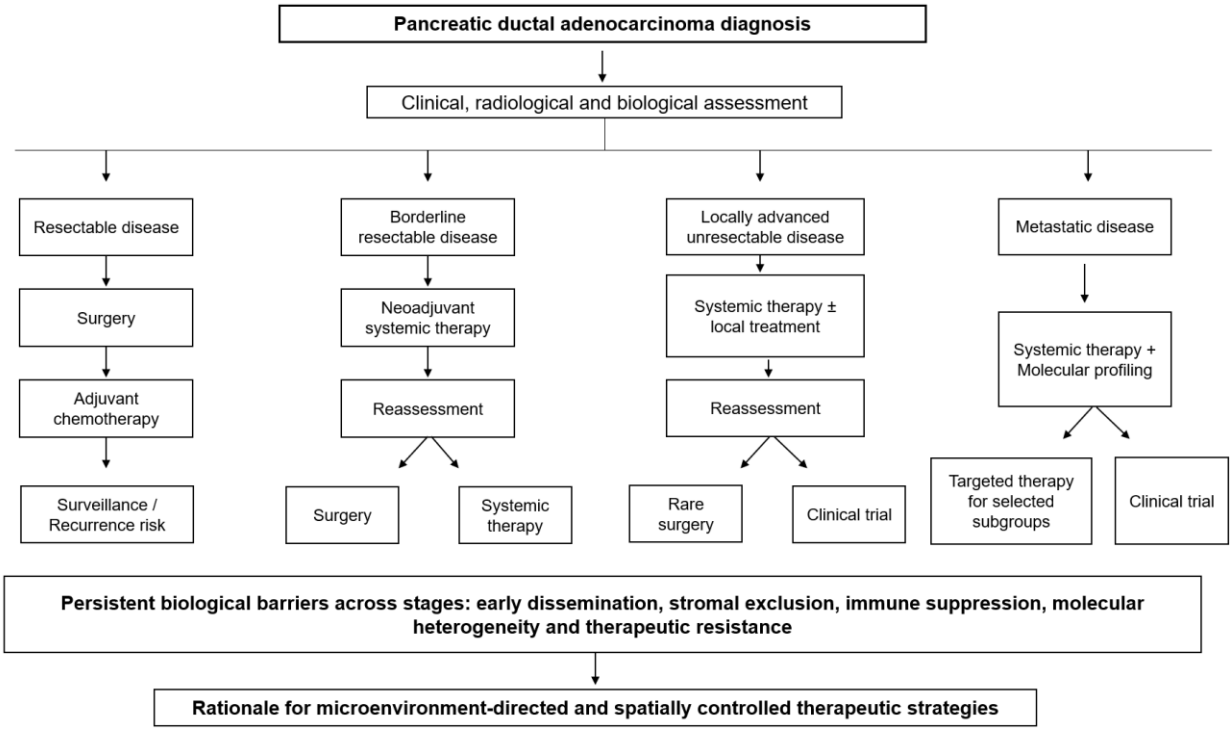


Figure 3: Current stage-adapted management of PDAC and rationale for microenvironment-directed therapeutic strategies.

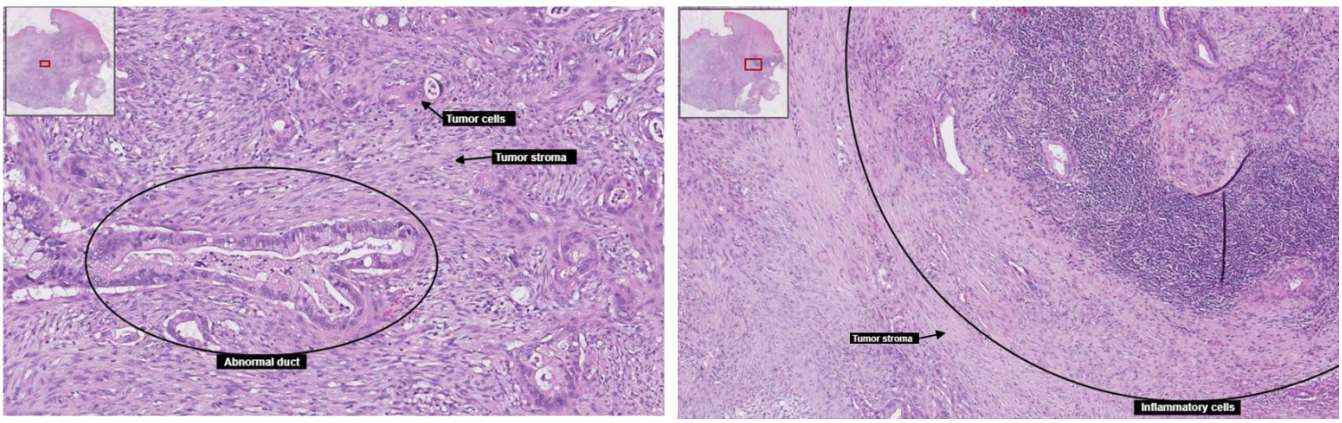
After diagnosis, PDAC patients are classified according to clinical, radiological and biological assessment into resectable, borderline resectable, locally advanced unresectable or metastatic disease. Treatment is based on surgery when feasible and systemic therapy across stages, with molecular profiling guiding targeted therapies in selected metastatic subgroups. However, persistent biological barriers (including early dissemination, stromal exclusion, immune suppression, molecular heterogeneity and therapeutic resistance) continue to limit clinical benefit. This provides a rationale for the development of microenvironment-directed and spatially controlled therapeutic strategies. Adapted from Conroy et al., 2023, and Boggi et al., 2024[41,42]*.*

Beyond survival statistics, PDAC also imposes a major clinical burden through cachexia, abdominal pain, biliary obstruction, weight loss and rapid functional decline, all of which frequently limit treatment tolerance and therapeutic options[43]. This clinical aggressiveness is further reinforced by epidemiological trends, as PDAC incidence is increasing worldwide. Importantly, mortality remains closely aligned with incidence, underscoring the persistent lack of effective curative strategies at the population level. Together, these observations emphasize that improving outcomes in PDAC will require more effective systemic therapies, earlier detection, refined patient stratification and therapeutic strategies that directly address the biological mechanisms driving resistance. This need directly motivates a closer examination of the molecular and microenvironmental features that underlie PDAC progression and therapeutic failure.

4. The PDAC tumor microenvironment: a stromal-dominant and immune-excluded niche

PDAC is one of the most stromal-rich solid tumors[44]. Histological sections commonly show scattered malignant epithelial glands embedded within a much larger stromal compartment. Inflammatory cell aggregates can be present within this stroma, while few inflammatory cells are observed in direct contact with malignant epithelial cells. This spatial organization is consistent with an immune-excluded pattern, in which immune cells accumulate in stromal regions without efficiently reaching the tumor-cell compartment **(Figure 4A).** This compartment is formed by a prominent desmoplastic reaction composed of activated cancer-associated fibroblasts (CAFs), a dense extracellular matrix rich in collagen and hyaluronan, aberrant vasculature, and a complex infiltrate of immune cells **(Figure 4B)**[45–48]. This stroma is an active driver of disease progression. It influences tumor-cell survival, mechanical constraint, vascular perfusion, immune infiltration, and treatment response. Malignant epithelial cells therefore represent only one component of a broader tissue ecosystem, which helps explain why therapies directed exclusively at tumor-cell killing often fail to produce durable responses.

A



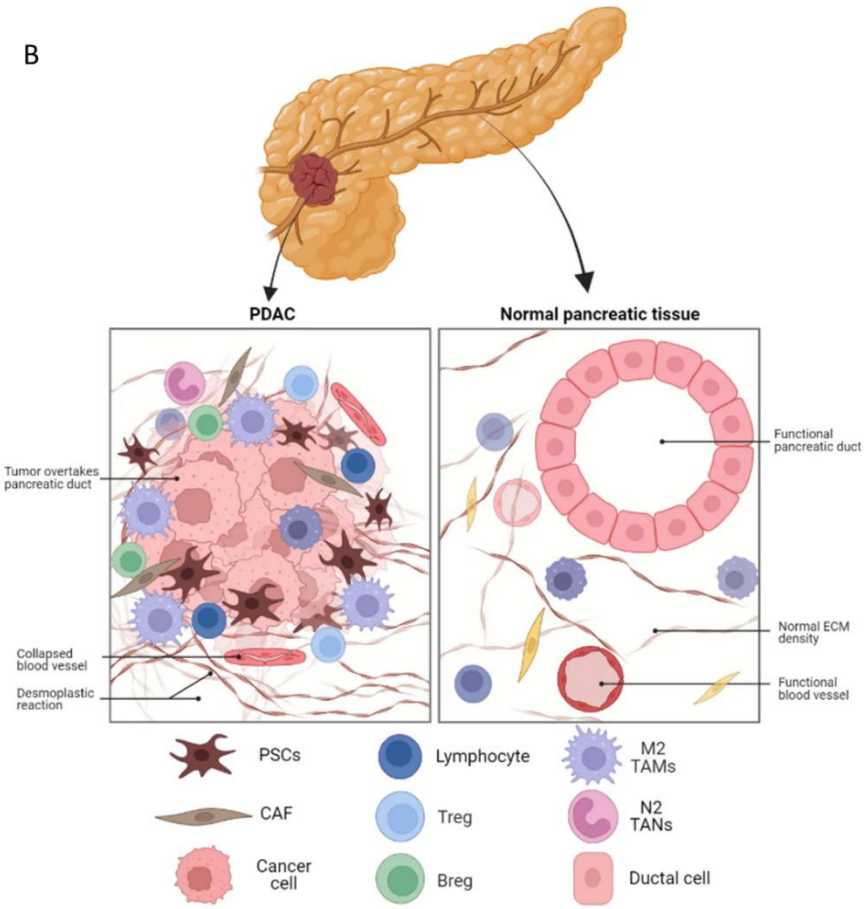


Figure 4: Histological architecture and major components of the pancreatic ductal adenocarcinoma microenvironment.

(A) *Representative hematoxylin and eosin-stained section of human pancreatic adenocarcinoma showing irregular neoplastic glands embedded in abundant desmoplastic stroma. Inflammatory cell aggregates are visible within stromal regions, with limited direct contact with malignant epithelial cells. This image illustrates the low tumor cellularity and the spatial separation between the inflammatory infiltrate and the tumor-cell compartment that can characterize PDAC. Image adapted from the Human Protein Atlas; annotations added.* ***(B)*** *Schematic comparison of normal pancreatic tissue and the PDAC microenvironment. PDAC is characterized by a dense desmoplastic reaction, altered extracellular matrix organization, impaired vasculature, cancer-associated fibroblasts, pancreatic stellate cells, and diverse immune-cell populations. Adapted from Joseph et al., 2024*[49]*.*

Low tumor cellularity and malignant epithelial compartment

Compared with many epithelial cancers, PDAC lesions often contain abundant stromal tissue, inflammatory infiltrates, extracellular matrix and non-malignant accessory cells, while the fraction of neoplastic epithelial cells can be relatively low and spatially discontinuous[44]. This low tumor cellularity has several therapeutic implications. First, it reduces the accessibility of malignant cells to drugs and immune effectors. Second, it increases the relative influence of stromal and immune compartments on treatment response. Third, it suggests that successful therapeutic intervention may not require direct genetic modification of every malignant cell. A limited number of transduced cells can act as

local sources of diffusible immunomodulatory or matrix-remodeling factors. This concept is directly relevant to tumor niche engineering, in which the therapeutic objective is not necessarily to eliminate every transduced cell, but to impose a local biological perturbation that propagates through the tumor ecosystem.

The malignant epithelial compartment itself is heterogeneous. Tumor cells may differ in differentiation state, epithelial or mesenchymal features, proliferative activity, metabolic adaptation and antigen expression. This heterogeneity contributes to variable sensitivity to chemotherapy, targeted therapy and immunotherapy, and provides a substrate for clonal selection under therapeutic pressure. In the context of antigen-directed approaches, including CAR T cells or targeted lentiviral vectors, this heterogeneity is particularly relevant because surface antigens may be expressed at different levels across lesions, patients or tumor-cell states.

Pancreatic stellate cells and origin of the fibrotic stroma

Pancreatic stellate cells are resident mesenchymal cells that play a central role in the development of the pancreatic fibrotic reaction[50]. In the healthy pancreas, stellate cells remain in a relatively quiescent state and participate in tissue homeostasis. During pancreatic injury, inflammation and tumorigenesis, they become activated and acquire a myofibroblast-like phenotype characterized by increased contractility, extracellular matrix production and secretion of growth factors and cytokines. Activated pancreatic stellate cells contribute to collagen deposition, tissue stiffness, interstitial pressure and impaired vascular perfusion, all of which are major barriers to drug delivery and immune-cell trafficking[50].

In PDAC, pancreatic stellate cells interact bidirectionally with malignant epithelial cells. Tumor-derived signals can activate stellate cells, while activated stellate cells in turn support tumor-cell proliferation, invasion and survival through paracrine signaling and matrix remodeling[51]. This reciprocal crosstalk contributes to a self-reinforcing fibrotic loop in which tumor progression and stromal activation are mutually amplified. For therapeutic purposes, this implies that targeting the tumor-cell compartment alone may be insufficient if the stromal program remains intact. Conversely, strategies that modulate stellate-cell-derived matrix organization may alter the physical and biochemical properties of the tumor niche.

Cancer-associated fibroblasts: heterogeneity and functional states

Cancer-associated fibroblasts constitute one of the most abundant and functionally important stromal populations in PDAC. CAFs secrete growth factors, cytokines and matrix components that support tumor proliferation and invasion, while the dense extracellular matrix increases interstitial pressure, compresses blood vessels and limits the penetration of both cytotoxic drugs and immune effector cells into the tumor core[46,52]. Beyond these physical constraints, CAFs can also actively organize

immune exclusion through chemokine-dependent mechanisms. In a KRAS-driven pancreatic cancer model, FAP-expressing CAFs were shown to produce CXCL12, which accumulated around tumor cells and limited T cell access; disruption of the CXCL12-CXCR4 axis restored T cell infiltration and sensitized tumors to PD-L1 blockade[53].

However, CAFs do not represent a uniform stromal population. Single-cell and functional studies have identified multiple CAF states with distinct phenotypes, localization patterns and biological functions. Myofibroblastic CAFs, often referred to as myCAFs, are typically enriched close to malignant glands and characterized by high expression of contractile and matrix-associated programs, including αSMA and collagen-related genes. Inflammatory CAFs, or iCAFs, are more strongly associated with cytokine and chemokine secretion, including IL-6-related inflammatory programs, and can promote tumor growth, myeloid recruitment and immunosuppression[54]. Antigen-presenting CAFs, or apCAFs, express MHC class II-related genes and may participate in local immune regulation, although their ability to productively activate T cells remains limited and context-dependent[55]. Other CAF-associated signatures, including FAP-, podoplanin-, periostin- or inflammatory-matrix-associated subsets, further illustrate the diversity of stromal states present in human PDAC[56–58].

This heterogeneity has major therapeutic implications. CAF populations can exert pro-tumoral, immunosuppressive, matrix-producing, inflammatory or even tumor-restraining functions depending on context. Therefore, stromal targeting should not be reduced to any fibroblast depletion. A more rational strategy is to identify and remodel specific stromal functions that restrict immune-cell access or reinforce immunosuppression, while avoiding the complete collapse of potentially protective tissue architecture.

Tumor-associated macrophages and M2-like myeloid polarization

The immune compartment of PDAC is strongly shaped by myeloid cells, among which tumor-associated macrophages (TAMs) are particularly abundant[44]. PDAC-associated macrophages frequently display M2-like immunosuppressive and tissue-remodeling features associated with angiogenesis and tumor progression. These macrophages can secrete IL-10, TGFβ, arginase-associated mediators, matrix-remodeling enzymes and growth factors that suppress effector T cell activity while supporting tumor-cell invasion and stromal remodeling[59].

TAMs also interact with CAFs and malignant epithelial cells to reinforce the immunosuppressive niche. Tumor-derived and stromal-derived chemokines recruit monocytes and promote their differentiation toward suppressive macrophage states. In turn, TAM-derived cytokines can sustain fibroblast activation, extracellular matrix deposition and T cell dysfunction. This myeloid-fibroblast crosstalk contributes to the resistance of PDAC to immune checkpoint blockade and may also limit the efficacy of adoptively transferred effector cells, including CAR T cells.

MDSCs, Tregs and suppressive immune networks

In addition to macrophages, PDAC lesions are enriched in other immunosuppressive populations, including myeloid-derived suppressor cells and regulatory T cells. MDSCs can inhibit T cell activation through nutrient depletion, reactive oxygen and nitrogen species, arginase activity, suppressive cytokine production and interference with antigen presentation[60]. Regulatory T cells further suppress antitumor immunity through IL-10, TGFβ, CTLA-4-dependent mechanisms and competition for cytokine support[59,60]. Together, these populations create a suppressive immune network that limits endogenous antitumor T cell priming and blunts the activity of therapeutic immune effectors.

Importantly, this immunosuppressive architecture appears early during pancreatic carcinogenesis[61]. In KRAS-driven models, regulatory and myeloid suppressive populations can be detected already in precursor lesions, whereas effector T cells remain scarce and poorly activated[62]. This suggests that immunosuppression is a core component of PDAC development, and may not be the late consequence of advanced tumor burden.

Effector lymphocytes, NK cells and immune exclusion

In contrast to suppressive myeloid and regulatory compartments, cytotoxic immune effectors are often quantitatively and functionally limited in PDAC. CD8+ T cells may be absent, excluded to stromal regions, spatially separated from malignant epithelial cells **(Figure 4A)**, or present in a dysfunctional state characterized by impaired proliferation, reduced cytokine production and expression of inhibitory receptors. Natural killer cells can also be depleted or functionally impaired by hypoxia, suppressive cytokines and metabolic competition within the tumor niche.

This immune-excluded architecture is central to the failure of many immunotherapies in PDAC. Even when tumor-reactive T cells are generated by vaccination, checkpoint blockade or adoptive transfer, these cells must still extravasate, navigate through a dense matrix, resist suppressive cytokines and establish stable contact with antigen-positive tumor cells. Thus, the problem is the absence of a permissive intratumoral niche in which such lymphocytes can operate productively.

Endothelial cells, abnormal vasculature and hypoxia

The vascular compartment of PDAC is structurally and functionally abnormal. Despite the high metabolic demand of the tumor, PDAC lesions are frequently hypovascular and poorly perfused, in part because the dense extracellular matrix and high interstitial pressure compress blood vessels[46]. This abnormal vasculature reduces oxygen and nutrient delivery, limits drug penetration and contributes to hypoxia. Hypoxia can then promote epithelial plasticity, metabolic rewiring, invasive behavior and resistance to therapy.

For immunotherapy, abnormal vasculature constitutes an additional barrier. Efficient T cell entry into tumors requires adhesion, extravasation and chemokine-guided migration across endothelial structures. Vascular compression, endothelial dysfunction and inappropriate chemokine gradients

can therefore limit immune-cell trafficking before cells even encounter the stromal matrix[63]. This reinforces the idea that improving immune infiltration in PDAC requires modulation of both cellular recruitment signals and the physical properties of the tumor tissue.

Neural compartment and perineural invasion

Another characteristic feature of PDAC is its close association with the neural compartment. Perineural invasion is frequent and contributes to local progression, pain, recurrence and poor clinical outcome[64]. Tumor cells, stromal cells and nerves engage in reciprocal signaling involving neurotrophic factors, inflammatory mediators and extracellular matrix remodeling[65,66]. Although the neural compartment is not the primary focus of this thesis, its presence illustrates the broader principle that PDAC progression is governed by a multicellular tissue ecosystem rather than by malignant epithelial cells alone.

Acellular components of the PDAC niche: ECM, stiffness and biochemical barriers;

The acellular component of the PDAC microenvironment is dominated by a dense extracellular matrix composed of fibrillar collagens, hyaluronan, fibronectin, laminins, proteoglycans and matricellular proteins such as periostin, SPARC and tenascin-C. This matrix actively regulates tissue stiffness, growth factor availability, mechano-transduction, interstitial fluid pressure and immune-cell migration. Collagen-rich matrices increase tissue rigidity and provide tracks for tumor invasion, whereas hyaluronan contributes to water retention, interstitial pressure and vascular compression[46,47].

Matrix stiffness also influences cell signaling. Mechanical cues transmitted through integrins, focal adhesion kinases and cytoskeletal pathways can promote tumor-cell survival, invasion and therapy resistance[67]. In parallel, dense matrix architecture restricts the motility of lymphocytes and can physically separate immune cells from malignant epithelial nests. These properties explain why ECM remodeling has become a major therapeutic concept in PDAC. However, because ECM components can also restrain tumor dissemination in certain contexts, matrix-targeting strategies must be designed as controlled remodeling rather than complete stromal ablation.

From stromal depletion to stromal remodeling

The biological role of the PDAC stroma is complex. Although the dense extracellular matrix and fibroblast-rich compartment can restrict perfusion, drug delivery and immune-cell access, experimental depletion of stromal components has produced unexpected adverse effects. Inhibition of Sonic Hedgehog signaling reduced stromal content but promoted more aggressive and poorly differentiated tumors, while depletion of αSMA-positive myofibroblasts accelerated disease progression, reduced survival and reinforced immunosuppression[68,69]. These findings indicate that

the stroma cannot be treated only as a physical barrier to be removed. They support a more selective strategy based on local remodeling of the tumor niche.

This distinction is important for the concept of this thesis. In PDAC, the goal is not to remove the stromal compartment, but to remodel it in a controlled and probably limited way. The tumor niche must become more permissive to lymphocyte recruitment, tissue penetration, contact with tumor cells and maintenance of effector function. This strategy supports the use of local gene delivery to produce chemokines and stromal-remodeling factors.

5. What has been tried, and why it failed

To enhance immune recognition in PDAC, multiple vaccination strategies have been developed to improve antigen presentation and expand tumor-specific T cell clones[70]. These approaches have targeted a range of PDAC-associated antigens, including telomerase, KRAS, gastrin, CEA, MUC1 and mesothelin, using different platforms such as peptide-based vaccines, viral and Listeria vectors, DNA vaccines encoding neoantigens and various cell-based formulations[71,72]. GVAX, a lethally irradiated allogeneic tumor cell vaccine engineered to secrete GM-CSF, showed that vaccination can recruit activated immune aggregates into the tumor microenvironment and broaden the intratumoral T cell repertoire[73–76]. Several trials have also demonstrated robust antigen-specific immune responses in vaccinated patients. However, advanced candidates such as TeloVac, Primo Vax, PANVAC-V and algenpantucel-L failed to improve survival in phase III trials[77,78]. These results indicate that vaccine-induced immunity can be generated in PDAC, but is usually insufficient to produce meaningful clinical benefit in unselected patients.

Mechanistic studies have helped to explain this gap between immune activation and clinical benefit by highlighting the early established immunosuppression in PDAC. A direct link between oncogenic KRAS and the establishment of an immunosuppressive microenvironment has been described, whereby $KRAS^{G12D}$-dependent upregulation of GM-CSF drives the recruitment of myeloid-derived suppressor cells that dampen antitumor T cell activity[62]. This suppressive immune landscape is established early during pancreatic carcinogenesis. In KRAS-driven mouse models, Treg cells and MDSCs already dominate the immune landscape in PanIN lesions, while effector T cells are scarce and display little evidence of activation[79]. Vaccines are therefore used in a tissue context where myeloid and regulatory networks are already in place before invasive carcinoma develops. In this setting, vaccines can expand specific T cell clones, but these effectors then encounter a microenvironment that limits their trafficking, activation and persistence, thereby blunting their clinical impact and underscoring the need for combinations that simultaneously reshape the TME[77].

Immune checkpoint inhibitors have also shown limited efficacy in PDAC, except in the rare subset of MSI-high tumors[80]. MSI-high tumors result from defective DNA mismatch repair, leading to accumulation of replication errors, increased neoantigen load and greater sensitivity to PD-1 blockade. However, this subgroup remains uncommon in PDAC, which limits the clinical impact of

checkpoint inhibitors. In most cases, resistance is associated with low tumor mutational burden, limited neoantigen presentation and weak T cell infiltration. Other immunotherapeutic strategies, including CD40 agonists, oncolytic viruses and combinations with chemotherapy or radiotherapy, can modulate the tumor microenvironment and enhance immune activation[81]. However, their clinical benefit has remained modest. This suggests that transient immune activation or partial depletion of immunosuppressive populations is not sufficient to overcome the multiple barriers imposed by PDAC, including stromal exclusion, myeloid-driven suppression and limited persistence of effector T cells.

Chemotherapy adds another layer of complexity to these combinations. Cytotoxic agents can induce systemic myelosuppression and transiently reduce immune-cell populations, which may limit the persistence or function of antitumor lymphocytes[25]. At the same time, some chemotherapies can also exert favorable immunomodulatory effects. Gemcitabine has been reported to reduce MDSCs, Tregs and TGFβ1 in patients with pancreatic cancer, while 5-fluorouracil can deplete tumor-associated MDSCs in preclinical models[82,83]. Chemotherapy may therefore create a temporary window of immune permissiveness, but this effect remains incomplete and can be counterbalanced by systemic immune depletion and persistent stromal and myeloid barriers in PDAC.

Stromal-targeting approaches have also been explored, including strategies aimed at hyaluronan degradation, connective tissue growth factor inhibition, focal adhesion kinase inhibition or pharmacological modulation of fibroblast activation[84–86]. These strategies showed that the PDAC microenvironment can be therapeutically altered, but they have not yet produced broadly effective immune-based combinations. Their mixed outcomes support the need for spatially controlled approaches that act on defined barriers without systemic and non-selective stromal modulation.

Altogether, these studies show that conventional immunotherapeutic strategies can induce measurable immune activation in PDAC, but this activation rarely translates into durable clinical benefit. The main limitation is the inability of these cells to efficiently infiltrate pancreatic lesions, persist within a dense stromal architecture and maintain effector function in an immunosuppressive niche. This provides the rationale for adoptive cell therapy. ACT does not rely only on endogenous immune priming; it provides patients with large numbers of functional antitumor effector cells.

II. Adoptive cell therapy

1. Adoptive cell therapy and engineered lymphocytes

The limited efficacy of conventional immunotherapeutic approaches in pancreatic ductal adenocarcinoma has progressively shifted attention toward strategies capable of providing patients with a larger pool of tumor-reactive effector cells. In this context, ACT has emerged as a major branch of cancer immunotherapy, based on the principle that lymphocytes with antitumor activity can be isolated, expanded or genetically modified *ex vivo*, and subsequently reinfused to mediate a more

potent and durable immune response than endogenous immunity alone. The conceptual foundations of ACT were established through pioneering work by Steven Rosenberg and colleagues, who demonstrated that *ex vivo*-expanded tumor-infiltrating lymphocytes could induce tumor regression in selected patients[87]. These early studies showed that transferred immune cells could mediate clinically meaningful antitumor effects. They also highlighted key limitations of ACT in solid tumors, including limited availability of functional tumor-reactive lymphocytes, variable persistence after infusion, and sensitivity to inhibitory signals. The concept of adoptive transfer is rooted in the physiological mechanisms through which T lymphocytes recognize and eliminate abnormal cells. Under normal conditions, antigen-specific T cells are activated when their T cell receptor (TCR) recognizes peptide antigens presented by major histocompatibility complex (MHC) molecules on antigen-presenting cells. This interaction, together with co-stimulatory signals and cytokine support, initiates clonal expansion and acquisition of effector functions. Activated $CD8^+$ T cells can then kill target cells through perforin- and granzyme-mediated cytotoxicity and through the secretion of inflammatory cytokines such as interferon-γ and tumor necrosis factor. In cancer, however, this physiological process can be interrupted at multiple levels, including defective antigen presentation, impaired co-stimulation, chronic antigen exposure and suppressive signaling.

This provides the rationale for adoptive cell therapy. ACT supplies patients with large numbers of immune effector cells that have already been selected, expanded or genetically redirected before infusion. Chimeric antigen receptor (CAR) T cell technology was developed in part to circumvent these constraints. CARs are synthetic receptors that redirect T lymphocytes toward predefined cell-surface antigens independently of conventional antigen processing and MHC presentation[88–90]. Structurally, a CAR typically consists of an extracellular antigen-binding domain derived from a monoclonal antibody single-chain variable fragment (scFv), linked through hinge and transmembrane regions to intracellular signaling modules that activate the T cell upon antigen engagement[91]. By uncoupling target recognition from HLA restriction, CAR T cells can overcome one of the major mechanisms of immune escape observed in many solid tumors, including PDAC.

The evolution of CAR design has progressively improved the therapeutic potential of engineered T cells. First-generation CARs contained only the CD3ζ signaling domain and showed limited expansion and persistence *in vivo*[92]. Second-generation constructs incorporated a single co-stimulatory domain, most commonly CD28 or 4-1BB, substantially improving T cell proliferation, survival and antitumor activity. Third-generation CARs combined multiple co-stimulatory motifs, while more recent fourth-generation or “armored” CARs have extended the concept further by incorporating additional functional modules such as inducible cytokine secretion, chemokine release, dominant-negative receptors or switch receptors that allow engineered cells to better resist inhibitory signals within tumors[88,93].

These engineering strategies can improve CAR T cell activity, but they also increase the need for safety control. Excessive activation, prolonged persistence or constitutive cytokine release may promote severe toxicities, including cytokine release syndrome, neurotoxicity and on-target off-tumor

effects when the target antigen is also expressed by normal tissues[94,95]. This is a major issue in solid tumors, where most CAR targets are tumor-associated rather than tumor-specific.

Taken together, these successive generations reflect a broader conceptual shift: CAR engineering has progressively moved beyond simply triggering cytotoxicity toward actively programming persistence, metabolic fitness and interactions with the tumor microenvironment **(Figure 5)**.

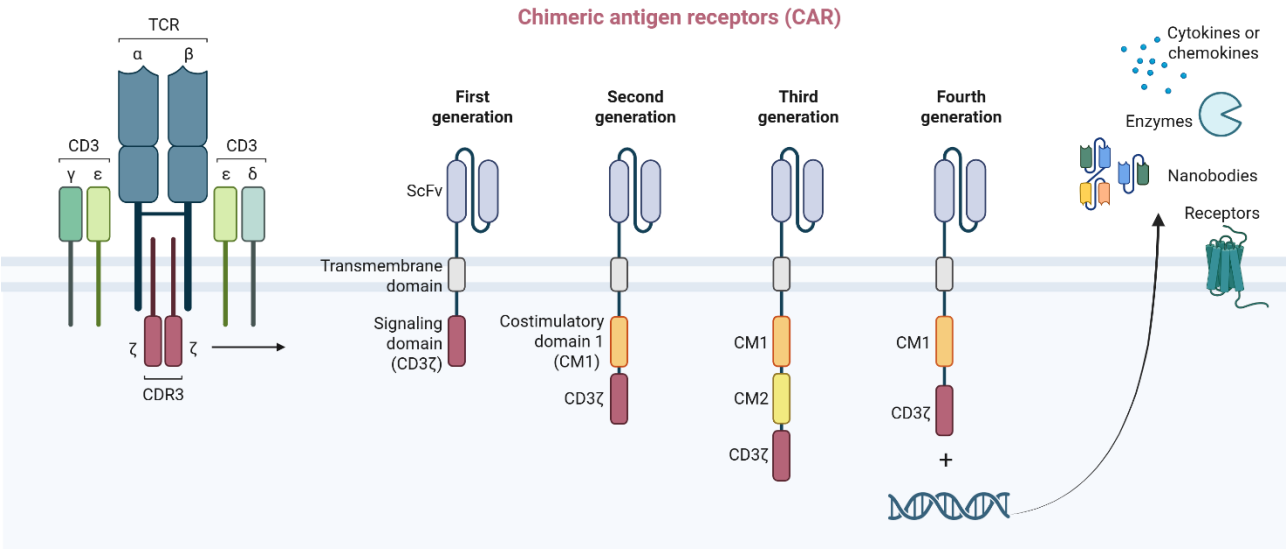


Figure 5: Structural evolution of chimeric antigen receptors (CARs) across successive generations. *Chimeric antigen receptors are synthetic immune receptors composed of an extracellular antigen-binding domain, typically derived from a single-chain variable fragment, linked to hinge, transmembrane and intracellular signaling domains. First-generation CARs contain CD3ζ as the sole activation module, whereas second- and third-generation CARs incorporate one or several co-stimulatory domains to improve T cell activation, expansion and persistence. More advanced armored CAR designs integrate additional functional modules, such as cytokine secretion, chemokine expression or resistance to inhibitory signals, in order to improve CAR T cell activity within hostile tumor microenvironments. Created with Biorender.com and adapted from Carcopino et al.*[93]*.*

The clinical success of CAR T cell therapy in hematological malignancies has provided strong validation for this approach. CAR T products targeting CD19 have induced durable remissions in patients with relapsed or refractory B-cell leukemias and lymphomas, establishing engineered lymphocytes as a transformative therapeutic modality in oncology[96,97]. However, translating this success to solid tumors has proven substantially more challenging. In these settings, therapeutic efficacy depends on the capacity of transferred cells to traffic into tumors, survive within hostile metabolic and stromal conditions, and maintain functional activity despite persistent immunosuppressive signals.

These limitations have led to several strategies to improve adoptive cell therapy in solid tumors. A first approach is to reinforce the therapeutic cell itself, for example by improving tumor homing, limiting exhaustion or protecting the cell from suppressive signals within the tumor microenvironment.

In pancreatic tumor models, enforced expression of CXCR6 enhanced the migration and antitumor activity of T cells toward CXCL16-rich tumors, while combined engineering of tumor recruitment and resistance to TGFβ-mediated suppression improved CAR T cell efficacy in solid tumors[98,99]. Other strategies have aimed to convert inhibitory signals into activating cues, as shown with PD-1-CD28 fusion receptors, or to increase resistance to exhaustion through transcriptional engineering[100,101].

A second approach is to expand adoptive immunotherapy beyond conventional αβ T cells. CAR-NK cells are being developed as alternative cytotoxic effectors, with potential advantages linked to their innate killing capacity and safety profile[102]. Macrophage-based cellular therapies have also emerged for solid tumors, using CAR-macrophages to promote tumor cell phagocytosis and modify the local immune microenvironment[103]. In parallel, stromal-targeting approaches have explored CAR T cells directed against fibroblast activation protein (FAP), with the aim of targeting tumor-supportive fibroblasts and weakening stromal barriers[104].

Another strategy is to generate CAR T cells directly *in vivo*. Targeted lentiviral vectors can deliver a CAR-encoding sequence to selected T cell subsets inside the organism, reducing the dependence on *ex vivo* manufacturing[105]. Proof-of-concept studies using CD8- or CD3-targeted lentiviral vectors have shown that functional CAR T cells can be generated *in vivo*, with antitumor or B-cell-depleting activity[106,107].

This therapeutic landscape is particularly relevant to PDAC because it reframes CAR T cell therapy as more than a targeting problem. In pancreatic cancer, antigen recognition is only one part of the problem. CAR T cells must also reach tumor cells, survive within a dense and suppressive niche, and remain functional after antigen encounter. This provides the rationale for combining CAR T cells with strategies that modify the local tumor ecosystem.

2. Why CAR T cells could work in PDAC

CAR T cells represent an attractive strategy for PDAC because they provide a way to impose a defined and concentrated antitumor immune pressure in a disease otherwise characterized by weak spontaneous T cell reactivity and frequent immune escape. By redirecting large numbers of cytotoxic lymphocytes toward predefined surface antigens independently of HLA-mediated antigen presentation, CAR T cells may bypass some of the mechanisms that limit endogenous immunity and conventional immunotherapies in PDAC[108–110].

Once engaged, CAR T cells proliferate, secrete effector cytokines and kill target cells through canonical cytotoxic mechanisms, but with a much higher frequency of tumor-specific effectors than is typically achieved by natural antitumor responses[88].

A first argument supporting CAR T cell development in PDAC is the presence of clinically relevant tumor-associated surface antigens. PDAC expresses several candidate targets, including mesothelin, CEACAM6, HER2 and claudin 18.2[111–114]. Although none of these antigens is perfectly tumor-specific, their overexpression in subsets of pancreatic tumors provides a rational basis for

redirected cellular therapy. Antigen selection must therefore define a therapeutic window. The ideal target should be abundant and accessible on tumor cells, present in most tumor lesions, and absent or weakly expressed in essential healthy tissues.

However, antigen selection remains a major bottleneck for CAR T cell therapy in PDAC. Most candidate targets are tumor-associated rather than tumor-specific, and their expression may be heterogeneous across patients, lesions and tumor-cell states. In addition, surface accessibility, antigen density and expression in essential healthy tissues are critical determinants of both efficacy and safety. This has motivated the use of single-cell and spatial profiling approaches to identify more selective and membrane-accessible targets for future CAR T cell development[108,115].

Among the antigens explored in PDAC, mesothelin is one of the most clinically advanced targets. Mesothelin is strongly expressed in a large proportion of pancreatic ductal adenocarcinomas, while its expression in normal tissues is mainly restricted to mesothelial cells lining the pleura, peritoneum and pericardium[116]. This expression profile has supported the development of mesothelin-targeted therapies, including recombinant immunotoxins, mesothelin-directed vaccines and CAR T cells[111,117,118]. Clinical responses with mesothelin-directed CAR T cells have remained limited, but early trials showed feasibility, acceptable short-term safety and evidence of CAR T cell trafficking to pancreatic tumor lesions[111,119]. Mesothelin therefore provides an important proof of concept for PDAC. It shows that pancreatic tumor cells can be reached and recognized by engineered T cells when a suitable surface antigen is present.

Claudin 18.2 has also emerged as an important gastrointestinal tumor-associated antigen, including in pancreatic cancer[113]. The preliminary activity of claudin 18.2-directed CAR T cells in gastrointestinal malignancies suggests that solid tumor CAR T therapy can generate clinical benefit when antigen expression is sufficiently enriched and the target is accessible at the tumor-cell surface. In PDAC, these observations support the idea that CAR T efficacy may depend on matching antigen selection, CAR design and disease context to act against pancreatic tumor cells.

Another reason CAR T cells remain conceptually relevant for PDAC is their potential to address minimal residual disease and micrometastatic dissemination. PDAC frequently recurs after macroscopically complete surgery, reflecting early systemic spread and persistence of occult tumor cells. Unlike local therapies, CAR T cells are living drugs capable of circulating, expanding after antigen encounter and, in some settings, persisting as memory-like populations. This property could be particularly valuable in a disease where relapse is often driven by disseminated residual disease.

A second argument is the modularity of CAR T cell engineering. In PDAC, this modularity is not limited to improving signal strength after antigen engagement. It also enables the design of lymphocytes with additional properties tailored to the pancreatic tumor context. CAR constructs can be engineered to resist inhibitory cytokines such as TGFβ, secrete cytokines or chemokines, incorporate switch systems to control activity, or include functional modules that improve persistence and adaptation to the tumor environment[93,109].

Experimental work in solid tumor models has shown that mitochondrial metabolism supports T cell migration within three-dimensional tumor-like environments and that enhancing mitochondrial activity can improve CAR T cell recruitment into tumor islets. In parallel, genetic reprogramming of human CAR T cells through engineered PGC-1α expression has been shown to promote mitochondrial biogenesis and improve antitumor efficacy *in vivo*, which is directly relevant to desmoplastic tumors like PDAC[120,121]. These findings are important because they link CAR T cell efficacy to the capacity of transferred cells to move, persist and remain metabolically competent within complex tumor architectures.

Together, these studies show that CAR T cell engineering can improve trafficking, resistance to suppression and effector persistence in solid tumors[99,100,122,123]. However, in PDAC, the tumor niche remains a major barrier. Dense stroma, poor immune-cell access and myeloid-driven suppression can still limit CAR T cell activity[119]. This supports strategies that act directly on the local tumor environment, in addition to engineering the therapeutic cell.

These cell-intrinsic modifications can be paired with interventions on the tumor niche. Examples include ECM-modifying agents such as hyaluronidase, stromal or myeloid-targeting approaches, checkpoint blockade, oncolytic viruses, radiotherapy and selected chemotherapy regimens[124–127]. These combinations aim to improve tumor access, reduce local suppression or increase inflammatory priming before or during CAR T cell therapy. They are particularly relevant in PDAC, where poor T cell entry, dense matrix organization and suppressive myeloid populations limit effector function.

CAR T cells can also amplify local immunity after antigen recognition. Activated CAR T cells release inflammatory mediators, including IFN-γ, that can activate myeloid cells, increase antigen presentation and support endogenous antitumor responses[128]. This effect could help convert a poorly inflamed tumor into a more immune-reactive lesion. However, it requires sufficient CAR T cell infiltration, antigen engagement and persistence within the tumor.

CAR T cells may be relevant in PDAC because their activity is not limited to direct tumor-cell killing. After antigen recognition, activated CAR T cells can also release inflammatory mediators that reshape local immune interactions and support endogenous antitumor responses **(Figure 6)**.

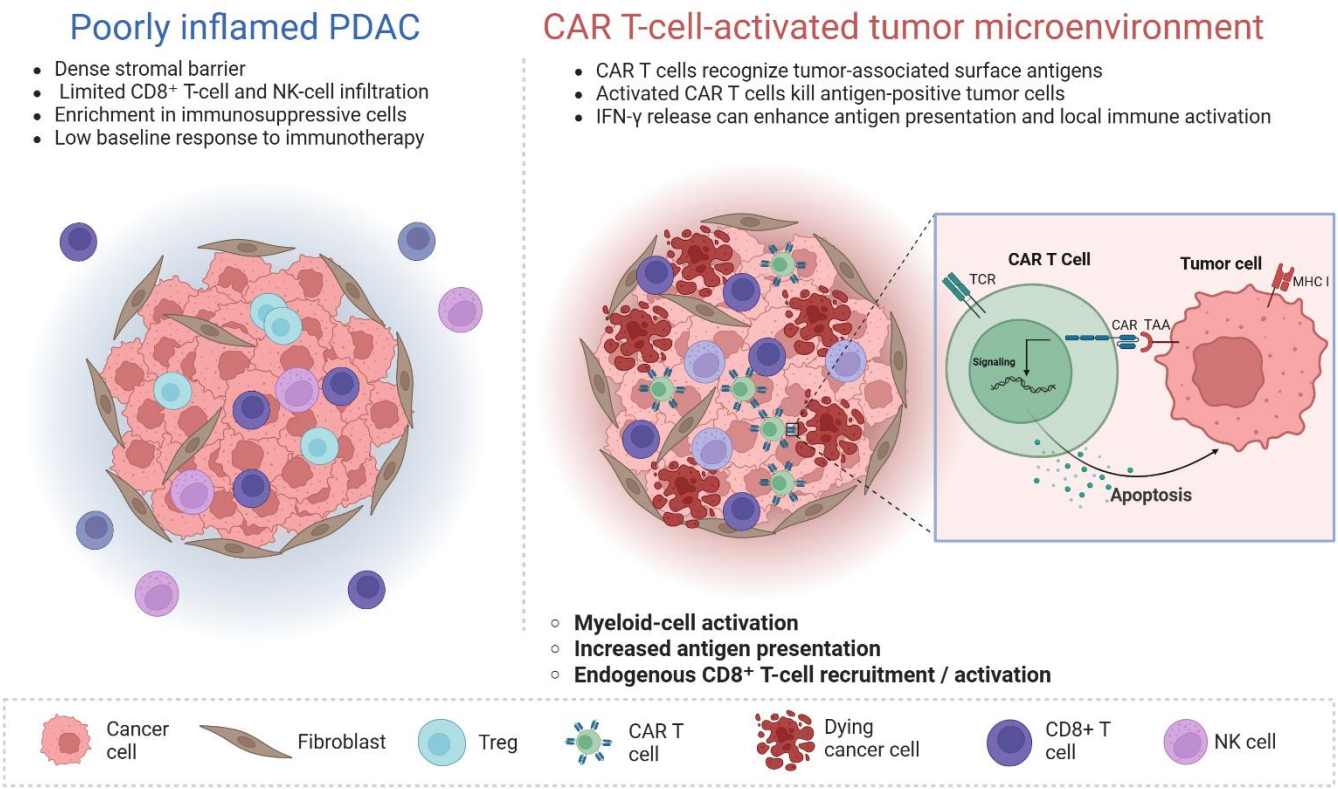


Figure 6: CAR T cell-mediated immune activation in poorly inflamed PDAC.

PDAC is commonly characterized by dense stroma, limited infiltration of cytotoxic lymphocytes and enrichment in immunosuppressive cell populations. After reaching the tumor bed, CAR T cells can recognize tumor-associated surface antigens independently of MHC presentation. This interaction triggers direct killing of antigen-positive tumor cells through cytotoxic mechanisms and promotes the release of inflammatory mediators such as IFN-γ. Local IFN-γ production can activate myeloid cells, increase antigen presentation and support endogenous antitumor immune responses. These effects may help shift a poorly inflamed tumor microenvironment toward a more immune-reactive state. This process requires sufficient CAR T cell infiltration, sustained antigen engagement and intratumoral persistence.

For these reasons, CAR T cells provide both a therapeutic backbone and a functional readout for niche-engineering strategies. Their activity can be followed at several levels: tumor entry, positioning near antigen-positive cells, activation, serial killing and persistence. If local delivery of chemokines or stromal-remodeling factors improves these parameters, the effect can be measured directly *in vitro*, in three-dimensional tumor models and *in vivo*. In this thesis, CAR T cells therefore provide the baseline for antitumor response, while targeted lentiviral niche engineering is used to remodel the local tumor ecosystem and make that response possible.

3. Why CAR T cells currently fail in solid tumors and PDAC

Preclinical and early clinical studies in pancreatic cancer have identified the tumor microenvironment as a major barrier to effective CAR T cell therapy[119]. In a phase I trial of mesothelin-specific CAR T

cells in metastatic PDAC, treatment was feasible and showed evidence of CAR T cell trafficking to tumor lesions, but clinical activity remained limited. Preclinical work has also shown that mesothelin-directed CAR T cells can fail as monotherapy in pancreatic tumor models and that their efficacy can be improved by local modification of the tumor microenvironment, for example using cytokine-armed oncolytic adenoviruses[129,130]. These observations indicate that antigen recognition is necessary, but not sufficient, for tumor control.

After systemic administration, CAR T cells must complete several steps before they can mediate productive antitumor activity. They must extravasate from the blood, penetrate the tumor tissue, remain metabolically active, encounter antigen-positive cells, become activated and sustain effector function in the presence of suppressive signals. Failure at any of these steps can limit tumor control. These obstacles can be grouped into three major and interdependent categories: physical and metabolic barriers, antigen heterogeneity or antigen loss, and an immunosuppressive tumor microenvironment[130,131]. This is consistent with previous work highlighting that successful CAR T cell activity in solid tumors requires efficient trafficking, stromal penetration, metabolic fitness and resistance to suppressive signals such as TGFβ[132] **(Figure 7)**.

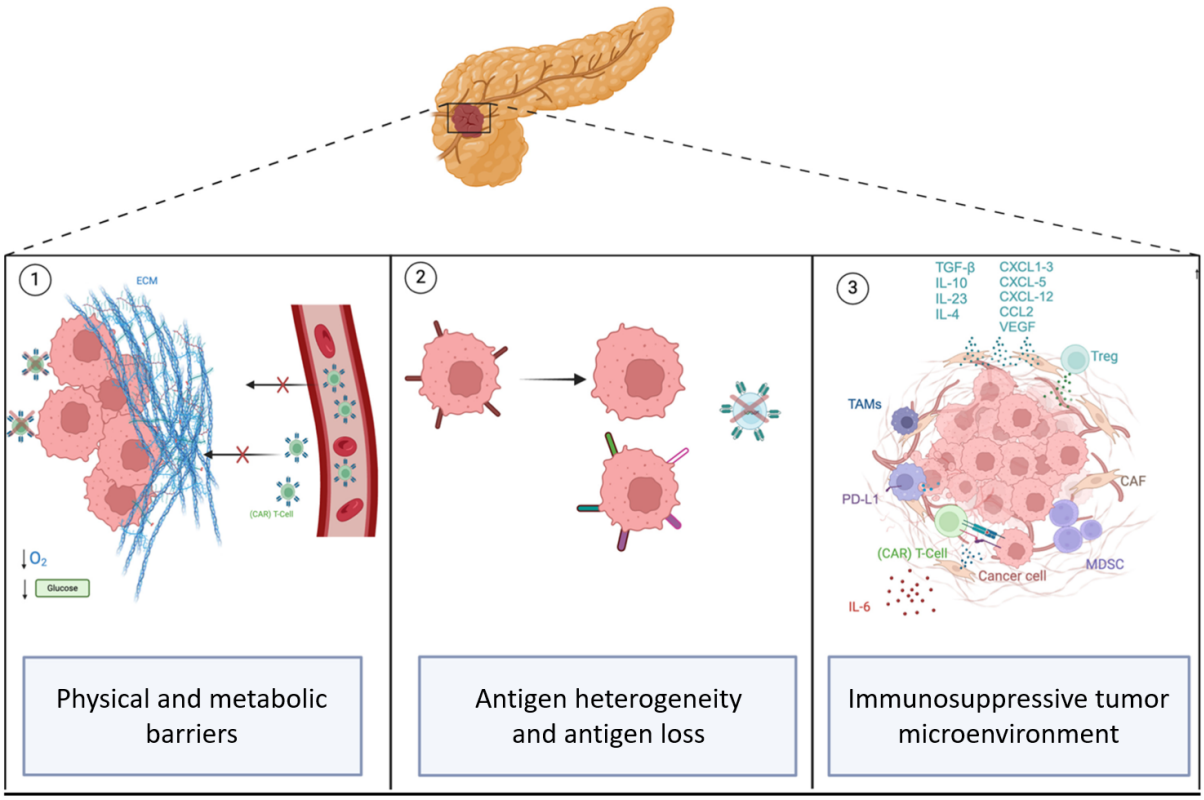


Figure 7: Main barriers limiting CAR T cell efficacy in pancreatic ductal adenocarcinoma.

CAR T cell activity in pancreatic ductal adenocarcinoma is restricted by multiple, interconnected tumor-intrinsic and microenvironmental barriers. Dense extracellular matrix deposition, abnormal vasculature, hypoxia and nutrient deprivation limit CAR T cell trafficking, survival and intratumoral persistence. In parallel, heterogeneous or unstable antigen expression can result in incomplete tumor recognition and antigen-negative immune escape. Finally, immunosuppressive stromal and immune populations, including cancer-associated fibroblasts, tumor-associated macrophages, myeloid-derived suppressor cells and regulatory T cells, together

with soluble mediators such as TGFβ, IL-10 and IL-6, impair CAR T cell activation, cytotoxicity and long-term function. These barriers support the rationale for combining CAR T cell therapy with strategies that remodel the pancreatic tumor microenvironment. Adapted from Guirguis et al., 2025[133]

The physical architecture of PDAC represents an early obstacle. The dense extracellular matrix, fibroblast-rich stroma and abnormal vasculature can restrict immune-cell entry and distribution, creating regions where antigen-positive tumor cells remain poorly accessible after systemic CAR T cell administration. Hyaluronan accumulation and stromal pressure can impair vascular function and drug delivery, while activated pancreatic stellate cells and fibroblasts can limit $CD8^+$ T cell access to tumor-cell regions[46,53,134,135]. This spatial exclusion is particularly problematic because CAR T cell cytotoxicity requires direct contact with target cells. As a result, even a potent CAR T product may show limited efficacy if it cannot efficiently enter tumor nests or maintain contact with malignant epithelial cells.

Metabolic stress adds a second layer of restriction. Hypoxia, nutrient deprivation, acidic pH and competition with tumor and stromal cells can impair T cell survival, migration and effector function[136]. These constraints are especially relevant in PDAC, where poor vascularization and high stromal density contribute to a hostile metabolic landscape. In this context, CAR T cell dysfunction may occur even when antigen recognition is intact, because the local environment limits the energetic and biosynthetic programs required for sustained cytotoxic activity.

Antigen heterogeneity further limits the durability of CAR T cell responses. Most PDAC targets are tumor-associated rather than tumor-specific, and their expression can vary between patients, between metastatic sites and within individual lesions[137]. This heterogeneity increases the risk of incomplete tumor elimination and selection of antigen-low or antigen-negative variants. At the same time, expression of candidate targets in some normal tissues constrains the intensity of CAR T cell targeting because of potential on-target, off-tumor toxicity[95]. Thus, antigen selection in PDAC involves a difficult balance between efficacy, coverage and safety.

The immunosuppressive tumor microenvironment constitutes a third major barrier. Cancer-associated fibroblasts, tumor-associated macrophages, myeloid-derived suppressor cells and regulatory T cells can inhibit CAR T cell activation and persistence through cell-cell interactions, nutrient competition, chemokine-mediated exclusion and soluble mediators such as GM-CSF, TGFβ and IL-6. In pancreatic cancer models, oncogenic KRAS-driven GM-CSF production promotes MDSC recruitment and limits $CD8^+$ T cell-dependent antitumor immunity[62]. $CSF1R^+$ macrophages and CCR2-dependent inflammatory monocytes also support pancreatic tumor growth through suppression of T cell responses[138,139]. In parallel, activated pancreatic stellate cells can sequester $CD8^+$ T cells away from juxtatumoral regions, while FAP^+ fibroblast-derived CXCL12 contributes to T cell exclusion and resistance to PD-L1 blockade[53,135]. TGFβ and IL-6 signaling have also been implicated in the maintenance of suppressive immune programs in pancreatic cancer, and their blockade can improve antitumor immune activity in preclinical models[140,141]. Importantly, these

suppressive pathways do not act independently from the stromal barrier. Fibroblasts and myeloid cells can simultaneously shape matrix organization, regulate chemokine gradients and produce inhibitory signals, thereby coupling physical exclusion with functional suppression[53,135,139].

These barriers have motivated efforts to pharmacologically modulate key stromal and immunosuppressive pathways, including TGFβ signaling, focal adhesion signaling, hyaluronan accumulation and angiotensin-dependent fibroblast activation, with the aim of rendering the PDAC microenvironment more permissive to immune attack. Galunisertib, a TGFβ receptor I inhibitor, provided a clinical signal when combined with gemcitabine in unresectable pancreatic cancer[142]. FAK inhibition reduced fibrosis and immunosuppression in PDAC models and rendered tumors responsive to checkpoint blockade[143]. Hyaluronan-targeting approaches improved vascular function and drug delivery in preclinical models, although PEGPH20 failed to improve survival in a phase III trial in metastatic PDAC[46,85,134]. Losartan reduced stromal collagen and improved therapeutic penetration in desmoplastic tumor models, and losartan-based neoadjuvant therapy showed encouraging downstaging and R0 resection rates in locally advanced PDAC[144,145]. However, these approaches have not yet translated into broadly effective immunotherapeutic combinations, suggesting that successful CAR T cell therapy in PDAC will require more spatially controlled and mechanistically integrated strategies.

Clinically, CAR T cell therapy in PDAC has mainly shown feasibility, manageable safety and early signs of activity, but durable responses remain uncommon[119,146,147]. Published studies have evaluated several targets, including mesothelin, HER2, EGFR, Claudin18.2 and PSCA, usually in small phase I cohorts or mixed solid-tumor populations. The main results are summarized in **Table 1.**

Study	CAR strategy / antigen target	Recruitment / patients	Main response data	Interpretation
Beatty et al., 2014[111]	Transient **mRNA CAR T cells targeting mesothelin**	Case reports from ongoing solid-tumor trials; included **1 patient with pancreatic ductal adenocarcinoma** and 1 patient with mesothelioma	In the PDAC patient, CARTmeso cells were detected in blood, ascites and tumor biopsy tissue. Disease was stable after 3 weeks of treatment.	Early proof of feasibility, tumor trafficking and short-term safety, but limited efficacy.

Beatty et al., 2018[119]	Transient **mRNA CAR T cells targeting mesothelin**	Phase I trial in **6 patients with chemotherapy-refractory metastatic PDAC**	No dose-limiting toxicity, severe CRS or neurotoxicity. Stable disease in **2/6 patients**, with PFS of **3.8 and 5.4 months**. FDG-PET showed lesion-level changes consistent with trafficking/activity.	Strongest early clinical proof for mesothelin CAR T cells in PDAC, but no objective durable responses.
Feng et al., 2018[112]	**HER2-directed CAR T cells**	Phase I trial in **11 patients with HER2-positive advanced biliary tract cancers or pancreatic cancers**; inclusion required HER2 expression in >50% of tumor cells	**1 partial response** lasting 4.5 months and **5 stable diseases** among evaluable patients. Median PFS was **4.8 months**. Toxicities were mostly manageable.	Shows feasibility of HER2 CAR T cells in a mixed BTC/PC cohort, but responses were limited and not PDAC-specific.
Liu et al., 2020[146]	**EGFR-directed CAR T cells**	Phase I trial in **16 patients with metastatic pancreatic cancer**; EGFR expression on tumor cells required to be >50%	Among **14 evaluable patients**, **4 partial responses** lasting 2–4 months and **8 stable diseases** were reported. Median PFS was **3 months**, and median OS was **4.9 months**.	One of the larger PDAC-specific CAR T studies, with measurable activity but short response duration.
Qi et al., 2024[147]	**CT041 / satri-cel, Claudin18.2-directed CAR T cells**	Pooled analysis of two early-phase trials in **24 patients with previously treated metastatic pancreatic cancer**	ORR **16.7%** with **4 partial responses**; DCR **70.8%**; median PFS **3.3 months** and median OS **10.0 months**. No predefined dose-limiting toxicities were reported in the pooled analysis.	Most convincing clinical signal so far in a PDAC-specific cohort, but still exploratory and not yet definitive.

Stein et al., 2024[148]	**BPX-601, PSCA-directed GoCAR T cells** with inducible MyD88/CD40 activation by rimiducid	Phase I dose-escalation trial in **33 patients**, including **24 metastatic PDAC** and 9 metastatic castration-resistant prostate cancer	The trial showed expansion/persistence and tumor infiltration signals, but objective responses were reported in prostate cancer patients, not clearly in the PDAC cohort.	Important cautionary study: enhanced CAR T cell activation can increase potency but also raises safety concerns.

Table 1: Clinical studies of CAR T cell therapy including patients with pancreatic cancer.
Published early-phase studies have tested CAR T cells targeting mesothelin, HER2, EGFR, Claudin18.2 and PSCA in pancreatic cancer or mixed gastrointestinal cancer cohorts. These trials mainly demonstrate feasibility, manageable safety and occasional signs of activity, including tumor trafficking, stable disease or partial responses in selected patients. However, responses remain limited and heterogeneous, indicating that antigen-directed CAR T cell activity alone is usually insufficient to achieve durable disease control in PDAC. Abbreviations: CAR, chimeric antigen receptor; DCR, disease control rate; ORR, objective response rate; PDAC, pancreatic ductal adenocarcinoma; PFS, progression-free survival; PSCA, prostate stem cell antigen.

Overall, these studies show that CAR T cells can be manufactured, administered and directed toward pancreatic tumor antigens. Several trials also reported tumor trafficking or transient disease control. However, responses were generally short-lived, heterogeneous and observed in small cohorts. These clinical data support the view that antigen engagement alone is not sufficient in PDAC, and that CAR T cell therapy will likely require combination strategies that improve tumor access, local persistence and resistance to immunosuppression.

III. Thesis project: targeted lentiviral TME niche engineering for CAR T cell therapy

Because CAR T cell failure in PDAC is largely imposed by the desmoplastic and immunosuppressive tumor microenvironment, a strategy could be to engineer the tumor niche. In this thesis, we propose a tumor-targeted niche-engineering approach in which selected pancreatic tumor or stromal cells are instructed to locally secrete chemokines and stromal-remodeling factors. The objective is to convert poorly infiltrated, mechanically constrained and immunosuppressive lesions into microenvironments that are more permissive to CAR T cell trafficking, persistence and effector function.
This strategy is conceptually distinct from the dominant approach of improving CAR T cell intrinsic potency.

1. Chemokine-based recruitment of effector lymphocytes

A key requirement for effective CAR T cell therapy is the presence of chemokine gradients capable of guiding effector cells from the circulation into the tumor bed. This step is particularly relevant in solid tumors, where transferred T cells must first extravasate, then follow local chemotactic cues, and finally reach malignant cells within a complex stromal architecture[149]. In PDAC, this process is inefficient. The tumor microenvironment is characterized by poor productive T cell infiltration, abnormal vasculature, dense extracellular matrix and suppressive stromal signaling. In this context, the problem is not only the amount of chemokine present in the tumor, but also its spatial organization, bioavailability and ability to generate a functional gradient that supports effector-cell entry[150].

CXCL9, CXCL10 and CXCL11 are interferon-inducible chemokines that bind CXCR3, a receptor expressed by activated T lymphocytes, including activated $CD8^+$ T cells and effector CAR T cells[63,150]. The CXCL9/10/11-CXCR3 axis has been linked to the recruitment of cytotoxic T cells and NK cells in several solid tumor settings, and CXCL9 and CXCL10 expression is often associated with T cell-inflamed tumors[151]. In PDAC, the role of this axis appears more context-dependent. CXCR3 ligand expression can be detected in pancreatic tumors, but this does not necessarily translate into efficient tumor-cell contact or productive antitumor immunity[152]. This supports the idea that a local and spatially controlled source of CXCR3 ligands may be required to convert an immune-excluded lesion into a more permissive site for effector-cell recruitment.

Local expression of CXCR3 ligands could therefore attract infused CAR T cells toward pancreatic tumor lesions and partially overcome the low baseline infiltration of endogenous T cells that characterizes this disease[152]. This strategy differs from approaches based on systemic delivery of soluble cytokines or chemokines, which are limited by unfavorable pharmacokinetics, short serum half-life, broad systemic distribution and dose-limiting toxicity[153–155].

Here, the tumor niche itself is engineered to produce a local chemotactic signal. This is well suited to targeted lentiviral delivery, because transduction of a fraction of antigen-expressing tumor cells may be sufficient to generate diffusible chemokine gradients within the lesion.

Beyond adoptively transferred cells, local CXCL9 or CXCL10 expression may also promote recruitment of endogenous $CXCR3^+$ effector lymphocytes. This could increase the likelihood of local immune amplification and contribute to the restoration of antitumor immune surveillance. Such amplification is important in heterogeneous tumors, where CAR T cells may not recognize every malignant cell[156]. Recruitment of endogenous $CD8^+$ T cells and NK cells could broaden the immune response beyond the initially targeted antigen and support bystander tumor control.

This principle is supported by chemokine-receptor engineering studies showing that CAR T cell trafficking can be enhanced by matching effector-cell chemokine receptor expression to tumor-derived chemokine gradients. For example, Cadilha et al. demonstrated that engineering CAR T

cells to exploit a CCL1-CCR8 recruitment axis improved tumor infiltration and synergized with TGFβ resistance to restore CAR T cell efficacy in solid tumor models[99]. These findings show that improved recruitment and protection from local suppression can act together. They also support the strategy of combining chemokine-based recruitment with stromal remodeling in PDAC.

Efficient trafficking alone is unlikely to be sufficient if infiltrating lymphocytes remain trapped in the stromal compartment, excluded from tumor nests, or rapidly suppressed by local inhibitory signals. Dense collagen-rich extracellular matrix, CAF-derived barriers and TGFβ signaling can limit T cell motility and function after recruitment. For this reason, active recruitment and stromal permissiveness should be considered as complementary requirements. In this thesis, CXCL10 expression is therefore used to promote effector-cell entry, while decorin is explored as a stromal-remodeling and TGFβ-modulating payload designed to make the recruited immune cells more effective within the PDAC microenvironment.

2. Decorin-mediated stromal remodeling and tumor sensitization

Parallel to improving T cell homing, there is a strong rationale for targeting the structural and immunosuppressive properties of the PDAC stroma. Decorin is a small leucine-rich proteoglycan naturally present in the extracellular matrix, where it interacts with collagen and contributes to the regulation of matrix organization[157]. In pancreatic cancer, decorin has been detected within the stromal compartment and has been proposed to influence tumor growth and response to chemotherapy, supporting its relevance in the specific context of PDAC[158]. By regulating collagen fibrillogenesis and extracellular matrix architecture, decorin may help reduce stromal rigidity, improve interstitial transport and facilitate immune-cell access to tumor regions that are otherwise physically constrained[159]. These structural effects are summarized in **Figure 8**, which highlights decorin interaction with the collagen network.

Interestingly, decorin may also act as a multifunctional regulator. In particular, decorin can bind and modulate TGFβ activity, a pathway that is central to fibroblast activation, extracellular matrix deposition and T cell suppression in PDAC[157]. This dual ability to regulate collagen organization and restrain TGFβ-dependent signaling makes decorin especially relevant in a desmoplastic and immune-restrictive tumor microenvironment. As shown in **Figure 8**, TGFβ sequestration by decorin may reduce TGFβ receptor signaling in both T cells and cancer-associated fibroblasts, with potential consequences on T cell function, CAF activation and stromal stiffness.

Decorin may also affect the tumor-cell compartment directly. Beyond its stromal effects, decorin has been shown to antagonize receptor tyrosine kinase signaling, including MET, EGFR and IGF-IR-related pathways, and to downregulate downstream oncogenic mediators such as β-catenin and MYC[160,161]. These properties suggest that decorin could simultaneously remodel the stromal barrier and weaken tumor-cell survival or proliferation programs. In the context of CAR T cell therapy, this

is conceptually important because efficient tumor killing depends on lymphocyte access and on the ability of target cells to remain vulnerable once immune contact has been established. **Figure 8** also includes the reported modulation of RTK-associated pathways by decorin, with expected effects on tumor-cell proliferation, survival and invasion, and on endothelial-cell angiogenic activity.

Although direct evidence linking decorin to improved CAR T cell function in PDAC remains limited, available preclinical data support this broader concept. Local decorin delivery has been shown to enhance T cell infiltration and improve CAR T cell activity in renal cell carcinoma models, while recent evidence indicates that decorin can facilitate T cell-mediated antitumor immunity and improve the efficacy of immune checkpoint blockade[162,163]. These findings suggest that decorin may do more than facilitate passive immune-cell migration through a loosened matrix; it may help restore an immune-compatible stromal state in which recruited effector cells can remain functional.

In addition, decorin has been reported to modulate macrophage responses through TLR2/4-dependent activation of NF-κB and MAPK signaling, leading to increased inflammatory cytokine production such as TNFα[164,165]. This activity may contribute to macrophage repolarization toward a less immunosuppressive state, although its relevance in PDAC and CAR T cell therapy remains to be directly demonstrated.

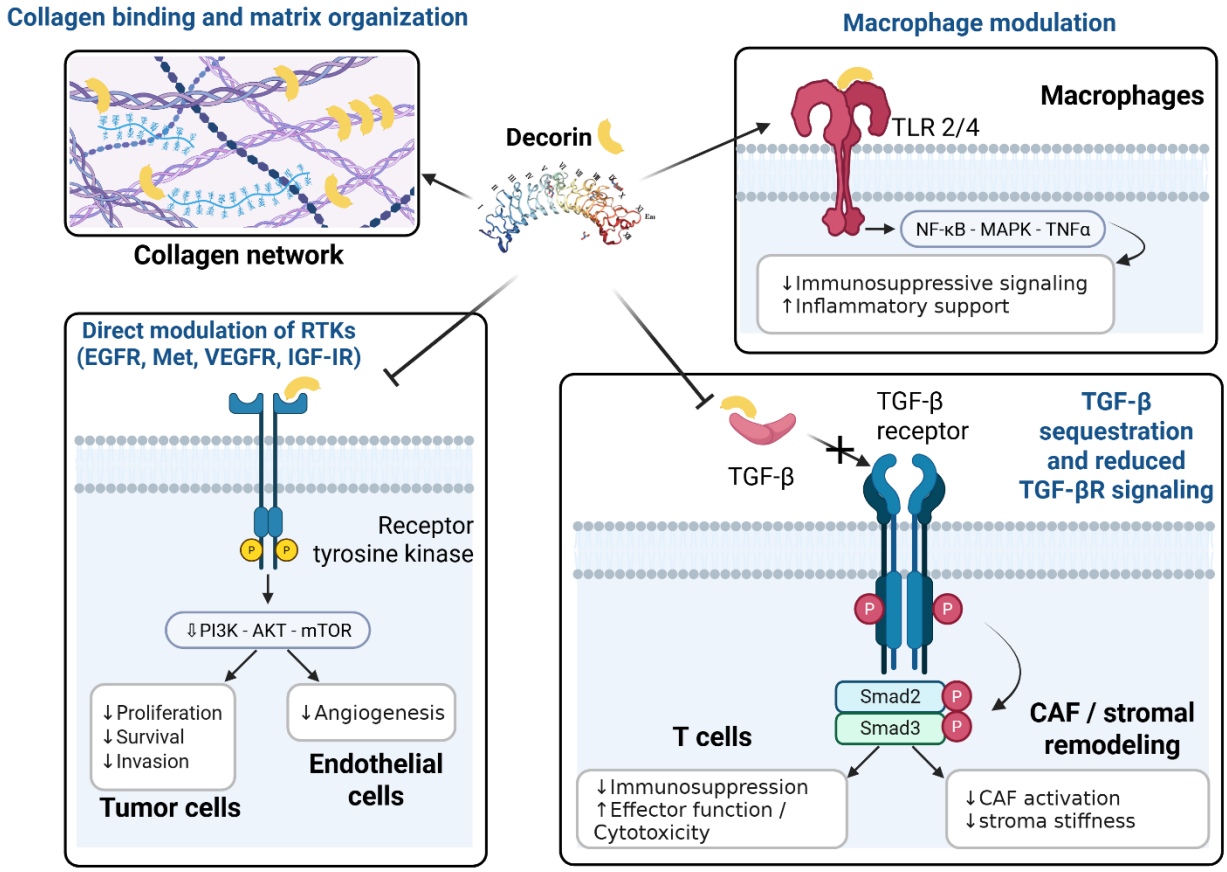


Figure 8: Major effects of decorin in the PDAC tumor microenvironment.

Decorin is a small leucine-rich proteoglycan that exerts multiple effects on the PDAC tumor microenvironment. It interacts with collagen and contributes to extracellular matrix organization. Decorin can also directly modulate receptor tyrosine kinase signaling, including EGFR, MET, VEGFR and IGF-IR-associated pathways, leading

to reduced tumor-cell proliferation, survival and invasion, as well as reduced angiogenesis. In parallel, decorin can bind and sequester TGFβ, thereby reducing TGFβ receptor signaling in T cells and cancer-associated fibroblasts. These effects may relieve T cell suppression and reduce CAF activation and stromal stiffness. Decorin has also been reported to modulate macrophage activity, contributing to a less immunosuppressive and more inflammatory microenvironment. Together, these properties support a more permissive stromal state and may improve immune-cell access and function in PDAC.

3. Rationale for combining chemokine recruitment and stromal remodeling

This thesis was designed to produce a gene therapy delivered in tumor cells to introduce stromal-modulating and tumor-sensitizing component intended to cooperate with chemokine-driven lymphocyte recruitment. CXCR3-ligand expression is expected to enhance CAR T cell recruitment and intratumoral positioning, whereas decorin may reduce matrix-associated constraints, attenuate TGFβ-driven stromal and immune suppression, and increase tumor-cell vulnerability to immune attack. In combination, these interventions could transform transient immune-cell entry into sustained intratumoral accumulation, productive tumor-cell engagement and durable antitumor activity. These beneficial effects are summarized in **Figure 9.**

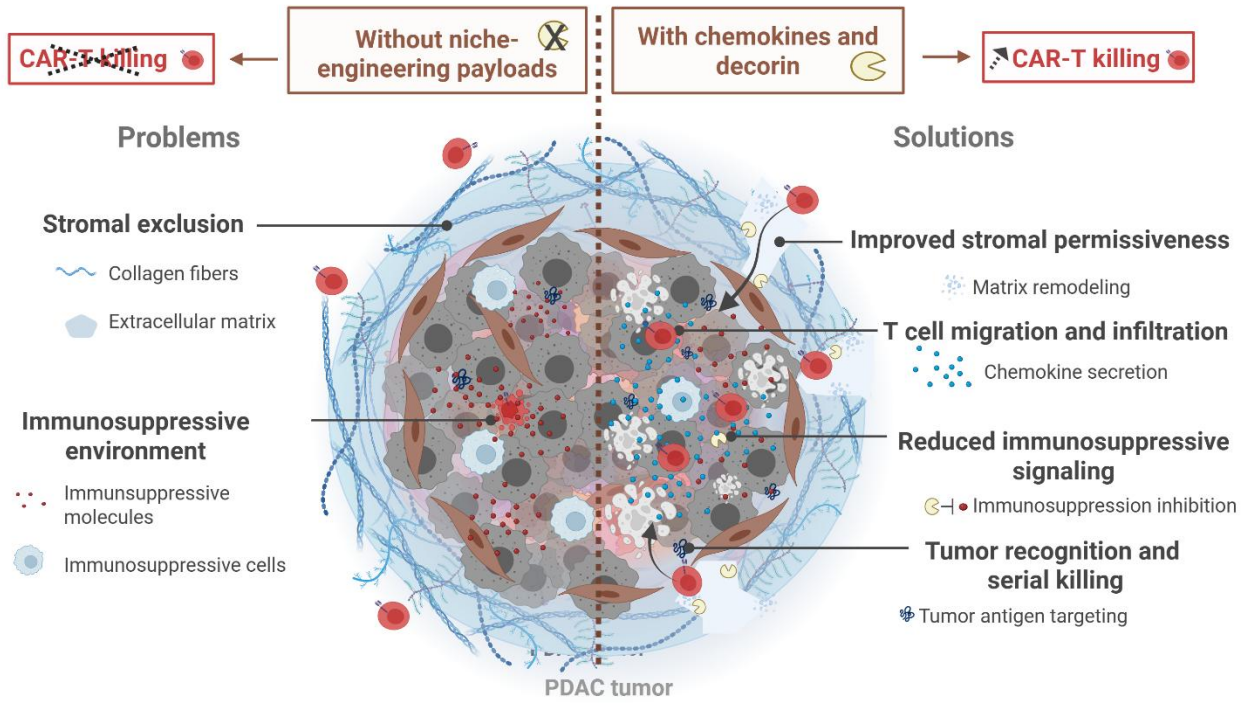


Figure 9: Chemokine- and decorin-based niche engineering to improve CAR T cell activity in PDAC. *This strategy aims to overcome stromal exclusion and immunosuppression in PDAC through local delivery of chemokines and decorin. Chemokines promote T cell migration and infiltration, while decorin supports stromal remodeling and reduces immunosuppressive signaling. Together, these effects are intended to improve tumor recognition and CAR T cell-mediated killing.*

Gene therapy approaches offer a unique opportunity to achieve localized and sustained modulation of the tumor microenvironment. Unlike systemic administration of recombinant proteins, vector-mediated gene delivery can ensure continuous production of therapeutic factors directly within the tumor, thereby enhancing efficacy while limiting systemic toxicity.

This localized expression is particularly important in the context of stromal and immune modulators, whose systemic administration could otherwise lead to off-target biological effects.

Importantly, spatial control of gene expression is critical in this context. Pathways such as TGFβ regulate immune tolerance, tissue repair, fibrosis and extracellular matrix organization in normal tissues[166–168]. Non-localized modulation could therefore induce unwanted inflammation, impair wound healing, alter tissue remodeling or affect cardiovascular and cutaneous homeostasis. This reinforces the need for targeted delivery systems capable of restricting transgene expression to the tumor site or its immediate microenvironment. This requirement directly motivates the use of targeted delivery systems, which provide the possibility of combining spatially restricted transgene expression with durable microenvironmental reprogramming.

4. Lentiviral vectors as precision delivery tools

The niche-engineering strategy described above depends on the ability to deliver modulatory genes, such as chemokines and decorin, in a spatially controlled and tumor-restricted manner. This requirement is central to cancer gene therapy. Earlier anticancer gene therapy approaches mainly aimed to kill transduced tumor cells directly, restore tumor-suppressor pathways or sensitize cancer cells to a prodrug. Examples include suicide-gene systems such as herpes simplex virus thymidine kinase combined with ganciclovir[169], toxin-gene strategies using potent cytotoxic proteins such as diphtheria toxin A chain[170], adenoviral delivery of p53[171], and TNF-α gene delivery in pancreatic cancer using TNFerade[172]. These strategies established gene transfer as a therapeutic approach in cancer, but they also highlighted the importance of spatial control. When a transgene encodes a suicide enzyme, a toxin, a pro-apoptotic factor or a potent inflammatory cytokine, off-target expression can directly damage healthy tissues or trigger unwanted inflammation.

The approach developed in this thesis follows a different therapeutic logic. The selected transgenes are intended to remodel the tumor microenvironment rather than directly eliminate the transduced cells. Chemokines are used to promote effector-cell recruitment, while decorin is used to modulate stromal barriers and TGFβ-associated suppression. This modulatory design may reduce direct cytotoxic risk at the level of the transduced cell, but it does not remove the need for tumor-restricted delivery.

Local gene transfer offers the possibility of converting selected tumor or stromal cells into intratumoral sources of therapeutic signals. In this context, lentiviral vectors represent a relevant platform because they can mediate stable transgene expression, including in non-dividing cells, as initially demonstrated by Naldini and colleagues[173,174]. Compared with other viral vector systems,

lentiviral vectors combine several properties that are attractive for tumor microenvironment engineering: they can transduce dividing and non-dividing cells, accommodate relatively large transgenes, support durable expression and be pseudotyped to modify cell tropism. Because the envelope glycoprotein displayed at the vector surface largely determines receptor usage and cellular entry, pseudotyping has become a central strategy to alter lentiviral tropism and refine transduction specificity[175].

5. From broad tropism to targeted pseudotyping

The most widely used lentiviral pseudotype is based on the vesicular stomatitis virus glycoprotein (VSV-G), which confers high physical stability, broad tropism and efficient production[173,176]. These properties make VSV-G-pseudotyped lentiviral vectors a robust experimental benchmark and an efficient tool for many *ex vivo* applications. However, broad tropism becomes a limitation when the therapeutic goal is *in vivo* delivery of biologically active transgenes. In this setting, non-specific transduction may expose healthy tissues to unwanted expression and dilute the local effect within the tumor.

Targeted pseudotyping aims to overcome this limitation by engineering viral entry so that transduction depends on recognition of a selected cell-surface molecule[175]. Retargeted envelopes incorporate antibody-derived or ligand-derived binding domains that redirect the vector toward predefined cell populations. In cancer, these targets are usually tumor-associated rather than strictly tumor-specific, so low-level expression in healthy tissues can remain a safety concern. Target selection must therefore account for antigen density, accessibility and distribution in both tumor and normal tissues.

This is particularly important for niche engineering, because the therapeutic effect depends on where the transgene is expressed. A chemokine or matrix-remodeling factor produced inside the tumor may promote immune infiltration, whereas the same factor produced systemically or in healthy tissues could lead to off-target biological effects.

Beyond broad tropism modification, retargeted lentiviral pseudotypes have enabled more precise cell-specific gene delivery. Measles virus glycoprotein-based lentiviral vectors have been engineered to redirect entry toward selected surface receptors, providing an important proof of concept for antibody- or ligand-guided lentiviral targeting[177]. Similarly, Sindbis virus envelope-based pseudotypes have been modified to redirect lentiviral vectors toward defined cellular targets, further supporting the feasibility of envelope engineering as a strategy for selective gene transfer[178].

Recent advances in vector engineering, including the development of synthetic and retargeted envelopes, have further expanded the versatility of lentiviral systems. These innovations enable more precise control over cell tropism and open new possibilities for selectively targeting tumor cells, stromal populations or immune cells within complex tumor ecosystems. Such selectivity is

particularly relevant in the context of PDAC, where therapeutic benefit is expected to confine expression of stromal and immune modulators to the tumor site or its immediate microenvironment. This conceptual framework is developed in our recent review, **“Engineering Precision Oncology: Targeting tumors and immune cells with lentiviral vectors”,** which synthesizes current pseudotyping strategies and highlights how envelope engineering can redirect lentiviral tropism toward defined tumor, stromal or immune-cell populations[179]. In the present thesis, several pseudotyped lentiviral vectors were compared to select the best solution to obtain spatially restricted gene transfer designed to induce local secretion of chemokines and stromal-remodeling molecules.

Molecular Therapy
Oncology
Review

Engineering precision oncology: Targeting tumors and immune cells with lentiviral vectors

Julia Rossi,[1,8] Chiara Martinello,[2,8] Riccardo Sorrentino,[1,8] Véronique Guyonnet-Duperat,[3] Samuel Amintas,[1,4] Maria Jimena Abrey Recalde,[1] Els Verhoeyen,[2,5,7] and Sandrine Dabernat[1,6,7]

[1]University Bordeaux, INSERM, BRIC, 1312 Bordeaux, France; [2]CIRI – International Center for Infectiology Research, Inserm, U1111, Université Claude Bernard Lyon 1, CNRS, UMR5308, Ecole Normale Supérieure de Lyon, Université Lyon, 69007 Lyon, France; [3]Plateforme VECT'UB, INSERM US 005 – CNRS UMS 3427- TBM-Core, Université de Bordeaux, 33000 Bordeaux, France; [4]CHU Bordeaux, Tumor Biology and Tumor Bank Laboratory, 33600 Pessac, France; [5]Université Côte D'Azur, INSERM, C3M, 06204 Nice, France; [6]CHU Bordeaux, Department of Biochemistry, Pellegrin Hospital, 33000 Bordeaux, France

Lentiviral vectors (LVs) are emerging as versatile tools for the efficient and stable delivery of therapeutic genes. Although VSV-G-pseudotyped LVs remain the standard for *ex vivo* genetic engineering, their broad tropism and serum sensitivity limit their applicability for *in vivo* cancer therapy, where precise targeting is essential for efficacy and safety. This review synthesizes two decades of advances in LV pseudotyping, comparing natural viral envelopes, engineered targeting strategies, and multicomponent glycoprotein systems that reshape vector tropism. We discussed donor-derived envelopes such as measles virus, baboon endogenous retrovirus, Nipah virus, and Sindbis virus, highlighting their value for transducing hematopoietic, immune, and tumor cells. We also examined next-generation retargeting innovations, including engineered receptor-binding domains, display of cytokines or antibody fragments, and VSV-G mutants that ablate natural receptor interactions, to enhance specificity for T cells, B cells, hematopoietic stem cells, and tumor-associated antigens. Finally, we review the recent emergence of engineered virus-like particles (VLPs) as precision tools for *in vivo* delivery of CRISPR-Cas9, base-editing, and prime-editing complexes. Collectively, these advances position receptor-targeted lentiviral and VLP systems as promising platforms for the next generation of precision oncology, enabling selective *in vivo* CAR T/NK cell generation, targeted tumor modification, and cell-restricted gene editing.

INTRODUCTION

Although gene therapy was initially dedicated to inherited disorders, applications to cancer emerged more recently. The most recent illustration is the genetic engineering of T cells for cancer cell therapy, promising the restoration of immunity within the tumor, producing durable responses in a subset of patients.[1] Cancer gene therapy applications are growing to the point that more than 65% of the ongoing gene therapy clinical trials are for cancer treatment.[2] More than 30 gene therapies, including cancer treatments, have received official approval, 60% for *in vivo* administration.[3] Cancer gene therapy requires efficient and selective gene delivery within complex multicellular ecosystems composed of malignant cells embedded within diverse stromal and immune cell populations.

In vivo gene delivery systems include non-viral and viral vectors. Non-viral systems, including physical methods, lipid nanoparticles, and polymeric carriers, offer advantages, such as low immunogenicity, scalability, and versatility. However, their limited cell entry and selectivity likely contribute to why the large majority (83%) of the approved gene therapies are viral based.[3]

Viral vectors have developed natural mechanisms for efficient cellular entry, genome integration, and expression

Lentiviral vectors (LVs), derived from the human immunodeficiency virus (HIV-1), can stably integrate delivered genes into the host genome and provide safety and efficacy as proven in many clinical trials leading to the approved medicines, Zynteglo for β-thalassemia and Libmeldi for metachromatic leukodystrophy.[4] Finally, lentiviral vectors are of particular interest with high gene delivery efficiency *in vivo*.[5] Clinical-grade vectors are also used *ex vivo* for chimeric antigen receptor (CAR) T cell engineering.[6]

LVs are derived from HIV-1, which targets CD4 T cells via its envelope glycoprotein. The viral genome has been extensively modified to remove all pathogenic and replication-competent elements while retaining the ability to efficiently integrate therapeutic genes into the host genome.[7,8] Safety is enhanced through the use of self-inactivating (SIN) sequences, split packaging systems, and pseudotyping.

https://doi.org/10.1016/j.omton.2026.201197.

[7]Senior author

[8]These authors contributed equally

Correspondence: Els Verhoeyen, CIRI – International Center for Infectiology Research, Inserm, U1111, Université Claude Bernard Lyon 1, CNRS, UMR5308, Ecole Normale Supérieure de Lyon, Université Lyon, 69007 Lyon, France.
E-mail: els.verhoyen@ens-lyon.fr
Correspondence: Sandrine Dabernat, University Bordeaux, INSERM, BRIC, U 1312, Bordeaux, France.
E-mail: sandrine.dabernat@u-bordeaux.fr

Published by Elsevier Inc. on behalf of The American Society of Gene and Cell Therapy.
This is an open access article under the CC BY-NC-ND license (http://creativecommons.org/licenses/by-nc-nd/4.0/).

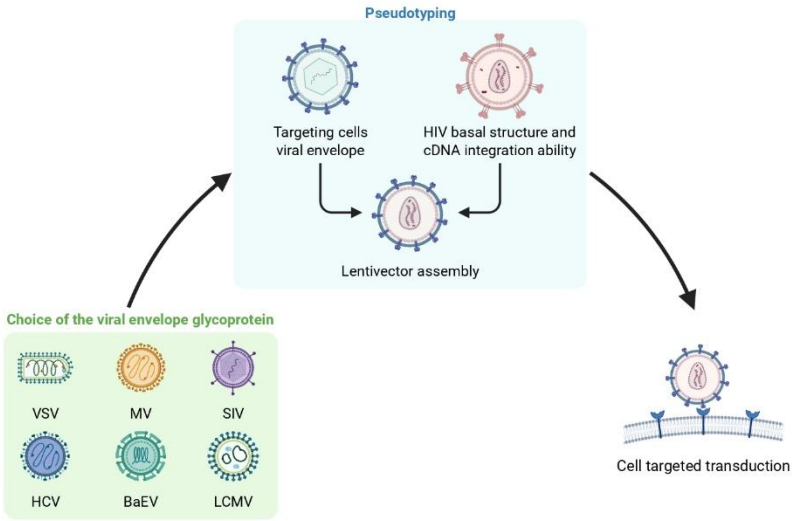


Figure 1. Schematic overview of lentivector pseudotyping maintaining viral donor tropism
Pseudotyping is performed on the HIV core structure, including packaging of viral RNA encoding for the transgene and capsid, carrying another viral envelope glycoproteins to redirect tropism. Created in BioRender. Amintas, S. (2025).

However, the use of integrating vectors with broad tropism can represent a serious safety concern, even in anticancer applications. For example, when used for CAR T cell engineering, the lentiviral transfer of the anti-CD19 CAR into a leukemic cell of a treated patient led to CAR-T cell therapy resistance and disease progression.[9]

Viral tropism is determined by the molecular interactions between viral surface proteins and the target cell. Pseudotyping is the process of producing viral particles in which the native envelope protein is replaced or engineered, thereby altering the particle's original tropism. This review examines LV pseudotyping strategies for retargeting defined cell-surface antigens.

Pseudotyping using the natural tropism of a donor envelope glycoprotein

Since the early 2000s, pseudotyping of HIV-derived LVs has been performed by replacing the native HIV envelope protein with the native envelope protein of a heterologous virus, without introducing recognition domain modifications through engineering or bispecific molecules. This made it possible to surface display on LVs well-known viral envelopes specifically targeting the desired type of cells, according to the known tropism of the donor virus. Lentivectors produced using this approach proved to be highly efficient, particularly for *ex vivo* experiments (Figure 1).

The most emblematic case is that of vesicular stomatitis virus glycoprotein-based LVs, commonly known as "VSV-G LVs". Such lentivectors achieved a high success for broad applications, thanks to their ability to target the low-density lipoprotein receptor (LDL), expressed by many different cell types,[10] but also because of VSV-G LV stability and the possibility of high-titer production.[11] This makes VSV-G a broad tropism lentivector, often exploited for its high gene transfer efficiency *in vitro* and *ex vivo* for gene therapy approaches. However, it reveals its weakness when specific cell targeting is required. Moreover, VSV-G LVs have been demonstrated to be unstable in human serum,[12] excluding any possible use for *in vivo* therapies. For this reason, many other viral envelopes were investigated.

An alternative comes from the measles virus (MV), which belongs to the *paramyxovirus* family. This viral family exploits a two-component entry system, meaning that receptor recognition and membrane fusion involve two separate glycoproteins functioning as paired dimers. The hemagglutinin H protein is responsible for receptor binding, while the fusion F protein drives membrane fusion and cell–cell syncytium formation.[13] For host-cell entry, MV relies on the signaling lymphocyte activating molecule (SLAM or CD150)[14] expressed mainly on immune cells. At later stages of infection, it exploits nectin-4 on the epithelial cells of the respiratory tract.[15] In addition, the development of the attenuated Edmonston vaccinal strain has broadened its tropism also to the ubiquitously expressed human CD46.[16]

MV glycoproteins are compatible with LV-pseudotyping upon shortening of their cytoplasmic tail. Due to their ability to mediate pH-independent cell entry leading to cytoskeletal rearrangements that favor the transport to the cell nucleus, they were excellent gene delivery tools. MV-LVs can also be produced at substantially high titers, a critical condition for large-scale production and efficient manufacturing processes.[17]

Given MV's lymphotropic receptor affinity, Frecha et al. developed an MV-LV enabling efficient transduction of quiescent human T[18] and B[7] cells without inducing cell-cycle progression or activation of the resting lymphocytes. MV-LVs were also exploited for gene delivery into B cell chronic lymphocytic leukemia.[19,20] Similarly, Levy et al. demonstrated that MV-LVs could transduce 100% of early-acting cytokine-stimulated human stem and progenitor cells (HSPCs) upon a single application. Remarkably, these MV-LVs also allowed transduction of up to 70% of non-stimulated quiescent human HSPCs, establishing a tool for efficient transduction of hematopoietic stem cells without compromising their stemness.[21]

Along with MV, baboon endogenous retrovirus (BaEV)-based lentivectors were implemented as an efficient gene transfer tool for blood

cells, either to treat blood malignancies or to enable CAR expression on T and natural killer (NK) cells, in cancer treatment. Notably, BaEV envelope targets ASCT1 and ASCT2, receptors expressed by many lymphocytes and their precursors. LV pseudotyping with BaEV viral envelope achieved efficient HSPC transduction,[22] reaching 90% at 10 MOI, compared to the 30% of transduction achieved by VSV-G LVs and 40% by RDTR-LV (from RD114 viral envelope). Another study highlighted the ability of BaEV-LVs and MV-LVs to transduce both quiescent and stimulated B cells up to 50%, while they were also able to transduce up to 100% of plasma B cells, especially mature B cells, plasmablasts, and plasmocytes, definitely outperforming VSV-G.[23] BaEV-LVs demonstrated a higher efficiency and stability of transduction, probably thanks to higher expression of ASCT1/ASCT2 receptors with respect to CD46. Indeed, transduction of T-ALL leukemia-initiating cells (LIC) was doubled when BaEV-LVs were used.[24] Transduction was further increased by 3- or 4-fold in T cells and thymocytes.[25] Similarly, BaEV-LVs exhibited superior transduction efficiency over MV-LVs for NK cells, with about 80% of transduced activated NK cells and 20% of freshly isolated cells, compared to 10% and 2% transduction achieved by MV-LVs.[26] Moreover, BaEV-LVs were able to transduce up to 70% NK cells from patients and generate stable CAR NK cells, giving the opportunity to explore new cell therapy-based anti-cancer approaches.[27,28] Although BaEV-LVs show high efficiency *in vitro*, *in vivo* applications remain limited. Indeed, *in vivo* experiments on NSG mice were always carried out by performing *ex vivo* transductions followed by cell transplantation. The BaEV pseudotyped vector's inability to undergo direct *in vivo* transduction becomes clear from the omnipresence of its entry receptors ASCT1 and ASCT2 on multiple cell types. Several simian immunodeficiency virus (SIV)-based lentivectors were also tested[20] in the context of lymphocytes and hematopoietic cells. Murine leukemia virus (MLV-A), Gibbon Ape leukemia virus (GALV), RD114 feline endogenous virus, and VSV-G envelopes were used to pseudotype SIV vectors. Notably, native RD114 and GALV glycoprotein cytoplasmic tails were incompatible with SIV vector core unless substituted with the cytoplasmic tail of MLV-A, leading to transduction increase. Among these vectors, RD114-LV was the most efficient one, achieving 25% of HSPC transduction and 55% of peripheral blood lymphocytes (PBLs). In contrast, only 3% of HSPCs and 15% of PBLs were transduced by MLV-A or GALV LVs, and 23% of $CD34^+$ cells and 15% of PBLs by VSV-G. These differences can, for the majority, be attributed to the differential expression of the natural receptors of these viral envelopes.

Beyond blood cells and progenitors, lentivectors have also been pseudotyped for liver-specific delivery. An HIV vector was pseudotyped with the Sendai virus F envelope protein (SV-F), capable of binding the asialoglycoprotein receptor expressed by hepatocytes and hepatoma cells.[29] SV-F LV was able to efficiently transduce liver cancer cells, such as HepG2, Hep3B, Huh6, and Huh7 but not non-hepatic cells (HeLa cells and HT1080 cells), demonstrating a greater specificity than the broad tropism of VSV-G. Hepatitis C virus (HCV) envelope glycoprotein,[30] recognizing the CD81 receptor, was used to produce HCV-LVs, which efficiently transduced Huh7 hepatocarcinoma cells and spared almost all non-hepatic cell lines. However, some specificity issues remained, since non-hepatic cells like HT1080, HT29, and MCF7 were weakly transduced.[30]

Lymphocytic choriomeningitis virus glycoproteins (LCMV-GP)-based LVs were used to treat malignant glioma.[31] LCMV-LV transduced *in vitro* about 90% glioma cells, compared to 60% transduced by VSV-G. Furthermore, *in vivo* analysis was performed by intracerebral implantation of glioma cells and viral intratumoral injection, confirming LCMV-LV's strong preference for glioma cells, transducing 70% cells composing the solid tumor and a similar amount of infiltrating cells, while VSV-G efficiency was 10-fold lower. On the other hand, VSV-G was much more efficient in transducing normal brain cells, resulting in 40% of transduced cells compared to 4% infected by LCMV-LV.

Although these studies have shown the possibility of reaching high transduction efficiencies in certain cell types, these LVs often demonstrated good transduction levels in other, non-targeted cell types. Indeed, the specificity of transduction for *in vivo* experiments was often achieved by intratumoral or local injections of LVs.

Together, these studies confirm that LVs pseudotyped by native donor glycoproteins can be useful for *ex vivo* applications to transduce cells known to be targets of the donor virus, but applicability for *in vivo* gene delivery needed by human cancer gene therapy seems limited.

Pseudotyping by retargeting a viral glycoprotein

Insertion of activated molecules together with VSV-G for LV pseudotyping

In the bloodstream and in the bone marrow, respectively, T cells and HSPCs are normally quiescent, non-dividing, and in the G0 state of the cell cycle. Multiple publications have shown that VSV-G pseudotyped vectors are refractory in transducing these resting/unstimulated T cell and HSPC gene therapy targets,[32–34] although they can transduce other non-proliferating cells.[35,36] In T cells, this has been attributed to lentiviral post-entry blocks upon transduction.[37]

Upgraded lentiviral vectors have been engineered to overcome these blocks in non-activated T cells. One targeting strategy consists of displaying a ligand on the vector surface, which, upon binding to its specific receptor, will induce signaling and stimulation of the target T cells at the time of transduction.

As a first proof of principle, a single-chain fragment variable (scFv) derived from an anti-CD3 monoclonal antibody, which binds and activates the T cell through the T cell receptor (TCR), was fused to a murine leukemia virus (MVL) envelope.[8] The MLV envelope harbors both its receptor-binding and fusion domains in a single envelope glycoprotein. Changing the binding of the MLV envelope glycoprotein from its natural receptor to CD3 on T cells compromised its fusion ability and actually diminished CD3-targeted transduction.

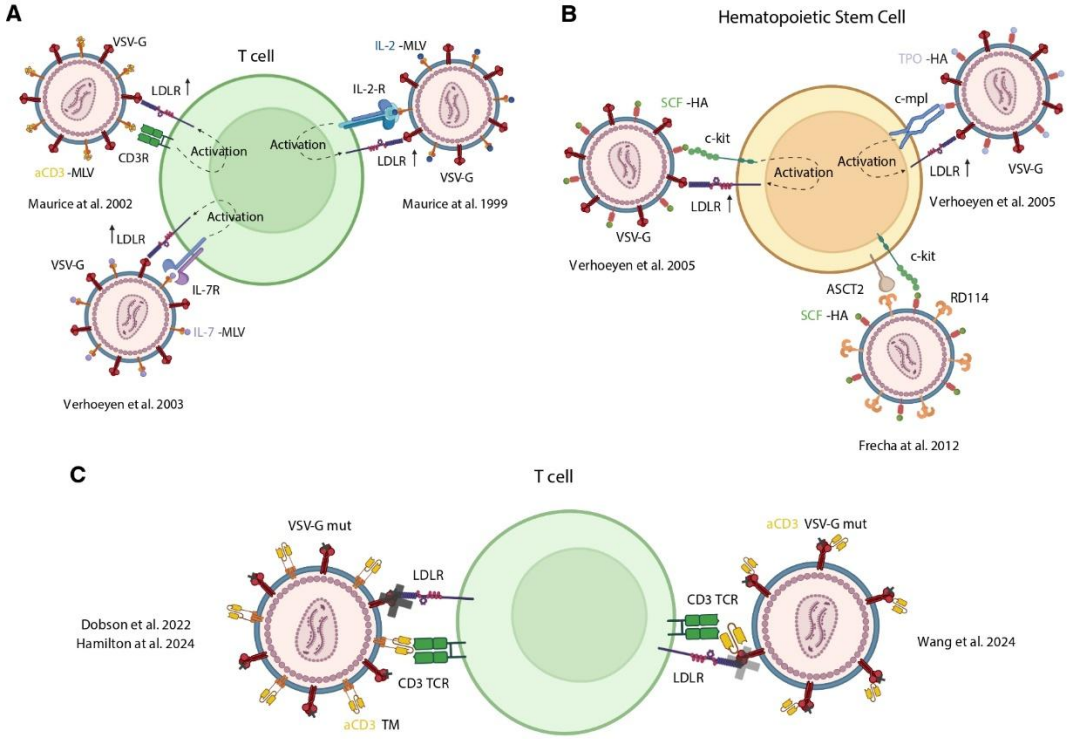


Figure 2. Schematic overview of lentivector VSV-G pseudotyping for "selective" targeting of T cells and HSCs

(A) Co-pseudotyping of native VSV-G and a T cell-stimulating molecule, such as cytokines (IL-2 and IL-7) or a CD3 scFv activating the T cell receptor by their insertion into an MLV envelope glycoprotein. (B) Co-pseudotyping of native VSV-G or RD114 and an HSC early-acting cytokine, such as SCF or TPO by their insertion into the influenza hemaglutinin (HA) envelope glycoprotein. (C) Retargeting of LVs by co-display of VSV-G, blinded for its natural receptor LDL, and a membrane-anchored CD3 scFv. Created in BioRender. Amintas, S. (2025).

To overcome this problem, co-expression of an "escorting" VSV-G envelope protein with the CD3-MLV envelope glycoprotein was required, by which the LV regained fusion with the target T cell (Figure 2A). These VSV-G/CD3-targeted vectors allowed a 100-fold increase in transduction of non-activated T cells as compared to single VSV-G pseudotyped vectors.[8,38] Similar to anti-CD3 and anti-CD28-mediated TCR stimulation, the VSV-G/CD3-targeted LVs induced naive T cells to switch to a memory phenotype. Moreover, TCR-stimulated T cells acquire a reduced half-life, lose immune competence, most probably because of exhaustion, and invert the physiological CD4/CD8 T cell ratio.[38] Equally important as high-level transduction is the conservation of naive T cell state for gene therapy, expected to achieve long-lasting immune reconstitution or treatment. Interestingly, exposure of T cells to interleukin-2 (IL-2), IL-15, and IL-7 cytokines renders them permissive to VSV-G-LVs in the absence of TCR triggering[38–40] without loss of naive T cell phenotype.[41–44] Thus, to avoid the phenotypic switch when transducing resting T cells, anti-CD3 scFV was replaced by IL-2 or IL-7 and fused to the amino terminus of the MLV-G.[38,45] Again, VSV-G was required as an accessory glycoprotein to permit fusion with the target T cells. VSV-G/IL-7-displaying LVs resulted in efficient transduction (up to 40%) of unstimulated naive and memory T cells, and, in contrast to anti-CD3-displaying LVs, conserved the functional characteristics of naive T cells.[38,46]

Another major limitation of current LVs is their inability to reach efficient gene transfer into human $CD34^+$ HSPCs, which are quiescent and undergo seldom "self-renewing" cell divisions. It was reported that high VSV-G-LV transduction levels in HSPCs can be achieved upon cytokine stimulation that promotes G0 to the G1 cell-cycle progression but at the cost of losing stemness.[32,47–49] To overcome this restriction, novel LVs were designed to display "early-acting cytokines" on their surface, such as thrombopoietin (TPO) or stem cell factor (SCF), or both cytokines on the same LV surface. TPO and SCF were selected as candidates because their respective receptors, c-Mpl and c-Kit, are present on HSPCs and, when activated synergistically, favor persistence, self-renewal, and maintenance of hematopoietic stem cells (HSCs) in the undifferentiated state[50–52] (Figure 2B).

SCF was displayed on the LV surface by fusion to the N terminus of the MLV-G, while TPO was fused to the influenza hemagglutinin, HA.[53] Double SCF/VSV-G- or TPO/VSV-G-LVs and triple envelope

VSVG/SCF/TPO displaying LVs allowed efficient gene delivery into quiescent HSPCs.[53] These surface-engineered LVs preferentially transduced and promoted the survival of resting HSPCs rather than cycling cells. Importantly, these novel LVs allowed superior gene transfer in the most immature HSPCs as compared to conventional LVs, even upon addition of these recombinant cytokines in soluble form. Transduced HSPCs *in vitro* displayed long-term engraftment and reconstituted hematopoiesis in non-obese diabetes (NOD)/severe combined immunodeficiency (SCID) mice, called humanized SCID mice. Later on, an upgraded version was developed, in which the accompanying fusion glycoprotein, VSV-G, was replaced by the RD114 envelope glycoprotein, resulting in SCF/RD114-LVs that allowed efficient transduction of HSCs *in vivo* by their direct inoculation into the bone marrow of humanized mice.[54] Interestingly, the long-hidden mystery of inefficiency to transduce unstimulated T cells and HSCs by VSV-G-LVs was solved much later by the discovery of the VSV-G receptor, the LDL-R.[10] Indeed, unstimulated T cells and HSPCs hardly express the LDL receptor, but TCR or IL-7 stimulation of T cells and SCF/TPO-stimulation of HSPCs upregulated this receptor.[34]

Expression of a targeting ligand together with the WT VSV-G envelope can promote "selective targeting" to some extent. Since the VSV-G envelope is polytropic because its entry receptor, LDL-R,[10] is present on multiple cell types, off-target events can easily occur, compromising specificity.[55] Therefore, recently an upgraded version of VSV-G/ligand displaying LVs was engineered by using a VSV-G glycoprotein that was mutated to disrupt binding to its native receptor, while retaining its fusion capacity (Figure 2C). This was possible by resolving the crystal structure of VSV-G in complex with the LDL-R-binding domains, which identified two crucial residues in VSV-G responsible for binding to the LDL receptor family. Mutating these residues (K47Q and R354A) altered VSV-G_{mut} binding to LDL-R without compromising its fusion ability.[56,57]

Furthermore, co-pseudotyping vectors with VSV-G_{mut} and surface-tethered dimerized IL-13 achieved specific transduction of IL-13R-expressing cells.[57] VSV-G_{mut} pseudotyped lentiviral vectors were also able to improve anti-CD3 scFv T cell tropism. In parallel, Yu et al. and more recently Hamilton et al. demonstrated that co-display of a membrane-anchored anti-CD19 scFv together with VSV-G_{mut} permitted transduction of $CD19^+$ B cells but not of the CD19-negative T cells.[58,59] This transduction targeting tool, called ENTER by the authors, can function as a platform to redirect LV tropism to any ligand expressed on a specific cell type. For example, the display of an antigen directed against the cytomegalovirus (CMV) alongside VSV-G_{mut} on the LV surface specifically bound to CMV TCR T cells and allowed targeted genetic payload delivery into T cells. The same was shown for targeting of specific BCRs on B cells.[57,59] Similarly, Hamilton et al. displayed next to VSV-G_{mut} and anti-CD3 scFv combined with its co-stimulatory anti-CD28 scFv, which resulted in specific activation and targeting of T cells for cargo delivery.[58]

The VSV-G_{mut}/targeting ligand pseudotyping strategy has advantages as compared to other viral envelopes, such as paramyxoviruses or Sindbis virus (SINV), used for retargeting, since high-titer particles can be produced. However, it is well known that VSV-G is human complement sensitive, which might reduce *in vivo* efficacy, while some paramyxovirus or alphavirus envelopes are less sensitive. Moreover, though *in vitro* specificity seems to be quite restricted, the insertion of 2 mutations in VSV-G does not completely abolish its natural tropism, e.g., for the liver. Several research teams are trying to introduce additional mutations into the VSV-G envelope to further reduce unspecific transduction. However, this might compromise the fusion capacity of the VSV-G envelope, limiting *in vivo* targeting of specific cell types. Nevertheless, several pharma companies are moving forward with this retargeted LV strategy (VSV-Gmut + membrane-anchored targeting moiety) toward clinical trials.[60,61] The Belgian company Esobiotec has developed a lentiviral platform (ENaBL) using a natural receptor-deficient VSVG mutant targeted to T cells using a nanobody binder directed against CD3. Additionally, the viral membrane overexpressed CD47, avoiding phagocytosis of the vectors *in vivo*. This LV platform was evaluated in a clinical trial by a single intravenous injection of this vector encoding an anti-BCMA CAR in multiple myeloma patients without prior lymphodepletion (NCT06691685). First-in-human data of four patients with relapsed or refractory disease showed the disappearance of cancer cells in the bone marrow by day 28.[62] Two out of four showed a complete response with lesion resolution, whereas the other two had a partial response with reduced tumor burden. CAR T cells were detected early on day 4–8 and increased till day 10–17. Some hematological toxicities (leukopenia, lymphopenia, and thrombopenia) were detected after vector infusion but resolved after two months. Cytokine release syndrome (CRS) was detected in all patients, whereas only one patient out of 4 developed immune effector cell-associated neurotoxicity syndrome (ICANS). As well as CRS, ICANS were controlled by glucocorticoids.[62]

The US biotech Umoja has generated CD22-directed CAR T cells using an anti-CD3 scFv grafted on cocal G glycoproteins (with a close structural similarity to VSVG) to deliver a CD19-targeted CAR. The US biotech Interius BioTherapeutics employs a ScFv targeting CD7 combined with the VSVG mutant glycoprotein to deliver an anti-CD20 CAR to $CD7^+$ T and NK cells. Preclinical data generated in mouse and cynomolgus macaque models have shown that this strategy generates $CD4^+$ and $CD8^+$ CAR T cells as well as CAR NK cells with subsequent depletion of $CD20^+$ B cells following a single intravenous administration.[63] While promising, at this point, the results of these studies and notably the tolerance of patients to the *in vivo* LV, as well as dose escalation effects, are not yet published and will require further clinical studies to assess.

In another strategy, the VSV-G_{mut} carried an insertion of a peptide or a targeting ligand to tumor cells to transform VSV-G-LV into an oncolytic virus specific for tumor cells.[61]

More recently, eight possible insertion sites in VSV-G were identified via computational analysis based on its crystal structure[56] for insertion of hepatocyte-specific peptides.[64] Seven insertion sites allowed

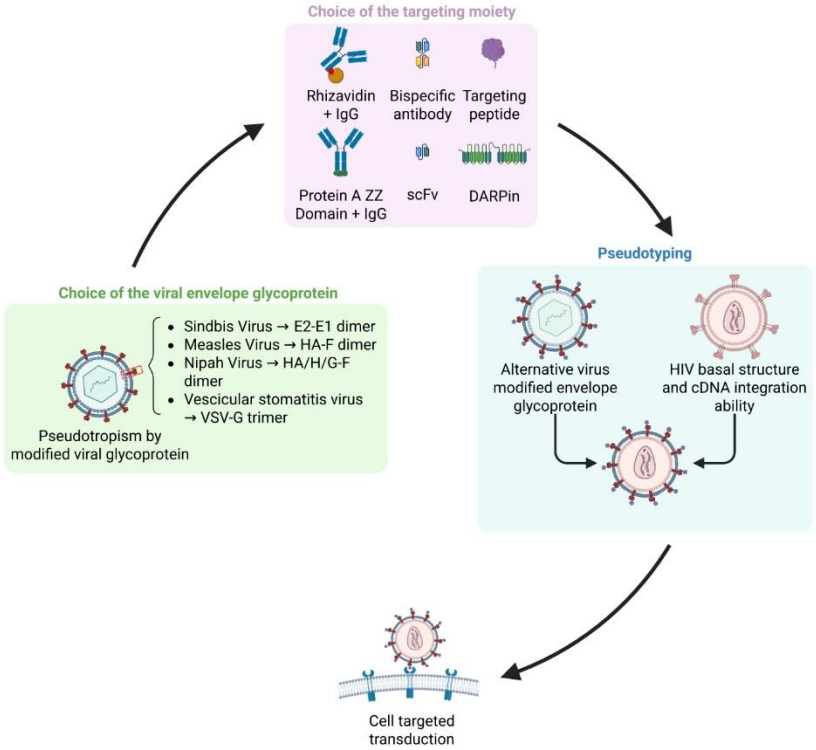


Figure 3. Schematic overview of lentivector pseudotyping redirecting viral tropism to implement *in vivo* therapeutic strategies

This method focuses on glycoprotein engineering by DARPins, targeting peptides, bispecific antibodies, scFvs, or antibody-binding proteins to develop LVs with a completely new tropism, conferring them a therapeutic role in the development of strategies against challenging diseases such as cancer. Created in BioRender. Amintas, S. (2025).

liver-specific transduction, one peptide showing better recognition for LDL-R upon *in vitro* screening. LV entry resulted in high accumulation of a transgene shIDOL in the liver, leading to reduced hypercholesterolemia and atherosclerotic lesions in mice. This VSV-G envelope was not mutated for its attachment to the LDL-R, but LDL-R attachment was enhanced by the specific LDL-R-binding peptide insertion. Though no obvious off-target transduction was shown in other tissues, caution is warranted since the LDL-R receptor is almost ubiquitous. A PD1-targeted LV was developed by incorporating the anti-PD1 nanobody into the VSV-Gmut glycoprotein,[65] resulting in higher viral titers at the cost of the specificity as compared to PD1-targeted MV glycoprotein H. This study showed that PD1-targeted LVs may offer a novel opportunity to modulate immune responses within the tumor microenvironment and might represent a new therapeutic strategy aimed at enhancing anti-tumor immunity.

Engineering the recognition monomer of a multimeric viral donor glycoprotein

Gene therapy approaches relying on a "two-component entry system"-LV might represent the most powerful tool for cell-targeted therapies. In these systems, the fusion and recognition functions are mediated by two distinct glycoproteins that operate as functional dimers. This separation allows for the specific retargeting of the vector to desired cell types while preserving high fusion efficiency, offering several advantages over the canonical single-glycoprotein systems, such as VSV-G[17] (Figure 3). As discussed in the following text, several donor viral glycoproteins can be engineered on their receptor recognition monomer.

Paramyxovirus. Initially, measles virus (MV) envelope retargeting was extensively explored in the context of oncolytic virotherapy.[66] This was achieved by introducing mutations in the MV-H protein in order to ablate the binding to its natural receptors[67,68] and by fusing the modified H protein with scFvs/DARPins targeting tumor-associated antigens[69] (Figure 3). These findings have paved the way for the translation of this tool into clinical trials,[70] highlighting the potential of MV envelope retargeting as an adaptable and versatile tool also for LV-based gene delivery applications. A relevant example of targeted cancer therapy is retargeted MV-LV with the H protein fused to the IL-13, enabling specific transduction *in vitro* of cancer cells expressing high levels of the human interleukin-13 receptor α2 (IL-13 Rα2), as well as *in vivo* of IL-13Ra2$^+$ glioma cell xenografted in immunodeficient mice.[71]

However, pseudotyping of LVs with MV-retargeted envelopes was primarily exploited to reach immune cells, with highly relevant applications in cancer therapy. CD20-retargeted LVs (MV-H fused to an anti-CD20 scFv) were highly efficient in delivering a therapeutic gene into primary human CD20$^+$ B lymphocytes (Figure 4). These vectors outperformed VSV-G LVs in efficient transduction of CD20$^+$ cells in co-cultures.[72] The selective uptake might involve CD20-mediated activation of resting B cells, facilitating cell-cycle entry and enhancing transduction efficiency.[73] Similarly, T cell sub-populations have been selectively targeted using CD8-LVs and CD4-LVs.[74,75] CD8-LVs pseudotyped with MV-H fused to a CD8-specific scFv delivered melanoma-specific TCRs both *ex vivo* and *in vivo*. In NOD-scid-IL2rγnull mice transplanted with human peripheral blood mononuclear cells (PBMCs), this resulted in enhanced cytotoxicity against melanoma cells compared to conventional vectors.[74] Moreover, CD4-LVs engineered with MV-H fused to a CD4-specific DARPin specifically targeted resting CD4$^+$ T cells *in vitro* and *in vivo*: upon administration into humanized mice, CD4-LVs

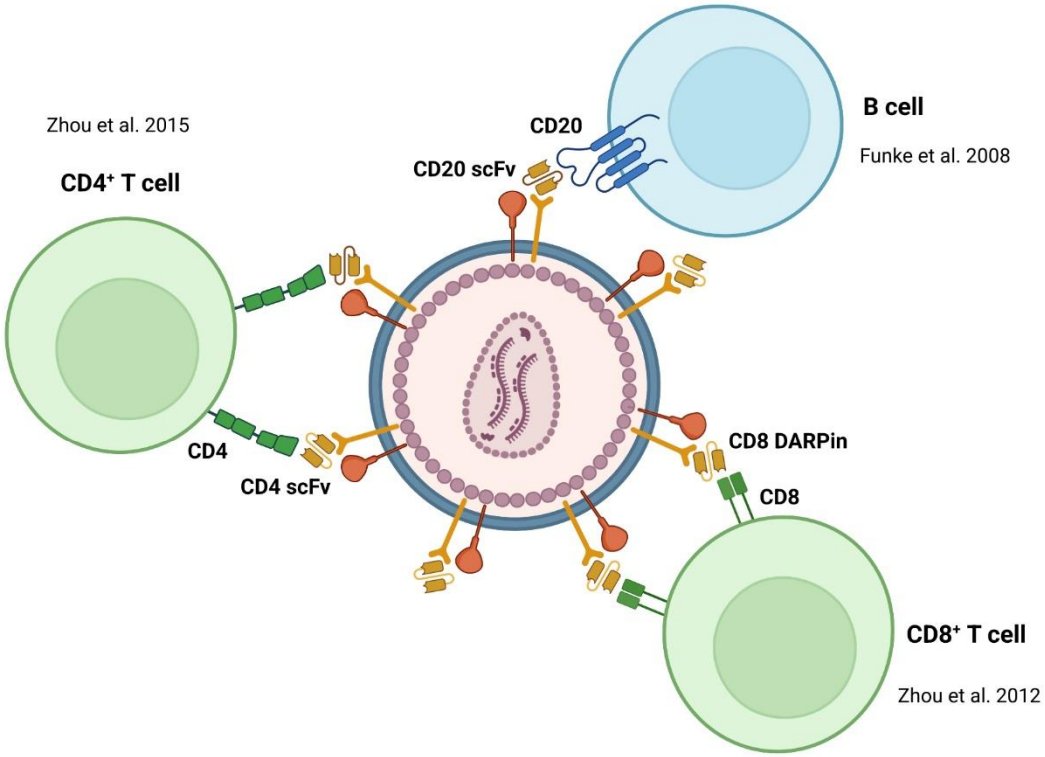


Figure 4. Schematic presentation of paramyxovirus envelope glycoproteins retargeted LVs to T cells and B cells
LVs are decorated with the paramyxovirus (measles or Nipah virus) fusion protein F (orange) and receptor recognition protein (yellow) that were blinded for the natural receptor binding and fused to CD4 scFv, CD8 Darpin, or CD20 scFv to target T cells and B cells. Created in BioRender. Amintas, S. (2025).

induced receptor internalization and activation signaling, leading to efficient gene transfer.[75]

Both these CD8-LV and CD4-LV have been exploited in the field of cancer gene therapy to enable systemic *in vivo* generation of CAR T cells.[76–78] In human PBMC-transplanted NSG mice, CD8-LVs induced $CD8^+$ CD19 CAR T cells that effectively cleared $CD19^+$ B cells and $CD19^+$ Nalm-6 tumor cells,[79,80] while CD4-LVs produced $CD4^+$ CD19 CAR T cells that not only eliminated tumor cells more rapidly and effectively but also maintained a predominantly naive and less exhausted phenotype. This suggests that $CD4^+$ CAR T cells may outperform $CD8^+$ CAR T cells, especially in high antigen burden scenarios, as $CD8^+$ T cells might be more prone to exhaustion.[81] In the huSGM3 mouse model, which supports enhanced human hematopoiesis and a more pronounced myeloid lineage differentiation, CAR T cell generation was diminished, likely due to macrophage-mediated clearance. However, surface engineering of LVs with phagocytosis-shielding CD47 restored CAR T cell generation while maintaining high T cell target specificity.[82]

Furthermore, these tools can also be relevant to specifically treat malignancies arising from a defined subset of the T cell population. For instance, in an *in vivo* CAR T cell therapy approach against a $CD4^+$ T cell lymphoma, CD8-LVs have been exploited to generate $CD8^+$ CD4 CAR T cells. Such selective targeting was crucial in preventing fratricide, a phenomenon where CAR T cells attack each other, which can occur if the entire T cell population is transduced. By ensuring that only $CD8^+$ T cells express the CD4 CAR, this approach has enhanced the safety and specificity of the therapy.[83] In a preclinical mouse model for $CD4^+$ follicular helper T cell lymphoma, direct injection of the CD8-targeted LV coding for an anti-CD4 CAR resulted in remarkably increased mouse survival. This strategy holds promise for both *in vivo* but also conventional *ex vivo* CAR T cell therapies, potentially improving the safety profile by minimizing unintended transduction of non-target cells.

However, the widespread use of the measles vaccine has led to the development of neutralizing antibodies in the general population, posing a significant challenge for therapies requiring systemic administration. Different strategies are being developed to overcome this hurdle, like LV-coating with nanoparticles (core-shell type iron oxide magnetic nanoparticles) or a cell-based delivery system to hide the particle while it is transported to the target site.[66] Additionally, a promising approach induced point mutations in the ectodomain of the H glycoprotein for blunting the antibody-binding sites, resulting

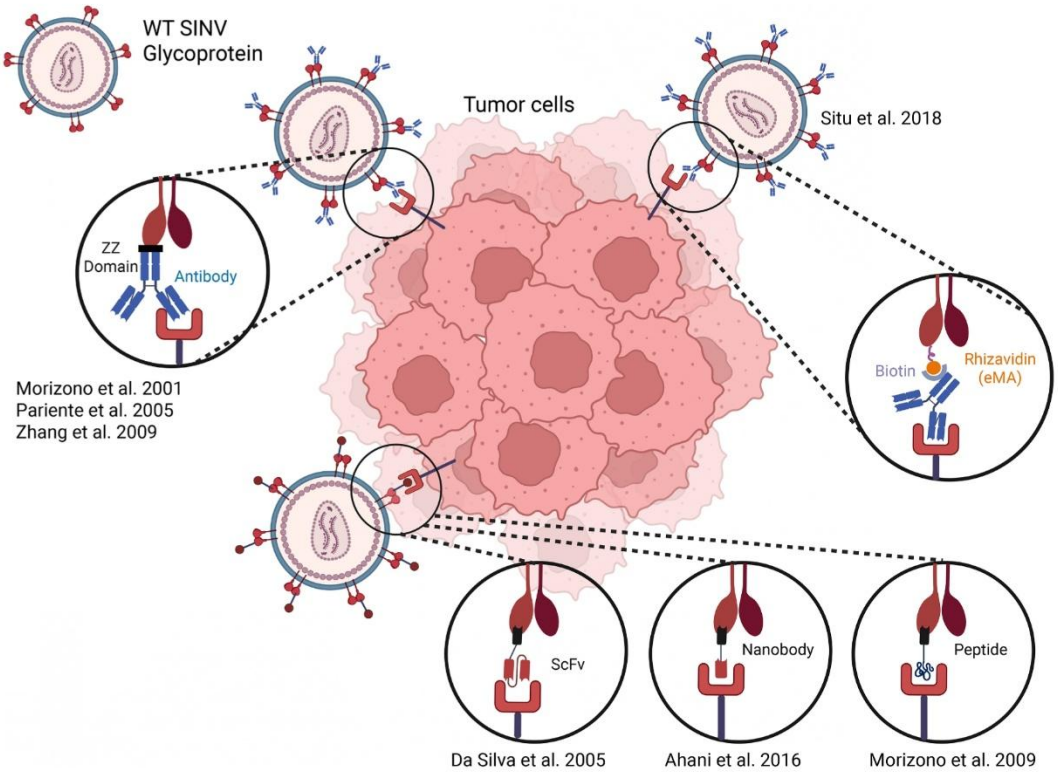


Figure 5. Schematic of the pseudotyping strategies engineering the E2 receptor monomer of Sindbis virus

The wild-type (WT) SINV glycoprotein possesses separate monomers for recognition and fusion. The ZZ domain can be added to the recognition monomer to attach the Fc domain of immunoglobulins, or an avidin to attach a biotinylated antibody. More recently, the monomer was engineered into a fusion protein with scFvs or nanobodies or ligands. Created in BioRender. Amintas, S. (2025).

in the generation of vectors for human *in vivo* use that bypass MV vaccine-induced antibody neutralization.[84]

Another line of research being explored is the use of glycoproteins from related viruses, such as the Nipah virus (NIV-G/F), which might represent a suitable candidate for the low prevalence of pre-existing humoral immunity in humans.[85] Nipah virus belongs to the *paramyxovirus* family and displays surface fusion F and receptor recognition G proteins, which form tetramers with β-propeller head domains that engage the receptors ephrin-B2[86] and, to a limited extent, ephrin-B3.[87,88] NIV-G has garnered particular attention among other viruses (e.g. *Tupaia paramyxovirus*)[89] for its potential to bypass the liver "sink",[90,91] a phenomenon where intravenously administered viral vectors are rapidly cleared by the liver, together with the possibility of producing up to two-orders of magnitude high titers and a less susceptibility to neutralization by the human serum.[86] NIV-retargeted LVs have already been exploited in the cancer gene therapy field, specifically in a CAR T cell therapy application. After ablation of the natural receptors, CD3-LVs displaying an agonistic CD3-specific scFv have been able to deliver the CAR construct not only selectively into T cells but also before activation. The generated CAR T cells were functionally active, eliminating the $CD19^+$ B cells *in vitro* and *in vivo* in humanized mice.[92]

Alphavirus. The envelope glycoprotein from the SINV has been extensively studied, and several generations have been developed to overcome the major problems encountered for the development of an efficient and specific gene therapy using different strategies shown in Figure 5. Tai and colleagues investigated the structural modifications of the SINV envelope glycoproteins to enhance their stability and functionality in pseudotyping applications, demonstrating that specific mutations in the E2 domain improved vector targeting and transduction efficiency on cells refractory to transduction, as dendritic cells, where they achieved 87% of transduction efficiency.[93] Morizono et al. pioneered the concept of engineering the SINV E2 glycoprotein by incorporating the ZZ domain from protein A from *Staphylococcus aureus*, recognizing the constant fragment of IgGs, associating in this way the Sindbis E2 glycoprotein with the antigen/antibody complex.[94] In this study, the authors assessed the efficiency and specificity of these SINVs by transducing luciferase into 293 T (HLA^+) and BHK (HLA^-) cells. A high signal for 293 T cells was detected, compared to a low signal for BHK cells. The complex

with an anti-CD4 antibody highly transduced HLA-CD4$^+$ but not HLA-CD4 in cocultures. This strategy was refined by mutating 5 domains of the E2 glycoprotein, making the so-called m168 LV, used later for every new SINV pseudotyping strategy. A high specificity and efficiency were reached in the tissue of interest *in vivo* by injecting the m168 LVs with an anti-HLA antibody, while low off-target transduction in other mouse organs was observed.[95] Similarly, another team targeted specifically and efficiently the PSCA antigen on LPSCA4 cells expressing high PSCA, using the 1G8 antibody, compared to LNCaP cells with low PSCA expression. To improve the specificity, the transgene was placed under the control of the prostate-specific antigen (PSE-BC) promoter. Both VSV-G and Sindbis LV achieved high transduction efficiency on LPSCA4 cells. VSV-G achieved low expression of the transgene, while SINV showed no ectopic expression, highlighting a synergistic effect of a specific promoter and a targeting viral glycoprotein to enhance specificity, both *in vitro* and *in vivo*.[96] Zhang et al. showed similarly that C4-2 cells, a prostate cancer cell line, were well transduced using SINV in combination with trastuzumab, a Her2 neutralizing antibody.[97]

To avoid any competition between immunoglobulins from the sera *in vivo* and the antibody targeting the antigen of interest, a new system has been implemented to increase the stability and specificity of this complex. Lentivectors were pseudotyped with an avidin monomer, rhizavidin (eMA) or with the monomeric streptavidin (mSAH) E2 fusion proteins, and incubated with biotinylated antibodies (anti-hTFR1, anti-mCD34, or anti-EGF) to reach high specificity and honorable efficiency. For example, HeLa cells (EGFR$^+$) were 31% GFP$^+$ with the eMA, and 39% with the mSAH, compared to only 1% for Jurkat cells (EGFR$^-$).[98] Alternatively, the E2 subunit, mutated to abrogate its natural tropism, and a bi-specific antibody directed against mutated E2 and the target cell (HER2 in this study) provided high specificity but modest efficiency.[99]

To further stabilize the receptor E2 fusion protein, scFv recognizing CCR5,[100] a nanobody specific to VEGFR2, the VEGF ligand targeting VEGFR,[101] and peptide binding integrins[102] were successfully developed with high specificity and various efficiencies. E2 fused with anchors that bind another peptide through either an isopeptide bond or a disulfide bond was developed to provide highly adaptable targeting tools. Used with DARPin specific to HER2, a strong efficiency of about 50% of HER2-positive cells was obtained.[103,104]

Collectively, these studies underscore the immense potential of Nipah virus and SINV envelope glycoprotein engineering in advancing lentiviral vector design, providing a versatile platform for targeted, efficient, and clinically relevant gene therapy applications. More efforts are now necessary to document the efficiency and specificity of these strategies *in vivo*.

Future applications: Retargeting of VLPs for gene editing

Viral particles can be engineered for receptor-targeted delivery of genetic information. Recently, virus-derived vehicles called virus-like particles (VLPs) have been employed to transfer proteins and RNA to specific cell types. VLPs are devoid of a viral genome but have the same lipid bilayer membrane and viral core as retroviral vectors. As for vectors, the tropism of these VLPs can be engineered by incorporating glycoproteins into the membranes.

One of the most promising "precision" gene therapy tools that have been discovered in the last decade is gene-editing tools, such as CRISPR-Cas9, base editing, and prime editing.[105] A huge hurdle in using these systems, though, in primary cells was the delivery of the therapeutic endonucleases with their guide RNAs (gRNAs) into primary cells. Indeed, for gene therapy of genetic diseases, viral-based delivery leaves the viral genome and the Cas9 nuclease into the corrected cell genomes. By fusing the MLV Gag protein to Cas9 and combining its co-expression with gRNA into a producer cell line, Mangeot and colleagues were able to incorporate the Cas9-gRNA complexes into MLV-based VLPs by active incorporation of the Gag-Cas9 fusion proteins. Once these VLP particles were pseudotyped with a VSV-G envelope, they allowed efficient release of the Cas9-gRNA into cells to allow efficient gene editing. Interestingly, co-pseudotyping with the BaEV and VSV-G envelope glycoproteins increased gene editing into cell lines, T cells, B cells, and CD34$^+$-cells.[106,107] Later, our team and others successfully generated HIV-derived VLPs by fusion of Cas9 to the HIV gag protein.[59,107] Others reported the successful transfer of base editors[108] and or prime editors,[109] respectively, using a similar VLP strategy for efficient gene editing in the liver, brain, and eye.

Finally, to change the tropism of VLPs carrying Cas9-gRNA Nielsen et al. borrowed the envelope proteins of different viruses for pseudotyping: (1) spike protein of severe acute respiratory syndrome coronavirus 2 that allowed specific entry into ACE2 receptor expressing cells, (2) Nipah virus glycoprotein resulted in cell entry via Ephrin-B2/B3 receptors, (3) measles virus glycoproteins (MV-H/F) delivered Cas9-sgRNA RNPs to CD46$^+$ cells with and without additional expression of SLAM receptor[110] and (4) HIV envelope to target specifically CD4$^+$ T cells.[59]

Therefore, precision oncology using viral-derived gene therapy is at its dawn. This field is rapidly growing, with already successful cures of patients suffering from genetic disorders.

ACKNOWLEDGMENTS

This work was supported by the "Réseau Recherche Impulsion Newmoon" of the University of Bordeaux, by the Joint support program for the University of Bordeaux and the Ludwig-Maximilians-Universität München (LMU, SD), by the Fondation pour la Recherche sur le Cancer, Fondation ARC www.fondation-arc.orggrant #2024050008233 (SD), and by the Institut National Du Cancer grant #085-2024-136 (SD, EV). J.R. is supported by a PhD grant from Fondation pour la Recherche Médicale (FRM). C.M. is supported by a MARIE SKŁODOWSKA-CURIE ACTIONS PhD; network GET-IN and the European community (EV). This project has received funding from the European Union's Framework Programme for Research and Innovation, Horizon Europe under grant agreement #101119880 (EV).

AUTHOR CONTRIBUTIONS

J.R., C.M., R.S., and S.A. have generated the figures. Additionally, J.R., C.M., and R.S. wrote the main manuscript together with S.D. and E.V. M.J.A.R., S.A., and V.G.-D. have critically revised the manuscript. All authors reviewed the manuscript.

DECLARATION OF INTERESTS

All authors declare no conflicts of interest.

REFERENCES

1. Lindner, S.E., Johnson, S.M., Brown, C.E., and Wang, L.D. (2020). Chimeric antigen receptor signaling: Functional consequences and design implications. Sci. Adv. *6*, eaaz3223. https://doi.org/10.1126/sciadv.aaz3223.
2. Alhakamy, N.A., Curiel, D.T., and Berkland, C.J. (2021). The era of gene therapy: From preclinical development to clinical application. Drug Discov. Today *26*, 1602–1619. https://doi.org/10.1016/j.drudis.2021.03.021.
3. Geng, G., Xu, Y., Hu, Z., Wang, H., Chen, X., Yuan, W., and Shu, Y. (2025). Viral and non-viral vectors in gene therapy: current state and clinical perspectives. EBioMedicine *118*, 105834. https://doi.org/10.1016/j.ebiom.2025.105834.
4. Poletti, V., and Mavilio, F. (2021). Designing Lentiviral Vectors for Gene Therapy of Genetic Diseases. Viruses *13*, 1526. https://doi.org/10.3390/v13081526.
5. Deng, L., Liang, P., and Cui, H. (2023). Pseudotyped lentiviral vectors: Ready for translation into targeted cancer gene therapy? Genes Dis. *10*, 1937–1955. https://doi.org/10.1016/j.gendis.2022.03.007.
6. Irving, M., Lanitis, E., Migliorini, D., Ivics, Z., and Guedan, S. (2021). Choosing the Right Tool for Genetic Engineering: Clinical Lessons from Chimeric Antigen Receptor-T Cells. Hum. Gene Ther. *32*, 1044–1058. https://doi.org/10.1089/hum.2021.173.
7. Frecha, C., Costa, C., Lévy, C., Nègre, D., Russell, S.J., Maisner, A., Salles, G., Peng, K.W., Cosset, F.L., and Verhoeyen, E. (2009). Efficient and stable transduction of resting B lymphocytes and primary chronic lymphocyte leukemia cells using measles virus gp displaying lentiviral vectors. Blood *114*, 3173–3180. https://doi.org/10.1182/blood-2009-05-220798.
8. Maurice, M., Verhoeyen, E., Salmon, P., Trono, D., Russell, S.J., and Cosset, F.L. (2002). Efficient gene transfer into human primary blood lymphocytes by surface-engineered lentiviral vectors that display a T cell-activating polypeptide. Blood *99*, 2342–2350. https://doi.org/10.1182/blood.v99.7.2342.
9. Ruella, M., Xu, J., Barrett, D.M., Fraietta, J.A., Reich, T.J., Ambrose, D.E., Klichinsky, M., Shestova, O., Patel, P.R., Kulikovskaya, I., et al. (2018). Induction of resistance to chimeric antigen receptor T cell therapy by transduction of a single leukemic B cell. Nat. Med. *24*, 1499–1503. https://doi.org/10.1038/s41591-018-0201-9.
10. Finkelshtein, D., Werman, A., Novick, D., Barak, S., and Rubinstein, M. (2013). LDL receptor and its family members serve as the cellular receptors for vesicular stomatitis virus. Proc. Natl. Acad. Sci. USA *110*, 7306–7311. https://doi.org/10.1073/pnas.1214441110.
11. Waehler, R., Russell, S.J., and Curiel, D.T. (2007). Engineering targeted viral vectors for gene therapy. Nat. Rev. Genet. *8*, 573–587. https://doi.org/10.1038/nrg2141.
12. DePolo, N.J., Reed, J.D., Sheridan, P.L., Townsend, K., Sauter, S.L., Jolly, D.J., and Dubensky, T.W., Jr. (2000). VSV-G pseudotyped lentiviral vector particles produced in human cells are inactivated by human serum. Mol. Ther. *2*, 218–222. https://doi.org/10.1006/mthe.2000.0116.
13. Yanagi, Y., Takeda, M., and Ohno, S. (2006). Measles virus: cellular receptors, tropism and pathogenesis. J. Gen. Virol. *87*, 2767–2779. https://doi.org/10.1099/vir.0.82221-0.
14. Tatsuo, H., Ono, N., Tanaka, K., and Yanagi, Y. (2000). SLAM (CDw150) is a cellular receptor for measles virus. Nature *406*, 893–897. https://doi.org/10.1038/35022579.
15. Mühlebach, M.D., Mateo, M., Sinn, P.L., Prüfer, S., Uhlig, K.M., Leonard, V.H.J., Navaratnarajah, C.K., Frenzke, M., Wong, X.X., Sawatsky, B., et al. (2011). Adherens junction protein nectin-4 is the epithelial receptor for measles virus. Nature *480*, 530–533. https://doi.org/10.1038/nature10639.
16. Dörig, R.E., Marcil, A., Chopra, A., and Richardson, C.D. (1993). The human CD46 molecule is a receptor for measles virus (Edmonston strain). Cell *75*, 295–305. https://doi.org/10.1016/0092-8674(93)80071-l.
17. Buchholz, C.J., Mühlebach, M.D., and Cichutek, K. (2009). Lentiviral vectors with measles virus glycoproteins – dream team for gene transfer? Trends Biotechnol. *27*, 259–265. https://doi.org/10.1016/j.tibtech.2009.02.002.
18. Frecha, C., Costa, C., Nègre, D., Gauthier, E., Russell, S.J., Cosset, F.L., and Verhoeyen, E. (2008). Stable transduction of quiescent T cells without induction of cycle progression by a novel lentiviral vector pseudotyped with measles virus glycoproteins. Blood *112*, 4843–4852. https://doi.org/10.1182/blood-2008-05-155945.
19. Frecha, C., Lévy, C., Cosset, F.L., and Verhoeyen, E. (2010). Advances in the Field of Lentivector-based Transduction of T and B Lymphocytes for Gene Therapy. Mol. Ther. *18*, 1748–1757. https://doi.org/10.1038/mt.2010.178.
20. Frecha, C., Lévy, C., Costa, C., Nègre, D., Amirache, F., Buckland, R., Russell, S.J., Cosset, F.L., and Verhoeyen, E. (2011). Measles Virus Glycoprotein-Pseudotyped Lentiviral Vector-Mediated Gene Transfer into Quiescent Lymphocytes Requires Binding to both SLAM and CD46 Entry Receptors. J. Virol. *85*, 5975–5985. https://doi.org/10.1128/jvi.00324-11.
21. Lévy, C., Amirache, F., Girard-Gagnepain, A., Frecha, C., Roman-Rodríguez, F.J., Bernadin, O., Costa, C., Nègre, D., Gutierrez-Guerrero, A., Vranckx, L.S., et al. (2017). Measles virus envelope pseudotyped lentiviral vectors transduce quiescent human HSCs at an efficiency without precedent. Blood Adv. *1*, 2088–2104. https://doi.org/10.1182/bloodadvances.2017007773.
22. Girard-Gagnepain, A., Amirache, F., Costa, C., Lévy, C., Frecha, C., Fusil, F., Nègre, D., Lavillette, D., Cosset, F.L., and Verhoeyen, E. (2014). Baboon envelope pseudotyped LVs outperform VSV-G-LVs for gene transfer into early-cytokine-stimulated and resting HSCs. Blood *124*, 1221–1231. https://doi.org/10.1182/blood-2014-02-558163.
23. Levy, C., Fusil, F., Amirache, F., Costa, C., Girard-Gagnepain, A., Negre, D., Bernadin, O., Garaulet, G., Rodriguez, A., Nair, N., et al. (2016). Baboon envelope pseudotyped lentiviral vectors efficiently transduce human B cells and allow active factor IX B cell secretion *in vivo* in NOD/SCIDγc-/- mice. J. Thromb. Haemost. *14*, 2478–2492. https://doi.org/10.1111/jth.13520.
24. Costa, C., Hypolite, G., Bernadin, O., Lévy, C., Cosset, F.L., Asnafi, V., Macintyre, E., Verhoeyen, E., and Tesio, M. (2017). Baboon envelope pseudotyped lentiviral vectors: a highly efficient new tool to genetically manipulate T-cell acute lymphoblastic leukaemia-initiating cells. Leukemia *31*, 977–980. https://doi.org/10.1038/leu.2016.372.
25. Bernadin, O., Amirache, F., Girard-Gagnepain, A., Moirangthem, R.D., Lévy, C., Ma, K., Costa, C., Nègre, D., Reimann, C., Fenard, D., et al. (2019). Baboon envelope LVs efficiently transduced human adult, fetal, and progenitor T cells and corrected SCID-X1 T-cell deficiency. Blood Adv. *3*, 461–475. https://doi.org/10.1182/bloodadvances.2018027508.
26. Colamartino, A.B.L., Lemieux, W., Bifsha, P., Nicoletti, S., Chakravarti, N., Sanz, J., Roméro, H., Selleri, S., Béland, K., Guiot, M., et al. (2019). Efficient and Robust NK-Cell Transduction With Baboon Envelope Pseudotyped Lentivector. Front. Immunol. *10*, 2873. https://doi.org/10.3389/fimmu.2019.02873.
27. Bari, R., Granzin, M., Tsang, K.S., Roy, A., Krueger, W., Orentas, R., Schneider, D., Pfeifer, R., Moeker, N., Verhoeyen, E., et al. (2019). A Distinct Subset of Highly Proliferative and Lentiviral Vector (LV)-Transducible NK Cells Define a Readily Engineered Subset for Adoptive Cellular Therapy. Front. Immunol. *10*, 2001. https://doi.org/10.3389/fimmu.2019.02001.
28. Tran, T.B.T., Bui, T.V.A., Tran, T.M.T., Nguyen, N.M., Nguyen, H.T.P., Tran, T.P.D., Nguyen, D.M.Q., Ngo, T.M.Q., Nguyen, T.B., Verhoeyen, E., et al. (2025). In Vitro Expansion and Transduction of Primary NK Cells Using Feeder Cells Expressing Costimulatory Molecules and IL-21. Cancer Sci. *116*, 1847–1860. https://doi.org/10.1111/cas.70090.
29. Sandrin, V., Boson, B., Salmon, P., Gay, W., Nègre, D., Le Grand, R., Trono, D., and Cosset, F.L. (2002). Lentiviral vectors pseudotyped with a modified RD114 envelope glycoprotein show increased stability in sera and augmented transduction of primary lymphocytes and CD34+ cells derived from human and nonhuman primates. Blood *100*, 823–832. https://doi.org/10.1182/blood-2001-11-0042.
30. Kowolik, C.M., and Yee, J.K. (2002). Preferential Transduction of Human Hepatocytes with Lentiviral Vectors Pseudotyped by Sendai Virus F Protein. Mol. Ther. *5*, 762–769. https://doi.org/10.1006/mthe.2002.0603.
31. Bartosch, B., Dubuisson, J., and Cosset, F.L. (2003). Infectious Hepatitis C Virus Pseudo-particles Containing Functional E1–E2 Envelope Protein Complexes. J. Exp. Med. *197*, 633–642. https://doi.org/10.1084/jem.20021756.
32. Miletic, D.H., Fischer, Y.H., Neumann, H., Hans, V., Stenzel, W., Giroglou, T., Hermann, M., Deckert, M., and Von Laer, D. (2004). Selective Transduction of

Malignant Glioma by Lentiviral Vectors Pseudotyped with Lymphocytic Choriomeningitis Virus Glycoproteins. Hum. Gene Ther. *15*, 1091–1100. https://doi.org/10.1089/hum.2004.15.1091.

33. Sutton, R.E., Reitsma, M.J., Uchida, N., and Brown, P.O. (1999). Transduction of human progenitor hematopoietic stem cells by human immunodeficiency virus type 1-based vectors is cell cycle dependent. J. Virol. *73*, 3649–3660. https://doi.org/10.1128/JVI.73.5.3649-3660.1999.

34. Sun, Y., Pinchuk, L.M., Agy, M.B., and Clark, E.A. (1997). Nuclear import of HIV-1 DNA in resting CD4+ T cells requires a cyclosporin A-sensitive pathway. J. Immunol. *158*, 512–517.

35. Amirache, F., Lévy, C., Costa, C., Mangeot, P.E., Torbett, B.E., Wang, C.X., Nègre, D., Cosset, F.L., and Verhoeyen, E. (2014). Mystery solved: VSV-G-LVs do not allow efficient gene transfer into unstimulated T cells, B cells, and HSCs because they lack the LDL receptor. Blood *123*, 1422–1424. https://doi.org/10.1182/blood-2013-11-540641.

36. Lewis, P., Hensel, M., and Emerman, M. (1992). Human immunodeficiency virus infection of cells arrested in the cell cycle. EMBO J. *11*, 3053–3058. https://doi.org/10.1002/j.1460-2075.1992.tb05376.x.

37. Weinberg, J.B., Matthews, T.J., Cullen, B.R., and Malim, M.H. (1991). Productive human immunodeficiency virus type 1 (HIV-1) infection of nonproliferating human monocytes. J. Exp. Med. *174*, 1477–1482. https://doi.org/10.1084/jem.174.6.1477.

38. Korin, Y.D., and Zack, J.A. (1998). Progression to the G1b phase of the cell cycle is required for completion of human immunodeficiency virus type 1 reverse transcription in T cells. J. Virol. *72*, 3161–3168. https://doi.org/10.1128/JVI.72.4.3161-3168.1998.

39. Verhoeyen, E., Dardalhon, V., Ducrey-Rundquist, O., Trono, D., Taylor, N., and Cosset, F.L. (2003). IL-7 surface-engineered lentiviral vectors promote survival and efficient gene transfer in resting primary T lymphocytes. Blood *101*, 2167–2174. https://doi.org/10.1182/blood-2002-07-2224.

40. Unutmaz, D., KewalRamani, V.N., Marmon, S., and Littman, D.R. (1999). Cytokine signals are sufficient for HIV-1 infection of resting human T lymphocytes. J. Exp. Med. *189*, 1735–1746. https://doi.org/10.1084/jem.189.11.1735.

41. Ducrey-Rundquist, O., Guyader, M., and Trono, D. (2002). Modalities of interleukin-7-induced human immunodeficiency virus permissiveness in quiescent T lymphocytes. J. Virol. *76*, 9103–9111. https://doi.org/10.1128/jvi.76.18.9103-9111.2002.

42. Fry, T.J., and Mackall, C.L. (2001). Interleukin-7: master regulator of peripheral T-cell homeostasis? Trends Immunol. *22*, 564–571. https://doi.org/10.1016/s1471-4906(01)02028-2.

43. Geiselhart, L.A., Humphries, C.A., Gregorio, T.A., Mou, S., Subleski, J., and Komschlies, K.L. (1950). IL-7 administration alters the CD4:CD8 ratio, increases T cell numbers, and increases T cell function in the absence of activation. J. Immunol. *166*, 3019–3027. https://doi.org/10.4049/jimmunol.166.5.3019.

44. Rathmell, J.C., Farkash, E.A., Gao, W., and Thompson, C.B. (1950). IL-7 enhances the survival and maintains the size of naive T cells. J. Immunol. *167*, 6869–6876. https://doi.org/10.4049/jimmunol.167.12.6869.

45. Cavalieri, S., Cazzaniga, S., Geuna, M., Magnani, Z., Bordignon, C., Naldini, L., and Bonini, C. (2003). Human T lymphocytes transduced by lentiviral vectors in the absence of TCR activation maintain an intact immune competence. Blood *102*, 497–505. https://doi.org/10.1182/blood-2003-01-0297.

46. Maurice, M., Mazur, S., Bullough, F.J., Salvetti, A., Collins, M.K., Russell, S.J., and Cosset, F.L. (1999). Efficient gene delivery to quiescent interleukin-2 (IL-2)-dependent cells by murine leukemia virus-derived vectors harboring IL-2 chimeric envelope glycoproteins. Blood *94*, 401–410.

47. Soares, M.V., Borthwick, N.J., Maini, M.K., Janossy, G., Salmon, M., and Akbar, A.N. (1998). IL-7-dependent extrathymic expansion of CD45RA+ T cells enables preservation of a naive repertoire. J. Immunol. *161*, 5909–5917.

48. Ahmed, F., Ings, S.J., Pizzey, A.R., Blundell, M.P., Thrasher, A.J., Ye, H.T., Fahey, A., Linch, D.C., and Yong, K.L. (2004). Impaired bone marrow homing of cytokine-activated CD34+ cells in the NOD/SCID model. Blood *103*, 2079–2087. https://doi.org/10.1182/blood-2003-06-1770.

49. Uchida, N., Sutton, R.E., Friera, A.M., He, D., Reitsma, M.J., Chang, W.C., Veres, G., Scollay, R., and Weissman, I.L. (1998). HIV, but not murine leukemia virus, vectors mediate high efficiency gene transfer into freshly isolated G0/G1 human hematopoietic stem cells. Proc. Natl. Acad. Sci. USA *95*, 11939–11944. https://doi.org/10.1073/pnas.95.20.11939.

50. Kittler, E.L., Peters, S.O., Crittenden, R.B., Debatis, M.E., Ramshaw, H.S., Stewart, F.M., and Quesenberry, P.J. (1997). Cytokine-facilitated transduction leads to low-level engraftment in nonablated hosts. Blood *90*, 865–872.

51. Kimura, S., Roberts, A.W., Metcalf, D., and Alexander, W.S. (1998). Hematopoietic stem cell deficiencies in mice lacking c-Mpl, the receptor for thrombopoietin. Proc. Natl. Acad. Sci. USA *95*, 1195–1200. https://doi.org/10.1073/pnas.95.3.1195.

52. Zielske, S.P., and Gerson, S.L. (2003). Cytokines, including stem cell factor alone, enhance lentiviral transduction in nondividing human LTCIC and NOD/SCID repopulating cells. Mol. Ther. *7*, 325–333. https://doi.org/10.1016/s1525-0016(03)00005-4.

53. Kirito, K., Fox, N., and Kaushansky, K. (2003). Thrombopoietin stimulates Hoxb4 expression: an explanation for the favorable effects of TPO on hematopoietic stem cells. Blood *102*, 3172–3178. https://doi.org/10.1182/blood-2003-03-0944.

54. Verhoeyen, E., Wiznerowicz, M., Olivier, D., Izac, B., Trono, D., Dubart-Kupperschmitt, A., and Cosset, F.L. (2005). Novel lentiviral vectors displaying "early-acting cytokines" selectively promote survival and transduction of NOD/SCID repopulating human hematopoietic stem cells. Blood *106*, 3386–3395. https://doi.org/10.1182/blood-2004-12-4736.

55. Frecha, C., Costa, C., Nègre, D., Amirache, F., Trono, D., Rio, P., Bueren, J., Cosset, F.L., and Verhoeyen, E. (2012). A novel lentiviral vector targets gene transfer into human hematopoietic stem cells in marrow from patients with bone marrow failure syndrome and *in vivo* in humanized mice. Blood *119*, 1139–1150. https://doi.org/10.1182/blood-2011-04-346619.

56. Burns, J.C., Friedmann, T., Driever, W., Burrascano, M., and Yee, J.K. (1993). Vesicular stomatitis virus G glycoprotein pseudotyped retroviral vectors: concentration to very high titer and efficient gene transfer into mammalian and nonmammalian cells. Proc. Natl. Acad. Sci. USA *90*, 8033–8037. https://doi.org/10.1073/pnas.90.17.8033.

57. Nikolic, J., Belot, L., Raux, H., Legrand, P., Gaudin, Y., and A Albertini, A. (2018). Structural basis for the recognition of LDL-receptor family members by VSV glycoprotein. Nat. Commun. *9*, 1029. https://doi.org/10.1038/s41467-018-03432-4.

58. Dobson, C.S., Reich, A.N., Gaglione, S., Smith, B.E., Kim, E.J., Dong, J., Ronsard, L., Okonkwo, V., Lingwood, D., Dougan, M., et al. (2022). Antigen identification and high-throughput interaction mapping by reprogramming viral entry. Nat. Methods *19*, 449–460. https://doi.org/10.1038/s41592-022-01436-z.

59. Hamilton, J.R., Chen, E., Perez, B.S., Sandoval Espinoza, C.R., Kang, M.H., Trinidad, M., Ngo, W., and Doudna, J.A. (2024). In vivo human T cell engineering with enveloped delivery vehicles. Nat. Biotechnol. *42*, 1684–1692. https://doi.org/10.1038/s41587-023-02085-z.

60. Yu, B., Shi, Q., Belk, J.A., Yost, K.E., Parker, K.R., Li, R., Liu, B.B., Huang, H., Lingwood, D., Greenleaf, W.J., et al. (2022). Engineered cell entry links receptor biology with single-cell genomics. Cell *185*, 4904–4920.e22. https://doi.org/10.1016/j.cell.2022.11.016.

61. Ammayappan, A., Peng, K.W., and Russell, S.J. (2013). Characteristics of Oncolytic Vesicular Stomatitis Virus Displaying Tumor-Targeting Ligands. J. Virol. *87*, 13543–13555. https://doi.org/10.1128/jvi.02240-13.

62. Xu, J., Liu, L., Parone, P., Xie, W., Sun, C., Chen, Z., Zhang, J., Li, C., Hu, Y., and Mei, H. (2025). In-vivo B-cell maturation antigen CAR T-cell therapy for relapsed or refractory multiple myeloma. Lancet *406*, 228–231. https://doi.org/10.1016/S0140-6736(25)01030-X.

63. Andorko, J.I., Russell, R.M., Schnepp, B.C., Grubaugh, D., Mullen, K.F., Wakabayashi, A., Carrington, L.J., O'Malley, T., Kuri-Cervantes, L., Culp, T.D., and Johnson, P.R. (2025). Targeted *in vivo* delivery of genetic medicines utilizing an engineered lentiviral vector platform results in CAR T and NK cell generation. Mol. Ther. *33*, 4937–4952. https://doi.org/10.1016/j.ymthe.2025.06.036.

64. Wang, W., Chen, X., Chen, J., Xu, M., Liu, Y., Yang, S., Zhao, W., and Tan, S. (2024). Engineering lentivirus envelope VSV-G for liver targeted delivery of

IDOL-shRNA to ameliorate hypercholesterolemia and atherosclerosis. Mol. Ther. Nucleic Acids *35*, 102115. https://doi.org/10.1016/j.omtn.2024.102115.

65. Zhuchkov, V.A., Kravchenko, Y.E., Frolova, E.I., and Chumakov, S.P. (2024). PD1-Targeted Transgene Delivery to Treg Cells. Viruses *16*, 1940. https://doi.org/10.3390/v16121940.

66. Aref, S., Bailey, K., and Fielding, A. (2016). Measles to the Rescue: A Review of Oncolytic Measles Virus. Viruses *8*, 294. https://doi.org/10.3390/v8100294.

67. Vongpunsawad, S., Oezgun, N., Braun, W., and Cattaneo, R. (2004). Selectively Receptor-Blind Measles Viruses: Identification of Residues Necessary for SLAM- or CD46-Induced Fusion and Their Localization on a New Hemagglutinin Structural Model. J. Virol. *78*, 302–313. https://doi.org/10.1128/jvi.78.1.302-313.2004.

68. Leonard, V.H.J., Sinn, P.L., Hodge, G., Miest, T., Devaux, P., Oezguen, N., Braun, W., McCray, P.B., Jr., McChesney, M.B., and Cattaneo, R. (2008). Measles virus blind to its epithelial cell receptor remains virulent in rhesus monkeys but cannot cross the airway epithelium and is not shed. J. Clin. Investig. *118*, 2448–2458. https://doi.org/10.1172/jci35454.

69. Nakamura, T., Peng, K.W., Harvey, M., Greiner, S., Lorimer, I.A.J., James, C.D., and Russell, S.J. (2005). Rescue and propagation of fully retargeted oncolytic measles viruses. Nat. Biotechnol. *23*, 209–214. https://doi.org/10.1038/nbt1060.

70. Galanis, E., Dooley, K.E., Keith Anderson, S., Kurokawa, C.B., Carrero, X.W., Uhm, J.H., Federspiel, M.J., Leontovich, A.A., Aderca, I., Viker, K.B., et al. (2024). Carcinoembryonic antigen-expressing oncolytic measles virus derivative in recurrent glioblastoma: a phase 1 trial. Nat. Commun. *15*, 493. https://doi.org/10.1038/s41467-023-43076-7.

71. Ou, W., Marino, M.P., Suzuki, A., Joshi, B., Husain, S.R., Maisner, A., Galanis, E., Puri, R.K., and Reiser, J. (2012). Specific Targeting of Human Interleukin (IL)-13 Receptor α2-Positive Cells with Lentiviral Vectors Displaying IL-13. Hum. Gene Ther. Methods *23*, 137–147. https://doi.org/10.1089/hgtb.2012.054.

72. Funke, S., Maisner, A., Mühlebach, M.D., Koehl, U., Grez, M., Cattaneo, R., Cichutek, K., and Buchholz, C.J. (2008). Targeted Cell Entry of Lentiviral Vectors. Mol Ther J Am Soc Gene Ther *16*, 1427–1436. https://doi.org/10.1038/mt.2008.128.

73. Kneissl, S., Zhou, Q., Schwenkert, M., Cosset, F.L., Verhoeyen, E., and Buchholz, C.J. (2013). CD19 and CD20 Targeted Vectors Induce Minimal Activation of Resting B Lymphocytes. Alici E. PLoS One *8*, e79047. https://doi.org/10.1371/journal.pone.0079047.

74. Zhou, Q., Schneider, I.C., Edes, I., Honegger, A., Bach, P., Schönfeld, K., Schambach, A., Wels, W.S., Kneissl, S., Uckert, W., and Buchholz, C.J. (2012). T-cell receptor gene transfer exclusively to human CD8+ cells enhances tumor cell killing. Blood *120*, 4334–4342. https://doi.org/10.1182/blood-2012-02-412973.

75. Zhou, Q., Uhlig, K.M., Muth, A., Kimpel, J., Lévy, C., Münch, R.C., Seifried, J., Pfeiffer, A., Trkola, A., Coulibaly, C., et al. (2015). Exclusive Transduction of Human CD4+ T Cells upon Systemic Delivery of CD4-Targeted Lentiviral Vectors. J. Immunol. *195*, 2493–2501. https://doi.org/10.4049/jimmunol.1500956.

76. Mhaidly, R., and Verhoeyen, E. (2019). The Future: In Vivo CAR T Cell Gene Therapy. Mol. Ther. *27*, 707–709. https://doi.org/10.1016/j.ymthe.2019.03.012.

77. Michels, A., Ho, N., and Buchholz, C.J. (2022). Precision medicine: In vivo CAR therapy as a showcase for receptor-targeted vector platforms. Mol. Ther. *30*, 2401–2415. https://doi.org/10.1016/j.ymthe.2022.05.018.

78. Weidner, T., Agarwal, S., Perian, S., Fusil, F., Braun, G., Hartmann, J., Verhoeyen, E., and Buchholz, C.J. (2021). Genetic *in vivo* engineering of human T lymphocytes in mouse models. Nat. Protoc. *16*, 3210–3240. https://doi.org/10.1038/s41596-021-00510-8.

79. Pfeiffer, A., Thalheimer, F.B., Hartmann, S., Frank, A.M., Bender, R.R., Danisch, S., Costa, C., Wels, W.S., Modlich, U., Stripecke, R., et al. (2018). *In vivo* generation of human CD 19- CAR T cells results in B-cell depletion and signs of cytokine release syndrome. EMBO Mol. Med. *10*, e9158. https://doi.org/10.15252/emmm.201809158.

80. Agarwal, S., Weidner, T., Thalheimer, F.B., and Buchholz, C.J. (2019). *In vivo* generated human CAR T cells eradicate tumor cells. OncoImmunology *8*, e1671761. https://doi.org/10.1080/2162402x.2019.1671761.

81. Agarwal, S., Hanauer, J.D.S., Frank, A.M., Riechert, V., Thalheimer, F.B., and Buchholz, C.J. (2020). In Vivo Generation of CAR T Cells Selectively in Human CD4+ Lymphocytes. Mol. Ther. *28*, 1783–1794. https://doi.org/10.1016/j.ymthe.2020.05.005.

82. Ho, N., Agarwal, S., Milani, M., Cantore, A., Buchholz, C.J., and Thalheimer, F.B. (2022). In vivo generation of CAR T cells in the presence of human myeloid cells. Mol. Ther., Methods Clin. Dev. *26*, 144–156. https://doi.org/10.1016/j.omtm.2022.06.004.

83. Krug, A., Saidane, A., Martinello, C., Fusil, F., Michels, A., Buchholz, C.J., Ricci, J.E., and Verhoeyen, E. (2024). In vivo CAR T cell therapy against angioimmunoblastic T cell lymphoma. J. Exp. Clin. Cancer Res. *43*, 262. https://doi.org/10.1186/s13046-024-03179-5.

84. Lévy, C., Amirache, F., Costa, C., Frecha, C., Muller, C.P., Kweder, H., Buckland, R., Cosset, F.L., and Verhoeyen, E. (2012). Lentiviral Vectors Displaying Modified Measles Virus gp Overcome Pre-existing Immunity in In Vivo-like Transduction of Human T and B Cells. Mol. Ther. *20*, 1699–1712. https://doi.org/10.1038/mt.2012.96.

85. Bender, R.R., Muth, A., Schneider, I.C., Friedel, T., Hartmann, J., Plückthun, A., Maisner, A., and Buchholz, C.J. (2016). Receptor-Targeted Nipah Virus Glycoproteins Improve Cell-Type Selective Gene Delivery and Reveal a Preference for Membrane-Proximal Cell Attachment. PLoS Pathog. *12*, e1005641. https://doi.org/10.1371/journal.ppat.1005641.

86. Negrete, O.A., Levroney, E.L., Aguilar, H.C., Bertolotti-Ciarlet, A., Nazarian, R., Tajyar, S., and Lee, B. (2005). EphrinB2 is the entry receptor for Nipah virus, an emergent deadly paramyxovirus. Nature *436*, 401–405. https://doi.org/10.1038/nature03838.

87. Negrete, O.A., Wolf, M.C., Aguilar, H.C., Enterlein, S., Wang, W., Mühlberger, E., Su, S.V., Bertolotti-Ciarlet, A., Flick, R., and Lee, B. (2006). Two Key Residues in EphrinB3 Are Critical for Its Use as an Alternative Receptor for Nipah Virus. G. McFadden, ed. *2*, e7. https://doi.org/10.1371/journal.ppat.0020007.

88. Negrete, O.A., Chu, D., Aguilar, H.C., and Lee, B. (2007). Single Amino Acid Changes in the Nipah and Hendra Virus Attachment Glycoproteins Distinguish EphrinB2 from EphrinB3 Usage. J. Virol. *81*, 10804–10814. https://doi.org/10.1128/jvi.00999-07.

89. Enkirch, T., Kneissl, S., Hoyler, B., Ungerechts, G., Stremmel, W., Buchholz, C.J., and Springfeld, C. (2013). Targeted lentiviral vectors pseudotyped with the Tupaia paramyxovirus glycoproteins. Gene Ther. *20*, 16–23. https://doi.org/10.1038/gt.2011.209.

90. Ganesan, L.P., Mohanty, S., Kim, J., Clark, K.R., Robinson, J.M., and Anderson, C.L. (2011). Rapid and Efficient Clearance of Blood-borne Virus by Liver Sinusoidal Endothelium. R.C. Desrosiers, ed. *7*, e1002281. https://doi.org/10.1371/journal.ppat.1002281.

91. Palomares, K., Vigant, F., Van Handel, B., Pernet, O., Chikere, K., Hong, P., Sherman, S.P., Patterson, M., An, D.S., Lowry, W.E., et al. (2013). Nipah Virus Envelope-Pseudotyped Lentiviruses Efficiently Target ephrinB2-Positive Stem Cell Populations *In Vitro* and Bypass the Liver Sink When Administered *In Vivo*. J. Virol. *87*, 2094–2108. https://doi.org/10.1128/jvi.02032-12.

92. Frank, A.M., Braun, A.H., Scheib, L., Agarwal, S., Schneider, I.C., Fusil, F., Perian, S., Sahin, U., Thalheimer, F.B., Verhoeyen, E., and Buchholz, C.J. (2020). Combining T-cell-specific activation and *in vivo* gene delivery through CD3-targeted lentiviral vectors. Blood Adv. *4*, 5702–5715. https://doi.org/10.1182/bloodadvances.2020002229.

93. Tai, A., Froelich, S., Joo, K.I., and Wang, P. (2011). Production of lentiviral vectors with enhanced efficiency to target dendritic cells by attenuating mannosidase activity of mammalian cells. J. Biol. Eng. *5*, 1. https://doi.org/10.1186/1754-1611-5-1.

94. Morizono, K., Bristol, G., Xie, Y.M., Kung, S.K., and Chen, I.S. (2001). Antibody-Directed Targeting of Retroviral Vectors via Cell Surface Antigens. J. Virol. *75*, 8016–8020. https://doi.org/10.1128/jvi.75.17.8016-8020.2001.

95. Morizono, K., Xie, Y., Ringpis, G.E., Johnson, M., Nassanian, H., Lee, B., Wu, L., and Chen, I.S.Y. (2005). Lentiviral vector retargeting to P-glycoprotein on metastatic melanoma through intravenous injection. Nat. Med. *11*, 346–352. https://doi.org/10.1038/nm1192.

96. Pariente, N., Morizono, K., Virk, M.S., Petrigliano, F.A., Reiter, R.E., Lieberman, J.R., and Chen, I.S.Y. (2007). A Novel Dual-targeted Lentiviral Vector Leads to Specific Transduction of Prostate Cancer Bone Metastases In Vivo After Systemic Administration. Mol. Ther. *15*, 1973–1981. https://doi.org/10.1038/sj.mt.6300271.

97. Zhang, K.X., Moussavi, M., Kim, C., Chow, E., Chen, I.S., Fazli, L., Jia, W., and Rennie, P.S. (2009). Lentiviruses with trastuzumab bound to their envelopes can target and kill prostate cancer cells. Cancer Gene Ther. *16*, 820–831. https://doi.org/10.1038/cgt.2009.28.

98. Situ, K., Chua, B.A., Bae, S.Y., Meyer, A.S., and Morizono, K. (2018). Versatile targeting system for lentiviral vectors involving biotinylated targeting molecules. Virology *525*, 170–181. https://doi.org/10.1016/j.virol.2018.09.017.

99. Parker, C.L., Jacobs, T.M., Huckaby, J.T., Harit, D., and Lai, S.K. (2020). Efficient and Highly Specific Gene Transfer Using Mutated Lentiviral Vectors Redirected with Bispecific Antibodies. mBio *11*. e02990-19–19. https://doi.org/10.1128/mBio.02990-19.

100. Aires da Silva, F., Costa, M.J.L., Corte-Real, S., and Goncalves, J. (2005). Cell type-specific targeting with sindbis pseudotyped lentiviral vectors displaying anti-CCR5 single-chain antibodies. Hum. Gene Ther. *16*, 223–234. https://doi.org/10.1089/hum.2005.16.223.

101. Ahani, R., Roohvand, F., Cohan, R.A., Etemadzadeh, M.H., Mohajel, N., Behdani, M., Shahosseini, Z., Madani, N., and Azadmanesh, K. (2016). Sindbis Virus-Pseudotyped Lentiviral Vectors Carrying VEGFR2-Specific Nanobody for Potential Transductional Targeting of Tumor Vasculature. Mol. Biotechnol. *58*, 738–747. https://doi.org/10.1007/s12033-016-9973-7.

102. Morizono, K., Pariente, N., Xie, Y., and Chen, I.S.Y. (2009). Redirecting lentiviral vectors by insertion of integrin-tageting peptides into envelope proteins. J. Gene Med. *11*, 549–558. https://doi.org/10.1002/jgm.1339.

103. Kasaraneni, N., Chamoun-Emanuelli, A.M., Wright, G.A., and Chen, Z. (2018). A simple strategy for retargeting lentiviral vectors to desired cell types via a disulfide-bond-forming protein-peptide pair. Sci. Rep. *8*, 10990. https://doi.org/10.1038/s41598-018-29253-5.

104. Kasaraneni, N., Chamoun-Emanuelli, A.M., Wright, G., and Chen, Z. (2017). Retargeting Lentiviruses via SpyCatcher-SpyTag Chemistry for Gene Delivery into Specific Cell Types. mBio *8*, e0186017. https://doi.org/10.1128/mBio.01860-17.

105. Gutierrez-Guerrero, A., Abrey Recalde, M.J., Mangeot, P.E., Costa, C., Bernadin, O., Périan, S., Fusil, F., Froment, G., Martinez-Turtos, A., Krug, A., et al. (2021). Baboon Envelope Pseudotyped 'Nanoblades' Carrying Cas9/gRNA Complexes Allow Efficient Genome Editing in Human T, B, and CD34+ Cells and Knock-in of AAV6-Encoded Donor DNA in CD34+ Cells. Front. Genome Ed. *3*, 604371. https://doi.org/10.3389/fgeed.2021.604371.

106. Gutierrez-Guerrero, A., Périan, S., Leray, A., Martinello, C., Abrey Recalde, M.J., Costa, C., Herrero, C.I., Bouzelha, M., Alvarez-Dorta, D., Gouin, S.G., et al. (2025). Ligand-modified rAAV6 vectors with nanoblades allow high-level gene knockin in HSPCs without compromising cell survival. Mol. Ther. Nucleic Acids *36*, 102495. https://doi.org/10.1016/j.omtn.2025.102495.

107. Haldrup, J., Andersen, S., Labial, A.R.L., Wolff, J.H., Frandsen, F.P., Skov, T.W., Rovsing, A.B., Nielsen, I., Jakobsen, T.S., Askou, A.L., et al. (2023). Engineered lentivirus-derived nanoparticles (LVNPs) for delivery of CRISPR/Cas ribonucleoprotein complexes supporting base editing, prime editing and *in vivo* gene modification. Nucleic Acids Res. *51*, 10059–10074. https://doi.org/10.1093/nar/gkad676.

108. Banskota, S., Raguram, A., Suh, S., Du, S.W., Davis, J.R., Choi, E.H., Wang, X., Nielsen, S.C., Newby, G.A., Randolph, P.B., et al. (2022). Engineered virus-like particles for efficient *in vivo* delivery of therapeutic proteins. Cell *185*, 250–265.e16. https://doi.org/10.1016/j.cell.2021.12.021.

109. An, M., Raguram, A., Du, S.W., Banskota, S., Davis, J.R., Newby, G.A., Chen, P.Z., Palczewski, K., and Liu, D.R. (2024). Engineered virus-like particles for transient delivery of prime editor ribonucleoprotein complexes *in vivo*. Nat. Biotechnol. *42*, 1526–1537. https://doi.org/10.1038/s41587-023-02078-y.

110. Nielsen, I.H., Rovsing, A.B., Janns, J.H., Thomsen, E.A., Ruzo, A., Bøggild, A., Nedergaard, F., Møller, C.T., Boesen, T., Degn, S.E., et al. (2024). Cell-targeted gene modification by delivery of CRISPR-Cas9 ribonucleoprotein complexes in pseudotyped lentivirus-derived nanoparticles. Mol. Ther. Nucleic Acids *35*, 102318. https://doi.org/10.1016/j.omtn.2024.102318.

6. Target antigens for LV retargeting in PDAC and associated tumor models

A central requirement for targeted lentiviral delivery is the choice of surface antigen. The ideal antigen should be accessible at the plasma membrane, expressed at sufficient density on the target population, absent or low on essential healthy tissues, and compatible with viral attachment and entry. In PDAC, no surface antigen fulfils all these criteria perfectly. Therefore, antigen selection must be guided by a balance between biological relevance, tumor expression, experimental tractability and safety considerations.

In this thesis, EpCAM, mesothelin and PSMA are used as target antigens to explore the modularity and specificity of scFv-retargeted lentiviral pseudotypes **(Figure 10)**.

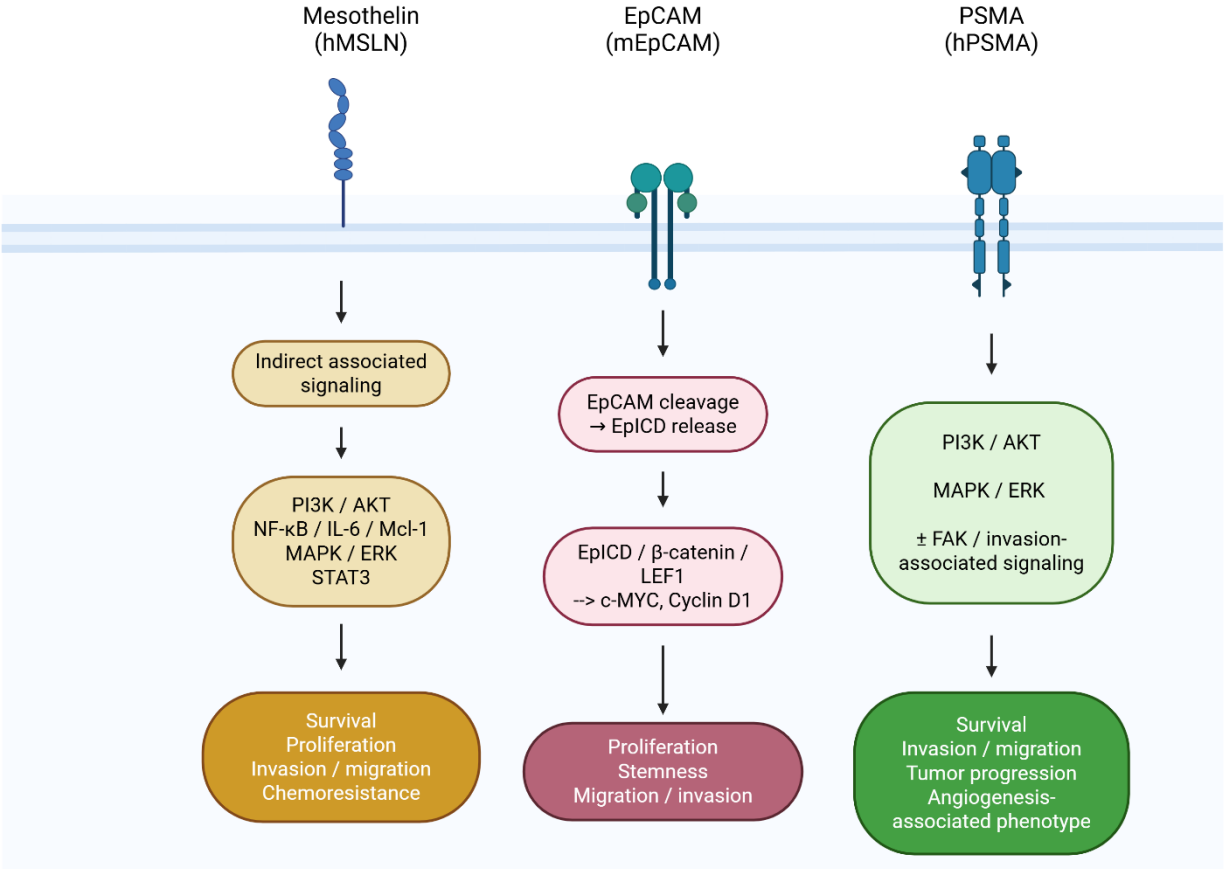


Figure 10: Tumor-associated surface antigens selected for lentiviral vector retargeting and associated pro-tumoral signaling pathways.

Schematic representation of mesothelin, EpCAM and PSMA at the tumor-cell plasma membrane and their associated pro-tumoral signaling pathways. Mesothelin is represented as a GPI-anchored surface glycoprotein linked to indirect activation of PI3K/AKT, NF-κB/IL-6/Mcl-1, MAPK/ERK and STAT3 signaling, supporting survival, proliferation, invasion/migration and chemoresistance. EpCAM is represented as a transmembrane glycoprotein that can undergo proteolytic cleavage and release EpICD, which participates in β-catenin/LEF1-dependent transcriptional programs involving c-MYC and Cyclin D1, promoting proliferation, stemness and migration/invasion. PSMA is represented as a type II transmembrane glycoprotein associated with PI3K/AKT,

MAPK/ERK and invasion-associated signaling, contributing to survival, invasion/migration, tumor progression and angiogenesis-associated phenotypes. Created with biorender.com.

Mesothelin: PDAC-associated antigen and clinically explored immunotherapy target

Mesothelin is a glycosylphosphatidylinositol-anchored cell-surface protein with restricted expression in normal mesothelial tissues and frequent overexpression in several solid tumors, including pancreatic cancer[116]. In PDAC, mesothelin is one of the most clinically explored tumor-associated antigens and has been targeted using vaccines, immunotoxins, antibody-drug conjugates and CAR T cell strategies[111,117–119]. This clinical and translational background makes mesothelin a particularly relevant antigen for the development of targeted gene delivery platforms in pancreatic cancer.

For lentiviral retargeting, mesothelin offers several advantages: it is extracellularly accessible, biologically relevant to PDAC, and already validated as an immunotherapy target. Nevertheless, its expression can be heterogeneous across tumors[116]. In this thesis, mesothelin targeting allows the retargeted LV platform to be tested against an antigen with direct relevance to PDAC immunotherapy.

EpCAM: epithelial tumor-cell targeting

Epithelial cell adhesion molecule (EpCAM) is a transmembrane glycoprotein expressed by epithelial cells and frequently overexpressed in epithelial cancers[180]. In PDAC and other carcinomas, EpCAM is relevant because it marks the malignant epithelial compartment, which represents the primary source of tumor propagation and a logical target for tumor-directed gene delivery[181]. Its extracellular domain makes it accessible to antibody-derived targeting moieties, and its broad use in tumor biology provides a strong rationale for evaluating EpCAM as a retargeting antigen.

However, EpCAM is not tumor-specific. Its expression in normal epithelial tissues raises potential on-target, off-tumor concerns for systemic applications. In the context of this thesis, EpCAM is therefore best considered not as a clinically optimized target antigen, but as a murine epithelial tumor antigen model used to evaluate whether scFv-mediated pseudotyping can redirect lentiviral transduction toward antigen-positive carcinoma cells in syngeneic settings. Using murine EpCAM enables retargeting strategies to be assessed in immunocompetent tumor models, where antigen-dependent transduction can be studied in a more physiologically relevant immune context than in xenograft systems. Thus, murine EpCAM provides a controlled syngeneic platform to compare antigen expression, targeting specificity and background transduction while preserving the contribution of the host immune system.

PSMA: validated prostate antigen and model-dependent solid tumor target

Prostate-specific membrane antigen (PSMA) is a type II transmembrane glycoprotein extensively validated as a diagnostic and therapeutic target in prostate cancer. Its strong clinical validation, extracellular accessibility and availability of well-characterized antibody-derived binders make PSMA a useful antigen for testing the modularity of targeted delivery platforms. In this thesis, PSMA should therefore be presented with precision. It is not a universal PDAC tumor-cell antigen, but it is valuable as a robust model antigen to demonstrate antigen-dependent retargeting, specificity and modularity of the lentiviral pseudotyping system. When used in engineered or selected PSMA-positive tumor models, it allows direct comparison between antigen-positive and antigen-negative conditions.

Why target several antigens rather than one?

Targeting several antigens addresses a central limitation of antigen-directed therapies in solid tumors: heterogeneity. A single antigen may be absent from some tumor cells, expressed at insufficient density, lost under therapeutic pressure, or inaccessible because of tissue architecture. Multi-antigen targeting strategies can therefore increase the probability of engaging relevant tumor regions and reduce the risk of antigen-negative escape.

For lentiviral niche engineering, multi-antigen targeting has an additional rationale. The objective is not necessarily to transduce every malignant cell, but to create local producers of immunomodulatory factors within the tumor ecosystem. Targeting different antigens may allow transduction of distinct cellular compartments or tumor-cell states, increasing the spatial distribution of therapeutic signal production. Thus, together, EpCAM, mesothelin and PSMA provide a modular antigen panel to test whether LV retargeting can be adapted to heterogeneous tumor contexts.

7. scFv as modular targeting domains for lentiviral retargeting

Structure and origin of scFv

Single-chain variable fragments (scFv) are recombinant antibody-derived binding domains composed of the variable regions of the heavy and light antibody chains connected by a flexible peptide linker. This format was first described in the late 1980s, when antibody variable domains were genetically fused into a single polypeptide while retaining antigen-binding activity[182,183]. This architecture preserves antigen-binding specificity in a compact, genetically encodable format. Because scFv can be derived from monoclonal antibodies with known specificity, they have become widely used in engineered immunotherapies, including CAR T cells, bispecific T cell engagers, immunotoxins and targeted viral vectors.

The main advantage of scFv is modularity. Changing the scFv can redirect the binding specificity of a therapeutic platform without necessarily changing the rest of its architecture. In the context of retargeted lentiviral vectors, this property is highly valuable: the same pseudotyping backbone can theoretically be adapted to different tumor-associated antigens by exchanging the targeting domain.

Why scFv are useful for LV targeting

For lentiviral retargeting, scFv provide a direct molecular bridge between antigen recognition and viral entry. By displaying or coupling an scFv to an engineered envelope system, vector attachment can be redirected toward antigen-positive cells. This makes it possible to compare different tumor-associated antigens, such as EpCAM, mesothelin and PSMA, within a shared recognition mode.
scFv-based retargeting is also conceptually aligned with precision oncology. Vectors are designed to recognize a molecular feature of the target cell. In PDAC, where local expression of secreted modulators must be spatially restricted, this additional layer of specificity is central to the therapeutic strategy.

OBJECTIVES OF THE THESIS

The central objective of this thesis is to determine whether local microenvironmental reprogramming can convert pancreatic tumors from poorly infiltrated, immunosuppressive lesions into niches permissive to productive immune-cell activity. To address this question, this work explores the use of pseudotyped lentiviral vectors to deliver non-cytotoxic stroma remodeling and immunomodulatory transgenes, directly within the pancreatic tumor microenvironment.
This strategy is based on the hypothesis that a limited number of successfully transduced tumor or stromal cells may act as local bioactive hubs, producing signals that amplify beyond the initially targeted population.
A first objective was to engineer and compare retargeted lentiviral pseudotypes directed against selected tumor-associated antigens, including EpCAM, mesothelin and PSMA. This objective aimed to determine how antigen choice, scFv targeting and pseudotype architecture influence transduction efficiency, antigen dependence and entry.
A second objective was to determine whether targeted lentiviral vectors can convert tumor or stromal cells into local producers of immunomodulatory factors, using chemokines and decorin.
A third objective was to assess whether local chemokine expression can enhance the recruitment and positioning of effector lymphocytes within PDAC models. This includes evaluating whether CXCR3-ligand expression can increase CAR T cell migration toward pancreatic tumor lesions and improve their spatial distribution within three-dimensional or *in vivo* tumor contexts.
A fourth objective was to investigate whether decorin-mediated stromal remodeling can reduce physical and functional barriers that limit immune-cell infiltration and activity.

Finally, this thesis aims to test whether these microenvironmental modifications cooperate with CAR T cell therapy to improve antitumor efficacy in preclinical PDAC settings. The overall experimental strategy of this thesis is summarized in **Figure 11**.

An important safety rationale of this approach is that the selected transgenes are intended to be modulatory rather than directly cytotoxic. This does not eliminate the need for tumor-restricted delivery, but it distinguishes the strategy from suicide-gene or toxin-based systems, in which off-target transduction could directly damage healthy tissues. In the present framework, the therapeutic effect is expected to arise from local immune recruitment and stromal reprogramming rather than from forced elimination of the transduced cells.

Taken together, this thesis aimed to establish proof of principle that tumor-targeted lentiviral niche engineering can enhance CAR T cell efficacy in PDAC.

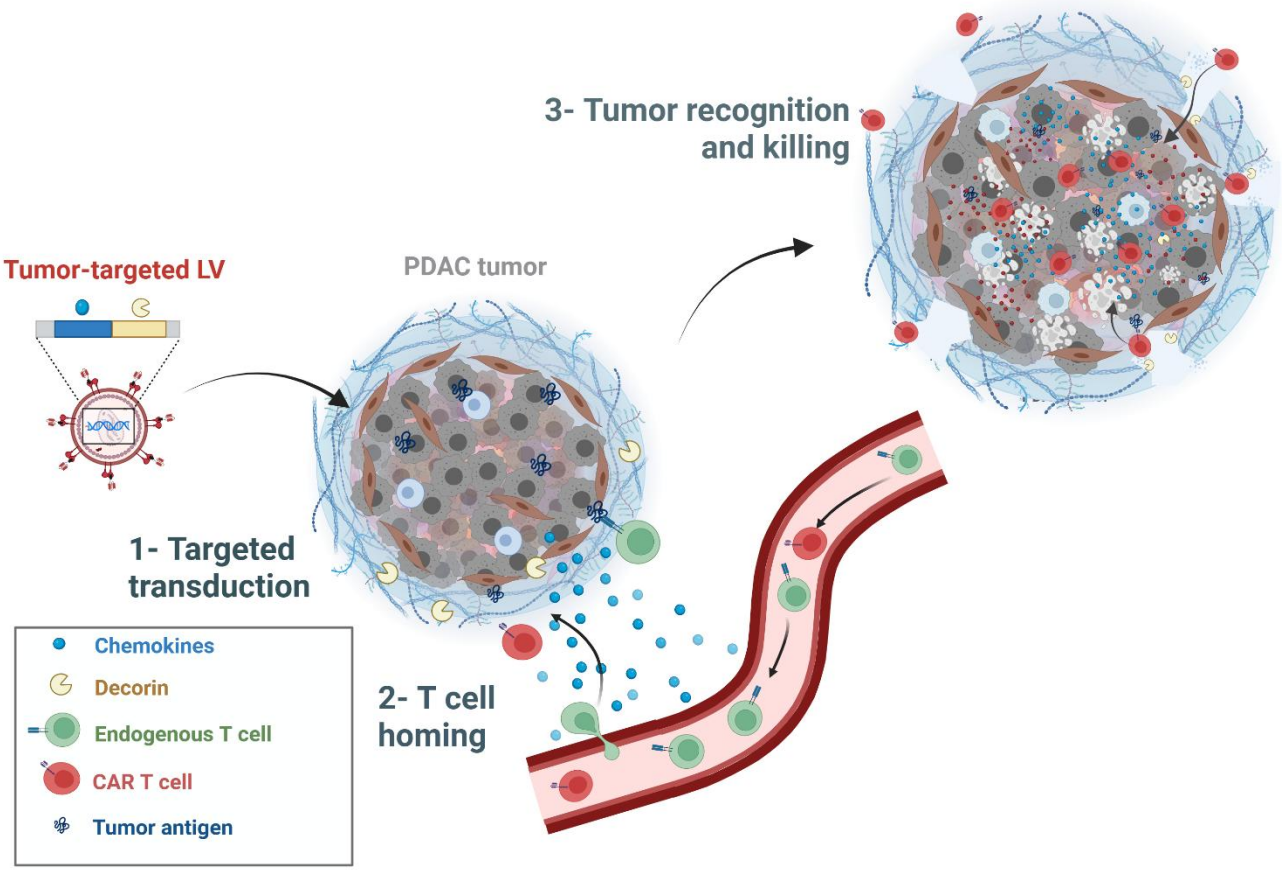


Figure 11: Tumor-targeted lentiviral niche engineering to enhance CAR T cell activity in PDAC

Tumor-targeted lentiviral vectors are designed to selectively transduce antigen-positive PDAC cells and deliver immunomodulatory payloads such as chemokines and decorin. This strategy aims to promote T cell homing, remodel stromal barriers and improve tumor recognition and killing by endogenous T cells and CAR T cells.

MATERIALS AND METHODS

The following section describes the main experimental procedures, reagents and analytical methods used throughout this thesis. Because some Results chapters are presented in manuscript format, selected methodological details are also repeated within the corresponding manuscript sections to preserve their internal structure and readability.

Plasmid construction

Lentiviral transfer plasmids were designed to express fluorescent reporters, luciferase reporters or therapeutic payloads, depending on the experimental setting. Reporter constructs encoded PGK-GFP for transduction efficiency readouts. For *in vivo* experiments, reporter constructs encoded MND-luciferase-IRES-ZsGreen. Therapeutic constructs encoded immunomodulatory or stromal-modulating proteins, including CXCL10 and decorin.

Retargeted envelope plasmids were generated using glycoprotein backbones derived from Sindbis virus (SINV), measles virus (MV), Nipah virus (NiV) or engineered vesicular stomatitis virus glycoprotein (VSV-G) platforms. The scFvs used in this study targeted human mesothelin, murine EpCAM or human PSMA.

Anti-human mesothelin clone SS1 and anti-mouse EpCAM clone G8.8 single-chain variable fragment (scFv) sequences were kindly provided by Dr. Sebastian Kobold, Munich, Germany. The anti-PSMA scFv sequence was kindly provided by Dr. Giulio Fracasso, Verona, Italy, from the pMIMOscFvD2B plasmid[184]. The anti-human CD8 scFv was obtained from the construct previously described by Zhou et al.[185]

For SINV-G, expression vectors of E2 were constructed by inserting the sequences of different scFvs between flexible linkers at amino acid (aa) 71 of E2 2.2 1L1L, as previously described[184]. For multi-antigen targeting experiments, two or three antigen-directed SINV E2 glycoproteins were co-transfected with the same final plasmid input to generate bispecific or trispecific lentiviral particles.

MV-based constructs used modified H and F glycoproteins, whereas NiV-based constructs used modified G and F glycoproteins. The MV and NiV plasmids were kindly provided by Dr. Els Verhoeyen. Following the same strategy, the scFv sequences were PCR amplified and individually cloned into the plasmids coding for MV-H (between *Sfi*I and *Not*I)[186] and NIV-G (between *Age*I and *Not*I)[187] using the In-Fusion HD Cloning Kit (Takara Bio).

The VSV-G envelope plasmid pMD2.G (#12259; Addgene) was provided by the Vectorology Vect'UB facility, University of Bordeaux. Site-directed mutagenesis was used to introduce in-frame scFv insertion cassettes targeting murine EpCAM or human mesothelin between residues T351 and T352 of VSV-G. This position was selected based on previous structural and functional work showing that this region is compatible with the insertion of exogenous targeting ligands in VSV-G[188].

All plasmid sequences were verified by Whole Plasmid sequencing before use.

Structural modeling of scFv-glycoprotein fusion constructs

The complete amino acid sequences of selected scFv-glycoprotein fusion constructs were analyzed *in silico* before experimental characterization. Fusion sequences were submitted to Alphafold servor structural prediction platform, to generate three-dimensional prediction models.

For each construct, predicted structures were inspected to evaluate global folding, preservation of the parental viral glycoprotein scaffold and exposure of the inserted scFv. The predicted orientation of the scFv relative to the glycoprotein backbone was also examined to assess whether the targeting domain was likely to remain accessible for antigen binding.

When available, published structures or reference models of the corresponding parental viral glycoproteins were used for comparison with the predicted fusion constructs. Final structures were visualized and colored using PyMOL version 3.0.0. Structural modeling was performed to assess the predicted compatibility of scFv insertion with the folding of the corresponding viral glycoprotein scaffold.

Cell culture

Human and murine cell lines were cultured at 37°C in a humidified incubator with 5% CO_2. HEK293T cells were used for lentiviral vector production. Panc02-WT, hFF-hTERT, SUIT-2 and MIA PaCa-2 cells were maintained in Dulbecco's modified Eagle's medium (DMEM, 4.5 g/L glucose; Gibco) supplemented with 10% fetal bovine serum (FBS) and 1% penicillin-streptomycin. The murine pancreatic tumor cell line T110299, derived from a KPC Ptf1a-Cre; LSL-$KRAS^{G12D}$; LSL-Trp53^fl/R172H^ mouse model, was kindly provided by Prof. Jens Siveke, University Hospital Essen, Germany, and was cultured under the same conditions. Prostate cancer cell lines PC3, PC3-PIP, 22Rv1 and LNCaP were cultured in RPMI 1640 medium (Gibco) supplemented with 10% FBS and 1% penicillin-streptomycin.

Human pancreatic cancer preclinical models included SUIT-2 and MIA PaCa-2 cell lines. Syngeneic murine pancreatic tumor models included Panc02-derived cell lines and T110299 cells. Prostate cancer models included PC3-PIP PSMA-positive and PC3-WT PSMA-negative cells, together with 22Rv1 and LNCaP cells when indicated. hFF-hTERT fibroblasts were used as non-tumoral control cells.

Antigen-modified cell lines were generated to stably express human mesothelin, murine EpCAM, human PSMA, or combinations of these antigens. Panc02-WT and T110299 cells were retrovirally engineered to express murine EpCAM (UniProt Q99JW5). Panc02-OVA-EpCAM cells were used as a murine pancreatic tumor model expressing murine EpCAM and have been modified with retroviral

vectors to express the chicken-derived ovalbumin antigen (UNIPROT entry P01012). T110299 EpCAM-negative and EpCAM-positive cells were used as additional murine tumor controls. MIA PaCa-2 and SUIT-2 cells were engineered to overexpress full-length human mesothelin by transduction with pMXs containing human MSLN cDNA (UniProt Q13421), generating MIA PaCa-2-hMSLN and SUIT-2-hMSLN cells. SUIT-2-EpCAM-PSMA cells were used as a poly-antigen human pancreatic tumor model expressing endogenous mesothelin, and murine EpCAM and human PSMA. Antigen-positive and antigen-negative populations were isolated by flow cytometry activated sorting after antibody staining when the percentage of the antigen is not specified otherwise.
Cells were passaged before confluence using trypsin and were tested monthly for mycoplasma contamination. For all experiments, cells were used at low to intermediate passage number after thawing.

Lentiviral vector production

Lentiviral vectors were produced by the Vectorology Vect'UB facility (TBMCore UAR 3427, University of Bordeaux) using HEK293T cells. Cells were co-transfected with a lentiviral transfer plasmid, the psPAX2 packaging plasmid (Addgene #12260) and the appropriate envelope plasmid encoding VSV-G, SINV-derived, MV-derived or NiV-derived glycoproteins, depending on the pseudotyping platform used. Reporter vectors used for the different experiments are mentioned in the specific associated sections. For monospecific targeted vectors, a single antigen-directed envelope plasmid was used during production. For bispecific or trispecific SINV-based vectors, two or three antigen-directed SINV envelope plasmids were co-transfected at equivalent proportions to allow co-display of multiple targeting glycoproteins on the same lentiviral particles.
Plasmid transfection was performed using calcium phosphate precipitation according to the facility protocol. Briefly, plasmid mixtures containing the transfer, packaging and envelope plasmids were prepared in calcium chloride and added to HEPES-buffered saline before distribution onto HEK293T cultures. Supernatants were collected 48 h after transfection and concentrated by Centricon® ultrafiltration (3,000 × g, 2-3 h, 4 °C). Concentrated vector stocks were aliquoted and stored until use. Vector production was quantified by p24 ELISA using the INNOTEST® HIV Antigen mAb kit (Fujirebio Europe). For *in vivo* experiments, in order to inject the same quantity of infectious particles of the different pseudotypes tested, viral titers were quantified by performing functional infectious titers. Antigen-positive target cells were transduced with serially diluted vector preparations. GFP expression was measured by flow cytometry 96 hours after transduction. Dilutions yielding 1-20% GFP-positive cells were used for titer calculation to remain within a linear range. Transductional titers were expressed as transducing units per milliliter (TU/mL) and calculated using the following formula: Titer (TU/mL)=(%GFP/100)×(Dilution factor/Volume of virus added (µL))×Number of cells seeded×1000.

For experimental comparisons, vectors were normalized either by p24 content or by infectious titer, as indicated in the corresponding figure legends.

Viral binding assay

Cell-surface binding of pseudotyped lentiviral particles was assessed by flow cytometry using an antibody directed against the G4S linker present in scFv-based envelope constructs. Target cells were detached using Accutase to preserve surface antigen expression and incubated with pseudotyped lentiviral particles normalized to equal p24 amounts across conditions.

Cells and viral particles were incubated for 30 min at 4°C on ice to allow surface binding while limiting particle internalization. After incubation, cells were washed once with cold PBS to remove unbound particles. Bound scFv-displaying particles were detected by staining with the Alexa Fluor 488-conjugated G4S Linker Rabbit monoclonal antibody (E7O2V; Cell Signaling Technology, #50515) for 30 min at 4°C. Cells were then washed once with cold PBS before acquisition.

Samples were acquired on a BD Accuri™ C6 Plus cytometer (BD Biosciences) and analyzed as Alexa Fluor 488-positive events. Viral binding was quantified as the Alexa Fluor 488 mean fluorescence intensity.

Cell transduction

Target tumor cells were seeded in 48-well plates at 1 × 10^4 cells per well and transduced with lentiviral particles at the indicated vector quantities, normalized according to p24 ELISA quantification or calculated infectious titer. 96 hours after transduction, cells were detached, washed with PBS supplemented with 2 mM EDTA, and analyzed by flow cytometry using a BD Accuri™ C6 Plus cytometer (BD Biosciences). Transduction efficiency was determined as the percentage of GFP-positive cells.

For antigen-dependence experiments, antigen-positive and antigen-negative cell lines were transduced in parallel with matched vector preparations. For receptor-density experiments, transduction levels were compared across cell lines expressing low, intermediate or high levels of the target antigen. For bispecific and trispecific SINV vectors, single-antigen and multi-antigen target cells were transduced with equal p24 input to compare the effect of combined receptor engagement.

For T cell transduction, peripheral blood T cells were prestimulated for 3 days using human CD3/CD28 TransAct reagent (Miltenyi Biotec, #130-111-160) in the presence of IL-2 (100 ng/mL; Miltenyi Biotec, #130-097-743). After stimulation, T cells were seeded at 3 × 10^4 cells per well in RetroNectin®-coated 96-well plates (Takara, #T100B; 12 µg/mL in PBS), prepared according to the manufacturer's recommendations. Cells were then transduced with lentiviral vectors at the indicated vector doses. Cytokines were replenished every 3 days. At 3- and 6-days post-transduction, cells

were analyzed by flow cytometry, and transduction efficiency was determined as the percentage of GFP-positive cells.

Saturation binding assay

Saturation binding assays were performed to quantify PSMA expression at the cell surface of prostate cancer cell lines. PC3-WT, PC3-PIP, 22Rv1 and LNCaP cells were seeded in 24-well plates at 2 × 10^5 cells per well, 24 h before the assay, and maintained at 37°C in 5% CO_2.
Cells were incubated with increasing concentrations of [^{177}Lu]Lu-PSMA-617, ranging from 0.1 to 100 nM, in the presence or absence of the competitive PSMA inhibitor 2-PMPA (10 µM; Sigma-Aldrich). After 2 h at 4°C, cells were washed twice with ice-cold DPBS (Gibco) to remove unbound tracer and lysed with 500 µL of 1 M NaOH.
Cell-associated radioactivity was quantified using a γ-counter (Wizard², PerkinElmer, USA). Specific binding was calculated by subtracting nonspecific binding measured in the presence of 2-PMPA from total binding. Binding affinity (Kd) and receptor density (Bmax) were determined by nonlinear regression using GraphPad Prism 10.2.3 (GraphPad Software, USA).
Experiments were performed in three independent replicates, with four technical replicates per condition.

Spheroid formation, imaging and spatial analysis

Multicellular spheroids were generated in 96-well ultra-low attachment plates (Corning, #7007). Antigen-expressing cells were first seeded to form the inner spheroid layer and centrifuged for 5 min at 100 × g to promote cell aggregation. After 24 h, antigen-negative tdTomato-positive cells were added to generate the outer layer, at a 1:3 ratio relative to the inner-layer cell number. Plates were centrifuged again under the same conditions. After an additional 24 h, spheroids were exposed to lentiviral particles at a MOI of 10, calculated relative to the number of inner-layer cells. Spheroids were maintained under standard culture conditions and monitored for 3 days.
For flow cytometry analysis, spheroids were mechanically dissociated into single-cell suspensions and stained with Fixable Viability Dye eBioscience™ eFluor™ 780 (#65-0865). Cells were then analyzed by flow cytometry to determine GFP expression according to tdTomato fluorescence and antigen expression status.
Spheroids were imaged using a CellCyte imaging system equipped with an Olympus 4× objective. Images were acquired using the spheroid module in transmitted light, GFP/FITC and mCherry channels over a 3-day period. Identical acquisition settings were used throughout each experiment. Images were processed using ImageJ/Fiji. Brightness and contrast were adjusted uniformly across images using identical display settings. For spatial analysis, concentric regions of interest were

defined from the spheroid center to the periphery using the tdTomato channel and then applied to the GFP channel. Concentric annuli were generated in 50-pixel increments using the Enlarge function and combined using the XOR command in the ROI Manager. Area, mean gray value and perimeter were measured for each annulus. GFP fluorescence intensity was then expressed as a radial profile across successive 50-pixel intervals from the spheroid center to the periphery.

Collagen-embedded 3D tumor cultures

Collagen-embedded 3D tumor cultures were generated from tumor cells grown under standard adherent culture conditions. Cells were detached using trypsin, counted, centrifuged to obtain a cell pellet and gently resuspended in a neutralized collagen mixture containing collagen, NaOH and 10× PBS. The collagen mixture was maintained on ice throughout preparation to prevent premature polymerization.

A 1 µL drop of the cell-containing collagen suspension was seeded into each well of a flat-bottom 96-well plate and incubated for 5 min at 37°C to allow collagen polymerization. Pre-warmed culture medium was then gently added on top of the polymerized collagen droplets. Cells were maintained under standard culture conditions and allowed to grow directly within the collagen fiber network.

These collagen-embedded spheroids were used either for lentiviral vector transduction assays or CAR T cell killing assays. For transduction experiments, lentiviral particles were added at the indicated vector doses 24 hours after collagen polymerization. GFP expression was monitored by imaging and quantified by flow cytometry after collagenase digestion. For CAR T cell killing assays, CAR T cells were gently added on top of the collagen droplets at the indicated effector-to-target ratios, and tumor cell killing was monitored over time by Incucyte live-cell imaging.

CAR T cell production

Human anti-mesothelin CAR T cells were generated from CD14-negative peripheral blood mononuclear cells obtained from healthy donors. Cells were cultured in complete human T cell medium composed of RPMI 1640 supplemented with 2,5% Human Serum, 2 mM L-Glutamine, 100 IU/ml Penicillin, 100 µg/ml Streptomycin and 1 mM Sodium Pyruvate. Recombinant human IL-2 and IL-15 were added freshly during activation and expansion.

CD14-negative PBMCs were activated using human CD3/CD28 Dynabeads and maintained under standard culture conditions for 48 hours before retroviral transduction. Activated T cells were transduced with retroviral supernatants produced from the 293Vec-RD114-CAR-MSLN producer cell line.

Briefly, the anti-mesothelin CAR construct was generated using the retroviral pMP71 backbone, kindly provided by Prof. Christopher Baum, Hannover, Germany. The CAR cassette encoded an

anti-human mesothelin antigen-recognition scFv fused to the corresponding hinge, transmembrane and intracellular signaling domains used for T cell activation. For retroviral vector production, 293Vec-RD114 packaging cells were used, kindly provided by Dr. Manuel Caruso, Québec, Canada. The pMP71 vector carrying the CAR-MSLN sequence was stably introduced into 293Vec-RD114 cells to generate a retroviral producer cell line. Single-cell clones were isolated and screened for retroviral production by assessing the transduction efficiency of primary human T cells.

The selected 293Vec-RD114-CAR-MSLN producer clone was used to generate retroviral supernatants for the transduction of activated human T cells.

Transduction was performed by spinoculation for 1.5 hours at 3000g at 32°C on RetroNectin-coated non-tissue culture-treated plates. Cells were then maintained in complete human T cell medium supplemented with IL-2 and IL-15.

After transduction, T cells were expanded by regular medium renewal and cytokine supplementation every second day. Cell density was adjusted at 10^6 cells per mL during expansion to maintain active proliferation. Transduction efficiency was assessed by flow cytometry 4 days after transduction, based on CAR detection. Human CAR T cells were used for *in vitro* functional assays and *in vivo* adoptive transfer experiments after 8 days expansion.

OT-I T cell preparation

OT-I T cells were prepared from spleens collected from OT-I mice (C57BL/6-Tg(TcraTcrb)1100Mjb/J; The Jackson Laboratory). OT-I mice express a transgenic T cell receptor specific for the ovalbumin-derived SIINFEKL peptide presented by the MHC class I molecule H-2K^{b}. This model was used to generate antigen-specific murine CD8^{+} T cells recognizing Panc02-OVA-EpCAM.

Spleens were mechanically dissociated through a 30 µm cell strainer to obtain single-cell suspensions. Cells were centrifuged and erythrocytes were lysed for 2 min using sterile-filtered ACK lysis buffer containing 0.15 M NH_4Cl, 1.0 mM $KHCO_3$ and 0.1 mM Na_2EDTA in water, pH 7.2-7.4.

Splenocytes were adjusted to 2 × 10^{6} cells/mL and cultured in complete murine T cell medium composed of RPMI 1640 supplemented with 10% heat-inactivated fetal calf serum, 100 IU/mL penicillin-streptomycin, 2 mM L-glutamine, 1 mM sodium pyruvate and 1 mM HEPES. Recombinant IL-2 (10 UI/ml), IL-15 (20 ng/ml), β-mercaptoethanol 50 µM, 4 x 10^{5} sodium acid-free mouse T cell Activator beads/ml (Mouse T cell activator CD3/CD28 Dynabeads, Invitrogen, #11452D) were added to support T cell expansion.

Every 48 hours, cells were counted and adjusted to 1 × 10^{6} cells/mL in fresh complete murine T cell medium supplemented with IL-2, β-mercaptoethanol and IL-15. OT-I T cells were used for *in vitro* assays or *in vivo* adoptive transfer experiments after four expansion cycles.

Cytokine protein level quantification

Murine and human IFNγ were quantified using ELISA sets from BD Biosciences (555138 and 555142, respectively). Murine and human CXCL10 were quantified using DuoSet ELISA from R&D Systems (DY466 and DY266, respectively). Murine and human Decorin were quantified using DuoSet ELISA from R&D Systems (DY1060 and DY143, respectively).

Migration assay

T cell migration was assessed using Transwell plates (Corning) with 3 µm pore-size membranes for murine T cells and 5 µm for human T cells. CAR T cells or OT-I T cells were harvested, counted and resuspended in migration medium composed of OptiMEM supplemented with 1% BSA.

For T cell migration toward recombinant chemokines, recombinant CXCL10 was diluted in the same migration medium and added to the lower chamber at a final concentration of 100 ng/mL. Migration medium alone was used as a negative control. A total of 0.5×10^6 T cells were added to the upper chamber of each Transwell insert. Each condition was performed in triplicate. Plates were incubated for 3 h at 37°C to allow chemokine-directed migration. After incubation, cells that had migrated into the lower chamber were collected and analyzed by flow cytometry using a BD FACS Canto II flow cytometer. Absolute migrated cell numbers were determined using CountBright™ Absolute Counting Beads (Invitrogen, #C36950). Briefly, 3 µL of counting beads diluted in 50 µL PBS were added to each FACS tube before acquisition. The absolute number of migrated cells was calculated from the ratio of cell events to bead events.

When indicated, T cell migration was also assessed toward tumor cells plated in the lower chamber of the Transwell system. Tumor cells were seeded in the bottom chamber 48 hours before the assay and allowed to adhere and secrete the different therapeutic elements. Depending on the experimental condition, tumor cells expressed and secreted chemokine alone or chemokine together with decorin. Control wells contained mock-transduced tumor cells or migration medium alone. CAR T cells or OT-I T cells were first stained with CellTrace™ Violet 5 µM (C34557) to distinguish them from tumor cells, and added to the upper chamber in migration medium and allowed to migrate for 3 h at 37°C. Migrated CTV^+ T cells were then collected from the lower chamber and quantified by flow cytometry using CountBright™ Absolute Counting Beads, as described above. This setup was used to evaluate whether chemokine secretion by engineered tumor cells, with or without decorin co-expression, promoted T cell recruitment.

Tumor-cell killing assay using Incucyte

Tumor-cell killing was monitored in real time using the Incucyte live-cell imaging system. Tumor cells were seeded in 96-well plates and allowed to adhere overnight. For 3D assays, tumor spheroids were generated before immune-cell addition as described above. Tumor cells expressed the red fluorescent reporters tdTomato.

CAR T cells or OT-I T cells were added at the indicated effector-to-target ratios. For cytotoxicity measurements, Incucyte Cytotox Green reagent was added according to the manufacturer's instructions. Plates were imaged every 3 hours for 2D assays and every 6 hours for spheroids experiments, using phase contrast and fluorescence channels (Red for tumor cells and green for cytotox green dye).

For 2D killing assay, killing was quantified using Cytotox green reagent. Cytotox Green accumulation was monitored over time and quantified as Green Integrated Intensity per Well / Phase Area Confluence, normalized to the time of effector cell addition. For spheroids killing experiments, the red tumor cell signal was monitored as Total Red Object Integrated Intensity, expressed as RCU × µm² per well, and normalized to the time of effector cells addition.

Conditions without effector cells and with untransduced T cells were used to measure spontaneous tumor-cell growth and basal cell death. Mock-transduced tumor cells were used as controls for therapeutic-vector conditions.

Flow cytometry

Cells were collected, washed in PBS + EDTA 2mM and stained with fixable viability dye eFluor™ 780 (Invitrogen). T cells surface staining was performed using CXCR3, CD45 and CD3 antibodies. For tumor-cell antigen analysis, antibodies against human mesothelin, murine EpCAM and human PSMA were used.

Samples were acquired on BD Accuri™ C6 Plus cytometer (BD Biosciences) or BD FACSCanto II (BD Biosciences). Data were analyzed using FlowJo v10. Gates were defined using unstained cells, single-stained controls or non-transduced controls, depending on the experiment. Dead cells and debris were excluded before quantification.

In vivo experiments

NOD.Cg-Prkdc^{scid} Il2rg^{tm1Wjl}/SzJ (NSG) mice were bred and maintained in a specific pathogen-free facility at the University of Bordeaux (agreement no. 55841). All procedures were approved by the Institutional Animal Care and Use Committee. Mice aged 8 weeks or more were randomized into treatment groups. Tumor growth and general health were assessed every other day.

For subcutaneous xenograft implantation, mice were induced with 5% isoflurane in air at a flow rate of 2 L/min and maintained with 2% isoflurane throughout the procedure. 5×10^5 tumor cells in 100 µL PBS were injected subcutaneously into the right flank. Tumor size was measured using calipers and tumor volume was calculated using the formula: volume = length × width² / 2. When tumors reached 100-150 mm³, around 7 days after implantation, the appropriate viruses (as described in the Results section) were injected intratumorally or intra-veneously in 100 µL PBS. Tumor bioluminescence was monitored twice a week after intraperitoneal administration of D-luciferin (IVISbrite D-Luciferin Potassium Salt Bioluminescent Substrate 150mg/kg resuspended in PBS, Revvity). Imaging was performed on a photon imager (photonIMAGERTM, RT Biospace Lab), and signals (ph/s/sr) were quantified using M3Vision software (BIOSPACE LAB). For ACT experiments, OT-I T cells were injected intravenously at $1x10^6$ cells per mouse, 14 days after tumor implantation.

For *in vivo* vector targeting experiments, PC3 PSMA-positive and PSMA-negative tumors were implanted subcutaneously in opposite flanks or in separate animals, depending on the experiment. Once tumors reached 100-150 mm³, mice received intravenous injection of TU-normalized lentiviral vectors pseudotyped with anti-PSMA SINV glycoproteins or control VSV-G in 100µL PBS. Tumor-free mice were included when indicated to assess off-target biodistribution. Reporter expression was analyzed by *in vivo* imaging and by *ex vivo* analysis of tumors and organs as mentioned above.

For orthotopic pancreatic tumor experiments, $5x10^4$ SUIT-2-hMSLN-luciferase cells were injected into the pancreas of NSG mice under anesthesia, induced with 5% isoflurane in air at a flow rate of 1 L/min and oxygen at a flow rate of 1 L/min and maintained with 2.5% isoflurane throughout the procedure. Tumor engraftment and growth were monitored by bioluminescence imaging after intraperitoneal injection of D-luciferin. Mice were randomized into treatment groups based on tumor signal before therapeutic intervention. Anti-mesothelin CAR T cells were injected intravenously at the indicated dose, 8 days after tumor implantation. Tumor progression was followed by serial bioluminescence imaging.

At endpoint, mice were euthanized and tumors, liver, spleen, lungs, kidneys and other relevant organs were collected. Tissues were processed for flow cytometry, histology, immunofluorescence or bioluminescence analysis.

Proteomic analysis

Protein samples were analyzed by the Bordeaux Proteome platform using an in-gel digestion and label-free quantitative mass spectrometry workflow. Samples were separated by short migration on 10% acrylamide SDS-PAGE gels, stained with colloidal blue and processed for in-gel trypsin digestion after reduction and alkylation. Peptides were extracted, acidified and analyzed by LC-MS/MS on an Orbitrap Fusion Lumos Eclipse mass spectrometer using a 146-min DIA acquisition method.

Raw files were processed using Proteome Discoverer 3.3 with Chimerys as the search algorithm. Spectra were searched against the Homo sapiens UniProt database RPS_GC_2026_01_Homo_sapiens_UP000005640_9606, supplemented with a contaminant database. Trypsin was used as the digestion enzyme, with up to two missed cleavages allowed. Carbamidomethylation of cysteine was set as a static modification. Oxidation of methionine, protein N-terminal acetylation, methionine loss and methionine loss combined with acetylation were included as dynamic modifications.

Protein quantification was performed using a label-free precursor ion intensity-based workflow. Unique and razor peptides were used for protein quantification, and protein abundance was calculated using a TOP3 approach. Normalization was performed using human proteins. Normalized proteomic datasets were log2(x + 1)-transformed. A total of 5,848 unique proteins were retrieved. Missing values were imputed using the MissForest implementation with default parameters from the DreamAI R package, as previously described[189]. Data were batch-corrected by culture group using the ComBat R package. Principal component analysis was performed to visualize sample clustering.

Differential protein abundance was analyzed at the protein level by pairwise comparisons between treatment groups. Tumor-cell comparisons were analyzed in unpaired mode, whereas CAR T cell-only and CAR T cell coculture comparisons were analyzed in paired mode to account for donor matching. Differentially expressed proteins were identified using an adjusted p value < 0.05, corresponding to a false discovery rate of 5%, together with the log2 fold-change thresholds specified in the corresponding figure legends.

Gene Ontology enrichment analysis was performed for Biological Process, Molecular Function and Cellular Component terms using the clusterProfiler package. Gene set enrichment analyses were performed on pre-ranked protein-level differential abundance tables using the t value from pairwise statistical comparisons and the fgsea package. Hallmark, Reactome, KEGG, Gene Ontology and C7 immunologic signature gene sets were used when indicated. Enriched pathways were selected based on a normalized enrichment score > 2 and an adjusted p value < 0.05.

Heatmaps of selected proteins were generated from normalized protein abundance values using the ComplexHeatmap R package and displayed as row z-scores when indicated. Volcano plots, PCA plots, enrichment plots and violin plots were generated using ggplot2. Violin plots were generated from donor-level normalized abundance values, with paired statistical comparisons when indicated.

Statistical analysis

All experiments were performed at least in biological duplicate and technical triplicate unless stated otherwise. Results are presented as mean ± standard deviation (SD) for in vitro experiments and as mean ± standard error of the mean (SEM) for in vivo experiments, unless otherwise indicated in the figure legends. Statistical analyses were performed using GraphPad Prism 8.0.2 or 11.0.1.

For viral binding assays, ratios were calculated relative to the antibody-only condition within each independent experiment and $\log_2$-transformed before statistical analysis. Differences between pseudotypes were analyzed using a mixed-effects model with experiment as a matched factor, followed by Tukey's multiple-comparisons test.

For comparisons between two groups, statistical significance was evaluated using two-tailed Student's t tests when data distribution and experimental design were appropriate. Paired tests were used for donor-matched CAR T cell experiments, whereas unpaired tests were used for independent experimental groups. For comparisons involving more than two groups, one-way ANOVA was used, followed by Tukey's multiple-comparisons test as indicated in the figure legends.

For time-course cytotoxicity experiments, statistical analyses were performed on endpoint values, area under the curve or slopes over the indicated time intervals, as specified in the corresponding figure legends. Nonlinear regression analyses for binding parameters were performed using the least-squares method.

Proteomic statistical analyses were performed as described in the proteomic analysis section. A p value < 0.05 was considered statistically significant.

RESULTS

I. Comparative evaluation of lentiviral pseudotyping platforms for tumor-targeted gene delivery

The first part of this Results section is presented as a manuscript entitled “Comparative lentiviral pseudotyping identifies Sindbis virus glycoprotein as a versatile platform for highly specific in vivo tumor targeting.” This study addresses the choice of viral envelope as a central determinant of targeted lentiviral delivery. It compares several scFv-retargeted pseudotyping platforms, including Sindbis virus, Measles virus, Nipah virus and engineered VSV-G envelopes, using matched tumor antigens and solid tumor models. The aim was to identify which platform could support efficient, antigen-dependent and tumor-restricted gene transfer, and to define the parameters that influence productive entry. The manuscript first evaluates targeted transduction in two-dimensional tumor cell models, then examines antigen abundance, three-dimensional tumor organization, antigen heterogeneity and *in vivo* biodistribution. Together, these results establish SINV-derived glycoproteins as the most robust and versatile platform tested for receptor-targeted lentiviral delivery to solid tumors.

Comparative lentiviral pseudotyping identifies Sindbis virus glycoprotein as a versatile platform for highly specific *in vivo* tumor targeting

J Rossi[1], N Richet[1], C Martinello[2], S Kobold[3,4,5,6], L Ali[7], C Morgat[7,8], R Sorrentino[1], L Sarmiento[1], S Michaelides[3], MJ Abrey-Recalde[1], L Mora Charrot[9], J Izotte[9], J Gillibert-Duplantier[10], I Moranvillier[1], M Lalanne[1], J Baud[1], C Charbonnieras[10], S Périan[11], JM Blouin[1], E Richard[1,12], S Amintas[1,13], A Bedel[1,12], F Moreau-Gaudry[1], V Guyonnet-Dupérat[10#], E Verhoeyen[2,11#], and S Dabernat[1,12#]

#, co-corresponding authors

Affiliations

1 Univ. Bordeaux, INSERM, BRIC, U 1312, F-33000 Bordeaux, France

2 Université Côte D'Azur, INSERM, C3M, 06204 Nice, France

3 Institute of Clinical Pharmacology, LMU University Hospital, LMU Munich, Munich, Germany

4 German Cancer Consortium (DKTK), Partner Site Munich, a partnership between the DKFZ Heidelberg and the LMU University Hospital, LMU Munich, Germany.

5 Einheit für Klinische Pharmakologie (EKLiP), Helmholtz Zentrum München - German Research Center for Environmental Health Neuherberg, Germany.

6 German Center for Lung Research (DZL), partner site Munich

7 INCIA, University of Bordeaux, CNRS, EPHE, UMR 5287, Bordeaux, F-33000, France

8 Radiopharmacy & Nuclear Medicine Department, Bordeaux University Hospital, Bordeaux, F-33000, France

9 Univ. Bordeaux, Animalerie A2, Service Commun des Animaleries, 33076 Bordeaux, France

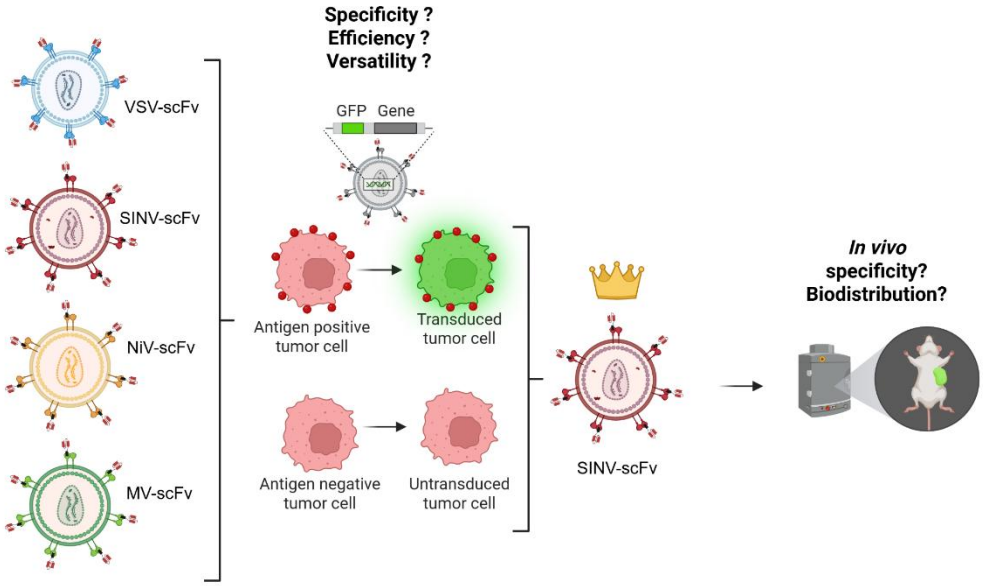
10 Plateforme VECT'UB, INSERM US 005 - CNRS UMS 3427- TBMCore, Université de Bordeaux, F-33000 Bordeaux, France

11 CIRI - International Center for Infectiology Research, Inserm, U1111, Université Claude Bernard Lyon 1, CNRS, UMR5308, Ecole Normale Supérieure de Lyon, Université Lyon, 69007 Lyon

12 CHU Bordeaux, Department of Biochemistry, Pellegrin Hospital, 33000 Bordeaux, France

13 CHU Bordeaux, Tumor Biology Department, Haut Leveque Hospital, 33600 Pessac, France

Graphical abstract



Abstract

In vivo cancer gene therapy necessitates constraining viral entry specifically into cancer cells. We performed a systematic comparison of single-chain variable fragment (scFv)-retargeted LVs pseudotyped with viral glycoproteins from Sindbis (SINV), measles (MV), and Nipah (NiV) viruses using matched targeting modules and tumor cell models.

SINV-derived pseudotypes were the only vectors to reproducibly combine gene transfer and strong antigen specificity. In contrast, MV-, NiV-, and engineered VSV-G-based targeted pseudotypes showed little or no productive transduction. Computational structural analyses did not reveal major instability of the retargeted envelopes, suggesting that productive entry was primarily constrained by platform-specific infectivity. Close analysis of predicted antigen epitope/scFv interaction revealed a 50Å maximal distance for functional fusion membrane using the NiV platform. Focusing on SINV, we found that transduction increased with antigen abundance.

In layered 3D spheroids, compared to VSV-G, SINV-scFv pseudotypes retained antigen-dependent spatial specificity, produced more homogeneous gene delivery and promoted gene transfer within antigen-positive tumor compartments more efficiently. Expanding SINV targeting to multiple tumor antigens improved transduction in antigen-heterogeneous models. *In vivo*, SINV-scFv vectors mediated antigen-dependent transduction after intratumoral and intravenous administration.

Together, these results identify SINV pseudotyping as a robust and versatile platform for *in vivo* targeted LV delivery.

Introduction

Gene therapy, originally developed to treat inherited genetic diseases, has become an increasingly powerful strategy in oncology. The first approved gene therapies were applied to cancer (1,2), but their use remained limited until the recent genetic engineering of immune cells, particularly T cells, which transformed cancer immunotherapy. They restored tumor-specific responses and achieved durable remissions in subsets of patients (3). Reflecting this progress, cancer now represents the main focus of the field, accounting for more than half of all clinical trials and the majority of approved gene therapy products (4).

The main challenge for cancer gene therapy is the precise and efficient delivery of therapeutic transgenes into tumor cells while minimizing off-target effects in healthy tissues (5). Solid tumors add a layer of complexity, as they are composed not only of heterogenous malignant cells but also stromal and immune populations that can influence therapeutic outcomes. These neighboring subpopulations may dilute the target tumor cells. Achieving safe and effective treatment, therefore, requires delivery systems that combine efficiency, durability, and tumor specificity.

Lentiviral vectors (LVs), derived from HIV-1, offer an attractive shuttle system (6), especially for in vivo gene transfer (7). With the ability to stably integrate large transgenes into both dividing and non-dividing cells (8,9), LVs have demonstrated strong safety and efficacy across diverse settings, including approved *ex vivo* therapies such as CAR T cell products (10,11). However, the broad tropism and integrative nature of conventional LVs, pseudotyped with the vesicular stomatitis virus glycoprotein (VSV-G), raise safety concerns for *in vivo* delivery of gene therapy.

To overcome this limitation, multiple pseudotyping strategies have been developed with variable targeting modules attached to glycoproteins to redirect entry toward tumor-associated antigens (11,12). These approaches are conceptually attractive, assuming that by selecting an antigen preferentially expressed on tumor cells, lentiviral vectors can, in principle, achieve high specificity (11). This antigen-centric paradigm has guided many retargeting efforts in the field. However, retargeting approaches have rarely been compared across various donor glycoproteins. The distance of the attachment site relative to the plasma membrane was shown to be crucial using different recognition moieties attached to Nipah glycoprotein (NiV-G) or Measles glycoprotein (MV-H) targeting several surface antigens (13).

Single-chain variable fragments (scFvs) provide a biologically driven targeting strategy by mimicking antibody/antigen recognition. They are particularly well-suited for recognizing tumor-associated antigens, their biology is well-known, and their cloning engineering has been optimized to reach the same affinity as a full monoclonal antibody (14). Many scFv-based LV pseudotyping strategies have been reported against diverse surface antigens. Published work suggests that the outcome of scFv-based lentiviral retargeting is shaped by the underlying glycoprotein platform itself, with measles-,

Nipah-, Tupaia-, VSV-G-, and canine distemper-derived systems displaying distinct infectious titers and gene-transfer efficiencies (13,15-17).

Overall, side-by-side comparative studies using the same recognition moiety against the same target antigen on the same cell background are lacking, particularly in the context of tumor antigen targeting, where lentiviral vectors are of strong interest for gene therapy applications (11). To meet this need, we performed a systematic comparative analysis of multiple lentiviral pseudotyping glycoproteins engineered to incorporate identical scFv-based targeting modules across distinct tumor-associated antigens. The most effective pseudotyping configuration was then challenged for *in vivo* delivery using both intratumoral and systemic administration in xenograft models.

Results

Comparative pseudotyping reveals divergent targeting efficiencies across viral glycoproteins.

We hypothesized that LV pseudotyping based on scFv-targeting modules might depend (i) on the nature of the viral glycoprotein to which it is attached and (ii) on the targeted antigen. To test these hypotheses, we built fusion glycoprotein envelopes against epithelial tumor antigens frequently expressed in solid cancers, including human mesothelin (MSLN) and murine EpCAM (18,19), and tested them on pancreatic cancer *in vitro* models. The engineered viral glycoproteins cover distinct entry and fusion mechanisms. We compared scFv protein fusion to viral donor glycoproteins presenting uncoupled recognition and fusion protein entities, from SINV, MV, and NiV. We also generated targeted VSV-G variants by inserting scFvs into the VSV-G ectodomain. Because VSV-G is a single glycoprotein responsible for both receptor engagement and membrane fusion, we selected a previously described permissive insertion site between residues T351 and T352, which had been shown to allow display of foreign targeting ligands while preserving VSV-G functionality (20). AlphaFold structural predictions indicate that scFv insertion does not induce major predicted disruption of the envelope glycoproteins (**Figure 12A** the scFv moiety is red on each glycoprotein**,** **Table 2**).

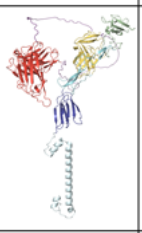
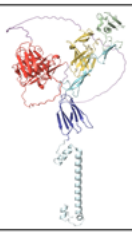
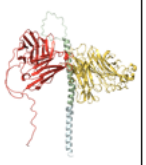
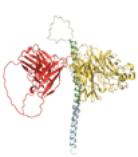
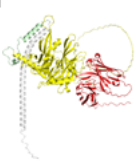
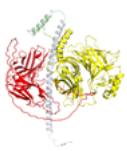
Origin	VSV		SINV		NIV		MV	
Family	Rhabdoviridae		Alphavirus		Paramyxovirus		Paramyxovirus	
Viral Glycoprotein	**VSV-G** (combined receptor recognition and fusion)		E1/E2/E3 heterodimers forming the spikes **E2** for recognition		F/G dimers **G** for recognition and **F** for fusion		F/H dimers **H** for recognition and **F** for fusion	
Entry mechanism	Endocytosis		Endocytosis		Membrane fusion		Membrane fusion	
Natural tropism	broad tropism via LDLR		broad cell tropism via surface proteins (e.g. heparin)		respiratory, CNS, endothelial, and urinary tropism via ephrin-B2/B3 receptors		immune-cell tropism via SLAM/CD150 receptors	
Target antigen	**EpCAM**	**hMSLN**	**EpCAM**	**hMSLN**	**EpCAM**	**hMSLN**	**EpCAM**	**hMSLN**
Alphafold Modelisation								
Infectious titrer	**0.00** TU/mL	**0.00** TU/mL	**6.23.10^5** TU/mL	**1.74.10^7** TU/mL	**1.33.10^4** TU/mL	**1.93.10^4** TU/mL	**3.85.10^4** TU/mL	**3.33.10^4** TU/mL
Specific infectivity	**0.00** TU/ng p24	**0.00** TU/ng p24	**54.82** TU/ng p24	**153.2** TU/ng p24	**0.28** TU/ng p24	**0.41** TU/ng p24	**2.03** TU/ng p24	**0.18** TU/ng p24
ΔG	**193.6** kcal/mol	**140.7** kcal/mol	**445.4** kcal/mol	**447.2** kcal/mol	**304.7** kcal/mol	**310.3** kcal/mol	**136.6** kcal/mol	**584.1** kcal/mol
$\Delta\Delta G$ $\Delta G_{pseudotyped} - \Delta G_{native}$	**108,7** kcal/mol	**55,77** kcal/mol	**311.3** kcal/mol	**313,1** kcal/mol	**130.2** kcal/mol	**136.1** kcal/mol	**-6.84** kcal/mol	**220.3** kcal/mol

Table 2: Comparative structural and functional characterization of retargeted lentiviral envelope platforms.

VSV-G-, SINV-, NiV- and MV-derived glycoproteins were compared according to their viral origin, glycoprotein organization, entry mechanism, natural tropism, predicted AlphaFold-based structure, infectious titer, specific infectivity and predicted stability parameters. Retargeted envelopes were engineered to display scFvs directed against either EpCAM or hMSLN. Infectious titers are expressed as TU/mL, and specific infectivity as TU/ng p24. ΔG values correspond to the predicted stability of the engineered envelope models, whereas ΔΔG was calculated as the difference between the predicted stability of the pseudotyped envelope and its corresponding native glycoprotein. Despite higher predicted ΔΔG values, SINV-derived pseudotypes showed the highest infectious titers and specific infectivities, indicating that predicted global destabilization alone does not account for functional pseudotyping efficiency.

Murine T110299 cells, negative or positive for EpCAM expression, human MIA PaCa-2-WT cells and human SUIT-2 cells, with low and high MSLN expression respectively (see **Supplementary Figure 18A,B**) were transduced with lentivirus pseudotyped scFv-retargeted VSV, SINV, NIV or MV glycoproteins, carrying a GFP reporter. All cell lines were highly transduced (>90%) with LVs pseudotyped with the native VSV Glycoprotein *(data not shown).*

We first asked whether the transduction efficiencies were similar using the same physical amount of LV particles (same p24 input = 50 ng). For both models, VSV, NIV and MV scFv-pseudotyped vectors did not show any transduction of the 4 cells lines (between 0%, up to 1 +/- 0.52 % of transduced cells) whereas only the SINV scFv-pseudotyped lentivectors achieved high levels of transduction, in the targeted antigen-expressing cells (T110299-EpCAM-positive, MIA PaCa-2 and SUIT-2 cells, 27.4 ± 5.8%, 39.9 ± 6.8% and 76.6 ± 4.7%, respectively) **(Figure 12B,C)**. Importantly, the T110299-

EpCAM-negative cells showed 1.56 +/- 0.91% of transduced cells, suggesting a very low level of aspecific transduction **(Figure 12B)**. Next, we compared the specific infectivity across the different glycoprotein pseudotypes **(Table 2).** Quantification of infectious units relative to particle content revealed major differences in specific infectivity, with SINV preparations reaching 55 and 153 TU/ng p24 (6.23x10^5 and 1.74x10^7 TU/mL) for EpCAM and MSLN models, respectively, compared with 0.28 and 0.41 TU/ng p24 for NiV and 2.03 and 0.18 TU/ng p24 for MV. Therefore, the superior performance of SINV under p24-normalized conditions is strongly influenced by a substantially higher functional particle yield. Finally, at a high particle input, MV-scFv-EpCAM LVs mediated low but detectable transduction of EpCAM-positive cells, while remaining largely inactive on EpCAM-negative cells, indicating a partial rescue of transduction **(Figure 12D)**. Similarly, NIV-scFv-hMSLN LVs mediated low but detectable transduction of hMSLN-positive cells **(Figure 12E).**

To determine whether functional performance could be predicted by global structural stability, we performed *in silico* stability analysis of the engineered envelopes (**Table 2**). Predicted destabilization, reflected by increased ΔΔG relative to the corresponding native envelope, did not correlate with transduction efficiency. SINV-derived envelopes presented the highest increase in entropy, as compared to the native glycoprotein *in silico*, yet they generated the highest infectious titers and specific infectivities. Conversely, NiV- and MV-derived pseudotypes showed lower or intermediate drops in entropy despite the lower infectivity. These observations suggest that potential loss of stability is not involved in pseudotype functionality and/or productive assembly.

Before investigating further the markedly different performance of MV- and NiV-derived pseudotypes relative to SINV-derived vectors, we verified that each system used the expected entry pathway in our target cells. To this end, cells were treated with bafilomycin A1, an inhibitor of endosomal acidification, to discriminate pH-dependent endocytic entry from receptor-triggered membrane fusion. Bafilomycin A1 reduced 3.9 times SINV-scFv transduction, consistent with a requirement for endosomal acidification and pH-dependent fusion. In contrast, MV-mediated transduction was minimally affected, in agreement with the membrane-fusion entry mechanism of paramyxovirus-derived envelopes **(Figure 12F)**. These data confirm that the engineered pseudotypes retain entry-route features of their parental viral glycoproteins.

We next investigated whether the poor performance of non-SINV pseudotypes resulted from impaired binding to antigen-positive cells. To this end, we quantified cell-associated viral particles using an antibody recognizing the G4S linker present in the scFv module **(Figure 12G)** in the EpCAM targeting model. All retargeted particles showed detectable binding to EpCAM-positive cells, whereas binding to EpCAM-negative cells remained at background levels, confirming antigen-dependent attachment **(Figure 12H)**. Although SINV particles tended to generate higher cell-associated signals, binding differences with the other viral particles could not reflect the large differences observed in transduction efficiency. These data indicate that cell-surface attachment is not a limiting step for the lesser performing MV and NiV-derived pseudotypes.

EpCAM and mesothelin reside in different membrane environments. EpCAM is a transmembrane glycoprotein that can associate with tetraspanin-enriched membrane complexes and mild detergent-resistant membrane fractions (21), and mesothelin as a GPI-anchored protein likely enriched in cholesterol-rich ordered domains (22). We used methyl-β-cyclodextrin (MβCD) as a functional tool to deplete membrane cholesterol, expecting improvement of virus entry under mesothelin but not EpCAM recognition. We found no difference in transduction efficiency for MV and NiV-derived pseudotypes, suggesting that cholesterol-dependent membrane microdomains are unlikely to be the primary barrier to productive entry in our tumor cell models (**Supplementary Figure 18C,D**).

CD8-directed lentiviral retargeting has previously been demonstrated using both Measles and Nipah virus-derived targeting systems (13,23). We tested scFv-CD8-retargeting in NiV- and SIN-V-derived LVs and found comparable transduction efficiencies (8.62E+05 ± 9.72E+04 TU/mL and 6.56E+05 ± 1.31E+05 TU/mL, respectively**, Figure 12I)**, attesting the validity of scFv targeting module with NiV-G, and showing that NiV-G can be as efficient as SINV-G, when targeting specific receptors.

Together, these results identify SINV as the most efficient and robust platform among the retargeted glycoproteins tested. SINV-scFv pseudotyping combined antigen specificity, receptor-density-dependent transduction, high functional particle yield, and preserved pH-dependent entry, making it the preferred envelope scaffold for subsequent tumor-targeted lentiviral gene transfer experiments.

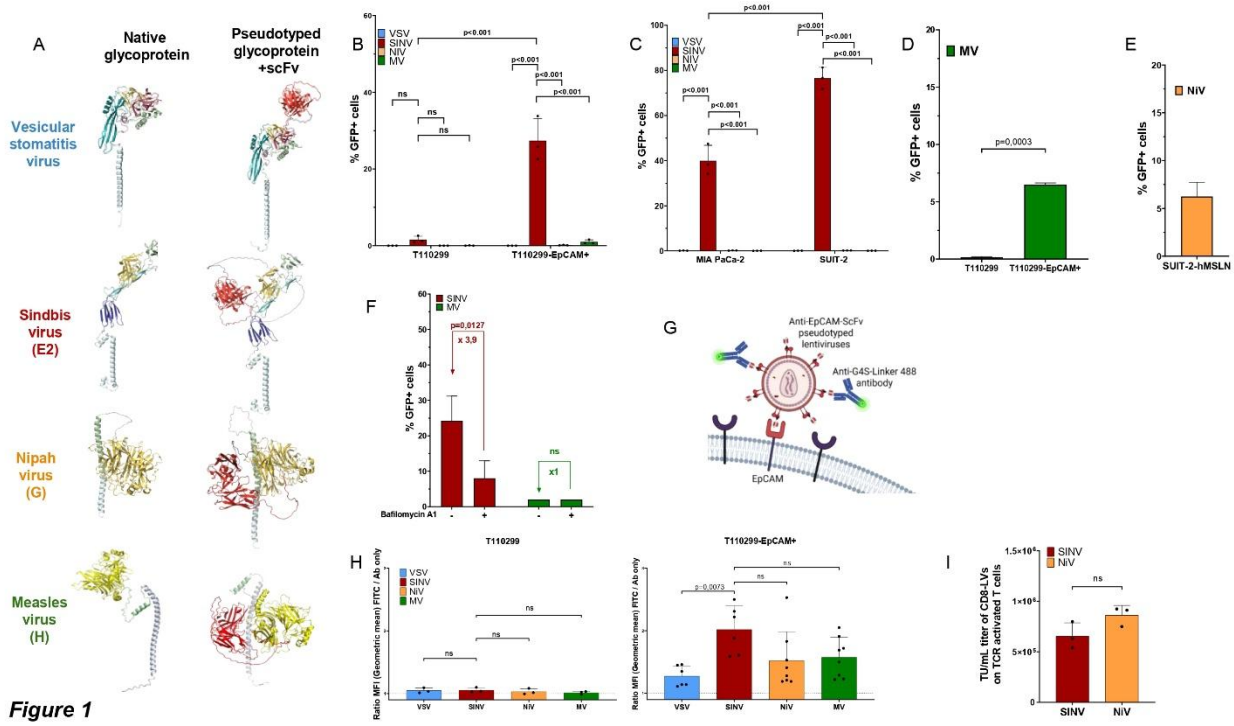


Figure 12: Comparative pseudotyping identifies SINV-scFv envelopes as the most efficient platform for antigen-directed lentiviral transduction.

(A) *AlphaFold-based structural models of native and scFv-engineered viral glycoproteins derived from VSV (Grey: Transmembrane Domain, Bordeaux: Lateral Domain, Yellow: PH Domain, Green: Trimerisation Domain, Emerald: Fusion Domain), SINV (E2: Grey: Transmembrane Domain, Cyan: β-sheet core (protein architecture and E1 interaction), Yellow: Domain A (recognition), Green: Domain B (stability), Blue: Domain C*

(E1 interaction)), NiV (G: Grey: Transmembrane Domain, Yellow: Globular head (recognition), Green: Stalk region (F gp interaction)) and MV (H: Grey: Transmembrane Domain, Green: Stalk region (responsible for dimerization), Yellow : Globular head (responsible for recognition)). scFv-targeting modules (red) were introduced into each envelope scaffold to redirect lentiviral vectors toward EpCAM or hMSLN. ***(B)*** *GFP expression in EpCAM-negative and EpCAM-positive T110299 cells after transduction with p24-normalized LVs pseudotyped with VSV-G-, SINV-, NiV- or MV-derived retargeted envelopes. (50ng p24)* ***(C)*** *GFP expression in MIA PaCa-2 and SUIT-2 pancreatic cancer cells after transduction with hMSLN-targeted pseudotypes. MIA PaCa-2 and SUIT-2 cells represent low and high hMSLN-expressing models, respectively. (50ng p24)* ***(B,C)*** *Data are shown as mean ± SD from n = 3 independent experiments. Statistical analysis was performed using a two-way ANOVA with Sidak's multiple-comparison test. Exact p values are indicated on the graphs for statistically significant comparisons; ns, not significant.* ***(D)*** *GFP expression after transduction of EpCAM-negative and EpCAM-positive cells with a high dose of MV-scFv-EpCAM LVs (p24=1400ng). Data are shown as mean ± SD from n = 2 independent experiments. Statistical analysis was performed using unpaired t test. Exact p value is reported in the figure* ***(E)*** *GFP expression after transduction of hMSLN-positive cells with a high dose of NIV-scFv-hMSLN LVs (p24=800ng).* ***(F)*** *Effect of bafilomycin A1 on EpCAM retargeted SINV- and MV-mediated transduction. Reduced SINV transduction upon bafilomycin A1 treatment is consistent with pH-dependent endosomal entry. Data are shown as mean ± SD from n = 3 independent experiments. Statistical analysis was performed using a two-way ANOVA with Sidak's multiple-comparison test. Exact p values are indicated on the graphs for statistically significant comparisons; ns, not significant,* ***(G-H)*** *Schematic and quantification of viral particle binding to EpCAM-positive and EpCAM-negative cells using an antibody directed against the G4S linker present in the scFv module. Binding was detected on antigen-positive cells but remained close to the background on antigen-negative cells. Data are shown as mean ± SD from n = 4 independent experiments. Statistical analysis was performed using a one-way ANOVA with Tukey's multiple-comparison test. Exact p values are indicated on the graphs for statistically significant comparisons; ns, not significant. The dotted line indicates the positivity threshold, calculated as followed: Positivity threshold=Mean from the antibody only condition+3*standard deviation* ***(I)*** *Functional comparison of SINV- and NiV-derived pseudotypes in an independent CD8-retargeting setting. Data are shown as mean ± SD from n = 3 independent experiments and from 2 independent labs. Statistical analysis was performed using unpaired t test. ns, not significant.*

Alphavirus-derived glycoproteins enable robust scFv-mediated targeting across multiple tumor antigens.

Because SINV-scFv pseudotyped lentivectors emerged as the most efficient candidates for tumor antigen-directed transduction, we next asked how their activity was influenced by antigen abundance. The pancreatic cancer cell lines used in this study displayed different levels of target antigen expression, as determined by RT-qPCR (**Supplementary Figure 18A,B**). As expected, classical VSV-G-pseudotyped lentivectors transduced all cell lines efficiently, reaching ~90% transduction irrespective of antigen expression level *(data not shown).* In contrast, SINV-scFv pseudotyped lentivectors transduced target cells in an antigen-dependent manner (**Figure 13A-B**).

For mesothelin-targeted vectors, transduction increased progressively across cell lines expressing low, intermediate, and high levels of mesothelin (MIA PaCa-2, SUIT-2, and SUIT-2-hMSLN, respectively), indicating a direct relationship between tumor antigen expression and transduction efficiency. In the same way, the SINV-based pseudotyping transduction was proportional to the hMSLN antigen expression levels with a correlation coefficient R^2 of 0,8689 ($p<0,0001$), as well as the EpCAM model (R^2 of 0,987, $p<0,0001$) **(Figure 13C)**.

To determine whether this relationship was generalizable across tumor types and receptor classes, we next examined prostate-specific membrane antigen (PSMA) in prostate cancer cell lines. Unlike EpCAM and mesothelin, PSMA is a type II transmembrane glycoprotein with well-documented endocytic behavior, making it a biologically relevant model to investigate how receptor identity and surface density influence productive SINV-mediated entry. In addition, PSMA provides a unique quantitative advantage, as its cell-surface abundance can be measured directly using radiolabeled [^{177}Lu]-PSMA-617. This enabled us to move beyond relative expression measurements and directly relate membrane-bound receptor copy number per cell to transduction efficiency. Using this system, we observed that SINV-scFv transduction initially increased with PSMA expression. In 22Rv1 and LNCaP cells, higher PSMA levels were associated with increased transduction efficiency (**Figure 13D**). 22Rv1 cells, expressing 31 353 ± 16 231 PSMA molecules per cell, were transduced at 15.5 ± 4.6%, whereas LNCaP cells, expressing 412 945 ± 173 771 PSMA molecules per cell, showed an approximately threefold higher transduction efficiency (50.2 ± 1.6%). However, this relationship was not maintained at very high receptor density. Although PC3-PIP cells expressed approximately threefold more PSMA molecules than LNCaP cells (1 373 394 ± 277 627 vs. 412 945 ± 173 771 molecules per cell), their transduction efficiency was reduced by ~20% (36.7 ± 1.7%) (**Figure 13D and Supplementary Figure 18E,F for** binding affinity (Kd) and quantification of receptors per cell). These data suggested that beyond a certain threshold, increasing PSMA density no longer promotes productive transduction and may instead become detrimental.

To test this hypothesis directly, we experimentally increased PSMA expression in LNCaP cells to levels comparable to those measured in PC3-PIP cells (**Figure 13E**). Strikingly, progressive PSMA overexpression in LNCaP cells resulted in an inverse correlation with SINV-scFv transduction efficiency (**Figure 13E-G;** $R^2 = 0.8781$, $p = 0.0006$). Together, these results indicate that PSMA-driven SINV transduction is not simply proportional to receptor abundance, but instead follows a saturable, non-linear relationship, consistent with the idea that excessive antigen density may impair productive viral entry, potentially through steric hindrance and/or reduced endocytic accessibility.

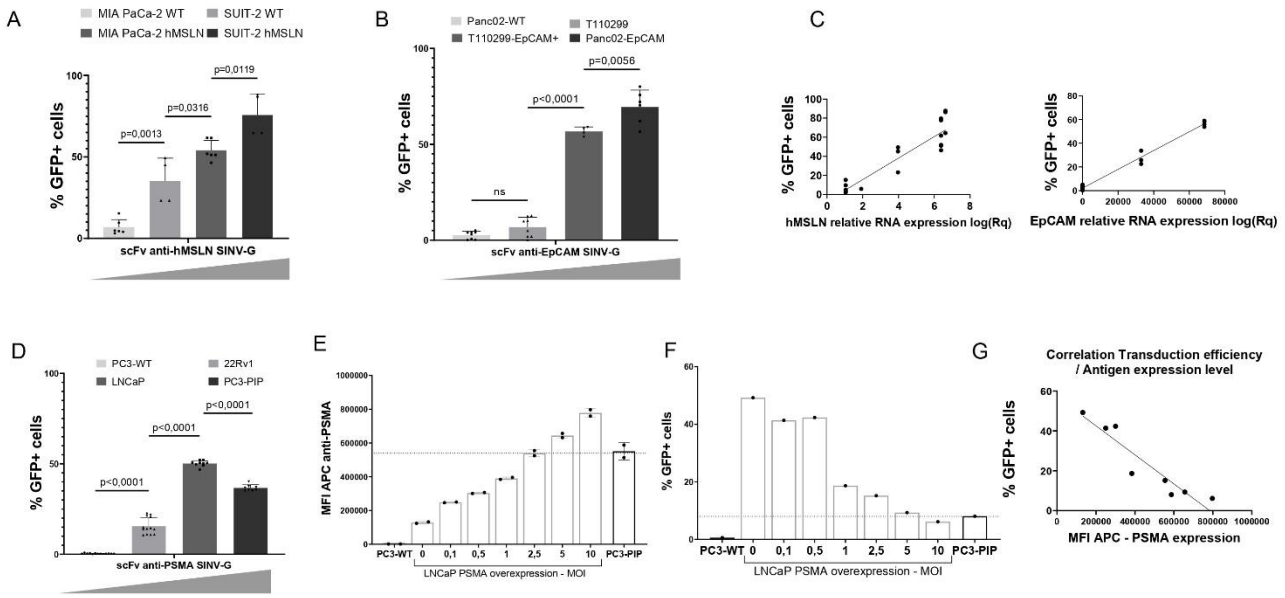


Figure 2

Figure 13: SINV-scFv pseudotyped lentiviral vectors mediate antigen-dependent transduction across multiple tumor antigens.

(A) *GFP transduction of hMSLN-low, -intermediate and -high pancreatic cancer cell lines with anti-hMSLN SINV-scFv LVs (50ng p24).* ***(B)*** *GFP transduction of EpCAM-negative and EpCAM-positive murine pancreatic cancer cells with anti-EpCAM SINV-scFv LVs. (50ng p24)* ***(A,B)*** *Data are shown as mean ± SD from n = 3 independent experiments, performed in duplicate. Statistical analysis was performed using a one-way ANOVA with Tukey's multiple-comparison test. Exact p values are indicated on the graphs for statistically significant comparisons; ns, not significant.* ***(C)*** *Correlation between hMSLN or EpCAM relative RNA expression and SINV-scFv-hMSLN or EpCAM-mediated transduction efficiency, respectively. For hMSLN model, the correlation coefficient R^2 is of 0,8689 (p<0,0001), and of 0,987, p<0,0001 for the EpCAM model* ***(D)*** *GFP transduction of prostate cancer cell lines expressing different levels of PSMA anti-PSMA SINV-scFv LVs. (50ng p24). Data are shown as mean ± SD from n = 5 independent experiments, performed in duplicate. Statistical analysis was performed using a one-way ANOVA with Tukey's multiple-comparison test. Exact p values are indicated on the graphs for statistically significant comparisons* ***(E)*** *PSMA surface expression in LNCaP cells following progressive PSMA overexpression, measured by APC-anti-PSMA flow cytometry. PC3-WT and PC3-PIP were used as negative and high PSMA-expressing controls.* ***(F)*** *Anti-PSMA SINV-scFv LV transduction of LNCaP cells with increasing PSMA expression levels. (10ng p24).* ***(E-F)*** *Representative results of n=3. Data are shown as mean ± SD. Each dot represents an independent biological replicate.* ***(G)*** *Correlation between PSMA surface expression and anti-PSMA SINV-scFv-mediated transduction efficiency. R^2 = 0.8781, p = 0.0006.*

A bilayer spheroid model reveals spatially restricted and homogeneous SINV-scFv-mediated gene transfer.

To determine whether the specificity and efficiency of SINV-scFv pseudotypes were preserved in a more tumor-relevant 3D context, we developed a bilayer spheroid model in which hMSLN-positive SUIT-2 cells were embedded in the core and surrounded by an antigen-negative PC3-WT-TdTomato outer layer **(Figure 14A)**. In this stringent 3D setting, WT VSV-G-pseudotyped LVs transduced both the inner and outer compartments, consistent with their broad tropism **(Figure 14B, upper panels)**. By contrast, anti-hMSLN SINV-scFv-pseudotyped LVs selectively transduced the hMSLN-positive inner compartment, with limited GFP signal in the antigen-negative peripheral layer **(Figure 14B, lower panels)**. Flow cytometry confirmed that SINV-scFv-hMSLN LVs efficiently transduced SUIT-2-hMSLN target cells while strongly reducing transduction of antigen-negative PC3-WT cells, whereas VSV-G LVs transduced both cell populations **(Figure 14C)**. Interestingly, VSV-G-LV showed a heterogeneous spatial pattern, whereas SINV-scFv-mediated gene delivery was markedly more homogeneous throughout the targeted core, as confirmed by radial fluorescence analysis **(Figure 14D)**. This analysis further showed that VSV-G-mediated GFP signal extended across both the SUIT-2-hMSLN core and the PC3-WT outer layer, while SINV-scFv-hMSLN-mediated transduction remained spatially confined to the target cell compartment. The same observations were made with anti-PSMA SINV-scFv targeting PSMA-positive core cells **(Supplementary Figure 19A-D)**. To further assess whether targeted SINV-scFv-mediated transduction was maintained in a more relevant 3D model containing matrix, SUIT-2-hMSLN spheroids were embedded in collagen before lentiviral transduction **(Figure 14E)**. In this extracellular matrix-containing model, both VSV-G and SINV-scFv-hMSLN LVs efficiently transduced SUIT-2-hMSLN spheroids, as shown by GFP fluorescence throughout the spheroid structure **(Figure 14F)**. Flow cytometry confirmed robust GFP expression after transduction with either pseudotype, with comparable percentages of GFP-positive cells between VSV-G and SINV-scFv-hMSLN LVs (~70%) **(Figure 14G)**. Thus, the antigen-retargeted SINV-scFv pseudotype retained efficient gene transfer in a collagen-embedded 3D model, indicating that the targeting strategy did not compromise transduction performance in an extracellular matrix-rich context.

These findings indicate that SINV-scFv pseudotypes combine target selectivity with topologically restricted transduction in 3D tumor models, while maintaining efficient gene delivery in collagen-embedded spheroids.

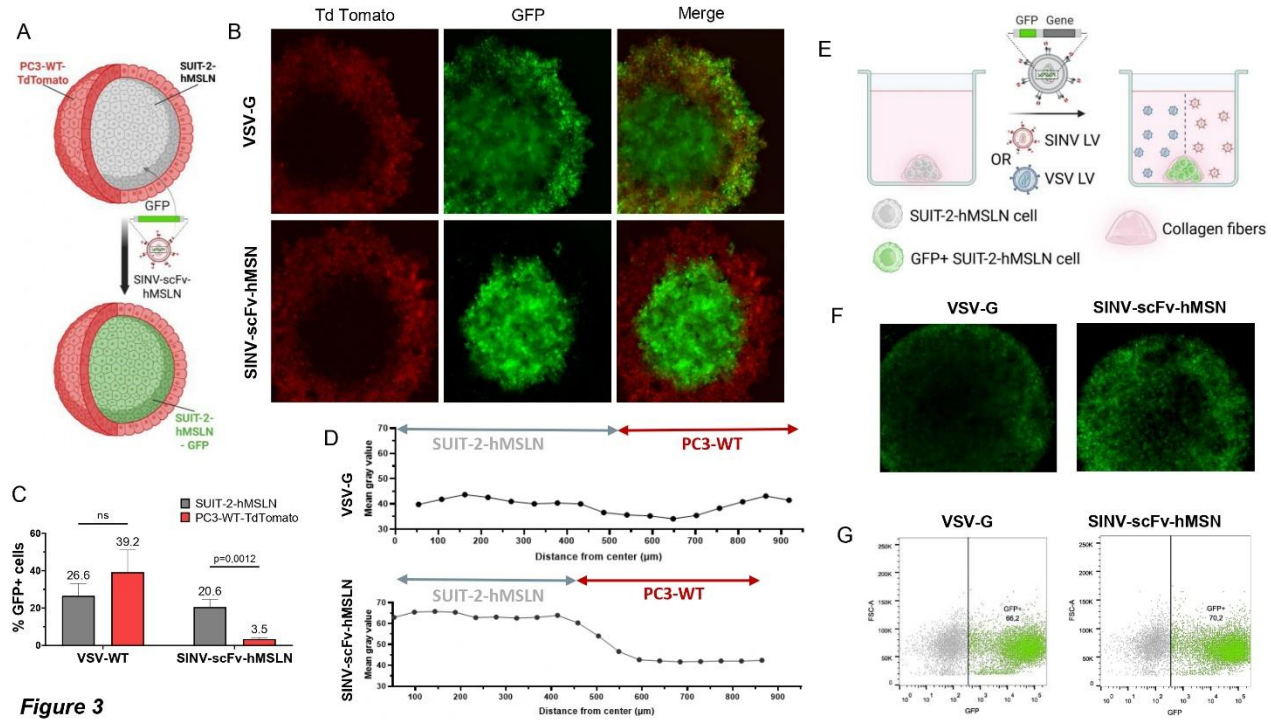


Figure 3

Figure 14: SINV-scFv-hMSLN pseudotyped lentiviral vectors mediate spatially restricted and efficient gene transfer in 3D tumor models.

(A) *Schematic representation of the bilayer spheroid model. hMSLN-positive SUIT-2 cells formed the inner spheroid core and were surrounded by antigen-negative PC3-WT-TdTomato cells. Spheroids were then exposed to GFP-encoding LVs pseudotyped with either VSV-G or SINV-scFv-hMSLN.* ***(B)*** *Representative fluorescence microscopy images of bilayer spheroids after transduction with VSV-G or SINV-scFv-hMSLN LVs at MOI 10. TdTomato marks antigen-negative PC3-WT cells, GFP marks transduced cells, and merged images show the spatial distribution of lentiviral transduction. VSV-G-mediated transduction was detected in both spheroid compartments, whereas SINV-scFv-hMSLN-mediated transduction was mainly restricted to the hMSLN-positive core.* ***(C)*** *Quantification of GFP-positive cells in SUIT-2-hMSLN and PC3-WT-TdTomato populations after transduction with VSV-G or SINV-scFv-hMSLN LVs. SINV-scFv-hMSLN LVs maintained efficient target cell transduction while reducing off-target transduction of PC3-WT cells. Data are shown as mean ± SD from n = 3 Statistical analysis was performed using a two-way ANOVA with Sidak's multiple-comparison test. Exact p values are indicated on the graphs for statistically significant comparisons. ns, not significant* ***(D)*** *Radial fluorescence intensity analysis of GFP signal across bilayer spheroids transduced with VSV-G or SINV-scFv-hMSLN LVs. The grey and red arrows indicate the localization of the SUIT-2-hMSLN core and PC3-WT outer layer, respectively. VSV-G-mediated GFP signal was broadly distributed across the spheroid, whereas SINV-scFv-hMSLN-mediated GFP signal remained spatially restricted to the target cell compartment.* ***(E)*** *Schematic representation of the collagen embedded spheroid model. hMSLN-positive SUIT-2 cells were seeded in a collagen matrix. Spheroids were then exposed to GFP-encoding LVs pseudotyped with either VSV-G or SINV-scFv-hMSLN.* ***(F)*** *Representative fluorescence microscopy images of SUIT-2-hMSLN spheroids embedded in collagen and transduced with VSV-G or SINV-scFv-hMSLN LVs at MOI 1. GFP fluorescence shows efficient transduction by both pseudotypes in an extracellular matrix-containing 3D model.* ***(G)*** *Representative flow cytometry plots showing GFP expression in collagen-embedded SUIT-2-hMSLN spheroids following transduction with VSV-G or SINV-scFv-hMSLN LVs.*

Multispecific SINV pseudotypes broaden antigen recognition without compromising transduction efficiency

Because tumor antigen expression is heterogeneous, targeting a single surface antigen may restrict vector entry to only a fraction of tumor cells. We therefore asked whether SINV-pseudotyped lentiviral vectors could be engineered to co-display multiple targeting specificities on the same viral particle.

We evaluated whether combining multiple targeting specificities on SINV pseudotypes could preserve gene transfer compared with mixtures of monospecific particles. MIA PaCa-2 cells, which express low levels of hMSLN **(Supplementary Figure 18B)**, were engineered to also express the EpCAM antigen. These cells, along with hFF-hTERT cells as a negative control for EpCAM and very low mesothelin expression, were transduced with either a cocktail of monospecific hMSLN- and EpCAM-targeted SINV-LVs or a bispecific hMSLN-EpCAM SINV-LV, using the same final viral input of 25 ng p24 **(Figure 15A)**. The monospecific cocktail mediated detectable transduction of MIA PaCa-2 cells and higher transduction of MIA PaCa-2-EpCAM cells, consistent with EpCAM providing an additional targetable antigen. The bispecific anti-hMSLN/EpCAM vector showed a higher transduction than the monospecific cocktail, particularly in EpCAM-expressing MIA PaCa-2 cells. hFF-hTERT control cells remained poorly transduced by targeted SINV vectors. These data suggest that co-display of hMSLN- and EpCAM-targeting moieties on the same particle is compatible with efficient transduction at matched viral input.

We then extended this strategy to a more complex antigenic setting using SUIT-2 cells to mimic the tumor antigenic heterogeneity. SUIT-2-WT cells, expressing hMSLN **(Supplementary Figure 18B)**, were compared with SUIT-2-EpCAM-PSMA cells, in which additional EpCAM and PSMA expression was introduced in a subpopulation of cells. Flow-cytometry analysis confirmed that SUIT-2-WT cells were largely negative for EpCAM and PSMA, whereas SUIT-2-EpCAM-PSMA transduced cells at low MOIs contained EpCAM-positive (around 10%), PSMA-positive (around 10%) and double-positive cells (around 2%), representing a minority of the total population (hMSLN-positive only, around 78%) **(Figure 15B)**. At a matched final input of 25 ng p24, hMSLN-containing bispecific vectors efficiently transduced SUIT-2-WT cells, consistent with functional hMSLN-dependent entry. The EpCAM-PSMA bispecific vector showed low activity on SUIT-2-WT cells but increased transduction in SUIT-2-EpCAM-PSMA cells, producing the expected proportion of transduced cells (around 22%), indicating that targeting SINV glycoproteins were functional **(Figure 15C)**.

In SUIT-2-EpCAM-PSMA cells, vectors incorporating anti-hMSLN together with anti-EpCAM and/or PSMA maintained robust transduction, with higher GFP positivity than in the corresponding SUIT-2-WT condition. Thus, the trispecific hMSLN/EpCAM/PSMA format preserves efficient gene transfer while broadening the range of targetable antigens.

Together, these data indicate that multispecific SINV pseudotypes can expand antigen recognition in heterogeneous tumor-cell populations without compromising transduction efficiency at dose-matched viral input.

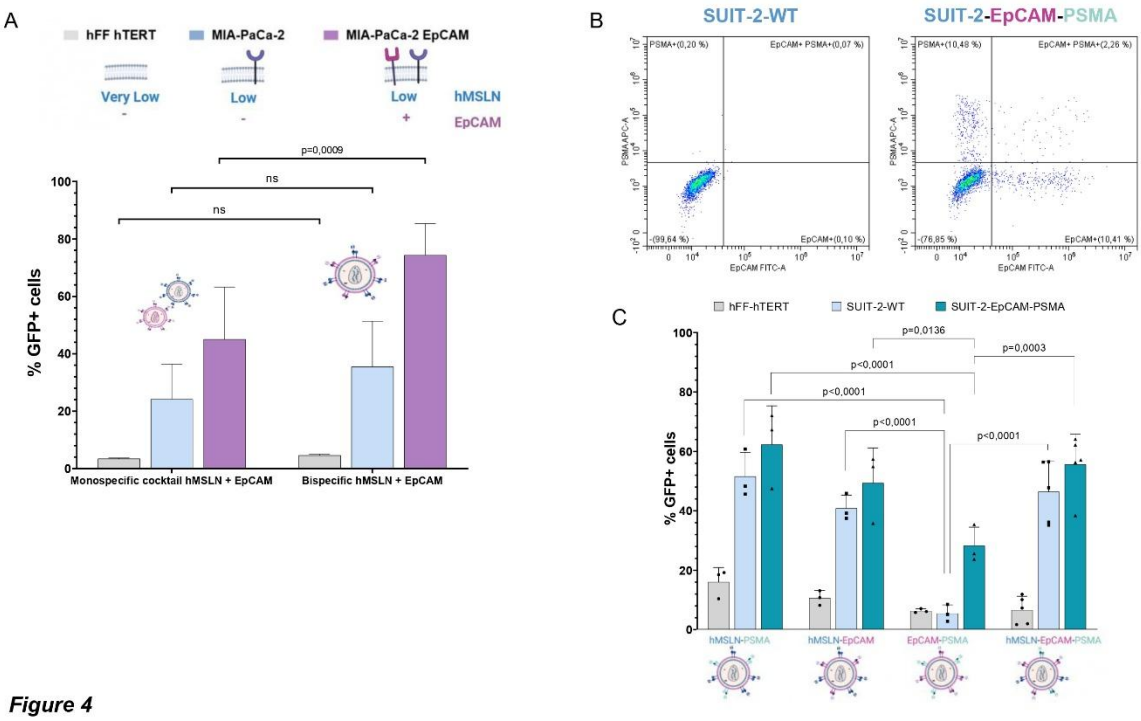


Figure 4

Figure 15: Multispecific SINV pseudotypes broaden antigen recognition while preserving transduction efficiency at matched viral input.

(A) *MIA PaCa-2 and MIA PaCa-2-EpCAM cells were transduced with either a cocktail of monospecific hMSLN- and EpCAM-targeted SINV-LVs or a bispecific hMSLN/EpCAM SINV-LV. hFF-hTERT cells were used as non-tumor control cells. All targeted SINV-LV conditions were normalized to the same final viral input of 25 ng p24. The bispecific hMSLN/EpCAM vector showed a higher transduction than the monospecific cocktail in MIA PaCa-2-EpCAM cells. Data are shown as mean ± SD from n = 5 independent experiments. Statistical analysis was performed using a two-way ANOVA Sidak's multiple-comparison test. Exact p values are indicated on the graphs for statistically significant comparisons; ns, not significant.* ***(B)*** *Representative flow-cytometry analysis of EpCAM and PSMA expression in SUIT-2-WT and SUIT-2-EpCAM-PSMA cells. SUIT-2-WT cells were largely negative for both antigens, whereas SUIT-2-EpCAM-PSMA cultures contained EpCAM-positive, PSMA-positive and double-positive subpopulations.* ***(C)*** *Percentage of GFP-positive cells after transduction of hFF-hTERT, SUIT-2-WT and SUIT-2-EpCAM-PSMA cells with bispecific or trispecific SINV-pseudotyped lentiviral vectors. All vectors were tested at the same final viral input of 25 ng p24. hMSLN-containing vectors efficiently transduced SUIT-2-WT cells, whereas the EpCAM/PSMA bispecific vector showed increased activity in SUIT-2-EpCAM-PSMA cells compared with SUIT-2-WT cells. The trispecific hMSLN/EpCAM/PSMA vector maintained robust transduction of SUIT-2-EpCAM-PSMA cells, supporting antigenic broadening without apparent loss of efficiency at matched viral input. Data are shown as mean ± SD from n = 3 Statistical analysis was performed using a two-way ANOVA with Tukey's multiple-comparison test. Exact p values are indicated on the graphs for statistically significant comparisons. Non-annotated comparisons were not statistically significant.*

SINV-scFv lentivectors achieve antigen-dependent *in vivo* gene transfer.

We evaluated scFv-SINV pseudotypes *in vivo*, carrying the luciferase reporter gene, using both local and systemic delivery settings. Following intratumoral injection, SIN-V vectors mediated transduction in PSMA-, EpCAM- and mesothelin-expressing subcutaneous tumors, demonstrating that targeted gene transduction remained functional *in vivo* across distinct tumor antigens **(Figure 16A)**. In EpCAM- and hMSLN-positive tumors, bioluminescence quantification at the tumor site showed no significant difference between VSV-G and the corresponding SINV-scFv LVs, indicating that local delivery of SINV-scFv vectors can achieve transduction levels comparable to broadly tropic VSV-G LVs in antigen-positive tumors **(Figure 16B).** We extended the *in vivo* exploration on the prostate model to assess antigen specificity and accessibility after systemic retro-orbital intravenous administration. In mice bearing PSMA-positive or PSMA-negative PC3 tumors, tumor localization was visualized by TdTomato imaging, whereas productive transduction was monitored by bioluminescence. Anti-PSMA-SINV vectors generated signal selectively in PSMA-positive tumors, but not in tumor-free animals or in mice bearing PSMA-negative tumors **(Figure 16C)**, demonstrating antigen-dependent specificity *in vivo*. By contrast, VSV-G-LVs were distributed preferentially in the liver and the bone marrow **(Figure 16C)**, regardless of the presence of a tumor, consistent with their broad *in vivo* tropism and non-targeted biodistribution. This selectivity was further challenged in mice simultaneously bearing one PSMA-negative (left flank) and one PSMA-positive (right flank) subcutaneous tumor. Following intravenous injection, the bioluminescent signal was only detected in the PSMA-positive lesion within the same animal **(Figure 16D,E)**, indicating that systemic scFv-SINV delivery can discriminate between antigen-negative and antigen-positive tumors *in vivo*.

Ex vivo bioluminescence analysis confirmed preferential transduction of PSMA-positive tumors following systemic anti-PSMA SINV-scFv LV delivery **(Supplementary Figure 20A)**. Major organs were analyzed to evaluate potential off-target biodistribution, including liver and spleen as classical sites of LV accumulation and lung and kidney as highly perfused organs relevant for systemic vector exposure. In line with the *in vivo* imaging, VSV-G LVs showed strong off-target signal in liver and spleen, whereas anti-PSMA SINV-scFv LVs showed limited non-tumoral organ transduction **(Supplementary Figure 20B)**. No substantial signal above the positivity threshold was detected in lung or kidney for either targeted SINV-scFv or VSV-G LVs.

Together, these data show that SINV-scFv pseudotyped LVs retain functional gene-transfer activity *in vivo* after both local and systemic administration, while conferring antigen-dependent tumor selectivity that is not achieved with broadly tropic VSV-G pseudotyping.

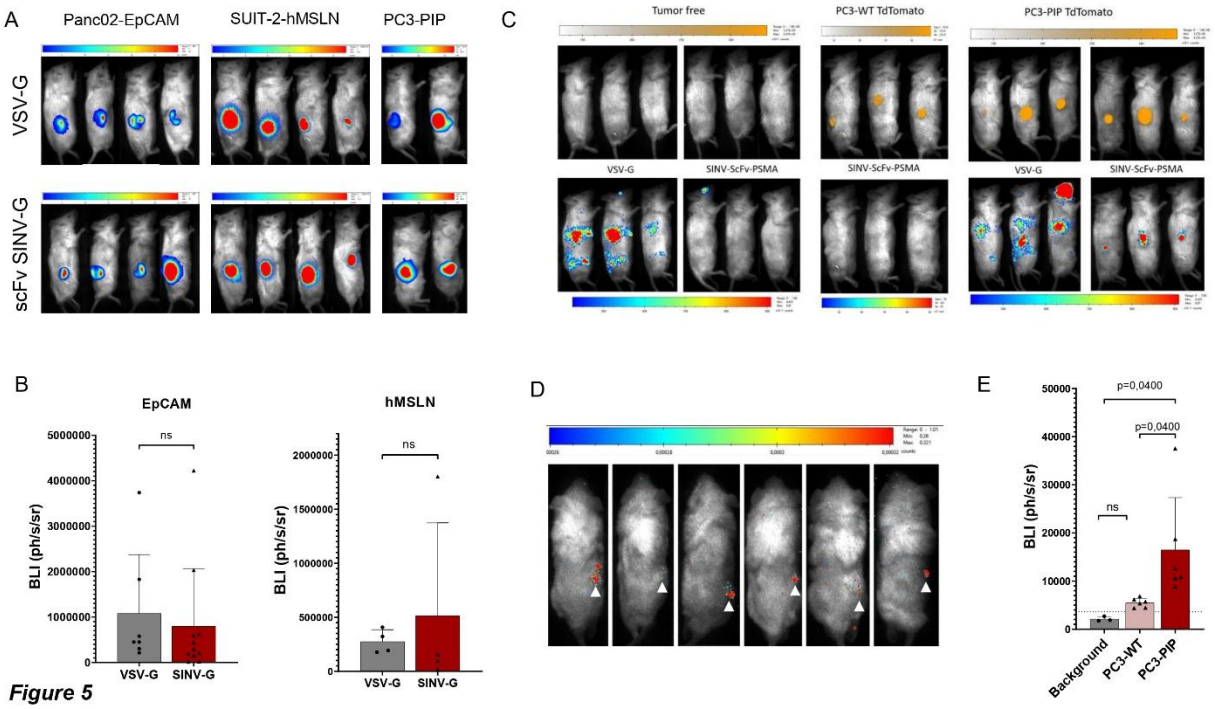


Figure 16: SINV-scFv pseudotyped lentiviral vectors mediate antigen-dependent gene transfer in vivo. ***(A)*** *Representative in vivo bioluminescence images of mice bearing subcutaneous Panc02-EpCAM, SUIT-2-hMSLN or PC3-PIP tumors after intratumoral injection of luciferase-encoding LVs pseudotyped with either VSV-G or the corresponding antigen-targeted SINV-scFv envelope (1x10^6 TU/mouse).* ***(B)*** *Quantification of ex vivo tumor-associated bioluminescent signal after intratumoral injection of VSV-G or SINV-scFv LVs in EpCAM- and hMSLN-positive tumor models. Data are shown as mean ± SD from n = 12 mice for the EpCAM model and n=4 mice for the hMSLN model. Statistical analysis was performed using unpaired t test. ns, not significant* ***(C)*** *Representative in vivo imaging following intravenous administration of luciferase-encoding VSV-G- or anti-PSMA SINV-scFv-pseudotyped lentiviral vectors in tumor-free mice or in mice bearing PSMA-negative PC3-WT-TdTomato or PSMA-positive PC3-PIP-TdTomato tumors. Vectors were administered at 5 × 10⁶ TU/mouse and imaging was performed 10 days after injection. TdTomato fluorescence was used to localize tumor sites, whereas bioluminescence imaging was used to detect productive lentiviral transduction through luciferase expression. Acquisition settings were kept identical within each imaging modality, and images are displayed with the indicated radiance scales.* ***(D)*** *Representative in vivo bioluminescence images of mice bearing paired PSMA-negative PC3-WT-TdTomato tumors on the left flank and PSMA-positive PC3-PIP-TdTomato tumors on the right flank following systemic administration of luciferase-encoding anti-PSMA SINV-scFv-pseudotyped lentiviral vectors. White arrowheads indicate tumor sites. Bioluminescence imaging was used to detect productive lentiviral transduction through luciferase expression. Vectors were administered intravenously at 5 × 10⁶ TU/mouse, and imaging was performed 10 days after injection. Signal was preferentially detected at PSMA-positive tumor sites, consistent with antigen-dependent in vivo transduction.* ***(E)*** *Quantification of tumor-associated bioluminescent signal after systemic delivery, showing preferential transduction of PSMA-positive tumors. The dotted line indicates the positivity threshold, calculated as followed: Positivity threshold=Mean+3*standard deviation. Data are shown as mean ± SD from n = 6 mice. Statistical analysis was performed using a one-way ANOVA with Holm-Sidak's multiple-comparison test. Exact p values are indicated on the graphs for statistically significant comparisons; ns, not significant.*

Discussion

In this study, we performed a systematic comparison of scFv-retargeted LV lentiviral pseudotypes across multiple tumor antigens, cell backgrounds and envelope platforms. This analysis identified SINV-based envelopes as the only platform that consistently supported efficient and antigen-restricted gene transfer under our experimental conditions, while MV-, NiV-, and engineered VSV-G-derived targeted pseudotypes showed markedly lower productive activity in the same settings. The efficiency of transduction of scFv-mediated lentiviral retargeting appeared strongly dependent on the donor glycoprotein. Under matched experimental conditions and using comparable scFv-based targeting modules across tumor antigens, SINV-derived pseudotypes were the only ones to combine robust transduction with strict antigen dependence, whereas MV- and NiV-based systems remained poorly active in our tumor models. The differences were not readily explained by gross structural anomalies of the engineered envelopes, but were clearly influenced by major differences in specific infectivity. This observation is consistent with the broader literature indicating that retargeted LV platforms are not functionally equivalent and can differ markedly in infectious yield and gene-transfer efficiency. In particular, high titers can be obtained when pseudotyping LVs with envelopes retaining compatibility with their cognate entry system, such as SLAM and CD46 for MV-LVs (24-26). Previous reports showed that pseudotype engineering maintained a good yield, and excellent specificity can be achieved. *Zhou et al.* demonstrated that scFv-CD8-targeted measles-pseudotyped LVs retained substantial titers (5×10^6 to 2×10^7 TU/mL) together with highly selective transduction of T cells *in vitro* and *in vivo* (23). Darpin-based anti-CD8-targeted Nipah-pseudotyped LVs recovered lower titers (10^5 TU/mL range) and further observed that engineered NiV yielded better titers than MV glycoproteins using the same recognition moiety on CD8 (Darpin module) (13). These observations further support that engineered LV pseudotypes are constrained by the type of recognition module, together with the pseudotyping platform. In our study, SINV pseudotypes reproducibly reached titers in the 10^6-10^7 TU/mL range, supporting their practical suitability for further *in vivo* evaluation.

We observed sharp differences in productive transduction between SINV and NiV or MV scFv-pseudotyping. Importantly, all scFv-pseudotyped vectors were able to bind target cells at comparable levels in our binding assay, indicating that the lower activity of MV- and NiV-derived pseudotypes was not simply due to the absence of cell attachment. After ruling out a problem of target engagement due to the membrane fluidity, we hypothesized that post-binding constraints, and in particular the geometry/distance of receptor engagement relative to the plasma membrane, could limit productive fusion. This interpretation is supported by the fact that receptor-targeted NiV-LVs are highly sensitive to the position of the targeted binding site, with efficient gene transfer favored by membrane-proximal receptor engagement (13). In their model, high-efficiency NiV-LV entry generally required receptor binding within approximately 50 Å of the target cell membrane, whereas

more distal binding sites markedly reduced gene transfer. Of note, CD8 represented a partial exception: although its Ig-like domain is positioned beyond this membrane-proximal range, its 47-residue stalk was proposed to be highly flexible, potentially allowing vector particles bound to the Ig-like domain to move closer to the plasma membrane and still support productive fusion. Based on our folding predictions **(Figure 17)**, our data confirm that receptor binding may occur in a geometry that was suboptimal for triggering productive MV- or NiV-mediated fusion, particularly when the targeted epitope was positioned too far from the plasma membrane. In contrast, SINV-GP-mediated entry is endocytic (27), which positions this platform as less sensitive to the precise membrane-proximal positioning of the targeted epitope.

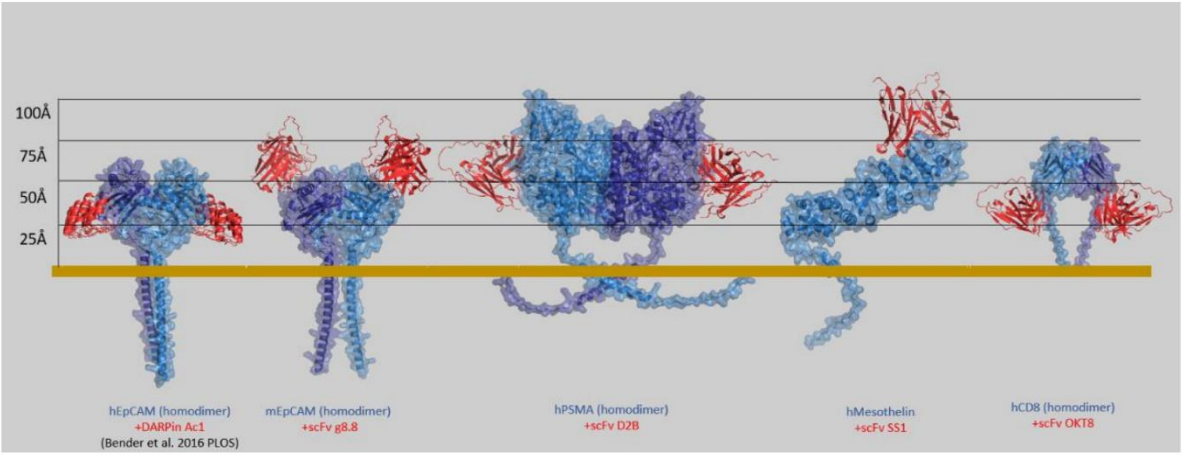


Figure 17: Structural modeling of target antigen-binder complexes relative to the plasma membrane. *Representative structural models of antigen-binder complexes were oriented relative to the plasma membrane (orange), using the membrane-proximal region of each antigen as reference. Antigen ectodomains are shown in blue/purple and targeting binders in red. The yellow bar indicates the plasma membrane, and horizontal guide lines indicate approximate distances from the membrane in Å. The hEpCAM/DARPin Ac1 complex, previously validated for receptor-targeted NiV-LV entry, is shown as a membrane-proximal reference. In contrast, the modeled mEpCAM/scFv g8.8, hPSMA/scFv D2B and hMesothelin/scFv SS1 complexes position the targeting module partially or predominantly beyond the approximately 50 Å membrane-proximal range proposed by Bender et al. for high-efficiency NiV-LV gene delivery. hCD8/scFv OKT8 is shown as a flexible exception: although the CD8 Ig-like domain extends beyond this range, the CD8α ectodomain is connected to the membrane by a flexible stalk that may allow closer vector-membrane apposition during entry. These models support the hypothesis that inefficient MV- and NiV-derived scFv-LV transduction may result from post-binding geometric constraints rather than from impaired target cell attachment alone.*

Importantly, we assessed pseudotype-dependent selectivity in heterocellular 3D tumor spheroids, providing a spatially resolved assay of pseudotype specificity. Whereas VSV-G pseudotyping resulted in expected broad transduction across both cellular compartments, SINV-scFv-LV-mediated

gene transfer was restricted to the targeted antigen-positive compartment. This 3D approach extends previous evaluations of pseudotyped lentiviral vectors. For example, LCMV-GP transduction efficiency was used to assess retargeting efficiency in glioblastoma patient-derived spheroids, compared to VSV-G, without directly testing specificity (28). To our knowledge, our strategy represents one of the few spatially resolved evaluations of lentiviral pseudotype specificity in a heterogeneous 3D tumor spheroid model.

Multiple reports show that productive entry is strongly influenced by receptor density. For example, entry of LVs pseudotyped with the 2.2ZZ SINV-derived glycoprotein combined with anti-CD4 antibodies was directly proportional to cell-surface CD4 concentrations (29). We confirm that increasing levels of antigen expression were associated with increasing transduction efficiency of SINV-pseudotyped LVs for several antigen-cell line combinations. Moreover, our analysis of cell lines expressing various levels of PSMA revealed that target antigen abundance may saturate and even decrease LV transduction efficiency, both across prostate cancer cell lines and in experimentally PSMA-overexpressing LNCaP cells. PSMA is not a passive surface marker but a constitutively internalized receptor whose uptake is further enhanced upon antibody engagement (30). Therefore, it is possible that increasing PSMA density does not simply increase viral capture in a linear manner, but may also alter the kinetics or routing of productive endocytic entry. These results suggest that productive SINV entry depends on an optimal range of receptor availability, beyond which excessive receptor density may impair uptake or post-binding trafficking, potentially through avidity-driven surface trapping, steric crowding, or rerouting into non-productive endocytic compartments.

Increasing transduction efficiency while keeping specificity has been a recurrent challenge in the vectorology field. Previous dual-targeting has been achieved by combining prostate PSCA-directed transduction with specific expression of transgenes in prostate tissue under a prostate-specific promoter (31). This strategy did improve the global selectivity of the system, but did not address cell heterogeneity in antigen expression. Alternatively, co-displaying a targeting ligand with a fusogenic module on the same LV particle achieved *in vivo* specific reporter gene delivery with efficiency similar to VSV-G enveloped particles (32), but remained valid for the unique tested antigen. In this study, we simultaneously exploited two or three tumor-associated surface antigens by LVs produced with all three engineered glycoproteins. Although we cannot be sure if the co-display of two or three tumor antigen-directed glycoproteins occurred on the same particles, our results showed that LVs retain the transduction efficiency of particles produced with one glycoprotein. These results open the possibility of targeting cells with several specific but low-density antigens and adapting targeting strategies to heterogeneous tumors.

Our work also contributes to validating *in vivo* strategies for specific and efficient LV-directed gene transfer. We confirmed that VSV-G-enveloped LV transduced mainly the liver, as previously described (33), but we showed that SINV-based envelope design can restrict productive transduction to antigen-expressing tumors while strongly reducing or even avoiding off-target liver and bone

marrow signal compared with VSV-G. The ability to distinguish PSMA-positive from PSMA-negative tumors within the same animal, together with avoiding liver and bone marrow transduction compared with VSV-G, positions SINV-scFv pseudotypes as a promising platform for safer, yet efficient *in vivo* lentiviral gene delivery. SINV-derived envelopes may also present translational advantages, as SINV is not targeted by routine human vaccination, unlike measles virus-based platforms (34). However, the xenograft models, although informative, do not fully capture the complexity of immunocompetent solid tumors or establish therapeutic efficacy with functional payloads. In particular, our study does not address how innate and adaptive immunity, complement, macrophage uptake, or anti-envelope immune responses would affect biodistribution and efficacy in immunocompetent hosts. These limitations are particularly relevant for systemic administration and will need to be addressed before therapeutic translation.

Together, these findings establish design principles for tumor-directed lentiviral delivery and position SINV-based pseudotyping as a particularly attractive platform for *in vivo* gene therapy of solid tumors. More broadly, our data indicate that successful retargeted LV engineering cannot be predicted from antigen binding alone, but requires integration of envelope biology, receptor density, membrane context, and tissue-level biodistribution.

Material & methods

Cell culture

Panc02-WT, hFF-hTERT, SUIT-2 and MIA PaCa-2 cells were maintained in Dulbecco's modified Eagle's medium (DMEM, 4.5 g/L glucose; Gibco) supplemented with 10% fetal bovine serum (FBS) and 1% penicillin-streptomycin. The murine pancreatic tumor cell line T110299, derived from a KPC Ptf1a-Cre; LSL-KRAS^{G12D}; LSL-Trp53^fl/R172H^ mouse (kindly provided by Prof. Jens Siveke, University Hospital Essen, Germany; Metzger et al.). Panc02-WT and T110299 cells were retrovirally engineered to express murine EpCAM (UniProt Q99JW5). MIA PaCa-2 and SUIT-2 cells were engineered for human mesothelin overexpression by transduction with pMXs containing full length human mesothelin (MSLN, UNIPROT entry Q13421) cDNA (35). Antigen-positive and -negative populations were isolated by flow cytometry after antibody staining. Prostate cancer cell lines PC3, PC3-PIP, 22Rv1, and LNCaP were cultured in RPMI 1640 medium (Gibco) supplemented with 10% FBS and 1% penicillin-streptomycin.

Plasmids

Anti-human mesothelin (MSLN) clone SS1 and anti-mouse epithelial cell adhesion molecule (EpCAM) clone g8.8 single-chain variable fragment (scFv) sequences were previously reported (36). The anti-prostate-specific membrane antigen (PSMA) scFv sequence was kindly provided by Giulio Fracasso (Verona, Italia), from the pMIMOscFvD2B plasmid. The anti-human CD8 scFv was

obtained from the construct previously described by Zhou et al. (23). Expression vectors of E2 were constructed by inserting the sequences of different scFvs between flexible linkers at amino acid (aa) 71 of E2 2.2 1L1L, as previously described (37). Following the same strategy, the scFv sequences were PCR amplified and individually cloned into the plasmids coding for MV-H (between *Sfi*I and *Not*I) (25) and NiV-G (between *Age*I and *Not*I) (13) using the In-Fusion HD Cloning Kit (Takara Bio). The VSV-G envelope plasmid (pMD2.G #12259; Addgene) was provided by the Vectorology Vect'UB facility (University of Bordeaux). Site-directed mutagenesis was used to introduce an in-frame insertion cassette of ScFv-EpCAM and scFv-hMSLN between residues T351 and T352 of VSV-G. This position was selected based on prior structural and functional work identifying this region as compatible with the insertion of exogenous ligands in VSV-G (20).

Amino acid FASTA files were uploaded to ColabFold, an AlphaFold2-based prediction platform (Mirdita et al., 2022), to generate three-dimensional (3D) structural models. Validation of predicted models was performed with MODELLER version 10.5 (Šali and Blundell, 1993) using the same sequences. Structural templates showing highest homology were identified using BLASTp (NCBI) and retrieved from the RCSB Protein Data Bank (PDB). Multiple sequence alignments in PIR format were prepared using ClustalX 2.1 (Larkin et al., 2007). Resulting structures were visualized and colored in PyMOL version 3.0.0 (Schrödinger, LLC).

Lentiviral vector production

Lentiviral vectors were produced by the Vectorology Vect'UB facility (TBMCore UAR 3427). 2.5µg of plasmid envelope (VSV-G, SINV-G, MV-H or NiV-G), 8µg of packaging (psPAX2, Addgene #12260), and 8µg of transfer (pPGK-eGFP) plasmids were co-transfected into HEK293T cells using calcium phosphate precipitation. For bispecific and trispecific envelopes, 1.25µg or 0.83µg of each plasmid envelope, respectively, were co-transfected. The $CaCl_2$-plasmid mix was distributed to HEK293T cultures at 70% confluence, seeded in 10-cm dishes at 0.5×10^6 cells 4 days prior. Supernatants were collected 48 h later and concentrated by Centricon® ultrafiltration (3,000 × g, 2-3 h, 4 °C). Viral titers were measured by p24 ELISA (INNOTEST® HIV Antigen mAb; Fujirebio Europe) and/or by infectious titer. For the latter, vectors pseudotyped with the different glycoproteins were pre-diluted and were added on antigen-positive cells. After 96h, the percentage of GFP-positive cells was determined by flow cytometry (eGFP). Dilutions yielding 1%-30% GFP-positive cells were used for titer calculation. Transductional titers were expressed as infectious units per milliliter (TU/mL) and calculated using the following equation: Titer (TU/mL)=(%GFP/100)×(Dilution factor/Volume of virus added (µL))×Number of cells seeded×1000.

Cell transduction

Target tumor cells (10^4 per well) were plated in 48-well plates and transduced with lentiviral particles at the indicated virus quantity according to p24 ELISA quantification. After 96 h, cells were detached,

washed with PBS + 2 mM EDTA, and analyzed by flow cytometry (BD Accuri™ C6 Plus, BD Biosciences) for GFP expression.

For T cells transduction, peripheral blood T cells were prestimulated for 3 days using human CD3/CD28 TransAct reagent (Miltenyi Biotec, #130-111-160) in the presence of IL-2 (100 ng/mL; Miltenyi Biotec, #130-097-743). After stimulation, 3 × 10^4 T cells per well were seeded in RetroNectin®-coated 96-well plates (Takara, #T100B; 12 µg/mL in PBS), according to the manufacturer's recommendations, and transduced with lentiviral vectors at the indicated vector doses. Cytokines were replenished every 3 days. At 3 and 6 days post-transduction, the percentage of GFP-positive cells was determined by flow cytometry.

Viral binding assay

Cell-surface binding of pseudotyped lentiviral particles was assessed by flow cytometry using an anti-G4S linker antibody recognizing scFv-based constructs containing a G4S linker. Target cells were detached with Accutase, and viral particles were added at an equal p24 amount across conditions. Cells were incubated for 30 min at 4°C on ice to limit particle internalization. Following incubation, cells were washed once with cold PBS to remove unbound particles. Bound pseudotyped particles were detected by staining with G4S Linker (E7O2V) Rabbit Monoclonal Antibody (Alexa Fluor 488 Conjugate; Cell Signaling Technology, #50515) for 30 min, followed by one additional wash with cold PBS. Samples were acquired on an Accuri flow cytometer and analyzed as Alexa Fluor 488-positive events.

Spheroid formation, imaging and spatial analysis

Multicellular spheroids were generated in 96-well ultra-low attachment plates (Corning, 7007). Antigen-expressing cells were seeded as the inner layer and centrifuged for 5 min at 100 × g to promote aggregation. After 24 h, antigen-negative TdTomato+ cells were added as the outer layer at a 1:3 ratio relative to the inner layer, followed by a second centrifugation step under the same conditions. After an additional 24 h, spheroids were exposed to lentiviral particles at an MOI of 10, calculated relative to the inner-layer cell number. Spheroids were maintained under standard culture conditions and followed for 3 days.

For flow cytometry analysis, spheroids were dissociated mechanically into single-cell suspensions and stained with a viability dye (Fixable Viability Dye eBioscience™ eFluor™ 780 #65-0865). The resulting cells were analyzed for colocalization of GFP, tdTomato and antigen expression by flow cytometry.

Spheroids were imaged using a Cellcyte imaging system equipped with an Olympus 4x objective. Images were acquired using the spheroid module in transmitted light, GFP/FITC, and mCherry channels over a period of 3 days, using identical acquisition settings throughout the experiment.

Images were processed in ImageJ/Fiji, with brightness and contrast adjusted uniformly across channels using identical display settings. For spatial analysis, concentric regions of interest (ROIs) were defined from the spheroid center to the periphery using the polygon selection tool on the TdTomato channel, then applied to the GFP channel. Concentric annuli were generated in 50-pixel increments using the Enlarge function and combined with the XOR command in the ROI Manager. Area, mean gray value, and perimeter were measured for each annulus, and fluorescence intensity was expressed as a radial profile across successive 50-pixel intervals.

Collagen-embedded 3D tumor cultures were generated by resuspending trypsinized tumor cells in a neutralized collagen I mixture containing collagen, NaOH and 10× PBS. One-microliter cell-collagen droplets were seeded into flat-bottom 96-well plates and polymerized for 5 min at 37°C before addition of pre-warmed culture medium. For transduction assays, lentiviral vectors were added 24 h after polymerization, and GFP expression was quantified by imaging and flow cytometry as described above, after collagenase digestion.

Saturation binding assay

PC3-WT, PC3-PIP, 22Rv1, and LNCaP cells (2×10^5 per well) were seeded in 24-well plates 24 h before the assay and incubated at 37 °C, 5% CO_2. [^{177}Lu]Lu-PSMA-617 was added at increasing concentrations (0.1-100 nM) with or without the competitive inhibitor 2-PMPA (10 µM; Sigma-Aldrich). After 2 h at 4 °C, cells were washed twice with ice-cold DPBS (Gibco) and lysed with 1 M NaOH (500 µL). Bound radioactivity was quantified by γ-counter (Wizard², PerkinElmer, USA). Binding affinity (Kd) and receptor density (Bmax) were determined by nonlinear regression in GraphPad Prism 10.2.3 (GraphPad Software, USA). Each experiment was performed in triplicate with quadruplicate technical replicates.

In vivo experiments

NOD.Cg-Prkdc^{scid} Il2rg^{tm1Wjl}/SzJ (NSG) mice were bred and maintained in a specific pathogen-free facility at the University of Bordeaux (agreement no. 55841). All procedures were approved by the Institutional Animal Care and Use Committee. Mice aged 8 weeks or more were randomized into treatment groups. Tumor growth and general health were assessed every other day.

For subcutaneous xenograft implantation, mice were induced with 5% isoflurane in air at a flow rate of 2 L/min and maintained with 2% isoflurane throughout the procedure. 5×10^5 tumor cells in 100 µL PBS were injected subcutaneously into the right flank. When tumors reached 100-150 mm³, the appropriate viruses (as described in the Results section) were injected intratumorally or intravenously in 100 µL PBS. Tumor bioluminescence was monitored twice a week after intraperitoneal administration of D-luciferin (IVISbrite D-Luciferin Potassium Salt Bioluminescent Substrate 150mg/kg resuspended in PBS, Revvity). Imaging was performed on a photon imager

(photonIMAGER™, RT Biospace Lab), and signals (ph/s/sr) were quantified using M3Vision software (BIOSPACE LAB).

Statistical analysis

All experiments were performed at least in biological duplicate and technical triplicate. Technical replicates, when present, were averaged before statistical analysis so that each biological replicate represented one independent data point. Data are presented as mean ± SD. Statistical analyses were performed using unpaired two-tailed Student's t tests, one-way ANOVA followed by Tukey's or Sidak's multiple-comparison tests, or two-way ANOVA followed by Tukey's or Sidak's multiple-comparison tests, as appropriate and as indicated in the figure legends. For viral binding assays, ratios were normalized to the Ab-only condition within each experiment and log2-transformed before analysis. A p-value < 0.05 was considered statistically significant. Graphs and analyses were generated using GraphPad Prism version 8.0.2.

Data availability statement

All published manuscripts reporting original research must include a data availability statement. The data availability statement must make the conditions of access to the minimum dataset that are necessary to interpret, verify and extend the research in the article transparent to readers.

Acknowledgments

The authors would like to thank Sandrine Hamon, Patrice Dutrinus and Stéphanie Lannelongue for administration assistance. We are grateful to Sabrina Fayet and Eva Manduchet for LV production optimization studies, Joann Kervadec for Alphafold structure prediction guidance and 3D modeling. We thank all the staff of A2 animal facility. We thank Atika Zouine and Vincent Pitard and Jean-Michel Griffon for technical assistance at the Flow cytometry facility, UAR 3427, INSERM US 05, Univ. Bordeaux, F-33000 Bordeaux, France. We also thank the vectorology platform Vect'UB (CNRS UMS 3427, INSERM US005, Univ. Bordeaux, F-33000Bordeaux, France) for providing viral particles and for technical support.

Funding

J.R. was supported by a fellowship from the French Ministry of Research (MESRI) and Fondation ARC www.fondation-arc.org ARCDOC42024120009208, benefited from state support managed by the Agence Nationale de la Recherche (French National Research Agency) under reference ANR-20-SFRI-0001 and supported by a mobility grant from the AFRCP "Transfert de Technologie 2022-2023" program. This work was supported by the "Réseau Recherche Impulsion Newmoon" of the University of Bordeaux, by the Joint support program for the University of Bordeaux and the Ludwig-Maximilians-Universität München (LMU, SD, SK), by the Fondation pour la Recherche sur le Cancer,

Fondation ARC www.fondation-arc.org, grant #2024050008233 (SD), and by the Institut National Du Cancer, INCa grant #085-2024-136 (SD, EV). C.M. is supported by a MARIE SKŁODOWSKA-CURIE ACTIONS PhD; network GET-IN and the European community (EV). This project has received funding from the European Union's Framework Programme for Research and Innovation, Horizon Europe under grant agreement #101119880 (EV). S.K. was supported by the BZKF (TANGO), the Deutsche Forschungsgemeinschaft (German Research Foundation, DFG; KO5055-2-1, KO5055/3-1 and SFB TRR 338SFB- TRR 338/3 2026 -452881907), the Elite Network of Bavaria (i-Target: immunotargeting of cancer), the Melanoma Research Alliance (409510), the Marie Sklodowska-Curie Training Network for Optimizing Adoptive T Cell Therapy of Cancer (955575), Marie Sklodowska-Curie Training Network for Tracking and Controlling Therapeutic Immune Cells in Cancer (101168810), the Else Kröner-Fresenius-Stiftung (IOLIN), the German Cancer Aid (DEFEAT-PDAC, AvantCAR.de and 70117182), Ernst Jung Stiftung, LMUexcellent, the Go-Bio-Initiative, the m4-Award of the Bavarian Ministry for Economical Affairs, Bundesministerium für Bildung und Forschung, European Research Council (ERC; Starting Grant 756017, PoC Grant 101100460 and CoG 101124203), Fritz-Bender Foundation, Deutsche José Carreras Leukämie Stiftung, Hector Foundation, Bavarian Research Foundation (BAYCELLATOR), the Bruno and Helene Jöster Foundation (360° CAR), the Monika Kutzner Foundation, the Rurainski foundation, the Brigitte and Dr. Konstanze Wegener Foundation.

Author contributions

J.R., S.D., E.V., N.R., V. GD, F.MG, designed the research; J.R., N.R., C.M., C.M., L.A., R.S., L.S., J.I., L. MC. J.GD., I.M., M.L., J.B., C.C., S.P. MJ.AR., performed the research; S.M., S.K. contributed in model design, analyzed the data J.R., S.D., E.V., N.R., C.M., F.MG., A.B., S.A., JM.B., E.R.; created figures J.R., N.R., C.M., L.I., R.S., S.A.; J.R. and S.D. wrote the paper, with feedback and support from all authors.

Declaration of interests

S. K. has received honoraria from Cymab, Plectonic, TCR2 Inc., Miltenyi, Galapagos, Novartis, BMS and GSK. S. K. is an inventor of several patents in the field of immuno-oncology. S. K. received license fees from TCR2 Inc and Carina Biotech. S.K. received research support from TCR2 Inc., Tabby Therapeutics, Catalym GmBH, Plectonic GmBH and Arcus Bioscience for work unrelated to the manuscript.

Keywords

Gene therapy, lentivector, pseudotyping, solid tumors, glycoprotein engineering

References

1. Zhang WW, Li L, Li D, Liu J, Li X, Li W, et al. The First Approved Gene Therapy Product for Cancer Ad-p53 (Gendicine): 12 Years in the Clinic. Hum Gene Ther. 2018 Feb;29(2):160–79. doi:10.1089/hum.2017.218 PubMed PMID: 29338444.

2. Andtbacka RHI, Kaufman HL, Collichio F, Amatruda T, Senzer N, Chesney J, et al. Talimogene Laherparepvec Improves Durable Response Rate in Patients With Advanced Melanoma. J Clin Oncol Off J Am Soc Clin Oncol. 2015 Sep 1;33(25):2780–8. doi:10.1200/JCO.2014.58.3377 PubMed PMID: 26014293.

3. Grupp SA, Kalos M, Barrett D, Aplenc R, Porter DL, Rheingold SR, et al. Chimeric antigen receptor-modified T cells for acute lymphoid leukemia. N Engl J Med. 2013 Apr 18;368(16):1509–18. doi:10.1056/NEJMoa1215134 PubMed PMID: 23527958; PubMed Central PMCID: PMC4058440.

4. Chancellor D, Barrett D, Nguyen-Jatkoe L, Millington S, Eckhardt F. The state of cell and gene therapy in 2023. Mol Ther. 2023 Dec 6;31(12):3376–88. doi:10.1016/j.ymthe.2023.11.001 PubMed PMID: 37927037; PubMed Central PMCID: PMC10727993.

5. Tang S, Chen X, Tong X, Zhu L. Overcoming the Delivery Challenges in CRISPR/Cas9 Gene Editing for Effective Cancer Treatment: A Review of Delivery Systems. Int J Med Sci. 2025 Jul 28;22(14):3625–49. doi:10.7150/ijms.112724 PubMed PMID: 40959562; PubMed Central PMCID: PMC12434829.

6. Naldini L, Blömer U, Gallay P, Ory D, Mulligan R, Gage FH, et al. In vivo gene delivery and stable transduction of nondividing cells by a lentiviral vector. Science. 1996 Apr 12;272(5259):263–7. doi:10.1126/science.272.5259.263 PubMed PMID: 8602510.

7. Wolff JH, Mikkelsen JG. Delivering genes with human immunodeficiency virus-derived vehicles: still state-of-the-art after 25 years. J Biomed Sci. 2022 Oct 9;29(1):79. doi:10.1186/s12929-022-00865-4 PubMed PMID: 36209077; PubMed Central PMCID: PMC9548131.

8. Lévy C, Amirache F, Girard-Gagnepain A, Frecha C, Roman-Rodríguez FJ, Bernadin O, et al. Measles virus envelope pseudotyped lentiviral vectors transduce quiescent human HSCs at an efficiency without precedent. Blood Adv. 2017 Oct 24;1(23):2088–104. doi:10.1182/bloodadvances.2017007773

9. Girard-Gagnepain A, Amirache F, Costa C, Lévy C, Frecha C, Fusil F, et al. Baboon envelope pseudotyped LVs outperform VSV-G-LVs for gene transfer into early-cytokine-stimulated and resting HSCs. Blood. 2014;124(8):1221–31. doi:https://doi.org/10.1182/blood-2014-02-558163

10. Maude SL, Laetsch TW, Buechner J, Rives S, Boyer M, Bittencourt H, et al. Tisagenlecleucel in Children and Young Adults with B-Cell Lymphoblastic Leukemia. N Engl J Med. 2018 Feb

1;378(5):439–48. doi:10.1056/NEJMoa1709866 PubMed PMID: 29385370; PubMed Central PMCID: PMC5996391.

11. Rossi J, Martinello C, Sorrentino R, Guyonnet-Duperat V, Amintas S, Abrey Recalde MJ, et al. Engineering Precision Oncology: Targeting tumors and immune cells with lentiviral vectors. Mol Ther Oncol. doi:10.1016/j.omton.2026.201197

12. Arduini A, Katiyar H, Liang C. Progress in Pseudotyping Lentiviral Vectors Towards Cell-Specific Gene Delivery In Vivo. Viruses. 2025 May 31;17(6):802. doi:10.3390/v17060802 PubMed PMID: 40573393; PubMed Central PMCID: PMC12197403.

13. Bender RR, Muth A, Schneider IC, Friedel T, Hartmann J, Plückthun A, et al. Receptor-Targeted Nipah Virus Glycoproteins Improve Cell-Type Selective Gene Delivery and Reveal a Preference for Membrane-Proximal Cell Attachment. PLoS Pathog. 2016 Jun;12(6):e1005641. doi:10.1371/journal.ppat.1005641 PubMed PMID: 27281338; PubMed Central PMCID: PMC4900575.

14. Kussia GG, Tessema TS. The Potential of Single-Chain Variable Fragment Antibody: Role in Future Therapeutic and Diagnostic Biologics. J Immunol Res. 2024 Jan 1;2024(1):1804038. doi:10.1155/2024/1804038

15. Enkirch T, Kneissl S, Hoyler B, Ungerechts G, Stremmel W, Buchholz CJ, et al. Targeted lentiviral vectors pseudotyped with the Tupaia paramyxovirus glycoproteins. Gene Ther. 2013 Jan;20(1):16–23. doi:10.1038/gt.2011.209

16. Berckmueller K, Thomas J, Taha EA, Choo S, Madhu R, Kanestrom G, et al. CD90-targeted lentiviral vectors for HSC gene therapy. Mol Ther J Am Soc Gene Ther. 2023 Oct 4;31(10):2901–13. doi:10.1016/j.ymthe.2023.08.003 PubMed PMID: 37550965; PubMed Central PMCID: PMC10556220.

17. Winter N, Kolbe C, Ferdos S, Steiner L, Bartelsen N, Lock D, et al. A novel pseudotype derived of the canine distemper virus for adapter-mediated lentiviral transduction in vivo. Mol Ther Methods Clin Dev. 2025 Sep 11;33(3):101526. doi:10.1016/j.omtm.2025.101526 PubMed PMID: 40734704; PubMed Central PMCID: PMC12305328.

18. Weidemann S, Perez D, Izbicki JR, Neipp M, Mofid H, Daniels T, et al. Mesothelin is Commonly Expressed in Pancreatic Adenocarcinoma but Unrelated to Cancer Aggressiveness. Cancer Invest. 2021 Oct;39(9):711–20. doi:10.1080/07357907.2021.1943747 PubMed PMID: 34143695.

19. Brown TC, Sankpal NV, Gillanders WE. Functional Implications of the Dynamic Regulation of EpCAM during Epithelial-to-Mesenchymal Transition. Biomolecules. 2021 Jul;11(7):956. doi:10.3390/biom11070956

20. Ammayappan A, Peng KW, Russell SJ. Characteristics of Oncolytic Vesicular Stomatitis Virus Displaying Tumor-Targeting Ligands. J Virol. 2013 Dec;87(24):13543–55. doi:10.1128/JVI.02240-13 PubMed PMID: 24089573; PubMed Central PMCID: PMC3838279.

21. Claas C, Wahl J, Orlicky DJ, Karaduman H, Schnölzer M, Kempf T, et al. The tetraspanin D6.1A and its molecular partners on rat carcinoma cells. Biochem J. 2005 Jul 1;389(Pt 1):99–110. doi:10.1042/BJ20041287 PubMed PMID: 15725074; PubMed Central PMCID: PMC1184542.

22. Dangaj D, Abbott KL, Mookerjee A, Zhao A, Kirby PS, Sandaltzopoulos R, et al. Mannose Receptor (MR) Engagement by Mesothelin GPI Anchor Polarizes Tumor-Associated Macrophages and Is Blocked by Anti-MR Human Recombinant Antibody. PLOS ONE. 2011 Dec 6;6(12):e28386. doi:10.1371/journal.pone.0028386

23. Zhou Q, Schneider IC, Edes I, Honegger A, Bach P, Schönfeld K, et al. T-cell receptor gene transfer exclusively to human CD8+ cells enhances tumor cell killing. Blood. 2012 Nov 22;120(22):4334–42. doi:10.1182/blood-2012-02-412973

24. Funke S, Maisner A, Mühlebach MD, Koehl U, Grez M, Cattaneo R, et al. Targeted Cell Entry of Lentiviral Vectors. Mol Ther J Am Soc Gene Ther. 2008 Aug;16(8):1427–36. doi:10.1038/mt.2008.128 PubMed PMID: 18578012; PubMed Central PMCID: PMC3927321.

25. Frecha C, Lévy C, Costa C, Nègre D, Amirache F, Buckland R, et al. Measles Virus Glycoprotein-Pseudotyped Lentiviral Vector-Mediated Gene Transfer into Quiescent Lymphocytes Requires Binding to both SLAM and CD46 Entry Receptors. J Virol. 2011 Jun 15;85(12):5975–85. doi:10.1128/jvi.00324-11

26. Nielsen IH, Rovsing AB, Janns JH, Thomsen EA, Ruzo A, Bøggild A, et al. Cell-targeted gene modification by delivery of CRISPR-Cas9 ribonucleoprotein complexes in pseudotyped lentivirus-derived nanoparticles. Mol Ther Nucleic Acids. 2024 Dec 10;35(4):102318. doi:10.1016/j.omtn.2024.102318 PubMed PMID: 39329149; PubMed Central PMCID: PMC11426049.

27. Kielian M, Chanel-Vos C, Liao M. Alphavirus Entry and Membrane Fusion. Viruses. 2010 Mar 26;2(4):796–825. doi:10.3390/v2040796 PubMed PMID: 21546978; PubMed Central PMCID: PMC3086016.

28. Huszthy PC, Giroglou T, Tsinkalovsky O, Euskirchen P, Skaftnesmo KO, Bjerkvig R, et al. Remission of Invasive, Cancer Stem-Like Glioblastoma Xenografts Using Lentiviral Vector-Mediated Suicide Gene Therapy. PLOS ONE. 2009 Jul 20;4(7):e6314. doi:10.1371/journal.pone.0006314

29. Liang M, Morizono K, Pariente N, Kamata M, Lee B, Chen ISY. Targeted transduction via CD4 by a lentiviral vector uses a clathrin-mediated entry pathway. J Virol. 2009 Dec;83(24):13026–31. doi:10.1128/JVI.01530-09 PubMed PMID: 19793825; PubMed Central PMCID: PMC2786851.

30. Liu H, Rajasekaran AK, Moy P, Xia Y, Kim S, Navarro V, et al. Constitutive and antibody-induced internalization of prostate-specific membrane antigen. Cancer Res. 1998 Sep 15;58(18):4055–60. PubMed PMID: 9751609.

31. Pariente N, Morizono K, Virk MS, Petrigliano FA, Reiter RE, Lieberman JR, et al. A Novel Dual-targeted Lentiviral Vector Leads to Specific Transduction of Prostate Cancer Bone Metastases In Vivo After Systemic Administration. Mol Ther. 2007 Nov 1;15(11):1973–81. doi:10.1038/sj.mt.6300271 PubMed PMID: 17653099.

32. Yang H, Joo KI, Ziegler L, Wang P. Cell type-specific targeting with surface-engineered lentiviral vectors co-displaying OKT3 antibody and fusogenic molecule. Pharm Res. 2009 Jun;26(6):1432–45. doi:10.1007/s11095-009-9853-y PubMed PMID: 19259792; PubMed Central PMCID: PMC2798122.

33. MacKenzie TC, Kobinger GP, Kootstra NA, Radu A, Sena-Esteves M, Bouchard S, et al. Efficient Transduction of Liver and Muscle after in Utero Injection of Lentiviral Vectors with Different Pseudotypes. Mol Ther. 2002 Sep 1;6(3):349–58. doi:10.1006/mthe.2002.0681

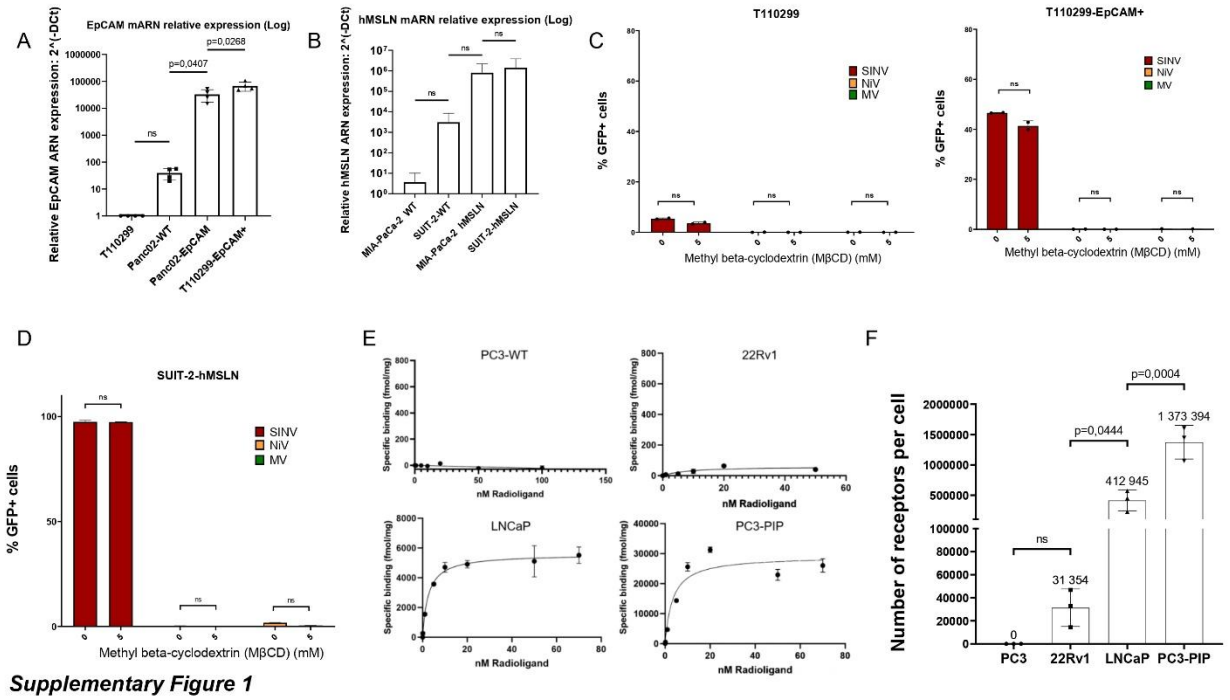
34. Miest TS, Yaiw KC, Frenzke M, Lampe J, Hudacek AW, Springfeld C, et al. Envelope-chimeric Entry-targeted Measles Virus Escapes Neutralization and Achieves Oncolysis. Mol Ther. 2011 Oct;19(10):1813–20. doi:10.1038/mt.2011.92 PubMed PMID: 21610701; PubMed Central PMCID: PMC3188758.

35. Karches CH, Benmebarek MR, Schmidbauer ML, Kurzay M, Klaus R, Geiger M, et al. Bispecific antibodies enable synthetic agonistic receptor-transduced T cells for tumor immunotherapy. Clin Cancer Res Off J Am Assoc Cancer Res. 2019 Oct 1;25(19):5890–900. doi:10.1158/1078-0432.CCR-18-3927 PubMed PMID: 31285373; PubMed Central PMCID: PMC7611266.

36. Cadilha BL, Benmebarek MR, Dorman K, Oner A, Lorenzini T, Obeck H, et al. Combined tumor-directed recruitment and protection from immune suppression enable CAR T cell efficacy in solid tumors. Sci Adv. 2021 Jun 11;7(24):eabi5781. doi:10.1126/sciadv.abi5781

37. Situ K, Chua BA, Bae SY, Meyer A, Morizono K. Versatile targeting system for lentiviral vectors involving biotinylated targeting molecules. Virology. 2018 Dec;525:170–81. doi:10.1016/j.virol.2018.09.017 PubMed PMID: 30290312; PubMed Central PMCID: PMC6269213.

Supplementary figures



Supplementary Figure 1

Figure 18 Supplementary: Characterization of tumor-antigen expression and membrane-modulation assays used for targeted lentiviral transduction.

(A) *Relative EpCAM mRNA expression in parental and EpCAM-engineered tumor cell lines, measured by RT-qPCR and displayed on a logarithmic scale.* ***(B)*** *Relative human mesothelin mRNA expression in parental and mesothelin-engineered tumor cell lines, measured by RT-qPCR and displayed on a logarithmic scale.* ***(A,B)*** *Data are shown as mean ± SD from n = 3 independent experiments, performed in duplicate. Statistical analysis was performed using a one-way ANOVA with Tukey's multiple-comparison test. Exact p values are indicated on the graphs for statistically significant comparisons; ns, not significant.* ***(C,D)*** *Effect of methyl-β-cyclodextrin (MβCD) treatment on targeted lentiviral transduction of T11029 EpCAM-negative and T11029 EpCAM-positive cells* ***(C)*** *and SUIT-2-hMSLN cells* ***(D)****. Cells were exposed to increasing concentrations of MβCD before transduction with SINV-, NiV- or MV-pseudotyped lentiviral vectors, and transduction efficiency was quantified as the percentage of GFP-positive cells****. (C,D)*** *Data are shown as mean ± SD from n = 2 independent experiments. Statistical analysis was performed using a two-way ANOVA with Sidak's multiple-comparison test. ns, not significant.* ***(E)*** *Saturation binding analysis of PSMA expression in prostate cancer cell lines using a radiolabeled PSMA ligand. Specific binding was measured in PC3, 22Rv1, LNCaP and PC3-PIP cells.* ***(F)*** *Quantification of PSMA receptor density per cell derived from the binding assays shown in* ***(E)****. PC3 and 22Rv1 cells showed low PSMA expression, whereas LNCaP and PC3-PIP cells displayed high PSMA receptor density. Data are shown as mean ± SD from n = 3 independent experiments, performed in quadruplicate. Statistical analysis was performed using a one-way ANOVA with Holm-Sidak's multiple-comparison test. Exact p values are reported in the figure legend; ns, not significant.*

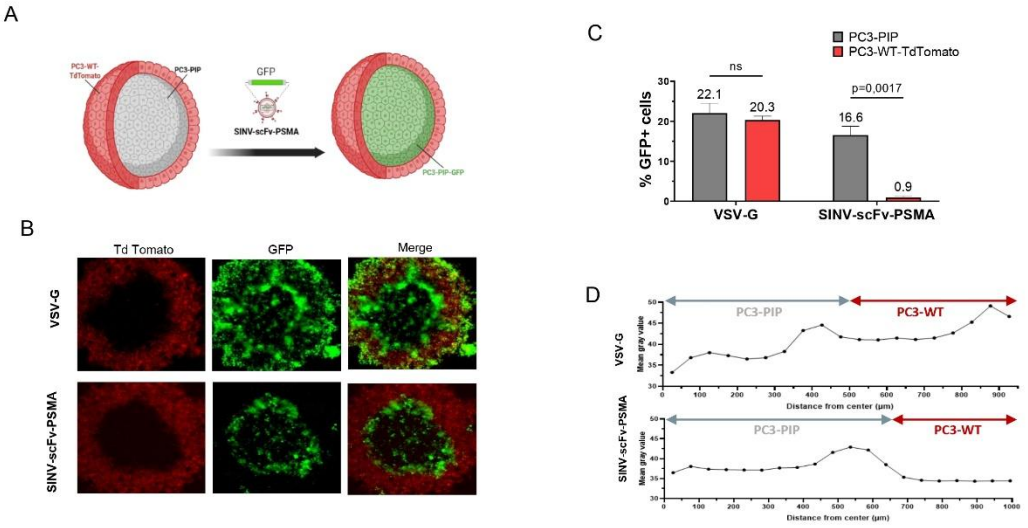


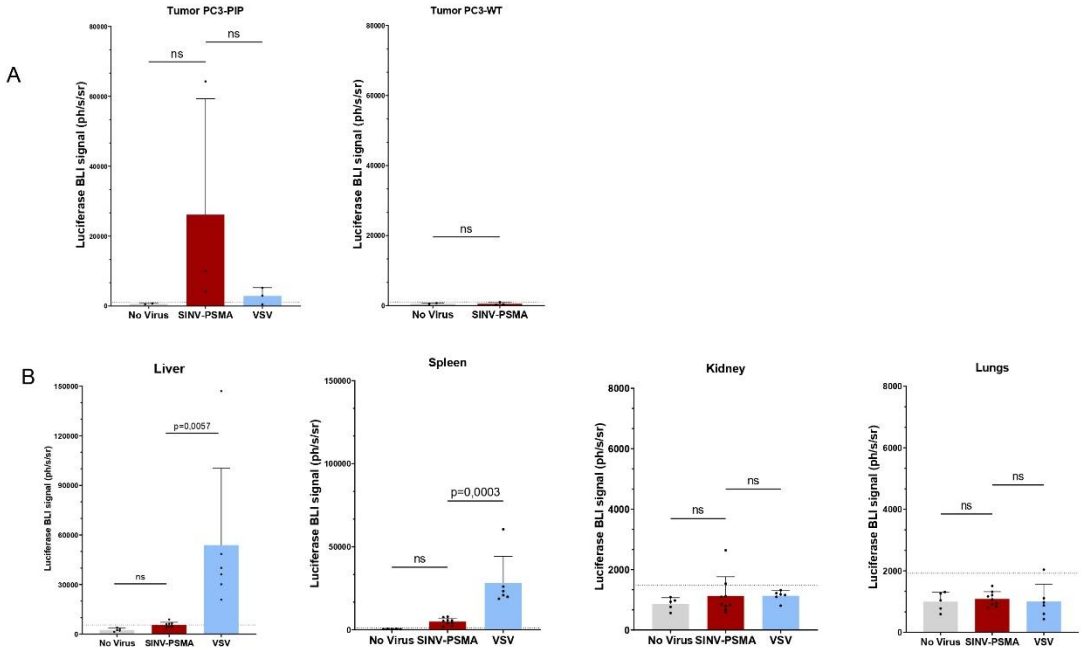
Figure 19 Supplementary: PSMA-targeted SINV pseudotypes selectively transduce PSMA-positive cells in mixed PC3 spheroids.

(A) *Schematic representation of the mixed spheroid transduction assay. PC3-WT-TdTomato cells were combined with PSMA-positive PC3-PIP cells to generate spatially organized spheroids, which were then transduced with GFP-encoding lentiviral vectors pseudotyped with VSV-G or PSMA-targeted SINV glycoproteins.*

(B) *Representative fluorescence microscopy images of mixed PC3-WT-TdTomato/PC3-PIP spheroids after transduction with VSV-G or SINV-scFv-PSMA pseudotyped lentiviral vectors. TdTomato signal identifies PC3-WT cells, whereas GFP signal indicates transduced cells. VSV-G mediated broad transduction across the spheroid, whereas SINV-scFv-PSMA preferentially transduced the PSMA-positive PC3-PIP compartment.*

(C) *Quantification of GFP-positive cells in PC3-WT-TdTomato and PC3-PIP populations after transduction with VSV-G or SINV-scFv-PSMA pseudotyped vectors. VSV-G transduced both populations, whereas SINV-scFv-PSMA selectively transduced PC3-PIP cells with minimal transduction of PC3-WT-TdTomato cells. Data are shown as mean ± SD from n = 3 Statistical analysis was performed using a two-way ANOVA with Sidak's multiple-comparison test. Exact p values are indicated on the graphs for statistically significant comparisons. ns, not significant.*

(D) *Spatial fluorescence intensity profiles across mixed spheroids transduced with VSV-G or SINV-scFv-PSMA pseudotyped vectors. The GFP signal after SINV-scFv-PSMA transduction was enriched in the PC3-PIP region and reduced in the PC3-WT-TdTomato region, supporting antigen-restricted transduction in a spatially organized tumor-cell model.*



Supplementary Figure 3

Figure 20 Supplementary: Ex vivo biodistribution analysis of systemic anti-PSMA SINV-scFv lentiviral delivery.

(A) *Ex vivo quantification of luciferase bioluminescence in PSMA-negative PC3-WT and PSMA-positive PC3-PIP tumors following systemic administration of no virus, anti-PSMA SINV-scFv LVs or VSV-G LVs. The dotted line indicates the positivity threshold.*
(B) *Ex vivo quantification of luciferase bioluminescence in liver, spleen, kidney and lung following systemic vector administration. VSV-G LVs showed prominent off-target signal in liver and spleen, whereas anti-PSMA SINV-scFv LVs displayed limited non-tumoral organ transduction.*

*The dotted line indicates the positivity threshold, calculated as followed: Positivity threshold=Mean from the no virus condition+3*standard deviation.*

Data are shown as mean ± SD from n = 3, mice per group. Statistical analysis was performed using a one-way ANOVA with Tukey's multiple-comparison test. Exact p values are indicated on the graphs for statistically significant comparisons; ns, not significant.

II. Chemokine- and decorin-based tumor niche engineering to enhance T cell recruitment and antitumor activity

After identifying retargeted SINV-pseudotyped lentiviral vectors as a suitable platform for antigen-dependent gene transfer, we next investigated whether tumor-directed gene delivery could be used to reshape local tumor-immune interactions. This part of the thesis focuses on therapeutic payloads designed to address two major barriers that limit T cell therapy in pancreatic ductal adenocarcinoma: inefficient effector-cell recruitment and stromal/TGFβ-associated restriction of antitumor function.

As an initial proof of concept, tumor cells were engineered to express the selected payloads. This allowed us to evaluate the biological consequences of local therapeutic gene expression independently of vector-entry efficiency. We selected the CXCR3 ligand CXCL10 to generate chemokine gradients able to attract activated cytotoxic T cells into the tumor compartment. We then combined this recruitment module with decorin, an extracellular matrix-associated proteoglycan selected for its ability to modulate collagen organization and interfere with TGFβ-dependent signaling. The central hypothesis was that chemokine expression would improve T cell access to the tumor, while decorin would make this access functionally productive by reducing matrix- and TGFβ-linked constraints.

This work was divided into two complementary sections. The first section focuses on human *in vitro* PDAC models and constitutes the basis of a manuscript currently in preparation. It evaluates CXCL10-decorin tumor niche engineering in SUIT-2-hMSLN and MIA PaCa-2-hMSLN cells combined with mesothelin-specific human CAR T cells. The second section presents a simplified murine *in vivo* proof-of-concept model based on Panc02-OVA-EpCAM tumors and adoptive transfer of OT-I T cells. This model was designed to test whether partial intratumoral payload expression could support antigen-specific T cell-mediated tumor control *in vivo*.

A. Preliminary evaluation of CXCL10-decorin tumor niche engineering in human mesothelin-positive PDAC models

This first section presents preliminary results from a manuscript currently under preparation, focused on the human *in vitro* model developed to evaluate the therapeutic relevance of tumor-cell secretion of CXCL10 and decorin for CAR T cell therapy in pancreatic cancer. At this stage, the manuscript is not yet ready for submission. SUIT-2-hMSLN cells were used as the main PDAC model and were engineered to directly secrete CXCL10 alone or in combination with decorin *in vitro*. These tumor cells were then combined with mesothelin-specific human CAR T cells to assess complementary

aspects of antitumor activity, including chemokine-driven migration, tumor-cell killing, IFNγ secretion, viable CAR T cell recovery, activity in collagen-embedded spheroids and resistance to TGFβ-mediated suppression.

This model was first designed to determine whether direct tumor-cell secretion of CXCL10 was sufficient to improve CAR T cell recruitment and function, or whether the addition of decorin was required to make this recruitment more functionally productive. The results support the feasibility of this approach in vitro and suggest that the CXCL10-decorin combination is associated with improved CAR T cell activity, including stronger tumor-cell killing in several experimental settings. MIA PaCa-2-hMSLN cells were then used as a second mesothelin-positive human PDAC model to begin testing whether the functional benefit of the dual payload could be maintained across distinct tumor-cell backgrounds, although additional experiments are still required to consolidate this point.

Finally, compartment-resolved proteomic analyses were performed to explore the tumor-cell and CAR T cell programs associated with CXCL10-decorin expression. These analyses provide a preliminary mechanistic framework, suggesting that decorin may act at the tumor-CAR T cell interface rather than as a simple soluble activator of isolated CAR T cells. In the next steps of the study, these in vitro findings will need to be strengthened by additional MIA PaCa-2-hMSLN experiments and by in vivo approaches testing targeted gene transfer, local transgene expression, CXCL10-decorin secretion and CAR T cell recruitment within the tumor microenvironment. This section therefore provides the current functional and mechanistic basis of the dual-payload strategy in human PDAC models, while defining the experiments required before the study can be finalized for publication.

Tumor-cell engineering for local decorin secretion enhances T cell therapy in pancreatic cancer by modulating matrix- and TGFβ-associated barriers

J Rossi1, N Richet1, S Michaelides2, L Mora Charrot3, J Izotte3, M Trefny2, E Carlini2, S Jang2, D Simnica2, M Henrich2, C Carcopino2, J Dörr2, S Claverol4, J Jaubert4, J Gillibert-Duplantier5, I Moranvillier1, MJ Abrey-Recalde1, C Charbonnieras5, A Bedel1,6, F Moreau-Gaudry1, V Guyonnet-Dupérat5, S Kobold2, 7, 8, 9 and S Dabernat1,6#

#, corresponding author

Affiliations

1 Univ. Bordeaux, INSERM, BRIC, U 1312, F-33000 Bordeaux, France

2 Institute of Clinical Pharmacology, LMU University Hospital, LMU Munich, Munich, Germany

3 Univ. Bordeaux, Animalerie A2, Service Commun des Animaleries, 33076 Bordeaux, France

4 Bordeaux Protéome, University of Bordeaux, F-33000 Bordeaux, France.

5 Plateforme VECT'UB, INSERM US 005 - CNRS UMS 3427- TBMCore, Université de Bordeaux, F-33000 Bordeaux, France

6 CHU Bordeaux, Department of Biochemistry, Pellegrin Hospital, 33000 Bordeaux, France

7 German Cancer Consortium (DKTK), Partner Site Munich, a partnership between the DKFZ Heidelberg and the LMU University Hospital, LMU Munich, Germany.

8 Einheit für Klinische Pharmakologie (EKLiP), Helmholtz Zentrum München - German Research Center for Environmental Health Neuherberg, Germany.

9 German Center for Lung Research (DZL), partner site Munich

Abstract

Pancreatic ductal adenocarcinoma (PDAC) remains largely refractory to immunotherapy, including CAR T cell therapy, because malignant cells are embedded in a dense, poorly permissive and immunosuppressive tumor microenvironment. Overcoming this barrier will likely require strategies that do more than redirect T cell specificity, by locally reshaping the tumor niche to improve immune-cell access and function. Here, we investigated a tumor niche-engineering approach in which pancreatic cancer cells were modified to produce CXCL10, to promote effector T cell recruitment, together with decorin, a matrix-associated regulator with stromal- and TGFβ-modulating properties.

Using human pancreatic cancer models and mesothelin-specific human CAR T cells, we show that CXCL10 provides a functional recruitment module, whereas the addition of decorin increases the antitumor impact of recruited CAR T cells. Compared with CXCL10 alone, the dual CXCL10-decorin payload enhanced CAR T cell-mediated tumor-cell killing, IFNγ secretion and recovery of viable CAR T cells after tumor engagement. It also improved CAR T cell activity in collagen-embedded spheroids and preserved a relative functional advantage under TGFβ exposure, two conditions that model key physical and suppressive barriers of PDAC. Compartment-resolved proteomics further linked decorin co-expression to remodeling of tumor-cell interface programs and to a post-engagement CAR T cell state enriched in biosynthetic, proteostatic and mitochondrial features.
Together, these findings support local induction of decorin production as a niche-engineering strategy to improve CAR T cell function in pancreatic cancer. More broadly, they suggest that combining chemokine-mediated immune recruitment with matrix- and TGFβ-associated barrier modulation may help convert a structurally restrictive tumor microenvironment into a more permissive site for T cell therapy.

Introduction

Pancreatic ductal adenocarcinoma (PDAC) remains one of the most lethal solid malignancies and responds poorly to conventional and immune-based therapies[1–4]. Chimeric antigen receptor (CAR) T cells are genetically engineered lymphocytes designed to recognize predefined cell-surface antigens through a synthetic receptor that combines an extracellular antigen-binding domain with intracellular T cell activation and costimulatory modules. This design enables major histocompatibility complex-independent tumor recognition and has produced deep and durable responses in several hematological malignancies, particularly B cell leukemias, lymphomas and multiple myeloma[5–8]. In contrast, clinical efficacy in solid tumors has been much more limited. This difference does not necessarily reflect an intrinsic inability of CAR T cells to kill epithelial tumor cells, but rather the fact that solid tumors impose additional constraints, including poor trafficking to tumor sites, inefficient penetration into tumor nests, antigen heterogeneity, metabolic stress and local immunosuppression. PDAC remains a relevant target for CAR T cell therapy because it expresses several actionable surface antigens, including mesothelin, HER2 and claudin 18.2, and because CAR-based recognition could in principle bypass the low neoantigen burden and defective antigen presentation that limit endogenous T cell responses in this disease.

Clinical experience with CAR T cells in PDAC has so far been underwhelming in early clinical phase trials. In a phase I study using mesothelin-directed mRNA CAR T cells in chemotherapy-refractory metastatic PDAC, treatment was feasible and biological activity was detected, but clinical efficacy remained modest, with disease stabilization in only a subset of patients and no durable objective

responses[6]. HER2-directed CAR T cells have also been tested in mixed biliary and pancreatic cancer cohorts, with limited activity in the pancreatic cancer subgroup[9].
However, these early studies also provided important proof-of-concept that CAR T cells can be administered safely and can show biological activity in patients with pancreatic cancer. More recently, claudin 18.2-directed CAR T cells have produced encouraging clinical signals in CLDN18.2-positive gastrointestinal cancers, including pancreatic cancer cases, supporting the idea that solid epithelial tumors are not uniformly resistant to CAR T cell therapy and that activity may emerge when appropriate antigen selection is combined with favorable trafficking, expansion and persistence conditions[10,11]. Together, these observations suggest that the main challenge in PDAC may not be target recognition alone, but the hostile tumor environment encountered by CAR T cells after infusion.

The barriers limiting CAR T cell therapy in PDAC are therefore best understood at the level of the tumor microenvironment. PDAC combines inefficient CAR T cell trafficking, exclusion of T cells from malignant epithelial regions, dense extracellular matrix deposition, antigen heterogeneity and local immune suppression[12–14]. These features are not independent obstacles. Instead, they interact within a stromal-dominant niche that simultaneously limits immune-cell access, increases the physical distance between effector cells and tumor cells, and exposes infiltrating lymphocytes to suppressive signals. This provides a rationale for therapeutic strategies that do not only engineer the T cell product, but also remodel the tumor niche in which these cells must operate.
PDAC is characterized by an intense desmoplastic reaction. The stroma is composed of cancer associated fibroblasts (CAFs), abundant fibrillar collagen, fibronectin, hyaluronan and other matrix components that increase tissue stiffness and create physical constraints around tumor cell clusters. The tumor-associated ECM acts as a structural barrier and contributes to immune regulation[15–17]. In particular, collagen-rich fibrosis can reduce interstitial space, alter tissue mechanics, limit immune-cell displacement and increase the distance between effector cells and malignant epithelial regions. Stromal signals can also actively exclude T cells from tumor-cell-containing regions. In preclinical pancreatic cancer models, CXCL12 produced by FAP-positive CAFs was linked to T cell exclusion and resistance to immunotherapy[18]. Moreover, TGFβ, enriched in PDAC tumors[19], further reinforces stromal remodeling, promotes immune exclusion, and directly suppresses cytotoxic T cell function by reducing effector molecules such as IFNγ, perforin and granzymes[20]. TGFβ signaling can also limit CAR T cell function, and genetic disruption of TGFβ receptor signaling has been shown to improve CAR T cell activity in TGFβ-rich tumor environments[21,22].

Therefore, in PDAC, the stroma is a major barrier to immune effector cells, including those that come from adoptive cell transfer. Strategies that improve effector-cell recruitment, increase access to tumor cells and limit suppressive stromal signaling are needed to improve CAR T cell therapy.

Improving tumor-directed trafficking has been explored in PDAC by engineering CAR T cells to express chemokine receptors that match chemokine gradients present in pancreatic tumors[14,21]. Local engineering of the tumor microenvironment can also create permissive conditions for CAR T cell activity in PDAC and other solid tumors. Combining tumor entry with protection from immune suppression was demonstrated by engineering CAR T cells with CCR8, a chemokine receptor matching the tumor-secreted CCL1 chemokine, to improve recruitment and a dominant-negative TGFβ receptor to shield them from TGFβ-mediated suppression[21]. This improved CAR T cell efficacy in pancreatic solid tumor models. These observations support the concept that chemokine-guided trafficking can be exploited to promote the delivery of effector T cells to solid tumors, including PDAC.

However, engineering each CAR T cell product to match patient- or tumor-specific chemokine patterns remains complex, because chemokine expression is heterogeneous across tumors and can change over time[23]. An alternative strategy is to introduce a defined chemokine gradient directly into the tumor bed. The CXCR3 ligands, CXCL9, CXCL10, and CXCL11, are the natural chemokines for recruitment of effector T cells to inflamed tissues. The CXCL10/CXCR3 axis is therefore a relevant candidate to promote local recruitment of CXCR3-positive cytotoxic T cells and CAR T cells into tumors[24,25].

Because chemokine-driven recruitment alone is unlikely to overcome the full spectrum of PDAC-associated barriers, an effective niche-engineering strategy may also need to target the stromal and suppressive signals encountered by T cells after tumor entry. This is particularly relevant in PDAC, where collagen-rich desmoplasia and TGFβ activity cooperate to restrict immune-cell access and cytotoxic function. We therefore selected decorin as a second payload because it connects two major features of the PDAC microenvironment: extracellular matrix organization and TGFβ-dependent stromal suppression.
Decorin is a small leucine-rich proteoglycan associated with the extracellular matrix. In pancreatic cancer, decorin has been detected mainly in the stromal compartment, with pancreatic stellate cells proposed as an important source[26]. This stromal localization is important because decorin interacts with fibrillar collagens and regulates collagen fibrillogenesis. Loss of decorin alters collagen fibril architecture and tissue mechanical properties, supporting a direct structural role in matrix organization[27,28]. Decorin can also bind TGFβ and restrain its biological activity, linking its matrix-regulatory function to a major profibrotic and immunosuppressive pathway in PDAC[29,30]. Through these activities, decorin may influence the stromal barrier at two complementary levels: collagen organization and TGFβ-driven stromal activation.

Decorin has also been associated with antitumor and immune-modulatory effects. Decorin promotes CD8 T cell infiltration, increases TNFα, IFNγ and perforin production by infiltrating T cells, and

enhances the anti-tumor efficacy of anti-PD1 therapy[31]. Decorin-carrying oncolytic adenovirus was shown to suppress TGFβ, increase IFNγ and improve the anti-tumor effect of gemcitabine in a pancreatic cancer model[32]. Although direct evidence linking decorin to CAR T function remains limited in PDAC, preclinical studies in solid tumors have shown that local decorin delivery can enhance T cell infiltration and improve CAR T activity in renal cell carcinoma[33]. Moreover, decorin can suppress tumor-cell proliferation and antagonize growth-promoting receptor signaling, including in pancreatic cancer[26,34,35]. Together, these data support decorin as a stromal-modulating candidate that may help create a more permissive tumor interface for recruited effector T cells. Here, we therefore positioned decorin as a local niche-engineering payload designed to complement CXCL10-mediated T cell recruitment. In this framework, CXCL10 promotes effector-cell access, while tumor-cell-derived decorin is intended to modulate the matrix- and TGFβ-associated barriers encountered by CAR T cells after tumor entry.

In this study, we tested a tumor niche-engineering strategy designed to combine local effector-cell recruitment with stromal modulation. We hypothesized that dual tumor secretion of CXCL10 and decorin would promote CAR T cell access to tumor cells and increase the functional impact of recruited effector cells within a matrix-rich and suppressive PDAC context. CXCL10 was used to provide a recruitment arm through the CXCR3 axis, while decorin was used as a stromal-modulating arm expected to act on collagen organization, TGFβ-associated suppression and the tumor-immune interface.

As a proof-of-concept for tumor-targeted niche engineering, we used pancreatic tumor cells as local producers of immunomodulatory payloads, thereby modeling the expected outcome of targeted lentiviral transduction within the tumor. We therefore engineered human pancreatic tumor cells to secrete CXCL10 alone or in combination with decorin and evaluated their interaction with mesothelin-specific human CAR T cells in complementary in vitro systems, including 2D coculture, collagen-embedded 3D spheroids and TGFβ-exposed conditions. Collagen-embedded spheroids were included to introduce a simplified matrix-rich barrier and to better model the spatial constraints that CAR T cells encounter in collagen-dense PDAC lesions. The strategy was first evaluated in SUIT-2-hMSLN cells and validated with MIA PaCa-2-hMSLN cells. To define the mechanisms associated with the dual payload, we performed compartment-resolved proteomic analyses of tumor cells, CAR T cells alone, and CAR T cells after coculture. This approach allowed us to distinguish tumor-cell-intrinsic changes, direct effects of recombinant decorin on CAR T cells, and CAR T cell states induced after tumor-cell engagement. We found that the CXCL10-decorin dual payload improved effector-cell-mediated tumor control under matrix-rich and TGFβ-suppressive conditions and was associated with proteomic changes consistent with a more permissive tumor-immune interaction. Together, these findings support a model in which CXCL10 promotes effector-cell

access, while decorin increases the functional impact of recruited T cells within a matrix-rich and suppressive pancreatic tumor context.

Results

CAR T cell migration is promoted by tumor-secreted CXCL10.

We built a strategy where combined tumor-secretion of CXCL10 and decorin is expected to improve trafficking and function of CAR T cells. For proof-of-concept, SUIT-2-hMSLN cells, a human model of PDAC, were engineered to express tdTomato alone, CXCL10-P2A-tdTomato, or Decorin-P2A-CXCL10-P2A-tdTomato from an EF1α-driven expression cassette cloned in a lentivector **(Figure 21A)**. Transduction efficiency was evaluated by flow cytometry based on tdTomato expression. All engineered populations showed high percentages of tdTomato-positive cells, indicating efficient and similar gene transfer across constructs **(Supplementary Figure 28A)**. We next quantified secretion of the encoded payloads in culture supernatants. CXCL10 was detected at similar levels in supernatants from CXCL10- and CXCL10-decorin-expressing SUIT-2-hMSLN cells **(Figure 21B)**, while Decorin was detected only in the dual CXCL10-decorin condition **(Figure 21C)**.

Next, we assessed whether tumor-cell-derived CXCL10 could recruit human mesothelin-specific CAR T cells using a transwell migration assay. Mock-transduced SUIT-2-hMSLN cells induced limited basal migration. CXCL10-expressing tumor cells increased CAR T cell migration, by 5.2-fold. Co-expression of Decorin did not impair this chemotactic effect and showed a similar migration profile compared with CXCL10 alone (6.4-fold, **Figure 21D**). Comparable results were obtained with MIA PaCa-2-hMSLN, another PDAC cell line, indicating that CXCL10-driven CAR T cell recruitment was not restricted to a single PDAC cell line (**Supplementary Figure 28B-D**).

Together, these results show that CXCL10 and Decorin can be co-expressed in human mesothelin-positive pancreatic tumor cells, while preserving chemokine secretion and functional recruitment of human CAR T cells.

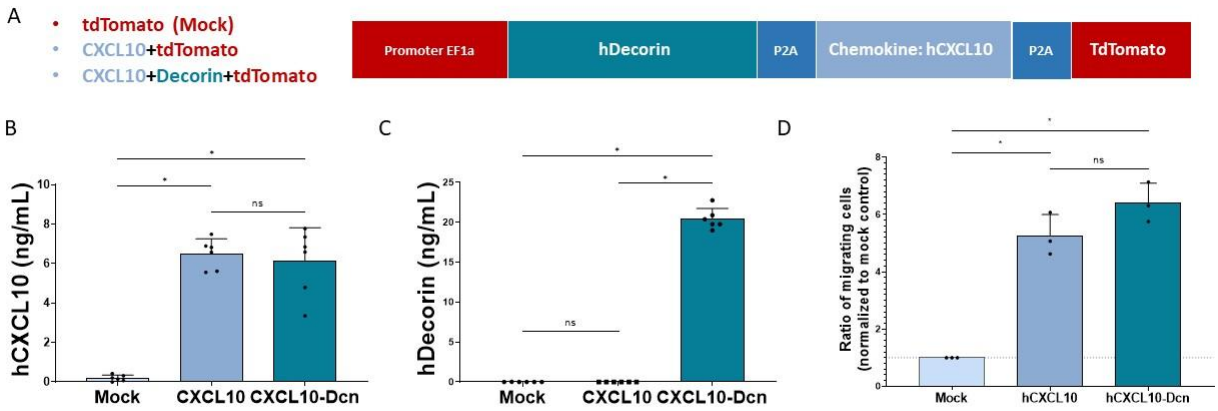


Figure 21: Tumor-secreted hCXCL10 and hDecorin can be co-expressed in mesothelin-positive PDAC cells while preserving CAR T cell recruitment.

(A) *Schematic representation of the EF1α-driven expression cassette encoding hDecorin, hCXCL10 and tdTomato separated by P2A sequences. Control cells expressed tdTomato alone, while single-payload cells expressed hCXCL10-tdTomato.* ***(B)*** *hCXCL10 secretion was quantified in culture supernatants by ELISA. hCXCL10 was detected in hCXCL10- and hCXCL10-hDecorin-expressing cells, but not in mock cells.* ***(C)*** *hDecorin secretion was quantified in culture supernatants by ELISA. hDecorin was detected only in cells transduced with the dual hCXCL10-hDecorin construct.* ***(B, C)*** *One dot represents one replicate.* ***(D)*** *Human anti-hMSLN CAR T cell migration toward engineered SUIT-2-hMSLN cells was assessed in a transwell assay and normalized to the mock condition. hCXCL10 expression increased CAR T cell migration, and hDecorin co-expression did not impair this effect. One dot represents one donor. Data are shown as mean ± SD. Statistical significance is indicated on the graph. ns: not significant.*

Anti-mesothelin CAR T cell cytotoxicity is enhanced by tumor-secreted decorin.

As decorin carries pleiotropic activities including promoting T cell function, we tested whether decorin co-expression modulated tumor-cell elimination during direct coculture with human mesothelin-specific CAR T cells produced from different donors. SUIT-2-hMSLN cells expressing tdTomato alone, CXCL10, or CXCL10 together with decorin were cocultured with human mesothelin-specific CAR T cells or untransduced T cells and tumor-cell death was monitored over time using Cytotox Green imaging **(Figure 22A)**.

Untransduced T cells induced only limited death, indicating low unspecific cytotoxicity. In contrast, mesothelin-directed CAR T cells showed antigen- and time-dependent tumor-cell killing. This increase was consistently stronger among different donors in the CXCL10-decorin condition against mock or CXCL10-only tumor cells **(Figure 22A)**. Quantification of cytotoxicity between 24 and 96 h confirmed that CXCL10-Dcn increased cytotoxicity accumulation rate by 2.2- and 2.5-fold, compared with mock and CXCL10 alone respectively, while CXCL10 alone did not alter killing, compared with

mock tumor cells **(Figure 22B)**. Endpoint killing quantification gave the same conclusion. CXCL10-Dcn increased the final killing by approximately four-fold over mock, whereas CXCL10 alone remained close to controls **(Figure 22C)**. A similar 2D cytotoxicity profile was observed using MIA PaCa-2-hMSLN cells, where CXCL10-Dcn increased cytotoxicity by 2.5-fold compared with mock conditions. This increase did not reach statistical significance in the pooled endpoint analysis, but supported the same trend across a second human PDAC cell line (**Supplementary Figure 29A,B**).

Next, we asked whether the enhanced tumor-cell killing observed with CXCL10-decorin was accompanied by stronger CAR T cell activation. IFNγ secretion was 1.3-fold higher in the CXCL10-decorin condition than in mock or CXCL10-only cocultures **(Figure 22D)**, indicating increased effector activation during tumor-cell engagement. We then quantified viable CAR T cells recovered at the end of coculture **(Figure 22E)**. The number of viable CAR T cells was 3.2-fold and 2.9-fold higher in the CXCL10-decorin condition than in mock and CXCL10-only cocultures, respectively. Together, these data indicate that decorin co-expression enhances the functional output of CAR T cells and is associated with improved recovery of viable CAR T cells after tumor-cell encounter.

To test the functional advantage of CXCL10-decorin in a 3D system, SUIT-2-hMSLN cells expressing tdTomato alone, CXCL10-tdTomato, or CXCL10-decorin-tdTomato were seeded as spheroids embedded in collagen **(Figure 22F)**. Untransduced T cells or human mesothelin-specific CAR T cells were added and monitored by live imaging. The tdTomato signal was used as a readout of tumor spheroid integrity.

In the presence of untransduced T cells, tdTomato-positive spheroids remained largely preserved over time, indicating limited nonspecific tumor-cell elimination **(Figure 22F)**.

In contrast, coculture with mesothelin-specific CAR T cells induced a progressive loss of tdTomato signal, consistent with tumor spheroid destruction. Live-imaging quantification showed that decorin co-expression enhanced CAR T cell-mediated spheroid elimination in an experiment representative of three independent CAR T cell donors **(Figure 22F).** A decrease in normalized red integrated intensity reflected loss of tdTomato-positive tumor-cell signal and therefore increased spheroid elimination **(Figure 22G)**. CAR T cells induced a progressive reduction of the red signal in all target conditions, with the strongest decrease in CXCL10-decorin-expressing spheroids. Pooled AUC analysis across three independent CAR T cell donors confirmed a lower tumor-signal burden in CXCL10-decorin spheroids, with a significant difference between mock and CXCL10-decorin conditions **(Supplementary Figure 29C)**.

Together, these results indicate that CXCL10 alone is sufficient to recruit CAR T cells, but decorin is required to obtain a clear increase in tumor-cell killing, IFNγ secretion, and recovery of viable CAR T cells during coculture.

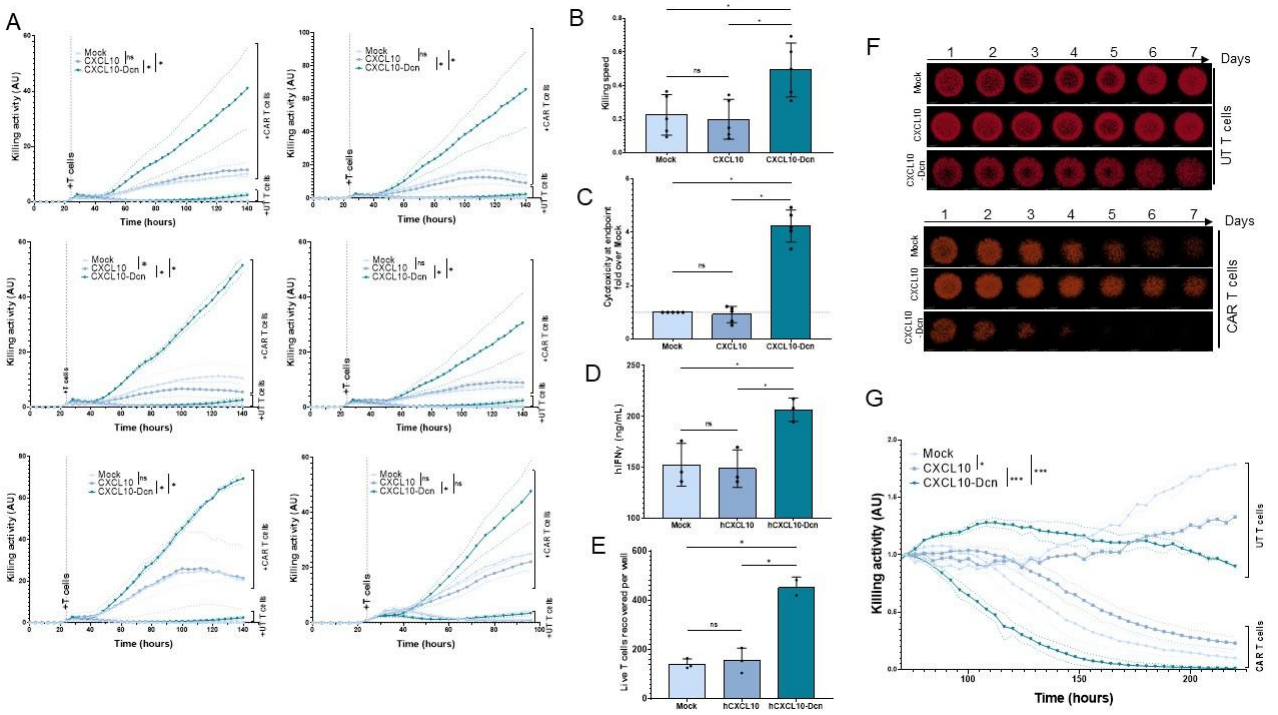


Figure 22: hCXCL10-hDecorin enhances mesothelin CAR T cell cytotoxicity and recovery of viable human CAR T cells in 2D and 3D coculture.

(A) *Real-time monitoring of tumor-cell death using an Incucyte Cytotox Green assay. SUIT-2-hMSLN cells expressing tdTomato alone, hCXCL10, or hCXCL10-hDecorin were cocultured with human mesothelin-specific CAR T cells or untransduced T cells. Cytotox Green accumulation was monitored over time and quantified as a normalized Cytotox Green signal. The signal was calculated as Green Integrated Intensity per Well / Phase Area Confluence and normalized to day 1, 0 h, 0 min. Each graph represents an independent CAR T cell donor. Increased Cytotox Green signal reflects accumulation of dead cells over time.* ***(B)*** *Cytotox Green slopes were calculated between 24 h and 96 h after T cell addition and used as a measure of cytotoxicity accumulation rate. hCXCL10-hDecorin significantly increased the Cytotox Green slope compared with mock and hCXCL10-only tumor cells, indicating faster CAR T cell-mediated killing.* ***(C)*** *Endpoint quantification of cytotoxicity at 140 h across independent CAR T cell donors. Cytotoxicity was expressed as a fold index over the mock condition. hCXCL10 expression alone did not significantly increase endpoint killing compared with mock tumor cells, whereas hCXCL10-hDecorin co-expression significantly increased CAR T cell-mediated killing. Each point represents one CAR T cell donor, calculated from the mean of technical duplicate.* ***(D)*** *hIFNγ secretion measured in coculture supernatants after 96 h. IFNγ was detected in CAR T cell cocultures with SUIT-2-hMSLN cells, with higher levels observed in the hCXCL10-hDecorin condition compared with mock and hCXCL10-only conditions.* ***(E)*** *Quantification of live T cells recovered after 96 h of coculture. Viable cells were quantified to assess the number of live CAR T cells remaining in each condition. A higher number of viable T cells was detected in the hCXCL10-hDecorin condition, suggesting improved CAR T cell persistence or accumulation during coculture.* ***(F)*** *Representative Incucyte images of tdTomato-positive SUIT-2-hMSLN collagen-embedded spheroids monitored over seven days. In the presence of untransduced T cells, tumor spheroids remained largely preserved. In contrast, coculture with mesothelin-specific CAR T cells induced*

progressive loss of tdTomato signal, reflecting tumor spheroid destruction. The strongest decrease in red signal was observed in the hCXCL10-hDecorin condition. ***(G)*** *Quantification of spheroid-associated tdTomato signal from the representative experiment shown in panel F. Tumor-cell signal was measured as Total Red Object Integrated Intensity, expressed as RCU × µm² per well, and normalized to T72h. A decrease in normalized red integrated intensity indicates loss of tdTomato-positive tumor-cell signal and therefore increased spheroid killing. Untransduced T cells had limited effect on spheroid signal, whereas CAR T cells induced a progressive decrease, most strongly in hCXCL10-hDecorin-expressing spheroids. (F,G) Representative data of n=3 independent donors. Data are shown as mean ± SD. Each point represents one biological replicate or independent CAR T cell donor, as indicated. For panels B-E, statistical analyses were performed using one-way ANOVA with multiple-comparison correction. Statistical significance is indicated on the graphs. ns, not significant; *p < 0.05. For panels A and G, statistical analysis of Cytotox Green kinetics was performed using a two-way repeated-measures ANOVA or mixed-effects model with time and tumor-cell condition as factors. The Time × Condition interaction was used to assess differences in killing kinetics.*

CAR T cell activity is partly preserved by decorin under TGFβ exposure

After validating the effect of CXCL10-decorin in 2D coculture and collagen-embedded spheroids, we tested whether the dual-payload strategy could preserve CAR T cell activity in the presence of TGFβ. Recombinant TGFβ was used to mimic a major soluble immunosuppressive factor of the PDAC tumor microenvironment, as TGFβ is elevated in pancreatic cancer and has been shown to suppress cytotoxic T cell and CAR T cell effector functions[18,20]. SUIT-2-hMSLN cells expressing tdTomato alone, CXCL10, or CXCL10-decorin were cocultured with human mesothelin-specific CAR T cells in the presence or absence of recombinant TGFβ added in the culture medium **(Figure 23A)**. As Mock and CXCL10 conditions remained comparable across these readouts, with no significant differences detected (data not shown), only the CXCL10 and CXCL10-Dcn conditions are shown to simplify figure presentation.

TGFβ reduced CAR T cell killing activity **(Figure 23A)**. In the presence of decorin, however, CAR T cells retained stronger killing kinetics **(Figure 23A)**. CXCL10-decorin increased cytotoxicity by 1.87- and 1.63-fold, compared with CXCL10 alone in condition with and without TGFβ, respectively **(Supplementary Figure 29D)**. This indicates that decorin enhanced CAR T cell killing even in the presence of TGFβ.

Endpoint killing quantification gave the same conclusion. CXCL10-decorin increased the final cytotoxicity signal by 2.15- and 2.58-fold compared with CXCL10-only tumor cells in untreated conditions and under TGFβ exposure, respectively **(Supplementary Figure 29D)**. Although TGFβ reduced the overall endpoint cytotoxicity, CXCL10-decorin maintained a higher killing signal than CXCL10 alone **(Supplementary Figure 29D)**. IFNγ secretion followed the same pattern. In the absence of TGFβ, CXCL10-decorin increased IFNγ secretion by 2.25-fold compared with CXCL10

alone. Under TGFβ exposure, IFNγ secretion remained higher in the CXCL10-decorin condition, even though the difference did not reach statistical significance **(Figure 23C).**

These data indicate that decorin does not abolish TGFβ-mediated suppression, but preserves a functional advantage for CAR T cells during tumor-cell engagement.

We next followed tdTomato fluorescence as a live readout of tumor spheroid persistence under TGFβ exposure. CXCL10-expressing spheroids retained more red signal over time, indicating less efficient tumor-cell elimination. By contrast, CXCL10-decorin-expressing spheroids showed a stronger decrease in red fluorescence, consistent with improved CAR T cell-mediated spheroid destruction despite TGFβ exposure ($p = 0.0023$) **(Figure 23D)**. Quantification of fluorescence loss during the linear phase confirmed that TGFβ reduced the killing rate in CXCL10-only cultures, whereas this effect was not significant when decorin was co-expressed **(Supplementary Figure 29E).**

Together, these results show that CXCL10-decorin mediates a CAR T cell functional advantage under TGFβ exposure. Decorin increased tumor-cell killing, maintained higher IFNγ secretion in untreated coculture, and improved elimination of collagen-embedded spheroids in a suppressive TGFβ-rich context.

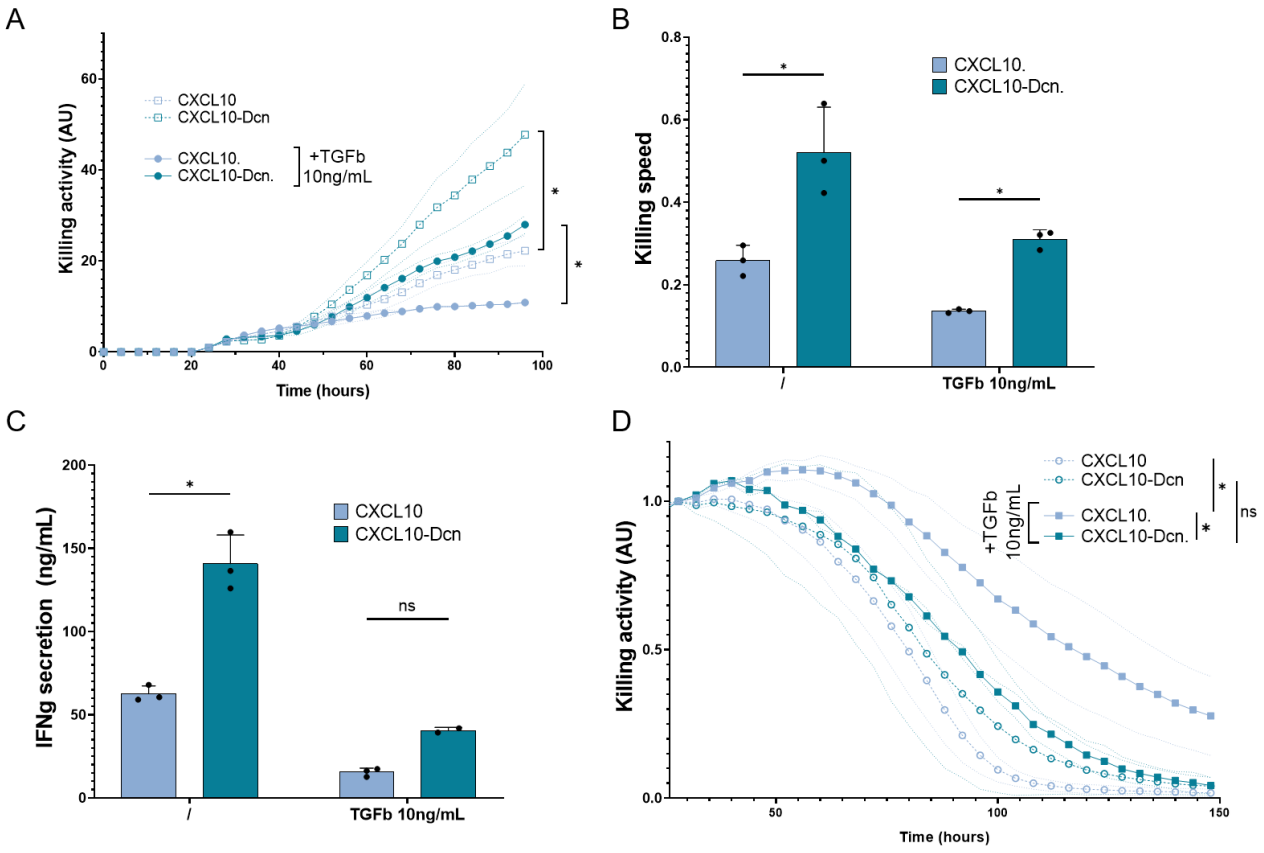


Figure 23: hCXCL10-hDecorin preserves a relative CAR T cell functional advantage under TGFβ exposure.

(A) *Real-time monitoring of tumor-cell death using an Incucyte Cytotox Green assay. SUIT-2-hMSLN cells expressing hCXCL10 or hCXCL10-hDecorin were cocultured with human mesothelin-specific CAR T cells in the absence or presence of recombinant TGFβ at 10 ng/mL. Cytotox Green accumulation was quantified as Green Integrated Intensity per Well / Phase Area Confluence and normalized to 1d0h0m. Increased signal reflects accumulation of dead cells over time* ***(B)*** *Quantification of the cytotoxicity accumulation rate from panel A. Slopes were calculated from the Cytotox Green curves and used as a readout of killing acceleration. hCXCL10-hDecorin increased the cytotoxicity accumulation rate compared with hCXCL10 alone, both in untreated conditions and under TGFβ exposure.* ***(C)*** *IFNγ secretion measured in coculture supernatants. CAR T cells secreted IFNγ upon coculture with SUIT-2-hMSLN cells, with higher levels observed in the hCXCL10-hDecorin condition than in the hCXCL10-only condition in the absence of TGFβ. TGFβ exposure reduced IFNγ secretion, but IFNγ levels remained higher in the hCXCL10-hDecorin condition, although this difference did not reach statistical significance compared with the other two conditions.* ***(D)*** *Kinetics of tdTomato-positive spheroid loss in cocultures exposed or not to 10 ng/mL TGFβ. Red fluorescence was quantified as Red Integrated Intensity per Well and normalized to the time of CAR T cell addition. Curves are shown for spheroids cocultured with CAR T cells in the absence or presence of TGFβ. In the presence of TGFβ, hCXCL10-expressing spheroids showed delayed reduction of red signal and were not significantly different, whereas hCXCL10-hDecorin-expressing spheroids displayed a stronger decrease in fluorescence than hCXCL10-only spheroids, indicating improved CAR T cell-mediated spheroid elimination under TGFβ exposure. Data are shown as mean ± SD where applicable. Statistical analysis was performed using two-way ANOVA with multiple-comparison correction, as appropriate. ns, not significant; *p < 0.05.*

Recombinant decorin partially counteracts the TGFβ-driven inhibitory proteomic state of CAR T cells

To gain mechanistic insight into how decorin affects CAR T cells, we compared T cell proteomes under inhibitory TGFβ conditions in the presence or absence of recombinant decorin **(Supplementary Figure 30)**. The analysis focused on functional programs associated with TGFβ-mediated inhibition of activated CD8 T cells, including cell expansion, DNA replication, cytoskeletal regulation, cytokine signaling, proteostasis, memory-associated programs and cytotoxic effector function[35].

As expected, TGFβ induced a clear proteomic shift compared with non-treated (NT) CAR T cells **(Figure 24A)**. The selected protein programs were consistent with a broad inhibitory effect of TGFβ on CAR T cells **(Figure 24B)**. Several proteins involved in proliferation, cell-cycle progression and DNA replication were reduced after TGFβ exposure, including SMC4, NCAPG, CDK1, SMC2, RRM1 and MKI67. TGFβ also altered proteins linked to trafficking, vesicle regulation and cytoskeletal organization, with induction of NLRC3, SLC1A4, ABLIM1 and TRPC4, and repression of AAMP, PPP1R9B and PDLIM1. In parallel, cytokine/NFκB/IFN-associated proteins, including IL2RG, MYD88 and ITGAX, were decreased. The cytotoxic effector program was also affected, as shown by reduced PRF1 abundance. Finally, TGFβ decreased LEF1, a transcription factor associated with

T cell memory and stemness. These results confirmed that *in vitro* exposure to TGFβ induced the expected inhibitory proteomic state in activated CAR T cells. Of note, we observed a limited proteomic response of CAR T cells treated with decorin compared with non-treated cells **(Supplementary Figure 31A)**, supporting the idea that decorin does not strongly modulate activation or reprogram CAR T cells by itself in the absence of TGFβ.

Next, we asked whether recombinant decorin could partially restore the CAR T cell proteome altered by TGFβ. We focused on proteins regulated by TGFβ and calculated a rescue score to determine whether adding decorin shifted each protein closer to its untreated level. In the heatmap, red indicates proteins shifted back toward the untreated state by decorin, whereas blue indicates proteins that remained altered or were further shifted away in the presence of decorin **(Figure 24C)**. Among the 25 proteins dysregulated by TGFβ, 14 proteins (56%) were restored or partially restored by decorin. This rescue pattern was most apparent for proteins associated with trafficking, cytoskeletal regulation and signaling. By contrast, 4 proteins (16%) were not modified by decorin, and 7 proteins (28%) were further dysregulated in the presence of decorin.

Representative proteins were then plotted individually **(Figure 24D)**. DOCK7, a trafficking- and cytoskeleton-associated protein, was reduced by TGFβ and partially restored by decorin in the presence of TGFβ. GZMA, an effector-associated granzyme, was also reduced by TGFβ and showed a trend toward recovery with decorin. In contrast, OSBPL8 and SIRT3, associated with lipid/membrane regulation and mitochondrial function, were increased by TGFβ and reduced when decorin was added.

To further assess the extent of this rescue, we compared recDcn + TGFβ-treated CAR T cells directly with untreated cells. Reactome enrichment and heatmap analyses showed that the recDcn + TGFβ condition remained distinct from NT, with persistent enrichment of several pathways and reduced mitochondrial translation and interferon signaling (**Supplementary Figure 32A,B**). These data support a partial, rather than complete, restoration of the TGFβ-altered CAR T cell proteome.

Together, these results indicate that recombinant decorin does not globally revert the TGFβ-induced proteomic state of isolated CAR T cells, but partially attenuates selected components of this response. This supports the relevance of this proteomic model for studying how decorin may modulate TGFβ-imposed constraints on activated CAR T cells before assessing its effect during tumor-cell engagement.

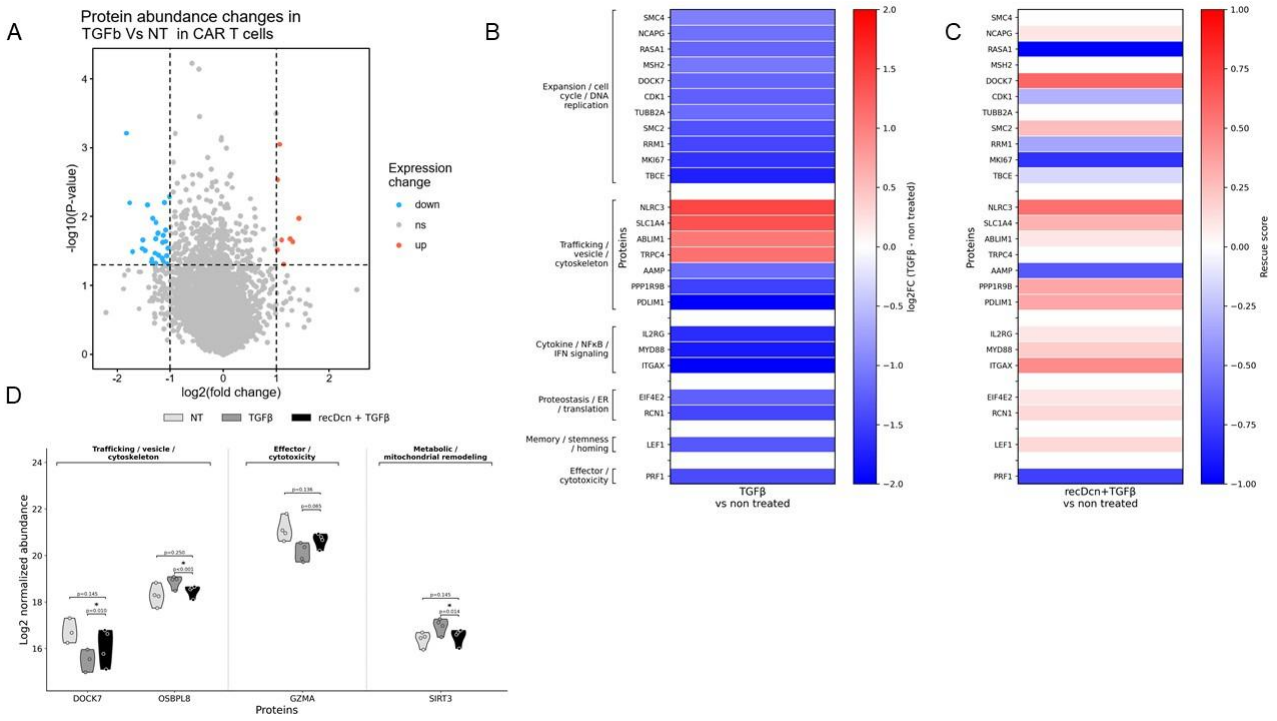


Figure 24: Recombinant decorin partially remodels the TGFβ-driven CAR T cell proteomic state.

(A) *Volcano plot showing protein abundance changes in activated CAR T cells treated with TGFβ compared with non-treated (NT) CAR T cells. Each dot represents one quantified protein. Red dots indicate proteins increased by TGFβ, blue dots indicate proteins decreased by TGFβ, and grey dots indicate non-significant proteins. Dashed lines indicate the selected thresholds for log2 fold change and p-value.* ***(B)*** *Heatmap of selected TGFβ-dysregulated proteins grouped into functional programs associated with TGFβ-mediated inhibition of activated CAR T cells. Values represent log2 fold change in TGFβ-treated CAR T cells relative to NT CAR T cells. Blue indicates reduced abundance and red indicates increased abundance.* ***(C)*** *Rescue score heatmap showing the effect of recombinant decorin under TGFβ exposure. Proteins are ordered as in panel B. Red indicates proteins for which recDcn + TGFβ shifts abundance back toward the NT state relative to TGFβ alone, while blue indicates proteins that remain distant from the NT state or are further shifted in the TGFβ-induced direction.* ***(D)*** *Violin plots showing donor-level log2 normalized abundance of selected representative proteins. DOCK7 and OSBPL8 were selected as trafficking, vesicle and cytoskeleton-associated proteins, GZMA as an effector-associated granzyme, and SIRT3 as a marker of mitochondrial remodeling. Each dot represents one donor. P values indicate paired comparisons between TGFβ and recDcn + TGFβ conditions. The number of points may vary when a protein was not quantified in all donor-condition samples. *p < 0.05.*

Decorin promotes a biosynthetic and proteostatic CAR T cell state after tumor engagement

Next, we analyzed the proteome of CAR T cells collected after coculture with tumor cells secreting CXCL10 or CXCL10-Dcn. CXCL10 induced only a limited proteomic shift compared with untreated (Mock) coculture **(Figure 25A)**. This indicates that CXCL10 expression by tumor cells has a modest impact on the CAR T cell proteome. Direct comparison of CXCL10-Dcn and CXCL10 showed a wider decorin-associated proteomic response, with many proteins increased in the CXCL10-Dcn condition **(Figure 25B)**. This indicates that the addition of decorin strongly impacts the CAR T cell proteome after tumor engagement.

To define biological programs associated with this shift, we focused on proteins linked to ribosome biogenesis, translation, protein processing and proteostasis, as these pathways emerged among the main programs enriched in the CXCL10-Dcn condition compared with mock and CXCL10 conditions **(Supplementary Figure 31B)**. Heatmap analysis showed proteins involved in these functions were consistently enriched in the CXCL10-Dcn, in comparison to Mock and CXCL10 conditions **(Figure 25C)**. This pattern supports an increase of biosynthetic and proteostatic activity when CAR T cells encounter and kill tumor cells in the presence of decorin. Representative proteins from these programs were then analyzed individually. RPL35 and EIF4B, linked to ribosomal function and translation, were increased in the CXCL10-Dcn condition compared with CXCL10. SPCS1 and DNAJC8, associated with protein processing and proteostasis-related functions, showed the same pattern **(Figure 25D)**. To test whether this proteomic signature was associated with increased protein synthesis, we performed a puromycin incorporation assay after coculture. CAR T cells were pulsed with puromycin for 10 min, and global nascent protein synthesis was assessed by anti-puromycin Western blotting and normalized to GAPDH **(Figure 25E,F)**. The CXCL10-Dcn condition showed higher puromycin incorporation than untreated (Mock) and CXCL10 conditions. This is consistent with the proteomic enrichment of translation and proteostasis-associated proteins in the CXCL10-Dcn condition.

Next, we compared the amplitude of decorin-induced proteome changes in CAR T cells according to their exposure to tumor cells, i.e. before and post-killing. A Venn diagram showed that the number of up- or downregulated proteins was much higher after tumor-cell engagement than in CAR T cells exposed to decorin alone (1108 vs 200) and 46 proteins were shared (**Figure 26A**). Among them, 29 proteins were regulated in the same way, and 17 were regulated in opposite ways (**Supplementary Figure 31C**). The shared regulated proteins were distributed in several pathways (**Figure 26B**). Interestingly, a correlation study of the different pathways, before and after exposure to tumor cells reveals a high correlation after decorin exposure (Pearson r=0.87), suggesting that decorin may support the acquisition of a post-engagement CAR T cell state compatible with effector

function. The clearest shared increases were seen for RPL29 and RPL21, whereas TRMT112, ETF1, and LGALS1 were significantly decreased (**Figure 26C**). As expected, the cytokine/NFκB/IFN signaling were uncorrelated (r near 0) suggesting that inflammatory signaling is context-dependent and reshaped by tumor-cell encounter. The shared regulated proteins involved in trafficking/vesicle/cytoskeleton and expansion/ cell cycle/DNA replication showed modest correlations before and after tumor cell killing (r= 0.4 and r = 0.52, respectively, **Figure 26B**).

Together, these data indicate that decorin leaves a clear molecular imprint on CAR T cells after tumor engagement, promoting a post-coculture state compatible with increased protein production, protein processing and cellular fitness.

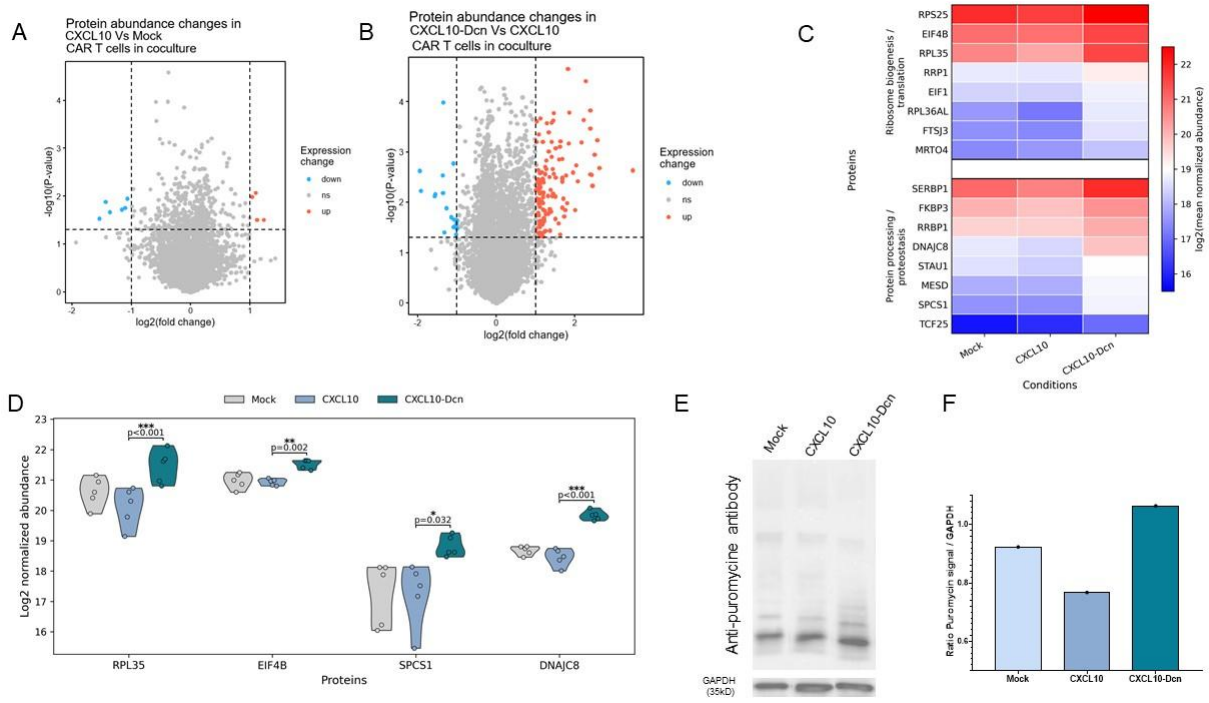


Figure 25: Decorin promotes a biosynthetic and proteostatic CAR T cell state after tumor engagement. ***(A)*** *Volcano plot showing protein abundance changes in CAR T cells after coculture with CXCL10-secreting tumor cells compared with Mock tumor cells. Each dot represents one protein. The x-axis shows log2(fold change), and the y-axis shows −log10(P-value). Vertical dashed lines indicate log2FC thresholds of ±1, and the horizontal dashed line indicates P = 0.05. Proteins significantly increased are shown in red, proteins significantly decreased are shown in blue, and non-significant proteins are shown in grey.* ***(B)*** *Volcano plot showing protein abundance changes in CAR T cells after coculture with CXCL10-Dcn-secreting tumor cells compared with CXCL10-secreting tumor cells. This comparison isolates the contribution of decorin on the CXCL10 background. The predominance of upregulated proteins in the CXCL10-Dcn condition indicates that decorin strongly modifies the post-coculture CAR T cell proteomic state.* ***(C)*** *Heatmap of selected proteins associated with ribosome biogenesis, translation, protein processing and proteostasis. Values are shown as row z-scores calculated from the mean log2 normalized abundance for each condition. Red indicates higher relative abundance and blue indicates lower relative abundance within each protein row. Proteins were grouped into two functional blocks: ribosome biogenesis/translation and protein processing/proteostasis. Most*

proteins in both blocks showed higher abundance in the CXCL10-Dcn condition, supporting a decorin-associated biosynthetic and proteostatic CAR T cell state after coculture. ***(D)*** *Violin plots showing representative proteins from the biosynthetic and proteostatic programs highlighted in panel C. RPL35 and EIF4B were selected as translation/ribosome-associated proteins, while SPCS1 and DNAJC8 were selected as protein processing/proteostasis-associated proteins. Dots represent individual CAR T cell donors. Mock is shown in light grey, CXCL10 in light blue and CXCL10-Dcn in teal. P-values indicate paired comparisons between CXCL10 and CXCL10-Dcn conditions. Exact P-values are shown on the graph; significance levels are indicated as *P < 0.05, **P < 0.01 and ***P < 0.001.* ***(E)*** *Representative Western blot of puromycin incorporation after CAR T cell coculture. CAR T cells recovered from Mock, CXCL10 or CXCL10-Dcn cocultures were pulsed with puromycin for 10 min. Global nascent protein synthesis was detected using an anti-puromycin antibody. GAPDH was used as loading control.* ***(F)*** *Quantification of the puromycin incorporation assay shown in panel E. Puromycin signal was normalized to the corresponding GAPDH signal. The graph shows the puromycin/GAPDH ratio from one independent experiment. No statistical analysis was performed because this experiment was performed once. This preliminary orthogonal readout is consistent with the increased translation and proteostasis-associated proteomic signature observed in the CXCL10-Dcn condition.*

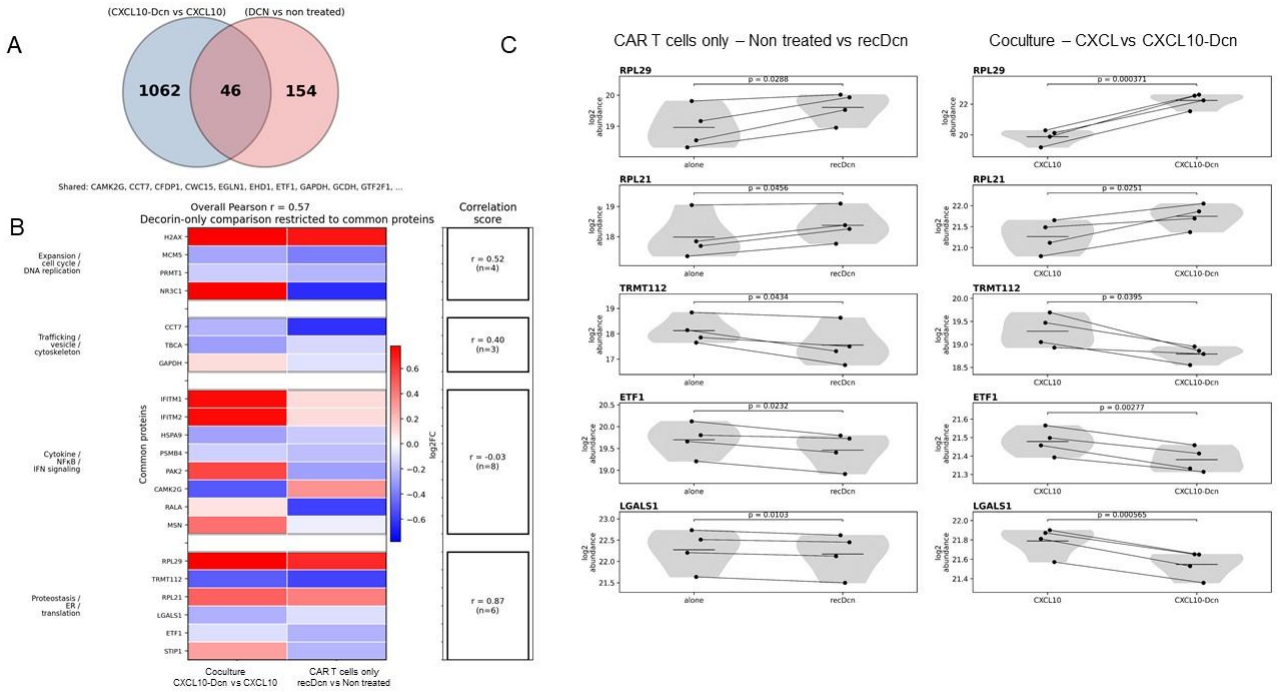


Figure 26: Decorin-containing conditions induce partially overlapping proteomic changes in CAR T cells before and after tumor-cell engagement.

(A) *Venn diagram showing the overlap between proteins deregulated in the coculture dataset after comparison of CXCL10-Dcn versus CXCL10 and proteins deregulated in the CAR T cell-only dataset after comparison of recDcn versus non-treated CAR T cells. Forty-six proteins were common to both comparisons.* ***(B)*** *Heatmap showing the log2 fold change of selected shared proteins from the overlap identified in panel A. Proteins were grouped according to functional categories: expansion/cell cycle/DNA replication, trafficking/vesicle/cytoskeleton, cytokine/NFκB/IFN signaling, and proteostasis/ER/translation. The left column shows the coculture comparison CXCL10-Dcn versus CXCL10, and the right column shows the CAR T cell-*

only comparison recDcn versus non-treated. Red indicates increased abundance and blue indicates decreased abundance in the first condition of each comparison. Pearson correlation was calculated across the shared proteins shown in the heatmap and within each functional block. The overall correlation was moderate (r = 0.57), with the strongest concordance observed in the proteostasis/ER/translation module (r = 0.87, n = 6). ***(C)*** *Violin plots showing log2-normalized abundance of selected proteins from the proteostasis/translation module. In the CAR T cell-only dataset, non-treated CAR T cells were compared with recDcn-treated CAR T cells. In the coculture dataset, CAR T cells recovered from CXCL10 cocultures were compared with CAR T cells recovered from CXCL10-Dcn cocultures. Dots represent individual donors, black lines connect paired donor values, and horizontal bars indicate the mean. P values were calculated using paired statistical testing.*

Tumor-cell proteomics identifies a coordinated decorin-associated remodeling program at the tumor cell interface.

The proteomic response of SUIT-2-hMSLN tumor cells to their secretion of CXCL10 alone showed little difference compared with Mock, as seen on the Volcano plot **(Figure 27A)**. This indicates that CXCL10 alone had a limited direct impact on the tumor-cell proteome. To isolate the contribution of decorin on the CXCL10 background, we then compared CXCL10-Dcn directly with CXCL10 only **(Figure 27B)**. This comparison revealed a focused decorin-associated proteomic response, with a limited number of strongly regulated proteins, suggesting that decorin does not induce a broad global proteomic shift but acts on selected tumor-cell programs.

Decorin is specifically induced by the engineering, as it was not detected in the mock and CXCL10-only conditions but it is not among the highest-abundance proteins in the panel and appears in the light blue range of color. The addition of decorin did not affect the classic extracellular matrix (ECM) matrisome[36], composed of collagen, laminin and proteoglycans **(Figure 27C)**. However, decorin induced changes in proteins involved in the remodeling of the tumor-cell interface **(Figure 27C**). ITGB8, S1PR3, EPHA2 and YAP1 provide the strongest support for this interpretation, as they are directly linked to adhesion, membrane signaling and mechanotransduction. In parallel, the decrease in KRT17, KRT80, TGM1 and KPRP is consistent with loss of an epithelial/barrier-like program, further supporting a decorin-associated reprogramming of how tumor cells interact with their extracellular environment. The strong induction of ITGB8 was accompanied by intracellular changes consistent with remodeling of cell-matrix signaling, including increased abundance of MAPK4/6 and membrane-trafficking regulators such as RAB5A, VAMP8 and NAPA **(Figure 27D)**. These changes support a coordinated decorin-associated remodeling program involving cell-matrix signaling, intracellular trafficking and regulation of the tumor-cell interface.

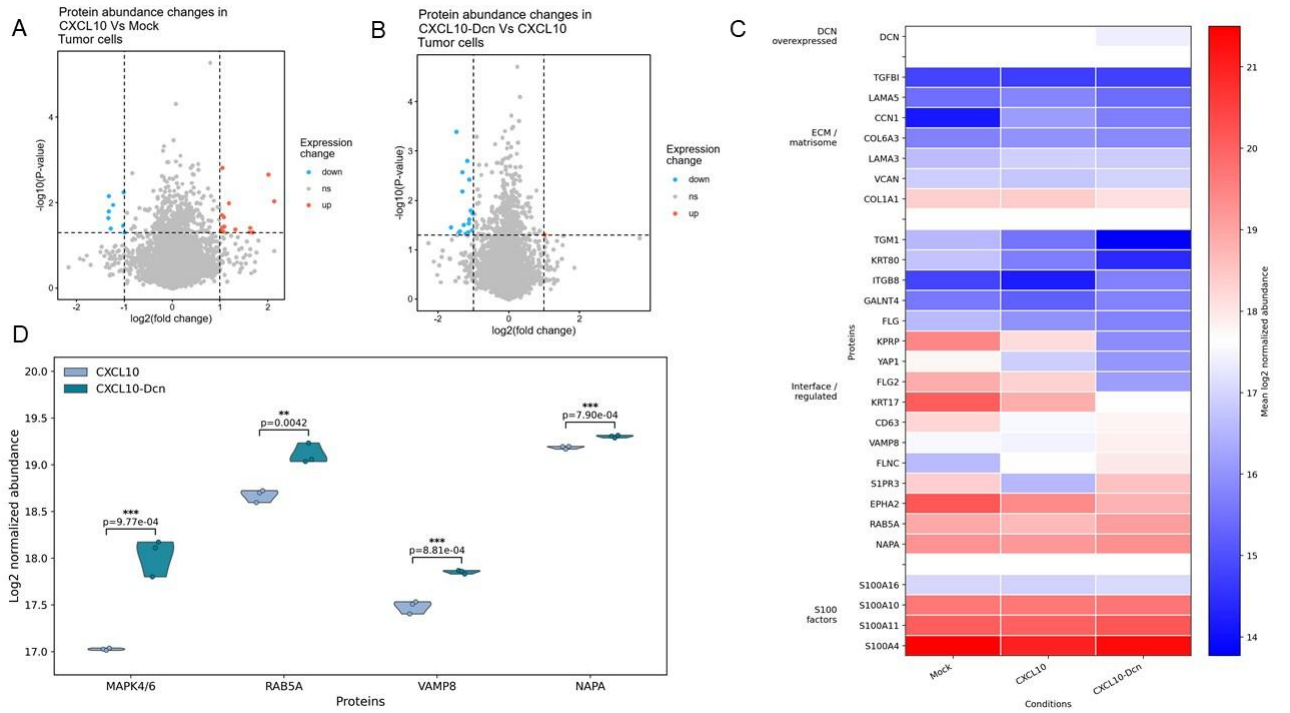


Figure 27: Tumor-cell proteomics identifies a coordinated decorin-associated remodeling program at the tumor cell interface.

(A) *Volcano plot showing differential protein abundance in SUIT-2-hMSLN tumor cells comparing CXCL10 vs Mock. CXCL10 induced a moderate but measurable proteomic shift. Dashed lines indicate the thresholds used to highlight differential proteins.* ***(B)*** *Volcano plot showing differential protein abundance in CXCL10-Dcn vs CXCL10 tumor cells. This comparison isolates the additional effect of decorin on the CXCL10 background and shows a focused decorin-associated proteomic response rather than broad global remodeling.* ***(C)*** *Heatmap of selected ECM/matrisome-associated and tumor-cell interface proteins across Mock, CXCL10 and CXCL10-Dcn conditions. Classical ECM/matrisome-associated proteins showed limited changes, whereas interface-associated proteins displayed stronger decorin-associated modulation. Proteins were selected for their relevance to collagen/laminin/proteoglycan-associated matrix components, adhesion, membrane signaling, cytoskeletal organization and epithelial barrier programs. Values are shown as mean log2 normalized protein abundance.* ***(D)*** *Quantification of selected intracellular signaling and membrane-trafficking proteins associated with the decorin-induced interface-remodeling signature. MAPK4 and MAPK6 were grouped as MAPK4/6 because they showed identical abundance behavior in the proteomic export. RAB5A, VAMP8 and NAPA were selected as membrane-trafficking regulators. Data are shown as log2 normalized protein abundance for CXCL10 and CXCL10-Dcn conditions. Statistical comparisons were performed using Welch's t test. Exact p values are indicated on the graph.*

Discussion

CAR T cell efficacy in pancreatic cancer is limited by the combination of poor T cell trafficking, dense extracellular matrix organization and TGFβ-associated immune suppression[6,16,18]. This study proposes a dual tumor-engineering strategy designed to address these barriers within the same local niche. CXCL10 provided a recruitment module, whereas decorin increased the functional value of

this recruitment by modifying the tumor context encountered by CAR T cells. Across human PDAC models, the CXCL10-decorin payload improved CAR T cell cytotoxicity, cytokine release, viable CAR T cell recovery and spheroid elimination, including under TGFβ exposure. These findings support the idea that chemokine-driven access alone is not sufficient when the tumor interface remains physically constrained or suppressive.

This conclusion is relevant for solid tumor immunotherapy. Increasing T cell recruitment can fail if recruited cells enter a niche that remains physically constrained or suppressive[21]. In this system, CXCL10 was used to improve access, not to act as a direct cytotoxic enhancer[38,39]. Decorin provided a complementary layer by acting on matrix- and TGFβ-associated features of the tumor microenvironment[40,41]. Although decorin delivery has previously been reported to improve CAR T cell activity in renal cell carcinoma[33], its relevance in PDAC is distinct because pancreatic tumors combine severe desmoplasia, immune exclusion and TGFβ-driven suppression. The novelty of the present approach therefore lies in coupling chemokine-mediated recruitment with local decorin production by pancreatic tumor cells, in order to reshape the niche where CAR T cells must act.

Several approaches have been developed to improve CAR T cell efficacy in solid tumors by acting on the tumor microenvironment rather than on antigen recognition alone. Therapeutic T cells can themselves be used to locally engineer the TME. For example, CAR T cells engineered to secrete a bifunctional αPD-L1/IL-12 fusion protein increased CAR T cell presence within the TME and remodeled suppressive immune features in solid tumor models[42]. TME conditioning can also be achieved with pharmacological agents. Dihydroartemisinin, an antimalarial derivative, was shown to enhance NKG2D CAR T cell therapy by improving CAR T cell activation, trafficking and cytotoxicity in pancreatic and prostate tumor models[43].
Other strategies have focused on improving CAR T cell homing, matrix penetration or resistance to suppressive cytokines, including chemokine receptor engineering[44], heparanase-mediated matrix degradation[45], and disruption of TGFβ signaling[22]. Together, these studies support the concept that solid tumor CAR T cell therapy requires strategies that condition the tumor context in which effector cells must operate.

Our approach follows this principle but uses tumor cells themselves as the local source of niche-modulating factors. In the present study, pancreatic tumor cells were engineered before coculture to secrete CXCL10 alone or together with decorin, thereby modeling the biological outcome expected from tumor-targeted delivery of these payloads. This experimental design allowed us to isolate the effect of tumor-cell-derived CXCL10 and decorin on CAR T cell recruitment, activation and function. CXCL10 was used to increase effector-cell access, whereas decorin was used to modulate matrix- and TGFβ-associated barriers at the tumor-T cell interface. The secreted nature of both payloads is central to this concept, because it suggests that their activity could extend beyond directly modified

tumor cells through local paracrine effects. Although the present work does not test targeted vector delivery *in vivo*, it provides functional evidence that inducing CXCL10-decorin production within pancreatic tumor cells can create a more permissive context for CAR T cell activity.

The proteomic analyses support this interpretation and suggest that decorin acts mainly as a context-dependent modulator rather than as a direct soluble activator of CAR T cells. In tumor cells, decorin co-expression was associated with a focused remodeling of membrane-, cytoskeleton-, epithelial/barrier- and interface-related programs, without broad depletion of the classical ECM matrisome. This distinction is important because it suggests that decorin may not simply dismantle the extracellular matrix, but rather reshape selected tumor-cell-associated features that influence tumor-T cell interaction. This is consistent with the view that the pancreatic matrisome is dynamic during development, maturation and PDAC progression[37,46,47]. Whether CXCL10-decorin can remodel a stromal compartment composed of fibroblasts, fibrillar matrix and variable tissue mechanics will need to be tested in models with distinct matrix densities and stromal architectures.

The CAR T-only proteomic dataset further indicates that decorin does not directly activate isolated CAR T cells in the absence of tumor-cell engagement. Instead, its effect became more relevant in the context of TGFβ-induced inhibition, where decorin partially attenuated selected components of the TGFβ-associated proteomic state without restoring a full untreated-like effector profile. This is consistent with the known ability of TGFβ to impose broad state changes in activated and reactivated CD8 T cells, including suppression of cytotoxic programs[22,48]. Thus, decorin may reduce some TGFβ-imposed constraints on CAR T cells, but is unlikely to fully overcome TGFβ-mediated inhibition on its own.

The stronger impact of decorin after coculture suggests that its main functional effect emerges during tumor-cell engagement. In this setting, CXCL10-decorin was associated with a CAR T cell state enriched in biosynthetic, proteostatic and mitochondrial features. This profile is relevant because proteostasis has recently emerged as an important determinant of CD8 T cell differentiation, persistence and tumor-infiltrating lymphocyte function[49]. Terminally exhausted T cells display impaired proteostasis and accumulation of unfolded proteins, whereas restoration of this program can improve T cell accumulation, cytokine production and antitumor activity[49]. Our data suggest that decorin may help preserve a more functionally competent CAR T cell state after antigen engagement, although the precise link between decorin, proteostasis and cytotoxic performance will require further validation.

Together, the functional and proteomic data support a sequential model for the dual payload. CXCL10 improves CAR T cell access to tumor cells. Decorin then acts locally by remodeling the tumor-cell interface and partially buffering TGFβ-associated inhibitory effects. This remodeled

context may support a post-engagement CAR T cell state with greater biosynthetic and proteostatic capacity, explaining why decorin had limited direct effects on isolated CAR T cells but a stronger functional and molecular impact after tumor-cell contact. Because the current human *in vitro* models do not fully reproduce the TGFβ-rich stromal environment of PDAC, the benefit of decorin may be underestimated here. In native tumors, where TGFβ is produced by stromal and immune compartments and contributes to fibrosis, immune evasion and cytotoxic T cell suppression, a decorin-containing payload could have broader effects[20,50,51].

Clinically, this strategy could be envisioned as a two-step combination approach. A tumor-targeted vector would first be delivered to pancreatic tumor sites to induce local CXCL10-decorin production and generate a more permissive immune niche. Antigen-directed CAR T cells could then be infused once the tumor has been locally conditioned to improve effector-cell access and function. For primary pancreatic tumors or locally advanced disease, local vector delivery could in principle be performed through image-guided or endoscopic ultrasound-guided injection, an approach already explored for intratumoral gene delivery in pancreatic cancer[52]. For metastatic disease, systemic delivery would require highly selective tumor-targeted vectors and careful control of off-tumor transduction. In both settings, the secreted nature of CXCL10 and decorin is central to the concept, because partial tumor transduction may be sufficient to generate a local bystander effect.

This translational path raises safety and design considerations. CXCL10-decorin expression would need to remain local and controlled to avoid non-specific immune recruitment, attraction of suppressive CXCR3-positive populations, or unwanted modulation of TGFβ and matrix organization[24,25,53,29,30]. Future work should define the minimal effective expression window and test whether partial tumor transduction can remodel matrix-diverse and TGFβ-rich PDAC models *in vivo*.

Several limitations should be considered. Most experiments were performed in reductionist human PDAC models that do not capture the full stromal, vascular and immune complexity of pancreatic tumors *in vivo*. The translational relevance of this strategy will depend on whether localized CXCL10-decorin delivery can generate a sufficient paracrine niche after partial tumor transduction. It also remains to be shown whether decorin-mediated remodeling is sufficient to improve CAR T cell penetration, tumor-cell contact and antitumor activity in tumors with different stromal architectures, including dense matrix-rich tumors and looser tumor models. These experiments will be important to define where this strategy is most likely to be effective.

Overall, this study identifies decorin as a context-dependent modulator of CAR T cell activity in pancreatic cancer models. Rather than acting as a direct CAR T cell stimulant, decorin appears to improve the tumor context in which recruited CAR T cells operate, combining partial relief of TGFβ-associated inhibition with remodeling of tumor-interface programs and reinforcement of post-engagement proteostatic features. These findings support local decorin production as a rational

adjunct to chemokine-mediated recruitment and provide a basis for testing dual niche-engineering strategies in more physiologically complex PDAC models.

Materials and methods

Cell culture

Human and murine cell lines were cultured at 37°C in a humidified incubator with 5% CO_2. SUIT-2-hMSLN and MIA PaCa-2-hMSLN cells were maintained in Dulbecco's modified Eagle's medium (DMEM, 4.5 g/L glucose; Gibco) supplemented with 10% fetal bovine serum (FBS) and 1% penicillin-streptomycin. MIA PaCa-2 and SUIT-2 cells were engineered to overexpress full-length human mesothelin by transduction with pMXs containing human MSLN cDNA (UniProt Q13421), generating MIA PaCa-2-hMSLN and SUIT-2-hMSLN cells. Antigen-positive populations were isolated by flow cytometry activated sorting after antibody staining when the percentage of the antigen is not specified otherwise. Cells were passaged before confluence using trypsin and were tested monthly for mycoplasma contamination.

Plasmids construction

Lentiviral transfer plasmids were generated to express CXCL10 and decorin payloads in human and murine pancreatic tumor cells. For human models, SUIT-2-hMSLN and MIA PaCa-2-hMSLN cells were engineered with vectors encoding tdTomato alone, hCXCL10-tdTomato, or hCXCL10-hDecorin-tdTomato. The P2A sequence was used to co-express decorin and CXCL10 from a single open reading frame. Inserts were cloned into lentiviral transfer plasmids by restriction enzyme digestion and ligation and verified by restriction digestion and Sanger sequencing.

Lentiviral vector production

Lentiviral vectors were produced by the Vectorology Vect'UB facility (TBMCore UAR 3427). 4µg of plasmid envelope (VSV-G), 8µg of packaging (psPAX2, Addgene #12260), and 8µg of transfer plasmids were co-transfected into HEK293T cells using calcium phosphate precipitation. The $CaCl_2$-plasmid mix was distributed to HEK293T cultures at 70% confluence, seeded in 10-cm dishes at 0.5×10^6 cells 4 days prior. Supernatants were collected 48 hours later and concentrated by Centricon® ultrafiltration (3,000 × g, 2-3 h, 4 °C). Viral titers were measured by infectious titer. For the latter, vectors pseudotyped with the different glycoproteins were pre-diluted and were added on

antigen-positive cells. After 96 hours, the percentage of fluorescent-positive cells was determined by flow cytometry (eGFP). Dilutions yielding 1%-30% positive cells were used for titer calculation. Transductional titers were expressed as infectious units per milliliter (TU/mL) and calculated using the following equation: Titer (TU/mL)=(%GFP/100)×(Dilution factor/Volume of virus added (µL))×Number of cells seeded×1000.

Transduction

Tumor cells were exposed to lentiviral particles at MOI 1 in complete medium and cells were expanded under standard culture conditions. Transduction efficiency was assessed by flow cytometry based on tdTomato expression.
Payload secretion was confirmed by ELISA in culture supernatants using human CXCL10 and decorin detection kits, as described below. CXCL10 bioactivity was assessed by transwell migration assays using activated T cells.

Cytokine protein level quantification

Human IFNγ was quantified using ELISA sets from BD Biosciences (555142). Human CXCL10 was quantified using DuoSet ELISA from R&D Systems (DY266). Human Decorin was quantified using DuoSet ELISA from R&D Systems (DY143).

CAR T cell production

Human anti-mesothelin CAR T cells were generated from CD14-negative peripheral blood mononuclear cells obtained from healthy donors. Cells were cultured in complete human T cell medium composed of RPMI 1640 supplemented with 2,5% Human Serum, 2 mM L-Glutamine, 100 IU/ml Penicillin, 100 µg/ml Streptomycin and 1 mM Sodium Pyruvate. Recombinant human IL-2 and IL-15 were added freshly during activation and expansion. CD14-negative PBMCs were activated using human CD3/CD28 Dynabeads and maintained under standard culture conditions for 48 hours before retroviral transduction. Activated T cells were transduced with retroviral supernatants produced from the 293Vec-RD114-CAR-MSLN producer cell line.
Briefly, the anti-mesothelin CAR construct was generated using the retroviral pMP71 backbone, kindly provided by Prof. Christopher Baum, Hannover, Germany. The CAR cassette encoded an anti-human mesothelin antigen-recognition scFv fused to the corresponding hinge, transmembrane and intracellular signaling domains used for T cell activation. For retroviral vector production, 293Vec-RD114 packaging cells were used, kindly provided by Dr. Manuel Caruso, Québec, Canada. The pMP71 vector carrying the CAR-MSLN sequence was stably introduced into 293Vec-RD114

cells to generate a retroviral producer cell line. Single-cell clones were isolated and screened for retroviral production by assessing the transduction efficiency of primary human T cells. The selected 293Vec-RD114-CAR-MSLN producer clone was used to generate retroviral supernatants for the transduction of activated human T cells. Transduction was performed by spinoculation for 1.5 hours at 3000g at 32°C on RetroNectin-coated non-tissue culture-treated plates. Cells were then maintained in complete human T cell medium supplemented with IL-2 and IL-15. After transduction, T cells were expanded by regular medium renewal and cytokine supplementation every second day. Cell density was adjusted at 10^6 cells per mL during expansion to maintain active proliferation. Transduction efficiency was assessed by flow cytometry 4 days after transduction, based on CAR detection. Human CAR T cells were used for *in vitro* functional assays after 8 days expansion.

Migration assay

T cell migration was assessed using Transwell plates (Corning) with 3 µm pore-size membranes for murine T cells and 5 µm for human T cells. CAR T cells or OT-I T cells were harvested, counted and resuspended in migration medium composed of OptiMEM supplemented with 1% BSA.
For T cell migration toward recombinant chemokines, recombinant CXCL9 or CXCL10 was diluted in the same migration medium and added to the lower chamber at a final concentration of 100 ng/mL. Migration medium alone was used as a negative control. A total of 0.5×10^6 T cells were added to the upper chamber of each Transwell insert. Each condition was performed in triplicate. Plates were incubated for 3 h at 37°C to allow chemokine-directed migration. After incubation, cells that had migrated into the lower chamber were collected and analyzed by flow cytometry using a BD FACS Canto II flow cytometer. Absolute migrated cell numbers were determined using CountBright™ Absolute Counting Beads (Invitrogen, #C36950). The absolute number of migrated cells was calculated from the ratio of cell events to bead events.
When indicated, T cell migration was also assessed toward tumor cells plated in the lower chamber of the Transwell system. Tumor cells were seeded in the bottom chamber 48 hours before the assay and allowed to adhere and secrete the different therapeutic elements. Depending on the experimental condition, tumor cells expressed and secreted chemokine alone or chemokine together with decorin. Control wells contained mock-transduced tumor cells or migration medium alone. CAR T cells were first stained with CellTrace™ Violet 5 µM (C34557) to distinguish them from tumor cells, and added to the upper chamber in migration medium and allowed to migrate for 3 hours at 37°C. Migrated CTV^+ T cells were then collected from the lower chamber and quantified by flow cytometry using CountBright™ Absolute Counting Beads, as described above. This setup was used to evaluate whether chemokine secretion by engineered tumor cells, with or without decorin co-expression, promoted T cell recruitment.

Collagen-embedded 3D tumor cultures

Collagen-embedded 3D tumor cultures were generated from tumor cells grown under standard adherent culture conditions. Cells were detached using trypsin, counted, centrifuged to obtain a cell pellet and gently resuspended in a neutralized collagen mixture containing collagen, NaOH and 10× PBS. The collagen mixture was maintained on ice throughout preparation to prevent premature polymerization. A 1 µL drop of the cell-containing collagen suspension was seeded into each well of a flat-bottom 96-well plate and incubated for 5 min at 37°C to allow collagen polymerization. Pre-warmed culture medium was then gently added on top of the polymerized collagen droplets. Cells were maintained under standard culture conditions and allowed to grow directly within the collagen fiber network. For CAR T cell killing assays, CAR T cells were gently added on top of the collagen droplets at the indicated effector-to-target ratios, and tumor cell killing was monitored over time by Incucyte live-cell imaging.

Tumor-cell killing assay using Incucyte

Tumor-cell killing was monitored in real time using the Incucyte live-cell imaging system. Tumor cells were seeded in 96-well plates and allowed to adhere overnight. For 3D assays, tumor spheroids were generated before immune-cell addition as described above. Tumor cells expressed the red fluorescent reporters tdTomato.

CAR T cells were added at the indicated effector-to-target ratios. For cytotoxicity measurements, Incucyte Cytotox Green reagent was added according to the manufacturer's instructions. Plates were imaged every 3 hours for 2D assays and every 6 hours for spheroids experiments, using phase contrast and fluorescence channels (Red for tumor cells and green for cytotox green dye).

For 2D killing assay, killing was quantified using Cytotox green reagent. Cytotox Green accumulation was monitored over time and quantified as Green Integrated Intensity per Well / Phase Area Confluence, normalized to the time of effector cell addition. This normalization accounted for potential differences in initial tumor-cell confluence between engineered tumor cells populations. For spheroid killing experiments, the red tumor cell signal was monitored as Total Red Object Integrated Intensity, expressed as RCU × µm² per well, and normalized to the time of effector cells addition.

Conditions without effector cells and with untransduced T cells were used to measure spontaneous tumor-cell growth and basal cell death. Mock-transduced tumor cells were used as controls for therapeutic-vector conditions.

Proteomic analysis

Protein samples were analyzed by the Bordeaux Proteome platform using an in-gel digestion and label-free quantitative mass spectrometry workflow. Samples were separated by short migration on

10% acrylamide SDS-PAGE gels, stained with colloidal blue and processed for in-gel trypsin digestion after reduction and alkylation. Peptides were extracted, acidified and analyzed by LC-MS/MS on an Orbitrap Fusion Lumos Eclipse mass spectrometer using a 146-min DIA acquisition method.

Raw files were processed using Proteome Discoverer 3.3 with Chimerys as the search algorithm. Spectra were searched against the Homo sapiens UniProt database RPS_GC_2026_01_Homo_sapiens_UP000005640_9606, supplemented with a contaminant database. Trypsin was used as the digestion enzyme, with up to two missed cleavages allowed. Carbamidomethylation of cysteine was set as a static modification. Oxidation of methionine, protein N-terminal acetylation, methionine loss and methionine loss combined with acetylation were included as dynamic modifications.

Protein quantification was performed using a label-free precursor ion intensity-based workflow. Unique and razor peptides were used for protein quantification, and protein abundance was calculated using a TOP3 approach. Normalization was performed using human proteins. Normalized proteomic datasets were log2(x + 1)-transformed. A total of 5,848 unique proteins were retrieved. Missing values were imputed using the MissForest implementation with default parameters from the DreamAI R package. Data were batch-corrected by culture group using the ComBat R package. Principal component analysis was performed to visualize sample clustering.

Differential protein abundance was analyzed at the protein level by pairwise comparisons between treatment groups. Tumor-cell comparisons were analyzed in unpaired mode, whereas CAR T cell-only and CAR T cell coculture comparisons were analyzed in paired mode to account for donor matching. Differentially expressed proteins were identified using an adjusted p value < 0.05, corresponding to a false discovery rate of 5%, together with the log2 fold-change thresholds specified in the corresponding figure legends.

Gene Ontology enrichment analysis was performed for Biological Process, Molecular Function and Cellular Component terms using the clusterProfiler package. Gene set enrichment analyses were performed on pre-ranked protein-level differential abundance tables using the t value from pairwise statistical comparisons and the fgsea package. Hallmark, Reactome, KEGG, Gene Ontology and C7 immunologic signature gene sets were used when indicated. Enriched pathways were selected based on a normalized enrichment score > 2 and an adjusted p value < 0.05.

Heatmaps of selected proteins were generated from normalized protein abundance values using the ComplexHeatmap R package and displayed as row z-scores when indicated. Volcano plots, PCA plots, enrichment plots and violin plots were generated using ggplot2. Violin plots were generated from donor-level normalized abundance values, with paired statistical comparisons when indicated.

Puromycin incorporation assay

Global protein synthesis was assessed by puromycin incorporation after CAR T cell coculture. Briefly, CAR T cells were recovered from cocultures with mock, CXCL10 or CXCL10-Dcn SUIT-2-hMSLN tumor cells and incubated with puromycin at 10 µg/mL for 10 min. Cells were then immediately washed with cold 1× PBS and lysed in RIPA buffer. Protein extracts were processed for western blotting. Membranes were incubated with an anti-puromycin antibody (clone 12D10, Sigma-Aldrich, MABE343) to detect newly synthesized puromycin-labeled proteins. GAPDH was used as a loading control. Anti-puromycin signal was detected using an anti-mouse IgG-HRP secondary antibody, and proteins were visualized using an ECL detection system. Densitometric quantification was performed using ImageJ. Puromycin incorporation was quantified as the total anti-puromycin signal normalized to the corresponding GAPDH signal.

Statistical analysis

All experiments were performed at least in biological duplicate and technical triplicate unless stated otherwise. Results are presented as mean ± standard deviation (SD), unless otherwise indicated in the figure legends. Statistical analyses of functional assays were performed using GraphPad Prism 8.0.2 or 11.0.1.

For comparisons between two groups, statistical significance was evaluated using two-tailed Student's t tests when data distribution and experimental design were appropriate. Paired tests were used for donor-matched CAR T cell experiments, whereas unpaired tests were used for independent experimental groups. For comparisons involving more than two groups, one-way ANOVA was used, followed by Tukey's multiple-comparisons test as indicated in the figure legends.

For time-course cytotoxicity experiments, statistical analyses were performed on endpoint values, area under the curve or slopes over the indicated time intervals, as specified in the corresponding figure legends. For donor-matched experiments, paired statistical analyses were used when applicable.

Proteomic statistical analyses were performed as described in the proteomic analysis section. A p value < 0.05 was considered statistically significant for functional assays. For proteomic analyses, adjusted p values were used as indicated in the proteomic analysis section and figure legends.

References

1. Burris HA, Moore MJ, Andersen J, Green MR, Rothenberg ML, Modiano MR, et al. Improvements in survival and clinical benefit with gemcitabine as first-line therapy for patients with

advanced pancreas cancer: a randomized trial. J Clin Oncol Off J Am Soc Clin Oncol. 1997 Jun;15(6):2403–13. doi:10.1200/JCO.1997.15.6.2403 PubMed PMID: 9196156.

2. Royal RE, Levy C, Turner K, Mathur A, Hughes M, Kammula US, et al. Phase 2 trial of single agent Ipilimumab (anti-CTLA-4) for locally advanced or metastatic pancreatic adenocarcinoma. J Immunother. 2010 Oct;33(8):828–33. doi:10.1097/CJI.0b013e3181eec14c PubMed PMID: 20842054; PubMed Central PMCID: PMC7322622.

3. Conroy T, Desseigne F, Ychou M, Bouché O, Guimbaud R, Bécouarn Y, et al. FOLFIRINOX versus Gemcitabine for Metastatic Pancreatic Cancer. N Engl J Med. 2011 May 12;364(19):1817–25. doi:10.1056/NEJMoa1011923

4. Hoff DDV, Ervin T, Arena FP, Chiorean EG, Infante J, Moore M, et al. Increased Survival in Pancreatic Cancer with nab-Paclitaxel plus Gemcitabine. N Engl J Med. 2013 Oct 31;369(18):1691–703. doi:10.1056/NEJMoa1304369

5. Maude SL, Laetsch TW, Buechner J, Rives S, Boyer M, Bittencourt H, et al. Tisagenlecleucel in Children and Young Adults with B-Cell Lymphoblastic Leukemia. N Engl J Med. 2018 Feb 1;378(5):439–48. doi:10.1056/NEJMoa1709866

6. Beatty GL, O'Hara MH, Lacey SF, Torigian DA, Nazimuddin F, Chen F, et al. Activity of Mesothelin-Specific Chimeric Antigen Receptor T Cells Against Pancreatic Carcinoma Metastases in a Phase 1 Trial. Gastroenterology. 2018 Jul;155(1):29–32. doi:10.1053/j.gastro.2018.03.029 PubMed PMID: 29567081; PubMed Central PMCID: PMC6035088.

7. Neelapu SS, Locke FL, Bartlett NL, Lekakis LJ, Miklos DB, Jacobson CA, et al. Axicabtagene Ciloleucel CAR T-Cell Therapy in Refractory Large B-Cell Lymphoma. N Engl J Med. 2017 Dec 28;377(26):2531–44. doi:10.1056/NEJMoa1707447

8. Ko AH, Jordan AC, Tooker E, Lacey SF, Chang RB, Li Y, et al. Dual Targeting of Mesothelin and CD19 with Chimeric Antigen Receptor-Modified T Cells in Patients with Metastatic Pancreatic Cancer. Mol Ther. 2020 Nov;28(11):2367–78. doi:10.1016/j.ymthe.2020.07.017

9. Feng K, Liu Y, Guo Y, Qiu J, Wu Z, Dai H, et al. Phase I study of chimeric antigen receptor modified T cells in treating HER2-positive advanced biliary tract cancers and pancreatic cancers. Protein Cell. 2018 Oct;9(10):838–47. doi:10.1007/s13238-017-0440-4 PubMed PMID: 28710747; PubMed Central PMCID: PMC6160389.

10. Qi C, Gong J, Li J, Liu D, Qin Y, Ge S, et al. Claudin18.2-specific CAR T cells in gastrointestinal cancers: phase 1 trial interim results. Nat Med. 2022 Jun;28(6):1189–98. doi:10.1038/s41591-022-01800-8

11. Qi C, Liu C, Gong J, Liu D, Wang X, Zhang P, et al. Claudin18.2-specific CAR T cells in gastrointestinal cancers: phase 1 trial final results. Nat Med. 2024 Aug;30(8):2224–34. doi:10.1038/s41591-024-03037-z PubMed PMID: 38830992.

12. Ostios-Garcia L, Villamayor J, Garcia-Lorenzo E, Vinal D, Feliu J. Understanding the immune response and the current landscape of immunotherapy in pancreatic cancer. World J Gastroenterol. 2021 Oct 28;27(40):6775–93. doi:10.3748/wjg.v27.i40.6775 PubMed PMID: 34790007; PubMed Central PMCID: PMC8567475.

13. Yeo D, Giardina C, Saxena P, Rasko JEJ. The next wave of cellular immunotherapies in pancreatic cancer. Mol Ther Oncolytics. 2022 Mar 17;24:561–76. doi:10.1016/j.omto.2022.01.010 PubMed PMID: 35229033; PubMed Central PMCID: PMC8857655.

14. Lesch S, Benmebarek MR, Cadilha BL, Stoiber S, Subklewe M, Endres S, et al. Determinants of response and resistance to CAR T cell therapy. Semin Cancer Biol. 2020 Oct;65:80–90. doi:10.1016/j.semcancer.2019.11.004

15. Jacobetz MA, Chan DS, Neesse A, Bapiro TE, Cook N, Frese KK, et al. Hyaluronan impairs vascular function and drug delivery in a mouse model of pancreatic cancer. Gut. 2013 Jan;62(1):112–20. doi:10.1136/gutjnl-2012-302529 PubMed PMID: 22466618; PubMed Central PMCID: PMC3551211.

16. Xiao Z, Todd L, Huang L, Noguera-Ortega E, Lu Z, Huang L, et al. Desmoplastic stroma restricts T cell extravasation and mediates immune exclusion and immunosuppression in solid tumors. Nat Commun. 2023 Aug 22;14(1):5110. doi:10.1038/s41467-023-40850-5

17. Provenzano PP, Cuevas C, Chang AE, Goel VK, Von Hoff DD, Hingorani SR. Enzymatic Targeting of the Stroma Ablates Physical Barriers to Treatment of Pancreatic Ductal Adenocarcinoma. Cancer Cell. 2012 Mar 20;21(3):418–29. doi:10.1016/j.ccr.2012.01.007 PubMed PMID: 22439937.

18. Feig C, Jones JO, Kraman M, Wells RJB, Deonarine A, Chan DS, et al. Targeting CXCL12 from FAP-expressing carcinoma-associated fibroblasts synergizes with anti–PD-L1 immunotherapy in pancreatic cancer. Proc Natl Acad Sci. 2013 Dec 10;110(50):20212–7. doi:10.1073/pnas.1320318110

19. Friess H, Yamanaka Y, Büchler M, Ebert M, Beger HG, Gold LI, et al. Enhanced expression of transforming growth factor beta isoforms in pancreatic cancer correlates with decreased survival. Gastroenterology. 1993 Dec;105(6):1846–56. doi:10.1016/0016-5085(93)91084-u PubMed PMID: 8253361.

20. Thomas DA, Massagué J. TGF-beta directly targets cytotoxic T cell functions during tumor evasion of immune surveillance. Cancer Cell. 2005 Nov;8(5):369–80. doi:10.1016/j.ccr.2005.10.012 PubMed PMID: 16286245.

21. Cadilha BL, Benmebarek MR, Dorman K, Oner A, Lorenzini T, Obeck H, et al. Combined tumor-directed recruitment and protection from immune suppression enable CAR T cell efficacy in solid tumors. Sci Adv. 2021 Jun 11;7(24):eabi5781. doi:10.1126/sciadv.abi5781

22. Tang N, Cheng C, Zhang X, Qiao M, Li N, Mu W, et al. TGF-β inhibition via CRISPR promotes the long-term efficacy of CAR T cells against solid tumors. JCI Insight. 5(4):e133977. doi:10.1172/jci.insight.133977 PubMed PMID: 31999649; PubMed Central PMCID: PMC7101140.

23. Kohli K, Pillarisetty VG, Kim TS. Key chemokines direct migration of immune cells in solid tumors. Cancer Gene Ther. 2022 Jan;29(1):10–21. doi:10.1038/s41417-021-00303-x

24. Groom JR, Luster AD. CXCR3 in T cell function. Exp Cell Res. 2011 Mar 10;317(5):620–31. doi:10.1016/j.yexcr.2010.12.017 PubMed PMID: 21376175; PubMed Central PMCID: PMC3065205.

25. Tokunaga R, Zhang W, Naseem M, Puccini A, Berger MD, Soni S, et al. CXCL9, CXCL10, CXCL11/CXCR3 axis for immune activation - A target for novel cancer therapy. Cancer Treat Rev. 2018 Feb;63:40–7. doi:10.1016/j.ctrv.2017.11.007 PubMed PMID: 29207310; PubMed Central PMCID: PMC5801162.

26. Köninger J, Giese NA, di Mola FF, Berberat P, Giese T, Esposito I, et al. Overexpressed Decorin in Pancreatic Cancer: Potential Tumor Growth Inhibition and Attenuation of Chemotherapeutic Action. Clin Cancer Res. 2004 Jul 21;10(14):4776–83. doi:10.1158/1078-0432.CCR-1190-03

27. Zhang G, Ezura Y, Chervoneva I, Robinson PS, Beason DP, Carine ET, et al. Decorin regulates assembly of collagen fibrils and acquisition of biomechanical properties during tendon development. J Cell Biochem. 2006 Aug 15;98(6):1436–49. doi:10.1002/jcb.20776 PubMed PMID: 16518859.

28. Danielson KG, Baribault H, Holmes DF, Graham H, Kadler KE, Iozzo RV. Targeted disruption of decorin leads to abnormal collagen fibril morphology and skin fragility. J Cell Biol. 1997 Feb 10;136(3):729–43. doi:10.1083/jcb.136.3.729 PubMed PMID: 9024701; PubMed Central PMCID: PMC2134287.

29. Yamaguchi Y, Mann DM, Ruoslahti E. Negative regulation of transforming growth factor-beta by the proteoglycan decorin. Nature. 1990 Jul 19;346(6281):281–4. doi:10.1038/346281a0 PubMed PMID: 2374594.

30. Border WA, Noble NA, Yamamoto T, Harper JR, Yamaguchi Y, Pierschbacher MD, et al. Natural inhibitor of transforming growth factor-β protects against scarring in experimental kidney disease. Nature. 1992 Nov;360(6402):361–4. doi:10.1038/360361a0

31. Zheng N, Xiang L, Xu G, Liu Y, Xu C, Zhang L, et al. Decorin facilitates T cell-mediated antitumor immunity and augments the efficacy of anti-PD1 immunotherapy. Cancer Immunol Immunother CII. 2026 Jan 27;75(2):45. doi:10.1007/s00262-025-04290-y PubMed PMID: 41591489.

32. Chen J, Tian WP, Wei XB, Zhang XW, Gao HY. Synergistic antitumor efficacy of a decorin-carrying oncolytic adenovirus combined with chemotherapy in pancreatic cancer. Front Oncol. 2026 Mar 17;16. doi:10.3389/fonc.2026.1702601

33. Zhang C, Fang L, Wang X, Yuan S, Li W, Tian W, et al. Oncolytic adenovirus-mediated expression of decorin facilitates CAIX-targeting CAR-T therapy against renal cell carcinoma. Mol Ther Oncolytics. 2021 Nov 29;24:14–25. doi:10.1016/j.omto.2021.11.018 PubMed PMID: 34977339; PubMed Central PMCID: PMC8688951.

34. Buraschi S, Pal N, Tyler-Rubinstein N, Owens RT, Neill T, Iozzo RV. Decorin antagonizes Met receptor activity and down-regulates {beta}-catenin and Myc levels. J Biol Chem. 2010 Dec 31;285(53):42075–85. doi:10.1074/jbc.M110.172841 PubMed PMID: 20974860; PubMed Central PMCID: PMC3009933.

35. Xie C, Mondal DK, Ulas M, Neill T, Iozzo RV. Oncosuppressive roles of decorin through regulation of multiple receptors and diverse signaling pathways. Am J Physiol - Cell Physiol. 2022 Mar 1;322(3):C554–66. doi:10.1152/ajpcell.00016.2022 PubMed PMID: 35171698; PubMed Central PMCID: PMC8917911.

36. Meehl MM, Ward MB, Krenciute G. Mapping clinical CAR-T cells: insights from scRNA-seq. Trends Mol Med. 2026 Jan;S147149142500293X. doi:10.1016/j.molmed.2025.12.006

37. Li Z, Tremmel DM, Ma F, Yu Q, Ma M, Delafield DG, et al. Proteome-wide and matrisome-specific alterations during human pancreas development and maturation. Nat Commun. 2021 Feb 15;12(1):1020. doi:10.1038/s41467-021-21261-w

38. Mikucki ME, Fisher DT, Matsuzaki J, Skitzki JJ, Gaulin NB, Muhitch JB, et al. Non-redundant requirement for CXCR3 signalling during tumoricidal T-cell trafficking across tumour vascular checkpoints. Nat Commun. 2015 Nov;6(1):7458. doi:10.1038/ncomms8458

39. Karin N. CXCR3 Ligands in Cancer and Autoimmunity, Chemoattraction of Effector T Cells, and Beyond. Front Immunol. 2020;11:976. doi:10.3389/fimmu.2020.00976 PubMed PMID: 32547545; PubMed Central PMCID: PMC7274023.

40. Zhang W, Ge Y, Cheng Q, Zhang Q, Fang L, Zheng J. Decorin is a pivotal effector in the extracellular matrix and tumour microenvironment. Oncotarget. 2018 Jan 3;9(4):5480–91. doi:10.18632/oncotarget.23869 PubMed PMID: 29435195; PubMed Central PMCID: PMC5797066.

41. Neill T, Schaefer L, Iozzo RV. Decorin: A Guardian from the Matrix. Am J Pathol. 2012 Aug 1;181(2):380–7. doi:10.1016/j.ajpath.2012.04.029 PubMed PMID: 22735579.

42. Murad JP, Christian L, Rosa R, Ren Y, Buckley AJ, Lee EHJ, et al. Solid tumour CAR-T cells engineered with fusion proteins targeting PD-L1 for localized IL-12 delivery. Nat Biomed Eng. 2026 Apr;10(4):613–29. doi:10.1038/s41551-025-01509-2 PubMed PMID: 41034514; PubMed Central PMCID: PMC13099387.

43. Saliu MA, Salisu MD, Suleiman RB, Liang W, Rabiu L, Abdalsalam NMF, et al. Dihydroartemisinin enhances NKG2D CAR-T cell therapy against solid tumors by inducing NKG2D ligands and remodeling the tumor microenvironment. Biomed Pharmacother Biomedecine Pharmacother. 2026 Feb;195:118974. doi:10.1016/j.biopha.2026.118974 PubMed PMID: 41529511.

44. Henze J, Tacke F, Hardt O, Alves F, Al Rawashdeh W. Enhancing the Efficacy of CAR T Cells in the Tumor Microenvironment of Pancreatic Cancer. Cancers. 2020 May 28;12(6):1389. doi:10.3390/cancers12061389 PubMed PMID: 32481570; PubMed Central PMCID: PMC7353070.

45. Caruana I, Savoldo B, Hoyos V, Weber G, Liu H, Kim ES, et al. Heparanase promotes tumor infiltration and antitumor activity of CAR-redirected T lymphocytes. Nat Med. 2015 May;21(5):524–9. doi:10.1038/nm.3833

46. Tian C, Clauser KR, Öhlund D, Rickelt S, Huang Y, Gupta M, et al. Proteomic analyses of ECM during pancreatic ductal adenocarcinoma progression reveal different contributions by tumor and stromal cells. Proc Natl Acad Sci U S A. 2019 Sep 24;116(39):19609–18. doi:10.1073/pnas.1908626116 PubMed PMID: 31484774; PubMed Central PMCID: PMC6765243.

47. Hong J, Jin HJ, Choi MR, Lim DWT, Park JE, Kim YS, et al. Matrisomics: Beyond the extracellular matrix for unveiling tumor microenvironment. Biochim Biophys Acta Rev Cancer. 2024 Nov;1879(6):189178. doi:10.1016/j.bbcan.2024.189178 PubMed PMID: 39241895.

48. Taber A, Konecny A, Oda SK, Scott-Browne J, Prlic M. TGF-β broadly modifies rather than specifically suppresses reactivated memory CD8 T cells in a dose-dependent manner. Proc Natl Acad Sci U S A. 2023 Nov 28;120(48):e2313228120. doi:10.1073/pnas.2313228120 PubMed PMID: 37988468; PubMed Central PMCID: PMC10691214.

49. Scharping NE, Ge X, Matias MI, Jiang F, Cafferata A, Heeg M, et al. Proteostasis sustains T cell differentiation potential and tumor-infiltrating lymphocyte function. Cell. 2026 May 14;189(10):2857-2874.e31. doi:10.1016/j.cell.2026.02.019 PubMed PMID: 42061400.

50. Principe DR, Timbers KE, Atia LG, Koch RM, Rana A. TGFβ Signaling in the Pancreatic Tumor Microenvironment. Cancers. 2021 Oct 11;13(20):5086. doi:10.3390/cancers13205086 PubMed PMID: 34680235; PubMed Central PMCID: PMC8533869.

51. Zhang T, Ren Y, Yang P, Wang J, Zhou H. Cancer-associated fibroblasts in pancreatic ductal adenocarcinoma. Cell Death Dis. 2022 Oct 25;13(10):897. doi:10.1038/s41419-022-05351-1

52. Hecht JR, Farrell JJ, Senzer N, Nemunaitis J, Rosemurgy A, Chung T, et al. EUS or percutaneously guided intratumoral TNFerade biologic with 5-fluorouracil and radiotherapy for first-line treatment of locally advanced pancreatic cancer: a phase I/II study. Gastrointest Endosc. 2012 Feb;75(2):332–8. doi:10.1016/j.gie.2011.10.007 PubMed PMID: 22248601; PubMed Central PMCID: PMC4380192.

53. Lunardi S, Jamieson NB, Lim SY, Griffiths KL, Carvalho-Gaspar M, Al-Assar O, et al. IP-10/CXCL10 induction in human pancreatic cancer stroma influences lymphocytes recruitment and correlates with poor survival. Oncotarget. 2014 Nov 25;5(22):11064–80. doi:10.18632/oncotarget.2519 PubMed PMID: 25415223; PubMed Central PMCID: PMC4294325.

54. Kong W, Longaker MT, Lorenz HP. Molecular Cloning and Expression of Keratinocyte Proline-rich Protein, a Novel Squamous Epithelial Marker Isolated During Skin Development *. J Biol Chem. 2003 Jun 20;278(25):22781–6. doi:10.1074/jbc.M210488200 PubMed PMID: 12668678.

55. de Koning PJA, Tesselaar K, Bovenschen N, Colak S, Quadir R, Volman TJH, et al. The cytotoxic protease granzyme M is expressed by lymphocytes of both the innate and adaptive immune system. Mol Immunol. 2010 Jan;47(4):903–11. doi:10.1016/j.molimm.2009.10.001 PubMed PMID: 19896187.

56. Kelly JM, Waterhouse NJ, Cretney E, Browne KA, Ellis S, Trapani JA, et al. Granzyme M mediates a novel form of perforin-dependent cell death. J Biol Chem. 2004 May 21;279(21):22236–42. doi:10.1074/jbc.M401670200 PubMed PMID: 15028722.

57. Makedonas G, Banerjee PP, Pandey R, Hersperger AR, Sanborn KB, Hardy GAD, et al. Rapid upregulation and granule-independent transport of perforin to the immunological synapse define a novel mechanism of antigen-specific CD8+ T cell cytotoxic activity. J Immunol Baltim Md 1950. 2009 May 1;182(9):5560–9. doi:10.4049/jimmunol.0803945 PubMed PMID: 19380804; PubMed Central PMCID: PMC2714586.

58. Davenport AJ, Cross RS, Watson KA, Liao Y, Shi W, Prince HM, et al. Chimeric antigen receptor T cells form nonclassical and potent immune synapses driving rapid cytotoxicity. Proc Natl Acad Sci. 2018 Feb 27;115(9):E2068–76. doi:10.1073/pnas.1716266115

59. Araki K, Morita M, Bederman AG, Konieczny BT, Kissick HT, Sonenberg N, et al. Translation is actively regulated during the differentiation of CD8+ effector T cells. Nat Immunol. 2017 Sep;18(9):1046–57. doi:10.1038/ni.3795 PubMed PMID: 28714979; PubMed Central PMCID: PMC5937989.

60. Wolf T, Jin W, Zoppi G, Vogel IA, Akhmedov M, Bleck CKE, et al. Dynamics in protein translation sustaining T cell preparedness. Nat Immunol. 2020 Aug;21(8):927–37. doi:10.1038/s41590-020-0714-5 PubMed PMID: 32632289; PubMed Central PMCID: PMC7610365.

61. Diop-Frimpong B, Chauhan VP, Krane S, Boucher Y, Jain RK. Losartan inhibits collagen I synthesis and improves the distribution and efficacy of nanotherapeutics in tumors. Proc Natl Acad Sci. 2011 Feb 15;108(7):2909–14. doi:10.1073/pnas.1018892108

Supplementary figures

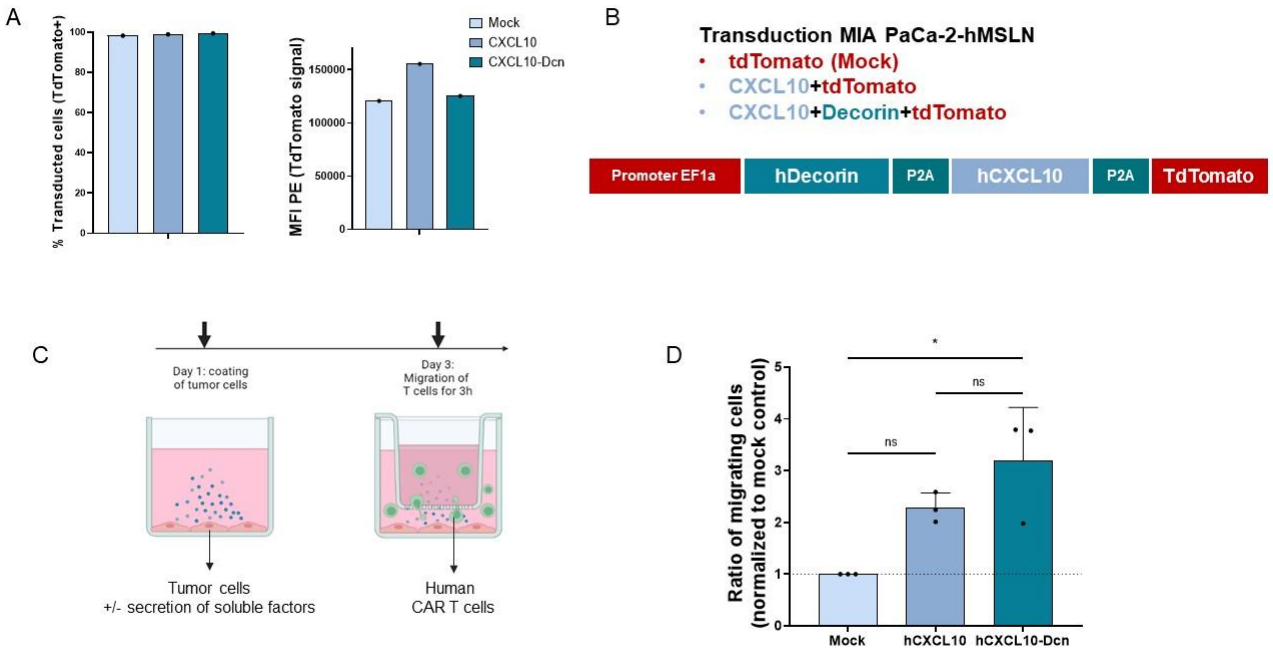


Figure 28 Supplementary: Tumor-secreted hCXCL10 and hDecorin can be co-expressed in two different models of mesothelin-positive PDAC cells while preserving CAR T cell recruitment.

(A) *Flow-cytometry quantification of tdTomato-positive SUIT-2-hMSLN cells and tdTomato mean fluorescence intensity after transduction. All engineered populations showed high transduction efficiency and comparable tdTomato fluorescence intensity, indicating similar reporter expression across conditions.* **(B)** *Schematic representation of the EF1α-driven expression cassette encoding hDecorin, hCXCL10 and tdTomato separated by P2A sequences. Control cells expressed tdTomato alone, while single-payload cells expressed hCXCL10-tdTomato.* ***(C)*** *Human anti-hMSLN CAR T cell migration toward engineered MIA PaCa-2-hMSLN cells was assessed in a transwell assay and normalized to the mock condition.* ***(D)*** *hCXCL10 expression increased CAR T cell migration, with and without hDecorin co-expression. Data are shown as mean ± SD. Statistical significance is indicated on the graph. ns: not significant.*

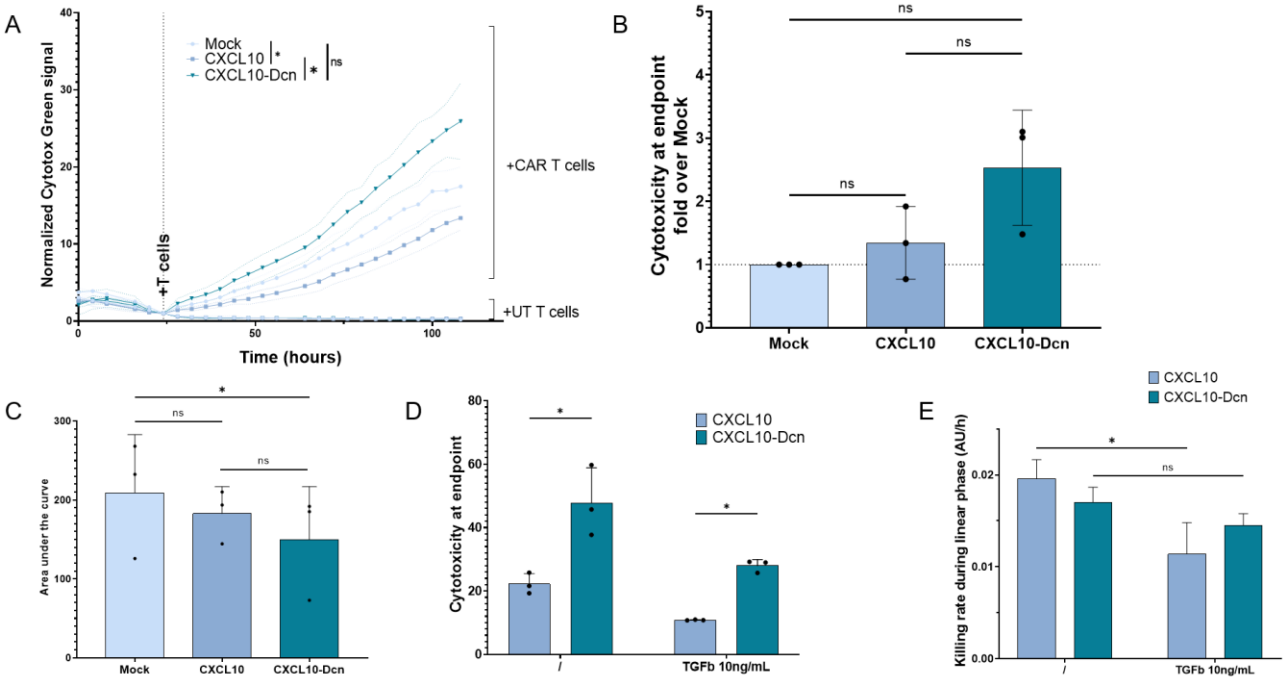


Figure 29 Supplementary: Additional functional analyses of CXCL10-decorin activity in human mesothelin-positive PDAC models.

(A) *Real-time monitoring of tumor-cell death in 2D culture using an Incucyte Cytotox Green assay. MIA PaCa-2-hMSLN cells expressing tdTomato alone, hCXCL10 or hCXCL10-hDecorin were cocultured with human mesothelin-specific CAR T cells or untransduced T cells. T cells were added at the indicated time point. Cytotox Green accumulation was monitored over time and quantified as normalized Cytotox Green signal. Increased signal reflects accumulation of dead cells over time. Dotted lines indicate variability between independent donors or replicates, as shown in the corresponding graph.* ***(B)*** *Endpoint cytotoxicity in 2D MIA PaCa-2-hMSLN cocultures, expressed as fold change over the mock condition. hCXCL10-hDecorin showed a higher mean endpoint cytotoxicity signal than mock and hCXCL10-only conditions, although the differences did not reach statistical significance.* ***(C)*** *Area under the curve analysis of tdTomato signal from SUIT-2-hMSLN spheroid killing assays across independent CAR T cell donors. Lower AUC indicates stronger reduction of tumor signal over time. hCXCL10-hDecorin showed a lower mean AUC than mock and hCXCL10-only conditions, consistent with increased spheroid elimination. The comparison between mock and hCXCL10-hDecorin reached statistical significance, whereas the other comparisons were not significant.* ***(D)*** *Endpoint quantification of Cytotox Green accumulation in 2D SUIT-2-hMSLN cocultures in the absence or presence of recombinant TGFβ. SUIT-2-hMSLN cells expressing hCXCL10 or hCXCL10-hDecorin were cocultured with mesothelin-specific CAR T cells. hCXCL10-hDecorin increased endpoint cytotoxicity compared with hCXCL10 alone, both in control conditions and under TGFβ exposure.* ***(E)*** *Killing rate calculated from the linear phase of the cytotoxicity curves shown in Figure 23D. Higher values indicate faster tumor-cell killing during the linear phase. TGFβ reduced the killing rate in hCXCL10-only cocultures, whereas hCXCL10-hDecorin maintained a higher killing rate under TGFβ exposure. Data are shown as mean ± SD. Each point represents one independent CAR T cell donor. Statistical analyses were performed as indicated in the corresponding panels, using one-way ANOVA with multiple-comparison correction or paired comparisons when appropriate. ns, not significant; *p < 0.05.*

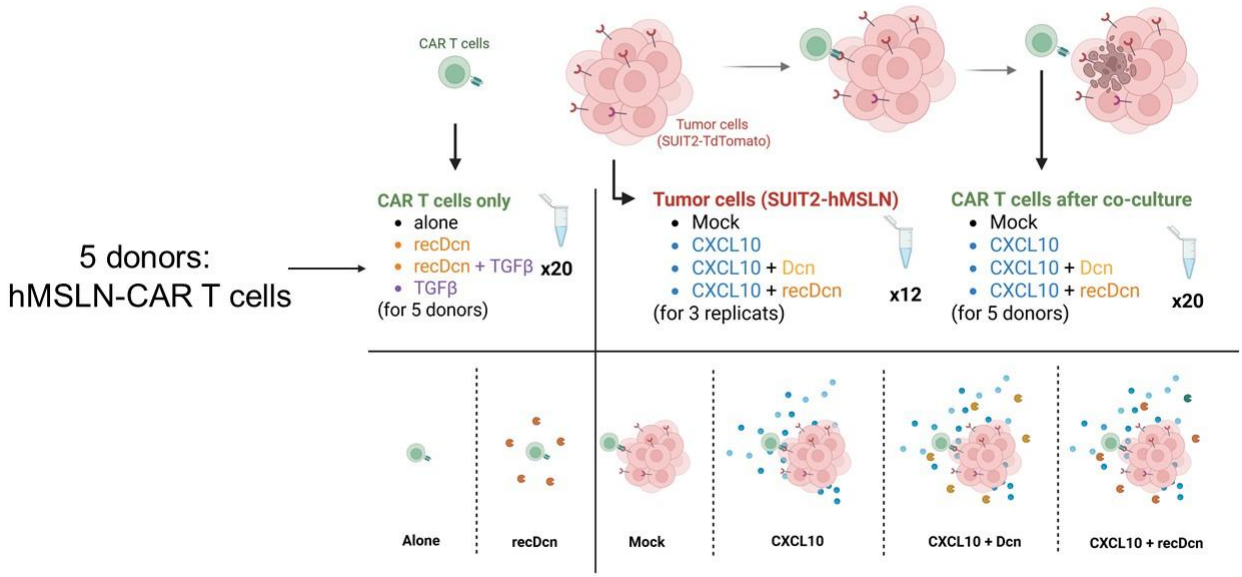


Figure 30 Supplementary: Experimental design of the compartment-resolved proteomic analyses.

Schematic representation of the proteomic workflow used to analyze the direct and context-dependent effects of decorin on tumor cells and CAR T cells. Human mesothelin-specific CAR T cells were generated from five independent donors and analyzed in three experimental compartments. First, CAR T cells were cultured in the absence of tumor cells under four conditions: untreated/alone, recombinant decorin (recDcn), TGFβ, or recDcn + TGFβ. Second, SUIT-2-hMSLN tumor cells were analyzed independently under four tumor-engineering conditions: Mock, CXCL10, CXCL10-Dcn, or CXCL10-recDcn, using three biological replicates per condition. Third, CAR T cells were recovered after coculture with the corresponding SUIT-2-hMSLN tumor-cell conditions from five independent donors. This design allowed the proteomic effects of decorin to be separated across tumor cells, isolated CAR T cells and CAR T cells after tumor engagement.

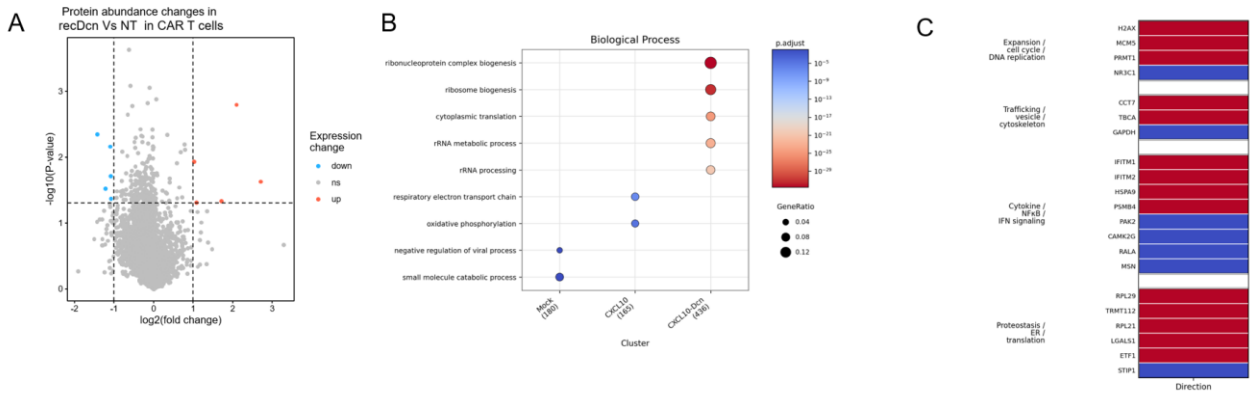


Figure 31 Supplementary: Proteomic analyses supporting decorin-associated remodeling of tumor cells and CAR T cells.

(A) *Volcano plot showing protein abundance changes in isolated CAR T cells treated with recombinant decorin compared with non-treated CAR T cells. Each point represents one protein. Red and blue indicate significantly increased and decreased proteins, respectively, and grey indicates non-significant proteins. Dashed lines indicate the selected thresholds for log2 fold change and statistical significance.*

(B) *GO Biological Process enrichment analysis of proteins grouped according to their dominant abundance pattern across coculture conditions. Enriched terms are shown for proteins associated with the Mock, CXCL10 and CXCL10-Dcn clusters. Dot size indicates the gene ratio, and color indicates the adjusted p value. CXCL10-Dcn-associated proteins were enriched in ribonucleoprotein complex biogenesis, ribosome biogenesis, cytoplasmic translation, rRNA metabolism and rRNA processing, while CXCL10-associated proteins included respiratory electron transport chain and oxidative phosphorylation terms.*

(C) *Heatmap showing the direction of regulation of selected proteins shared between the coculture comparison and the CAR T cell-only comparison. Proteins were grouped into functional categories related to expansion/cell cycle/DNA replication, trafficking/vesicle/cytoskeleton, cytokine/NFκB/IFN signaling, and proteostasis/ER/translation. Red indicates increased abundance and blue indicates decreased abundance in the decorin-containing comparison.*

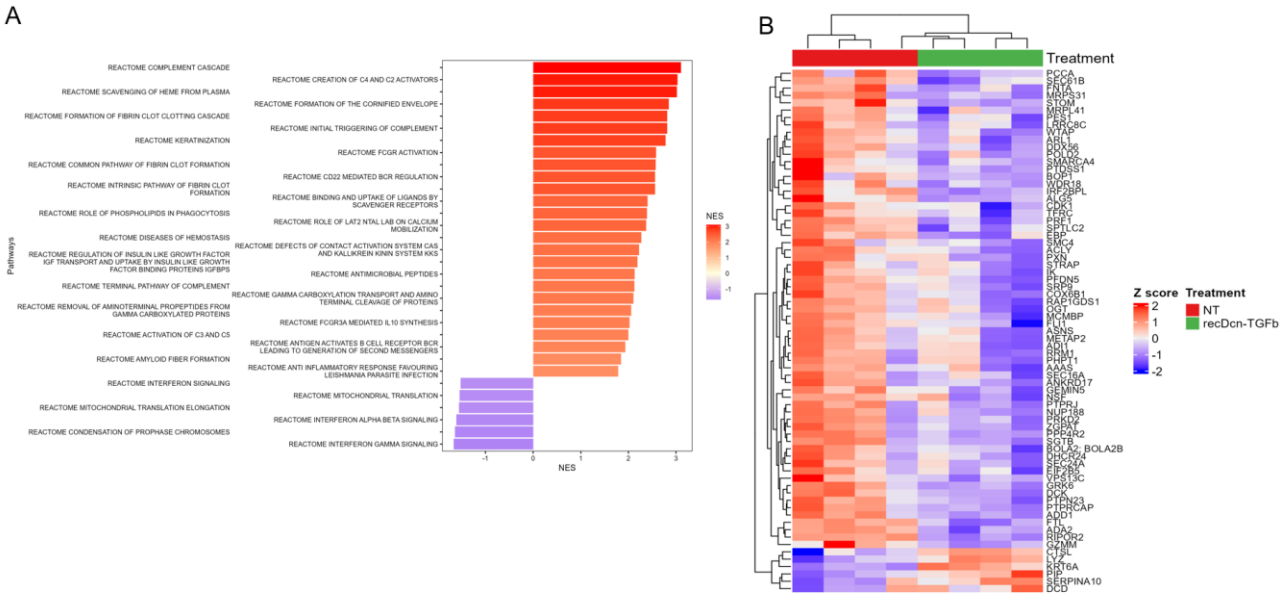


Figure 32 Supplementary: Recombinant decorin does not fully restore the proteomic state of TGFβ-treated CAR T cells.

(A) Unsupervised Reactome enrichment analysis comparing CAR T cells treated with recombinant decorin plus TGFβ (recDcn + TGFβ) to untreated (NT) CAR T cells. Pathways are ranked according to normalized enrichment score (NES). Positive NES values indicate pathways enriched in the recDcn + TGFβ condition, whereas negative NES values indicate pathways enriched in NT cells. (B) Heatmap of the most regulated proteins in the recDcn + TGFβ versus NT comparison, selected using |log2 fold change| > 1 and p value < 0.05. Protein abundance values are displayed as row z-scores of normalized expression values. Together, these analyses show that recDcn + TGFβ-treated CAR T cells remain proteomically distinct from untreated CAR T cells, supporting a partial rather than complete restoration of the TGFβ-altered state.

B. *In vivo* assessment of partial tumor niche engineering in simplified and orthotopic models

The second section presents two *in vivo* models designed to evaluate whether partial tumor expression of CXCL10 and decorin could improve T cell-mediated tumor control. The first model is a simplified murine proof-of-concept system based on Panc02-OVA-EpCAM tumors and OT-I T cells. The second model is an exploratory human orthotopic PDAC model based on SUIT-2-hMSLN tumors and mesothelin-specific CAR T cells. Together, these models were used to assess the impact of partial tumor niche engineering in a controlled antigen-specific setting and in a more complex orthotopic human CAR T cell setting.

For the murine proof-of-concept model, Panc02-OVA-EpCAM tumor cells were used in combination with OT-I T cells. Panc02-OVA-EpCAM is a murine pancreatic cancer cell line engineered to express EpCAM and the ovalbumin antigen, allowing antigen-specific recognition by OT-I $CD8^+$ T cells. This system provides a controlled model of antigen-specific $CD8^+$ T cell recognition through the OVA/OT-I axis.

NSG mice were selected to provide a clean experimental setting. Because these mice lack functional T cells, B cells and NK cells, any antitumor activity observed after adoptive T cell transfer can be attributed mainly to the transferred antigen-specific T cells. This model therefore allowed us to separate the effect of the therapeutic payloads from endogenous adaptive or NK-cell-mediated immune responses.

This murine *in vivo* model was used as a simplified system to test one specific question: whether partial tumor engineering is sufficient to support T cell-dependent tumor control. Only a fraction of the tumor cells expressed CXCL10 or CXCL10-decorin, allowing us to model an incomplete gene-delivery setting. This is relevant for tumor-directed gene therapy, where complete transduction of all malignant cells is unlikely. The comparison of tumors with or without OT-I transfer also made it possible to determine whether the payloads had intrinsic growth-inhibitory effects or whether their activity depended on adoptive T cell transfer.

In parallel, an exploratory orthotopic SUIT-2-hMSLN model was used to test whether the same partial tumor-engineering strategy could be transferred to a human mesothelin-positive PDAC setting *in vivo*. In this model, NSG mice received pancreatic implantation of SUIT-2-hMSLN tumor-cell mixtures containing a minority of payload-expressing cells, followed by systemic injection of mesothelin-specific human CAR T cells. This model was closer to the human CAR T cell system used *in vitro*, but it also introduced additional sources of variability, including orthotopic engraftment,

local pancreatic tumor growth and systemic CAR T cell trafficking. It was therefore used as an exploratory model to evaluate feasibility and identify the limits of translating the *in vitro* strategy *in vivo*.

B.1. Partial CXCL10 and decorin tumor secretion enhances antigen-specific T cell tumor control *in vivo* in a simplified Panc02-OVA-EpCAM/OT-I model

Panc02-OVA-EpCAM cells were engineered to express ZsGreen alone, mouse CXCL10-ZsGreen, or a dual mouse Decorin-P2A-CXCL10-IRES-ZsGreen cassette driven by the MND promoter **(Figure 33A).** Before *in vivo* implantation, engineered tumor cells were validated *in vitro*. Flow-cytometry analysis confirmed efficient transduction of Panc02-OVA-EpCAM cells, with high ZsGreen-positive fractions in the CXCL10 and CXCL10-Dcn conditions and a lower but detectable ZsGreen-positive fraction in the mock condition **(Supplementary Figure 34A)**.

Next, we measured payload secretion over time. CXCL10 was detected in the supernatants of both CXCL10- and CXCL10-Dcn-expressing cells, with increasing concentrations over 96 hours **(Supplementary Figure 34B)**. CXCL10 secretion was not significantly altered by decorin co-expression, indicating that the dual cassette preserved production of the chemokine module. Decorin was detected only in the CXCL10-Dcn condition, confirming specific production of the second payload **(Supplementary Figure 34C)**. Together, these results validated the generation of murine Panc02-OVA-EpCAM cells secreting CXCL10 alone or together with decorin.

The functional activity of secreted CXCL10 was assessed using a transwell migration assay with activated OT-I T cells. Migration medium alone induced minimal migration, whereas recombinant CXCL10 served as a positive control. Mock-transduced Panc02-OVA-EpCAM cells induced limited basal OT-I migration. In contrast, CXCL10- and CXCL10-Dcn-expressing tumor cells strongly increased OT-I migration **(Supplementary Figure 34D).** Migration induced by CXCL10-Dcn-expressing cells was comparable to that induced by CXCL10-expressing cells, indicating that decorin co-expression did not impair the chemotactic activity of CXCL10.

Next, we assessed whether partial expression of these payloads could modulate tumor control *in vivo*. Subcutaneous Panc02-OVA-EpCAM tumors were established in NSG mice using tumor-cell mixtures containing 80% parental cells and 20% engineered cells expressing mock, CXCL10, or CXCL10-Dcn payloads **(Figure 33B)**. This design was used to model partial tumor engineering, since complete transduction of all tumor cells is unlikely in a therapeutic gene-delivery setting. After tumor establishment, mice received intravenous OT-I T cell transfer where indicated. Conditions

without OT-I transfer were included to determine whether payload expression altered intrinsic tumor growth in this immunodeficient setting.

In the absence of OT-I transfer, mock, CXCL10 and CXCL10-Dcn tumors showed progressive growth, indicating that payload expression alone was not sufficient to control tumor progression in NSG mice. This control is important because each engineered tumor-cell population was generated and expanded separately before implantation, which could theoretically introduce payload-independent differences in intrinsic tumor growth. The comparable progressive growth observed in the groups without OT-I transfer indicates that the improved tumor control seen after OT-I administration was not due to baseline growth differences between tumor-cell preparations, but depended on the adoptively transferred antigen-specific T cells **(Figure 33C,D).** This supports the idea that CXCL10 and CXCL10-Dcn do not act primarily through direct tumor-growth inhibition in this model. After OT-I transfer, mock tumors showed partial growth delay, consistent with baseline antigen-specific activity of transferred OT-I cells. Tumors containing CXCL10-secreting cells showed a heterogeneous response, with some mice displaying improved control and others showing progressive tumor growth **(Figure 33C,D).** This indicates that CXCL10 expression can support OT-I-mediated tumor control in a subset of animals, but does not consistently prevent tumor progression.

In contrast, the CXCL10-Dcn + OT-I group showed a more favorable overall growth profile, with reduced tumor-growth burden and more consistent control across individual mice **(Figure 33C,D).** To specifically evaluate tumor behavior after OT-I transfer, we calculated the post-OT-I tumor expansion ratio by normalizing the endpoint tumor volume of each mouse to its tumor volume at the day of OT-I injection. This analysis showed reduced post-transfer tumor expansion in the CXCL10-Dcn + OT-I group compared with mock + OT-I tumors **(Figure 33E)**. The comparison between CXCL10 + OT-I and CXCL10-Dcn + OT-I did not reach statistical significance, indicating that the decorin-associated improvement should be interpreted as a more consistent tumor-control profile rather than a definitive superiority over CXCL10 alone in this small cohort.
We also followed normalized tumor growth after OT-I transfer to compare post-ACT progression independently of tumor size at the time of T cell injection. In this analysis, CXCL10-Dcn + OT-I tumors showed a lower mean expansion profile than the other OT-I-treated groups, but the difference was not statistically significant **(Figure 33F).** Thus, the normalized growth analysis is consistent with the endpoint expansion ratio, while confirming that the effect remains moderate in this limited cohort.

Together, these data indicate that partial intratumoral CXCL10 expression can enhance antigen-specific T cell control in some tumors, while addition of decorin is associated with a more reproducible tumor-control phenotype. The absence of tumor control in the corresponding groups without OT-I transfer supports a T cell-dependent paracrine niche-engineering mechanism. This simplified NSG model therefore provides an *in vivo* proof of concept that partial tumor engineering

can improve the activity of adoptively transferred antigen-specific T cells. These results suggest a trend toward improved and more consistent OT-I-dependent tumor control with CXCL10-Dcn. This interpretation is supported by the significant reduction in post-OT-I expansion ratio compared with mock + OT-I, although no significant difference between CXCL10 + OT-I and CXCL10-Dcn + OT-I. Altogether, these results support the use of CXCL10-decorin as a dual payload able to convert local T cell recruitment into more effective tumor control, while remaining dependent on the presence of transferred effector T cells.

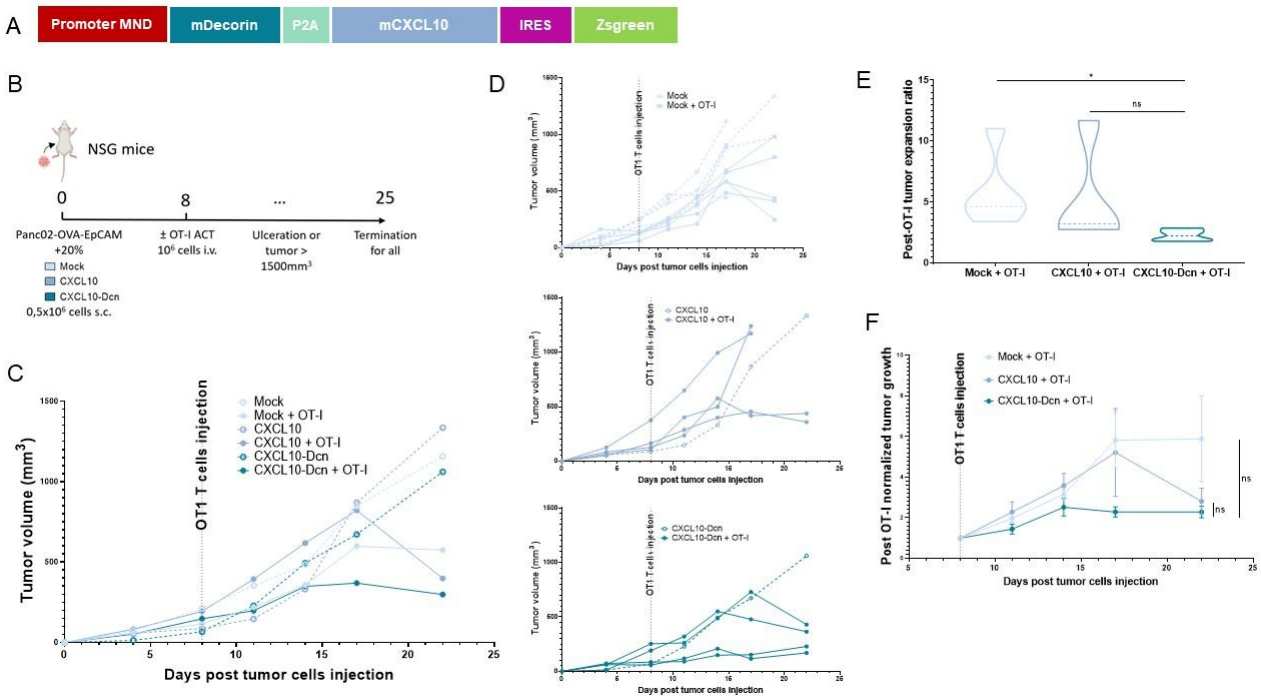


Figure 33: Partial CXCL10-decorin tumor engineering improves antigen-specific T cell-mediated tumor control in vivo.

(A) *Schematic representation of the dual murine decorin-CXCL10 lentiviral cassette. The construct contains the MND promoter, murine decorin, a P2A sequence, murine CXCL10, an IRES sequence and ZsGreen.* ***(B)*** *Experimental design of the in vivo proof-of-concept experiment. NSG mice were injected subcutaneously with Panc02-OVA-EpCAM tumor-cell mixtures containing 80% parental cells and 20% engineered cells expressing ZsGreen alone, mCXCL10-ZsGreen or mDecorin-P2A-mCXCL10-IRES-ZsGreen. Where indicated, mice received intravenous adoptive transfer of OT-I T cells on day 8 after tumor-cell injection. Tumor growth was monitored until ethical endpoint or study termination.* ***(C)*** *Tumor-growth kinetics of mock, CXCL10 and CXCL10-Dcn tumors with or without OT-I T cell transfer.* ***(D)*** *Individual tumor-growth curves for each payload condition, shown with or without OT-I T cell transfer. Dotted lines indicate mice that did not receive OT-I cells, and solid lines indicate mice that received OT-I cells.* ***(E)*** *Post-OT-I tumor expansion ratio, calculated by normalizing the endpoint tumor volume of each mouse to its tumor volume on the day of OT-I T cell injection. CXCL10-Dcn + OT-I tumors showed reduced post-transfer tumor expansion compared with mock + OT-I tumors. The comparison between CXCL10 + OT-I and CXCL10-Dcn + OT-I was not significant.* ***(F)*** *Normalized post-OT-I tumor growth in OT-I-treated groups, calculated relative to the tumor volume at the day of OT-I T cell injection. Data are shown as individual mice, mean ± SEM, or violin plots as indicated. Statistical significance was determined using one-way ANOVA with multiple comparisons for the post-OT-I expansion ratio. *p < 0.05; ns, not significant.*

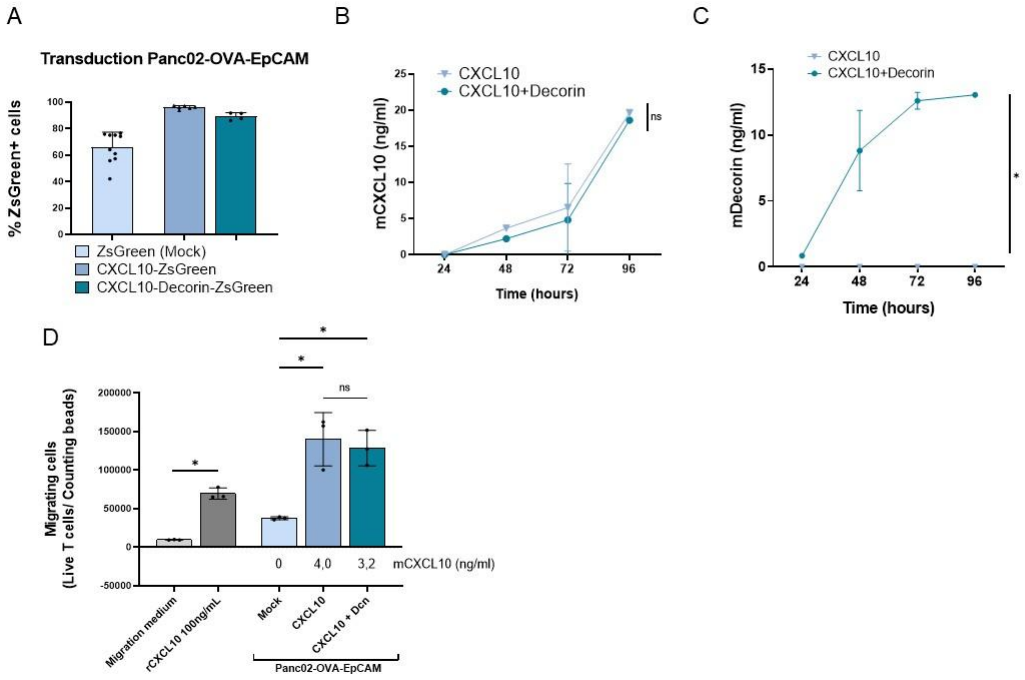


Figure 34 Supplementary: Validation of murine CXCL10 and CXCL10-decorin Panc02-OVA-EpCAM cells.

(A) *Flow-cytometry quantification of ZsGreen-positive Panc02-OVA-EpCAM cells after engineering with ZsGreen alone, mCXCL10-ZsGreen, or mDecorin-P2A-mCXCL10-IRES-ZsGreen constructs.* ***(B)*** *Quantification of mCXCL10 secretion in culture supernatants over 96 hours.* ***(C)*** *Quantification of mDecorin secretion in culture supernatants over 96 hours. Decorin was detected only in the CXCL10-Dcn condition.* ***(D)*** *Transwell migration assay using activated OT-I T cells exposed to migration medium, recombinant CXCL10, or supernatants from engineered Panc02-OVA-EpCAM cells. CXCL10- and CXCL10-Dcn-expressing tumor cells increased OT-I migration compared with mock cells, while decorin co-expression did not reduce CXCL10-driven migration. Data are shown as mean ± SD. Statistical significance was determined using one-way ANOVA with multiple comparisons for panels A and D and repeated-measures or two-way ANOVA for secretion kinetics in panels B and C, as appropriate. *p < 0.05; ns, not significant.*

B.2. Exploratory orthotopic SUIT-2-hMSLN model with systemic mesothelin CAR T cell transfer

To further evaluate whether the CXCL10-decorin strategy could be translated to a human CAR T cell setting *in vivo*, we established an exploratory orthotopic model using SUIT-2-hMSLN pancreatic tumor cells in NSG mice. SUIT-2-hMSLN cells were engineered to carry the luciferase transgene and follow tumor burden via bioluminescence. As in the murine proof-of-concept experiment, tumors were generated using mixtures containing 80% SUIT-2-hMSLN-Luciferase cells and 20% engineered cells expressing mock, CXCL10 or CXCL10-Dcn payloads. This design was used to model partial tumor engineering in a human mesothelin-positive PDAC setting. Tumor cells were injected into the pancreas in 50% Matrigel, and mice received intravenous mesothelin-specific human CAR T cells after tumor establishment **(Figure 35A).**

Tumor development was monitored by longitudinal bioluminescence imaging. Representative images showed detectable orthotopic tumor growth in all tumor-bearing groups, with increasing signal over time **(Figure 35B).** However, tumor progression was highly heterogeneous within each condition. This variability was also visible in the individual bioluminescence curves, where mice from the same group showed markedly different growth kinetics **(Figure 35C).** No consistent reduction in tumor burden was observed in the CXCL10 + CAR T or CXCL10-Dcn + CAR T groups compared with mock + CAR T controls. Endpoint *ex vivo* imaging confirmed that the strongest signal was detected in the pancreas, supporting the orthotopic localization of the tumor signal, but pancreatic tumor burden remained variable across all groups **(Figure 35D).** Importantly, CXCL10-Dcn did not increase bioluminescent signals in distant organs compared with mock or CXCL10 conditions. Signals detected in the liver, spleen, lungs, kidneys and ovaries remained low and comparable between groups, indicating that decorin expression did not promote detectable extra-pancreatic tumor dissemination under these experimental conditions.

These results indicate that this orthotopic SUIT-2-hMSLN model did not reveal a clear payload-dependent improvement in tumor control after systemic CAR T cell transfer. In contrast to the reductionist Panc02-OVA-EpCAM/OT-I model, this human orthotopic system introduced additional sources of variability, including pancreatic implantation efficiency, early tumor engraftment, local tumor growth kinetics and systemic CAR T cell trafficking to the pancreatic site. The use of only 20% payload-expressing tumor cells may also have limited the local concentration of CXCL10 and decorin in the orthotopic niche. Therefore, this experiment should be interpreted as an exploratory feasibility study rather than as definitive evidence against the biological activity of the dual payload.

Together, these data show that partial CXCL10-decorin tumor engineering was not sufficient to produce a measurable and reproducible antitumor effect in this orthotopic SUIT-2-hMSLN model

under the tested conditions. They also highlight the technical and biological constraints of evaluating niche-engineering strategies in orthotopic PDAC models, where tumor take, growth kinetics and CAR T cell access can vary substantially between animals. Further optimization of this model, including tumor-cell dose, timing of CAR T cell infusion, CAR T cell dose, payload-expressing fraction and local payload delivery, would be required to determine whether the effects observed *in vitro* can be reproduced *in vivo*.

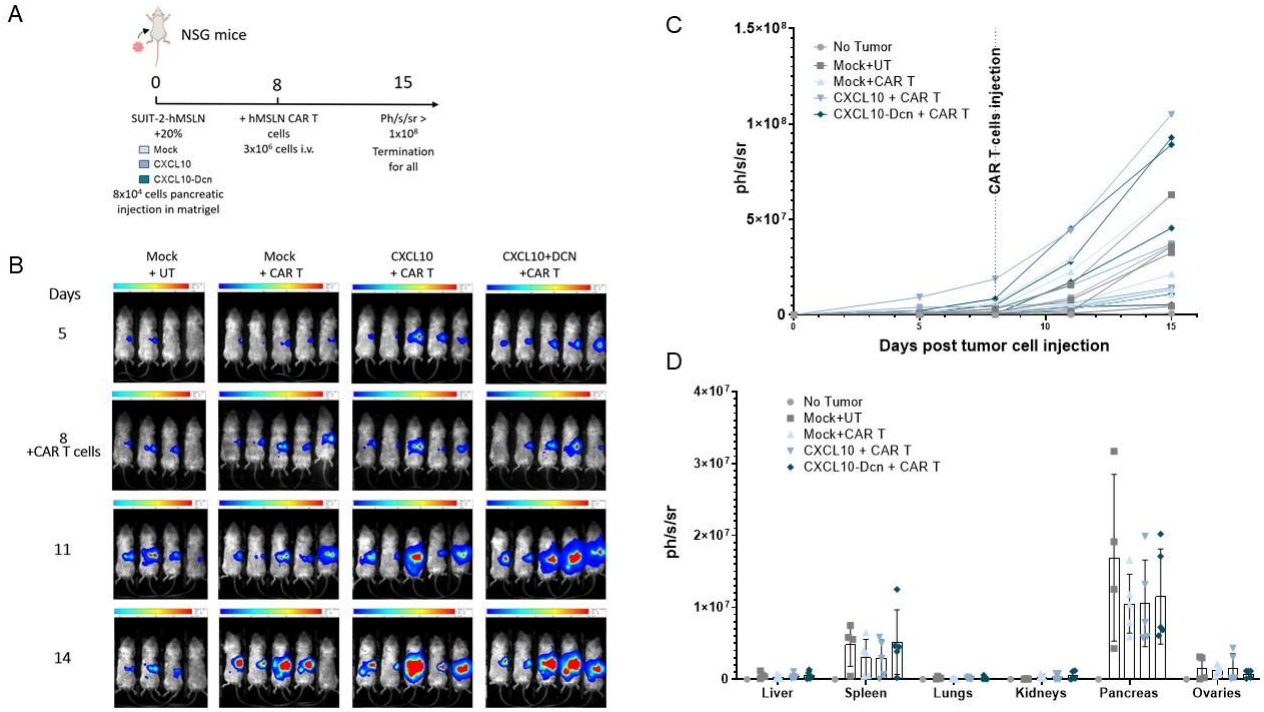


Figure 35: Exploratory orthotopic SUIT-2-hMSLN model with systemic mesothelin CAR T cell transfer.

(A) *Experimental design. NSG mice received orthotopic pancreatic injection of SUIT-2-hMSLN Luciferase+ tumor-cell mixtures containing 80% parental cells and 20% engineered cells expressing mock, CXCL10 or CXCL10-Dcn payloads. Tumor cells were injected in Matrigel. Where indicated, mice received intravenous mesothelin-specific human CAR T cells on day 8 after tumor-cell injection. Tumor progression was monitored by bioluminescence imaging until study termination.* ***(B)*** *Representative longitudinal bioluminescence images of tumor-bearing mice. Images are shown before CAR T cell injection and at subsequent time points after treatment.* ***(C)*** *Individual tumor-growth kinetics measured by bioluminescence imaging. The dotted line indicates the time of CAR T cell injection. Tumor growth was heterogeneous across animals, and no consistent difference was observed between mock + CAR T, CXCL10 + CAR T and CXCL10-Dcn + CAR T groups.* ***(D)*** *Endpoint ex vivo bioluminescence imaging of organs. Signal was mainly detected in the pancreas, supporting orthotopic tumor localization, with variable pancreatic tumor burden across groups. Data are shown as individual mice and mean ± SD where indicated.*

DISCUSSION

Pancreatic ductal adenocarcinoma remains a major challenge for immunotherapy because tumor-cell recognition alone is not sufficient to generate efficient tumor control. CAR T cells can kill antigen-positive tumor cells when productive contact is established, but their activity in PDAC is limited by poor tumor infiltration, dense extracellular matrix, abnormal tissue architecture and suppressive signals such as TGFβ. This places PDAC within a broader class of solid tumors in which the main therapeutic barrier is not only target recognition, but also the failure to generate a permissive tissue context for immune-cell entry, persistence and function. This interpretation is consistent with early clinical experience using mesothelin-directed CAR T cells in pancreatic cancer, where biological activity could be detected but durable objective responses remained limited, indicating that antigen targeting alone does not overcome the full resistance of the PDAC microenvironment[119]. Similar conclusions have emerged from preclinical studies combining mesothelin CAR T cells with cytokine-armed oncolytic vectors, where local remodeling of the tumor microenvironment was required to improve CAR T cell activity[129].

This thesis was built on the concept that these barriers may be addressed by local genetic engineering of the tumor niche. The objective was not to modify every malignant cell. The objective was to use a fraction of antigen-expressing tumor cells as local sources of diffusible factors able to modify tumor-immune interactions.

This paracrine logic is important for PDAC, where low tumor cellularity, stromal dominance and heterogeneous antigen expression make complete genetic modification of the tumor mass unrealistic. It is also conceptually aligned with recent gene-delivery strategies designed to restrict therapeutic protein production to the tumor site, thereby increasing intratumoral exposure while reducing systemic exposure[190].

The work addressed two connected levels. The first was technological: can lentiviral vectors be redirected toward tumor-associated antigens with enough specificity to support antigen-dependent gene delivery in experimental models? The second was biological: can local expression of selected payloads reshape the tumor niche in a way that improves T cell recruitment and antitumor activity? The central conclusion is that vector retargeting and payload biology must be considered together.

A key concept emerging from this work is that targeted niche engineering is likely governed by thresholds rather than by binary effects. Target antigen expression must reach a level sufficient for vector binding and productive transduction. The fraction of transduced tumor cells must produce enough payload to generate a biologically active local signal. CXCL10 must establish a chemokine gradient strong enough to recruit effector cells. Decorin must reach the tumor interface at a concentration and duration sufficient to modify matrix-associated or TGFβ-associated constraints. CAR T cells must then encounter tumor cells under conditions that allow synapse formation, survival

and repeated killing. This threshold-based interpretation may help reconcile the strong in vitro effects, the proof-of-concept activity observed in the OT-I model and the inconclusive outcome of the single orthotopic human experiment performed.

1. Retargeted lentiviral vectors as tools for tumor-restricted gene delivery

The first part of this thesis established the vector platform required for spatially controlled gene delivery. Conventional VSV-G-pseudotyped lentiviral vectors are efficient, stable and widely used, but their broad tropism limits their direct use for tumor-restricted delivery *in vivo*. In the context of cancer gene therapy, this lack of specificity is a central issue. Expression of a therapeutic payload outside the tumor may reduce efficacy and increase toxicity. This risk is particularly important for suicide genes, toxin genes or strong pro-apoptotic factors, where ectopic expression can directly damage healthy tissues. Chemokines, cytokines, matrix-remodeling proteins and immune-modulatory molecules are less directly cytotoxic, but their off-tumor expression may still perturb immune-cell trafficking, stromal organization or inflammatory signaling. This supports the need for tumor-restricted delivery even when the payload is not intrinsically lethal.

The comparative analysis of pseudotyping strategies showed that retargeting lentiviral vectors is not simply a question of adding an antigen-binding domain to a viral glycoprotein. Productive transduction requires several coordinated steps, including antigen recognition, particle binding, internalization, membrane fusion and post-entry events. Some pseudotyping platforms may bind target cells without mediating efficient gene transfer. This distinction is important because it shows that target recognition alone cannot be used as an indicator for functional delivery. This conclusion is consistent with previous work on engineered viral envelopes showing that cell-type-specific lentiviral transduction requires simultaneous control of receptor binding, native tropism, fusogenic activity and particle stability. Early SINV-pseudotyped lentiviral vectors displaying scFv domains established the feasibility of antibody-guided transduction, but subsequent studies also showed that envelope mutations, glycosylation and residual interactions with attachment factors can strongly influence specificity and efficiency[178,191].

Among the platforms tested, SINV-derived glycoproteins displaying scFv targeting domains provided the most robust antigen-dependent transduction. This was observed across several tumor-associated antigens, including EpCAM, mesothelin and PSMA, and was also extended to CD8 targeting using the same retargeting strategy. The ability to redirect the same envelope architecture toward tumor antigens and immune-cell markers places the SINV-scFv platform within the broader development of programmable lentiviral delivery systems. This is particularly relevant as retargeted

lentiviral vectors are now being explored not only for tumor-cell transduction, but also for direct *in vivo* immune-cell engineering[192].

These results show that the SINV-scFv platform can be adapted to distinct cell-surface targets by changing the scFv domain, including targets expressed by tumor cells or immune-cell subsets. The platform also allowed the production of vector preparations generated by co-transfection of two or three different scFv-envelope constructs, enabling simultaneous targeting of multiple antigens at the level of the vector preparation. This is particularly relevant for PDAC and other solid tumors, where antigen expression is heterogeneous and no single surface marker perfectly identifies all malignant cells. In this context, antigen loss or heterogeneous antigen density can limit both CAR T cell recognition and vector targeting. Multi-targeted vector preparations could therefore increase the fraction of tumor cells that receive the payload while maintaining a degree of tumor selectivity. This strategy is distinct from mixing independently produced monospecific vectors, because the different targeting envelopes are produced during the same transfection process. However, the precise composition of individual particles was not directly determined, and it remains possible that the preparation contains particles bearing one or several targeting envelopes.
This point is also relevant to antigen-density thresholds. For both CAR T cell recognition and vector retargeting, the presence of an antigen is not sufficient; the level and spatial distribution of antigen expression are likely to influence functional activity. In solid tumors, heterogeneous or low antigen density can reduce CAR T cell recognition and promote antigen-low escape variants. The same principle may apply to targeted lentiviral delivery, where antigen density could determine whether vector binding reaches the threshold required for productive transduction. Multi-targeted vector preparations may therefore help address not only antigen presence or absence, but also heterogeneous antigen density across tumor-cell states and lesions[129,193].

The *in vivo* data further support the relevance of SINV-scFv pseudotyping for tumor-directed gene transfer. Intratumoral administration allowed productive transduction in antigen-positive tumor models, and systemic administration of anti-PSMA SINV-scFv vectors showed antigen-associated transduction in PSMA-positive tumors with reduced broad off-target expression compared with VSV-G. These results do not yet establish clinical safety, but they demonstrate that antigen-directed lentiviral transduction can be achieved *in vivo*.
The main contribution of this part of the thesis is the demonstration that lentiviral retargeting can be used as a modular spatial-control layer for tumor microenvironment engineering. The envelope determines the cellular entry point, whereas the transgene determines the biological perturbation imposed locally. This separate targeting from function and makes the platform adaptable to different tumor antigens, payloads and biological barriers.

2. From targeted delivery to tumor niche engineering

The second part of the thesis aimed to build on this experimental vector-targeting approach to address a biological problem: the limited capacity of cytotoxic T cells to operate efficiently within the PDAC microenvironment. PDAC is characterized by low tumor cellularity, abundant desmoplastic stroma and spatial separation between immune cells and malignant epithelial cells. These properties suggest that therapeutic benefit may not depend only on the direct killing of individually transduced tumor cells. A more relevant objective was therefore to evaluate whether local payload expression could modify selected barriers to T cell recruitment and antitumor activity.

This idea is central to niche engineering. If a limited number of tumor cells can be selectively transduced, they can secrete factors that act on neighboring tumor cells, stromal components and immune effectors. This approach is well suited for secreted proteins such as chemokines and decorin. Their biological effect is not restricted to the cell that expresses them. They can generate gradients, modify extracellular matrix organization, regulate cytokine availability and influence immune-cell behavior within the local tumor environment.

This strategy also fits the biology of PDAC. The PDAC stroma is not a passive physical barrier that should simply be removed. Complete stromal depletion can worsen tumor behavior in some experimental settings, supporting a shift from stromal ablation toward controlled remodeling. In this context, targeted delivery of secreted payloads offers a way to modify selected features of the tumor niche without aiming to eliminate the stromal compartment. The next question was therefore whether a combined recruitment and remodeling payload could convert local T cell attraction into more productive antitumor activity.

3. A sequential payload model: recruitment, niche remodeling and effector output

The CXCL10-decorin payload was designed to address two non-redundant barriers. CXCL10 was intended to provide a localization signal for CXCR3-expressing T cells, whereas decorin was intended to condition the tumor interface encountered after recruitment. This distinction is essential for interpreting the functional data. In migration assays, CXCL10 expression by tumor cells increased OT-I and mesothelin CAR T cell migration, confirming that tumor-derived chemokine gradients can redirect antigen-specific T cells. However, in direct 2D coculture, the migration step is experimentally bypassed. Under these conditions, CXCL10 alone did not consistently increase tumor-cell killing, indicating that CXCL10 is not a direct enhancer of CAR T cell cytotoxicity once tumor-cell contact is imposed. This is consistent with the established role of the CXCL9/CXCL10/CXCL11-CXCR3 axis

as a trafficking module for activated effector T cells, rather than as a direct cytotoxicity-inducing pathway[151,194].

The decorin-containing payload changed this interpretation. Even in direct 2D coculture, where physical access is not limiting, CXCL10-Dcn increased CAR T cell-mediated killing, IFNγ secretion and recovery of viable CAR T cells. This indicates that decorin contributes to the post-contact phase of the antitumor response. The effect should not be interpreted as direct soluble activation of isolated CAR T cells, since recombinant decorin did not strongly activate CAR T cells in the absence of tumor engagement. Rather, the data support a model in which decorin modifies the tumor-cell context or the tumor/CAR T cell interface, making antigen-dependent engagement more productive. This post-contact interpretation is important because T cell exclusion and T cell dysfunction are mechanistically separable barriers. A chemokine gradient may improve localization, but productive killing also requires stable tumor contact, immune-synapse formation, cytotoxic granule release, metabolic support and resistance to suppressive cytokines[195–197]

This model is consistent with the current view of the PDAC stroma as an active regulator of immune-cell positioning and function. CAF-derived CXCL12 can restrict T cell access to malignant epithelial regions, and TGFβ-rich stromal programs can limit T cell penetration and effector activity. The therapeutic interpretation of the PDAC stroma has evolved substantially. Early studies supported the idea that stromal targeting could improve drug access, as Hedgehog pathway inhibition increased vascular density and gemcitabine delivery in KPC tumors, and hyaluronan depletion reduced physical barriers to drug penetration[46,134,198]. However, subsequent studies showed that depletion of αSMA$^+$ myofibroblasts or broad Hedgehog-dependent stromal programs could accelerate tumor progression, increase immunosuppression and reduce survival[68,199].

These apparently conflicting results are now better understood in light of CAF heterogeneity. PDAC fibroblasts include myofibroblastic, inflammatory and antigen-presenting states, with distinct localization, signaling programs and potential functions[54,200,201]. This supports a more selective therapeutic objective: not to remove the stromal compartment, but to remodel specific stromal features that restrict immune-cell access or function. Decorin-based niche engineering is closer to stromal reprogramming than to stromal depletion.

This interpretation is also consistent with studies linking collagen architecture and tissue stiffness to impaired T cell movement in solid tumors. Reducing collagen stabilization or targeting stromal barriers can improve T cell access and immunotherapy efficacy, supporting the idea that matrix remodeling may convert immune-cell recruitment into productive tumor engagement[202,203].

The use of CXCL10 also requires caution. CXCL10 is commonly associated with recruitment of CXCR3-expressing effector T cells, but its effect depends on the immune context. In pancreatic cancer, stromal IP-10/CXCL10 has been linked to recruitment of CXCR3$^+$ regulatory T cells and poor

clinical outcome[204]. This indicates that CXCL10 gradients may not selectively enrich cytotoxic lymphocytes in a fully immunocompetent tumor microenvironment. In this thesis, the human CAR T cell experiments and the NSG/OT-I model mainly tested the effector arm of CXCL10-dependent recruitment. Because these models lack a complete endogenous immune compartment, they could not fully address the impact of CXCL10 on suppressive CXCR3$^+$ populations.

This point is particularly relevant because regulatory T cells are closely connected to TGFβ biology. TGFβ can promote FOXP3 induction in conventional CD4 T cells and contributes to Treg maintenance and suppressive activity in defined contexts[205,206]. Therefore, a CXCL10-rich tumor niche that also contains abundant TGFβ could, in principle, support both effector-cell recruitment and regulatory immune suppression. In this context, decorin provides a mechanistic rationale for combination with CXCL10, although not direct evidence that this limitation is overcome. Decorin can interact with collagen, regulate extracellular matrix organization and modulate TGFβ availability or activity[207–209]. Local decorin expression could therefore reduce part of the TGFβ-dependent suppressive environment that favors regulatory immune programs, while CXCL10 promotes T cell recruitment. Whether this balance is sufficient to prevent CXCL10-driven recruitment or activation of suppressive CXCR3$^+$ Tregs remains to be directly tested in immunocompetent PDAC models.

4. Proteomic evidence for remodeling of the tumor-CAR T cell interface

The proteomic analyses support the idea that decorin acts at the tumor-CAR T cell interface, but they also define the limits of the current mechanistic interpretation. The compartment-restricted design was important because decorin could theoretically act on tumor cells, on CAR T cells directly, or on the interaction between the two. The strongest conclusion is that decorin did not behave as a broad soluble activator of isolated CAR T cells. In the CAR T-only dataset, TGFβ imposed the dominant proteomic shift, whereas recombinant decorin alone produced limited changes. This argues against a model in which decorin simply pre-activates CAR T cells before antigen encounter.

In tumor cells, the addition of decorin to CXCL10 was associated with proteins and pathways linked to adhesion, cytoskeletal organization, membrane-associated signaling and cell-matrix interaction. These changes are consistent with an interface-remodeling model, but they should not be overinterpreted as proof of a specific upstream pathway. Bulk proteomics measures protein abundance. It does not directly measure kinase activity, receptor activation, SMAD signaling, mechanotransduction or immune-synapse signaling.

This limitation is particularly important for CAR T cells because early CAR signaling is dominated by phosphorylation-dependent events, and phosphoproteomic studies have shown that CD28- and 4-1BB-based CARs generate distinct kinetic and quantitative signaling programs[210]. Similarly, time-resolved phosphoproteomics after TCR stimulation has shown that major signaling changes occur within minutes, before they are reflected by changes in total protein abundance[211].

The most informative proteomic signal was detected after coculture. CAR T cells collected from CXCL10-Dcn cocultures acquired a post-engagement state enriched in rRNA processing, translation initiation, translation elongation, protein quality control, unfolded protein response and mitochondrial metabolism. This suggests that decorin-conditioned tumor engagement is associated with a biosynthetic and proteostatic CAR T cell state compatible with sustained effector activity. This interpretation is supported by recent work showing that proteostasis is not only a housekeeping process in T cells, but a determinant of differentiation potential and tumor-infiltrating lymphocyte function. Progenitor-exhausted and tissue-resident memory-like T cells retain proteostasis-associated programs, whereas terminally exhausted TILs lose key E3 ubiquitin ligases, including NEURL3, RNF149 and WSB1, accumulate unfolded proteins and show impaired function[212]. Restoration of these ligases improved T cell fitness and antitumor activity in preclinical models[212].

In this context, the decorin-associated enrichment of protein processing, protein quality control and unfolded protein response pathways after tumor engagement is notable. It suggests that the improved cytotoxic phenotype observed with CXCL10-Dcn may be linked, at least in part, to a CAR T cell state better able to sustain the biosynthetic and proteostatic demands of repeated antigen encounter. However, this remains an association. The present data do not demonstrate that decorin restores proteostasis in the same sense as Scharping et al., nor do they identify NEURL3, RNF149, WSB1 or unfolded-protein accumulation as causal mediators in this model. This state may therefore reflect several non-exclusive mechanisms: stronger CAR signaling, improved CAR T cell survival, altered tumor-cell adhesion, modified mechanical constraints or reduced TGFβ-associated suppression.

A complementary phosphoproteomic or phosphokinome analysis would help define the signaling events upstream of this remodeling. This is particularly relevant for MAPK/ERK, PI3K/AKT, FAK/Src, Rho GTPase signaling and SMAD2/3, which are largely regulated through phosphorylation. Time-resolved phosphoproteomics after CAR T cell contact with mock, CXCL10 and CXCL10-Dcn tumor cells would distinguish early tumor-cell signaling from CAR T cell activation signaling. Kinase-activity inference could then test whether the decorin-associated post-killing state reflects stronger CAR signaling, altered mechanotransduction, improved survival signaling or reduced TGFβ-driven suppression[210,211,213,214].

Thus, the proteomic data strengthen the central model of the thesis but only partially reveal the mechanism. They show that decorin changes the molecular state associated with tumor-CAR T cell engagement. They do not yet identify the exact causal signaling pathway responsible and the major facors involved in improved cytotoxicity.

5. *In vivo* relevance of partial tumor engineering

The *in vivo* experiments tested a central translational assumption of this thesis: local expression of secreted payloads by only a fraction of tumor cells may be sufficient to modify the antitumor response. This is important because complete tumor transduction is unlikely with any targeted vector platform, especially in heterogeneous solid tumors. However, partial tumor engineering is expected to work only if a functional threshold is reached. This threshold likely depends on several parameters, including the fraction of engineered cells, the amount of payload produced per cell, payload diffusion and retention, antigen density on tumor cells, local T cell availability and the suppressive state of the tissue. This concept is consistent with the broader CAR T cell literature showing that antigen density can determine the strength of CAR T cell activation and tumor control, and with studies using locally armed oncolytic vectors showing that intratumoral expression of immune-modulatory payloads can enhance mesothelin CAR T cell activity in pancreatic cancer models[129,193].

The Panc02-OVA-EpCAM/OT-I model should be interpreted as a proof-of-concept system rather than as a fully representative PDAC model. Its strength is that it isolates antigen-specific T cell activity in a controlled setting, allowing the effect of partial CXCL10-Dcn expression to be tested directly. The improved tumor-control profile observed with CXCL10-Dcn supports the principle that a limited engineered tumor-cell fraction can influence antigen-specific T cell-mediated tumor control through secreted factors. However, the model uses a strong artificial antigen and lacks the endogenous immune complexity of PDAC, including suppressive myeloid cells, regulatory T cells, heterogeneous CAF states and native tumor-antigen presentation. Therefore, it demonstrates that partial niche engineering can work under permissive experimental conditions, but it does not establish that the same payload dose, engineered-cell fraction or timing would be sufficient in an immunocompetent pancreatic tumor. This distinction is consistent with studies in more complex PDAC models showing that engineered T cells can accumulate in pancreatic tumors and induce tumor-cell death, but that persistence and function remain limited by the local suppressive environment[53,215].

The orthotopic SUIT-2-hMSLN experiment defines the next translational boundary of the strategy. The absence of a therapeutic effect in this model indicates that partial payload expression, systemic CAR T cell delivery and an orthotopic human xenograft setting were not sufficient, under the tested conditions, to generate a robust *in vivo* effect. This result is informative because it identifies the

parameters that will likely determine future efficacy: the engineered tumor-cell fraction, the level and duration of payload expression, the timing and dose of CAR T cell infusion, the route of vector delivery and the ability of the payload to reach both primary and disseminated tumor sites. In this sense, the *in vivo* data support the biological rationale of partial niche engineering but also show that translation will require optimization of payload exposure and delivery strategy before the approach can be tested in more stringent immunocompetent or metastatic PDAC models.

6. Relationship to *in vivo* CAR T cell generation by retargeted lentiviral vectors

Recent work has pushed retargeted lentiviral vectors toward direct *in vivo* immune-cell engineering. Functionalized lentiviral vectors pseudotyped with chimeric dolphin morbillivirus-derived glycoproteins were retargeted to CD7 using camelid-derived nanobodies and combined with stimulatory αCD3/CD80 modules[192]. This system generated CAR T cells *in vivo* and mediated antitumor activity in a preclinical B-cell lymphoma model, while also addressing the problem of neutralizing antibody responses against measles-related envelopes. This study is important because it shows that retargeted lentiviral vectors can move beyond *ex vivo* gene transfer and act as programmable *in vivo* cell-engineering tools.

The strategy developed in this thesis is conceptually related, but it addresses a different biological barrier. Both approaches use retargeted lentiviral vectors to define which cells receive the genetic payload. However, *in vivo* CAR T cell generation targets immune cells to create the therapeutic effector directly inside the organism, whereas tumor niche engineering targets antigen-positive tumor cells to modify the local tissue environment in which therapeutic or endogenous immune cells act. These strategies are therefore complementary. *In vivo* CAR T cell generation may simplify manufacturing and immune-cell programming, while tumor niche engineering aims to make solid tumors more permissive to CAR T cell entry, persistence and effector function.

A future therapeutic approach could therefore combine immune-cell retargeting and tumor retargeting. One vector system could generate or support CAR T cells *in vivo*, while another tumor-targeted vector could condition the tumor niche through local expression of CXCL10, decorin or other payloads. This dual-vector concept is still speculative, but it illustrates the modularity of retargeted lentiviral platforms. The cell targeted by the vector and the payload delivered by the vector can be independently adapted to the biological barrier that needs to be overcome.

7. Limitations of the current work

Several limitations must be considered when interpreting this thesis.

The first limitation concerns the tumor models. The work relied largely on established tumor-cell lines engineered to express defined antigens such as EpCAM, mesothelin or PSMA. These models are useful for testing antigen-dependent vector targeting and CAR T cell function, but they do not fully reproduce the heterogeneity of patient-derived PDAC. Antigen density, tumor-cell state, stromal composition and immune contexture vary widely between patients and lesions. Future validation should include patient-derived organoids, *ex vivo* tumor slices and more complex multicellular models containing fibroblasts, matrix components and myeloid cells.

The second limitation concerns the immune models. The OT-I/OVA system provides a controlled and sensitive readout of antigen-specific T cell migration and killing, but it is more artificial than endogenous tumor-antigen recognition. The human CAR T cell experiments are more translational, but they were performed mainly in reductionist *in vitro* systems and immunodeficient mouse contexts. These settings do not include the full suppressive network of PDAC, including tumor-associated macrophages, regulatory T cells, myeloid-derived suppressor cells, abnormal vasculature and complex CAF states. These components may influence both vector delivery and T cell function.

The third limitation concerns decorin mechanism. The functional data show that decorin improves CAR T cell activity, especially in combination with CXCL10, but the exact mechanism remains incompletely defined. Decorin may act through collagen organization, TGFβ modulation, integrin-associated signaling, growth factor sequestration, receptor tyrosine kinase regulation or changes in tumor-cell adhesion. The proteomic data point toward remodeling of the tumor interface and a post-killing CAR T cell state enriched in biosynthetic and proteostatic pathways. These data generate hypotheses, but they do not prove causality. Direct validation will require targeted assays.

The fourth limitation concerns vector translation. SINV-scFv pseudotyping showed strong potential, but several parameters still need optimization before clinical translation. These include vector yield, particle stability, batch reproducibility, antigen-density thresholds, off-target transduction, biodistribution, immunogenicity and manufacturing under GMP-compatible conditions. The route of administration is another central translational issue. Systemic delivery is especially demanding because the vector must avoid neutralization, liver sequestration and uptake by non-target tissues. This problem is not specific to lentiviral vectors, but it is particularly relevant for tumor-targeted gene delivery, where systemic exposure increases the risk of off-tumor transduction and ectopic payload expression.
Intratumoral or regional administration may therefore be more realistic for early development, especially in locally advanced PDAC, where endoscopic ultrasound (EUS) -guided delivery could be used to target the primary pancreatic lesion. This approach is supported by previous clinical

experience showing that EUS-guided or image-guided intratumoral delivery of biologic agents has already been explored in locally advanced PDAC, including adenoviral TNFα gene delivery combined with chemoradiotherapy. These studies indicate that local injection into pancreatic tumors is technically feasible, but also highlight persistent limitations related to dose, toxicity, tissue distribution and clinical efficacy[216].

Another study illustrates, although not performed in PDAC, that regional administration can improve local exposure and reduce the dose required to achieve antitumor activity. This supports the rationale for evaluating local or regional delivery routes for both CAR T cells and tumor-targeted gene-delivery vectors[217].

However, a purely local route would not address disseminated disease or distant metastases. A sequential administration strategy could therefore be considered in future studies, combining local or regional delivery to engineer the primary tumor niche with systemic delivery designed to reach metastatic deposits. This local-systemic strategy is conceptually attractive, but it remains speculative. It would require dedicated optimization of vector dose, timing, biodistribution, antigen selectivity, payload diffusion and safety, because the constraints differ between a locally injected primary pancreatic tumor and systemically exposed metastatic sites.

This issue is reinforced by the biological differences between primary and metastatic PDAC niches. Single-cell analyses of matched primary tumors and liver metastases have shown that metastatic sites contain distinct tumor microenvironment compositions and intercellular interaction networks. Therefore, a payload strategy optimized for the primary pancreatic lesion may not behave identically in metastatic deposits[218].

The fifth limitation concerns payload safety. CXCL10 and decorin were selected because they are biologically relevant to immune recruitment and stromal remodeling. Their local expression may still have unintended effects. CXCL10 can recruit effector T cells, but it may also shape broader immune-cell recruitment depending on the cytokine context. Decorin can modulate matrix and TGFβ signaling, but excessive or prolonged stromal remodeling could produce unpredictable consequences. Future systems may require regulated promoters, dose-controlled expression, local administration, suicide switches or transient expression strategies.

8. Future directions

Future work should first resolve three mechanistic and translational questions. The first is whether decorin improves CAR T cell function primarily through matrix remodeling, TGFβ modulation or altered tumor-T cell contact. The second is whether partial payload expression can reach a reproducible functional threshold after true vector-mediated delivery in orthotopic and immunocompetent PDAC models. The third is whether local, regional or systemic administration can provide a therapeutic window in which tumor exposure is sufficient while off-tumor expression

remains limited. These three questions should be prioritized before broad therapeutic combinations are tested.

First, the mechanism of decorin action should be defined more precisely. Matrix organization could be analyzed by second harmonic generation imaging, a label-free nonlinear microscopy technique that visualizes fibrillar collagen organization, together with collagen I/III immunostaining, fiber-orientation analysis and measurement of matrix stiffness. TGFβ signaling could be assessed by pSMAD2/3 quantification, TGFβ target-gene expression and use of TGFβ pathway inhibitors or neutralizing antibodies. CAR T cell contact dynamics could be studied by live imaging to measure migration speed, dwell time, immune synapse formation and serial killing. These assays would help determine whether decorin improves CAR T cell function through matrix remodeling, signaling modulation or improved cell-cell contact.

Second, decorin structure-function relationships should be explored. Full-length decorin could be compared with mutants unable to bind collagen or with variants altered in TGFβ interaction. This would help distinguish matrix-dependent and TGFβ-dependent effects. Recombinant decorin, tumor-cell-expressed decorin and vector-delivered decorin should also be compared directly, because secretion kinetics, local concentration and matrix retention may differ between systems.

Third, the models should be made more representative of PDAC. Patient-derived organoids embedded in collagen or basement membrane matrices could be combined with pancreatic stellate cells, CAFs and macrophages. Tumor slices could preserve native architecture and allow short-term testing of vector penetration and immune-cell localization. Orthotopic models would better reproduce pancreatic vascularization, tissue pressure and local stromal organization than subcutaneous models. Immunocompetent models using physiological tumor antigens would be useful to assess whether CXCL10-Dcn also enhances endogenous antitumor immunity.

Fourth, the SINV-scFv platform should be optimized for translational use. This includes testing additional PDAC-relevant antigens, defining antigen-density thresholds for efficient transduction, improving vector production and studying biodistribution after local, regional and systemic administration. Combining multiple targeting domains may help address antigen heterogeneity. Safety could be improved by adding transcriptional restrictions, such as tumor-selective promoters.

Fifth, the therapeutic combinations should be expanded. CXCL10-Dcn niche engineering could be combined with mesothelin CAR T cells, checkpoint blockade, CXCR4/CXCL12 inhibition, TGFβ pathway blockade or chemotherapy regimens with immunomodulatory properties. The most rational combinations are those that act on non-redundant barriers. For example, CXCL10-Dcn could increase recruitment and improve the tumor interface, while checkpoint blockade could restore

exhausted endogenous or transferred T cells. Similarly, chemotherapy could reduce tumor burden and transiently reshape suppressive myeloid populations, creating a window in which niche engineering may have stronger effects.

Finally, the approach could be extended beyond PDAC. Dense extracellular matrix, immune exclusion and poor T cell infiltration are common features of several solid tumors. The modular nature of the platform means that the targeting antigen and the payload can be adapted to each tumor type. The central principle remains the same: a targeted vector delivers a local payload that makes the tumor microenvironment more permissive to immune attack.

Taken together, these findings argue for a shift in how CAR T cell therapy in PDAC is approached. The limiting factor is not only the design of the CAR or the choice of tumor antigen, but the ability of the tumor tissue to support lymphocyte entry, contact, persistence and effector function. Targeted lentiviral niche engineering addresses this issue by separating two levels of control: the cell type that receives the genetic payload and the local biological effect imposed by that payload. This work therefore supports a modular framework in which vector tropism, antigen density, payload diffusion, stromal remodeling and T cell function must be optimized together. The main challenge for translation will be to convert this proof-of-concept into a reproducible therapeutic window in models that preserve the spatial, stromal and immune complexity of PDAC.

CONCLUSION

This thesis supports targeted lentiviral niche engineering as a strategy to improve T cell therapy in PDAC. The work first identified SINV-scFv pseudotyping as a robust and modular platform for antigen-dependent gene delivery to solid tumor cells. It then showed that local expression of chemokines and decorin could address complementary barriers to antitumor immunity. CXCL10 validated the recruitment module in the human CAR T cell system. The addition of decorin improved CAR T cell cytotoxicity, IFNγ secretion, viable CAR T cell recovery and elimination of collagen-embedded spheroids, including under TGFβ exposure.

The proteomic analyses further support a model in which decorin remodels the tumor-CAR T cell interface. Decorin had limited direct autonomous effects on CAR T cells before tumor contact, but it was associated with a distinct post-killing CAR T cell state after coculture, enriched in biosynthetic, proteostatic and metabolic pathways. *In vivo*, partial tumor engineering with CXCL10-Dcn improved antigen-specific T cell-mediated tumor control in a controlled proof-of-concept model, supporting the idea that complete tumor transduction may not be required when the payload acts through paracrine niche remodeling under permissive conditions.

Overall, this work positions retargeted lentiviral vectors as more than delivery vehicles. They can serve as programmable tools for spatially controlled modification of the tumor microenvironment. In PDAC, where CAR T cell efficacy is limited by poor infiltration, stromal exclusion and suppressive signaling, this approach provides a rational strategy to complement adoptive cell therapy. Future studies should validate the mechanisms of decorin action, optimize vector safety and biodistribution, and test this strategy in more complex models that better reproduce the stromal, immune and metastatic architecture of human PDAC.

REFERENCES

1. Dato A, Bellino R. Surgical Anatomy of the Pancreas. In. 2025. doi:10.5772/intechopen.1007049

2. Basturk O, Hong SM, Wood LD, Adsay NV, Albores-Saavedra J, Biankin AV, et al. A Revised Classification System and Recommendations From the Baltimore Consensus Meeting for Neoplastic Precursor Lesions in the Pancreas. Am J Surg Pathol. 2015 Dec;39(12):1730–41. doi:10.1097/PAS.0000000000000533 PubMed PMID: 26559377; PubMed Central PMCID: PMC4646710.

3. Lee AYL, Dubois CL, Sarai K, Zarei S, Schaeffer DF, Sander M, et al. Cell of origin affects tumour development and phenotype in pancreatic ductal adenocarcinoma [Internet]. 2019 Mar 1. doi:10.1136/gutjnl-2017-314426

4. Yachida S, Jones S, Bozic I, Antal T, Leary R, Fu B, et al. Distant metastasis occurs late during the genetic evolution of pancreatic cancer. Nature. 2010 Oct 28;467(7319):1114–7. doi:10.1038/nature09515 PubMed PMID: 20981102; PubMed Central PMCID: PMC3148940.

5. Kleeff J, Korc M, Apte M, La Vecchia C, Johnson CD, Biankin AV, et al. Pancreatic cancer. Nat Rev Dis Primer. 2016 Apr 21;2:16022. doi:10.1038/nrdp.2016.22 PubMed PMID: 27158978.

6. Zhang H, Sashittal P, Karnoub ER, Jakatdar A, Umeda S, Hong J, et al. Genomic evolution of pancreatic cancer at single-cell resolution. Nat Genet. 2026 Feb;58(2):355–65. doi:10.1038/s41588-025-02468-9

7. Waddell N, Pajic M, Patch AM, Chang DK, Kassahn KS, Bailey P, et al. Whole genomes redefine the mutational landscape of pancreatic cancer. Nature. 2015 Feb 26;518(7540):495–501. doi:10.1038/nature14169 PubMed PMID: 25719666; PubMed Central PMCID: PMC4523082.

8. Golan T, Hammel P, Reni M, Cutsem EV, Macarulla T, Hall MJ, et al. Maintenance Olaparib for Germline BRCA-Mutated Metastatic Pancreatic Cancer. N Engl J Med. 2019 Jul 25;381(4):317–27. doi:10.1056/NEJMoa1903387

9. Kindler HL, Hammel P, Reni M, Van Cutsem E, Macarulla T, Hall MJ, et al. Overall Survival Results From the POLO Trial: A Phase III Study of Active Maintenance Olaparib Versus Placebo for Germline BRCA-Mutated Metastatic Pancreatic Cancer. J Clin Oncol Off J Am Soc Clin Oncol. 2022 Dec 1;40(34):3929–39. doi:10.1200/JCO.21.01604 PubMed PMID: 35834777; PubMed Central PMCID: PMC10476841.

10. Reyes-Castellanos G, Masoud R, Carrier A. Mitochondrial Metabolism in PDAC: From Better Knowledge to New Targeting Strategies. Biomedicines. 2020 Aug;8(8):270. doi:10.3390/biomedicines8080270

11. Abdel Hadi N, Reyes-Castellanos G, Gicquel T, Gallardo-Arriaga S, Cosialls E, Boet E, et al. Adaptation of redox metabolism in drug-tolerant persister cells is a vulnerability to prevent relapse in pancreatic cancer. Oncogenesis. 2025 Dec 9;14(1):48. doi:10.1038/s41389-025-00591-0

12. Moffitt RA, Marayati R, Flate EL, Volmar KE, Loeza SGH, Hoadley KA, et al. Virtual microdissection identifies distinct tumor- and stroma-specific subtypes of pancreatic ductal adenocarcinoma. Nat Genet. 2015 Oct;47(10):1168–78. doi:10.1038/ng.3398

13. Bailey P, Chang DK, Nones K, Johns AL, Patch AM, Gingras MC, et al. Genomic analyses identify molecular subtypes of pancreatic cancer. Nature. 2016 Mar;531(7592):47–52. doi:10.1038/nature16965

14. Chan-Seng-Yue M, Kim JC, Wilson GW, Ng K, Figueroa EF, O'Kane GM, et al. Transcription phenotypes of pancreatic cancer are driven by genomic events during tumor evolution. Nat Genet. 2020 Feb;52(2):231–40. doi:10.1038/s41588-019-0566-9

15. Klein L, Tu M, Krebs N, Urbach L, Grimm D, Latif MU, et al. Spatial tumor immune heterogeneity facilitates subtype co-existence and therapy response in pancreatic cancer. Nat Commun. 2025 Jan 6;16(1):335. doi:10.1038/s41467-024-55330-7

16. Hwang WL, Jagadeesh KA, Guo JA, Hoffman HI, Yadollahpour P, Reeves JW, et al. Single-nucleus and spatial transcriptome profiling of pancreatic cancer identifies multicellular dynamics associated with neoadjuvant treatment. Nat Genet. 2022 Aug;54(8):1178–91. doi:10.1038/s41588-022-01134-8 PubMed PMID: 35902743; PubMed Central PMCID: PMC10290535.

17. Oh K, Yoo YJ, Torre-Healy LA, Rao M, Fassler D, Wang P, et al. Coordinated single-cell tumor microenvironment dynamics reinforce pancreatic cancer subtype. Nat Commun. 2023 Aug 26;14(1):5226. doi:10.1038/s41467-023-40895-6

18. Kotecha K, Tree K, Ziaziaris WA, McKay SC, Wand H, Samra J, et al. Centralization of Pancreaticoduodenectomy: A Systematic Review and Spline Regression Analysis to Recommend Minimum Volume for a Specialist Pancreas Service. Ann Surg. 2024 Jun 1;279(6):953–60. doi:10.1097/SLA.0000000000006208 PubMed PMID: 38258578.

19. Panni RZ, Panni UY, Liu J, Williams GA, Fields RC, Sanford DE, et al. Re-defining a high volume center for pancreaticoduodenectomy. HPB. 2021 May 1;23(5):733–8. doi:10.1016/j.hpb.2020.09.009

20. Ballehaninna UK, Chamberlain RS. The clinical utility of serum CA 19-9 in the diagnosis, prognosis and management of pancreatic adenocarcinoma: An evidence based appraisal. J Gastrointest Oncol. 2012 Jun;3(2):105–19. doi:10.3978/j.issn.2078-6891.2011.021 PubMed PMID: 22811878; PubMed Central PMCID: PMC3397644.

21. Dickerson LD, Gittens J, Brunning C, Jackson R, Schmid MC, Mielgo A, et al. Neoadjuvant treatment versus upfront surgery in borderline resectable and resectable pancreatic ductal adenocarcinoma: meta-analysis. BJS Open. 2025 Mar 24;9(2):zrae172. doi:10.1093/bjsopen/zrae172 PubMed PMID: 40126570; PubMed Central PMCID: PMC11932015.

22. Papakonstantinou M, Fiflis S, Giakoustidis A, Christodoulidis G, Myriskou A, Louri E, et al. Survival after vascular resections in patients with borderline resectable or locally advanced pancreatic head cancer: A systematic review. Ann Hepato-Biliary-Pancreat Surg. 2024 Nov 30;28(4):423–32. doi:10.14701/ahbps.24-118 PubMed PMID: 39138646; PubMed Central PMCID: PMC11599818.

23. Melloul E, Lassen K, Roulin D, Grass F, Perinel J, Adham M, et al. Guidelines for Perioperative Care for Pancreatoduodenectomy: Enhanced Recovery After Surgery (ERAS) Recommendations 2019. World J Surg. 2020 Jul;44(7):2056–84. doi:10.1007/s00268-020-05462-w PubMed PMID: 32161987.

24. Deichmann S, Wellner U, Bolm L, Honselmann K, Braun R, Abdalla T, et al. Minimally invasive approaches in pancreatic cancer surgery. Eur Surg. 2024 May 1;56(3):76–85. doi:10.1007/s10353-023-00812-z

25. Conroy T, Desseigne F, Ychou M, Bouché O, Guimbaud R, Bécouarn Y, et al. FOLFIRINOX versus Gemcitabine for Metastatic Pancreatic Cancer. N Engl J Med. 2011 May 12;364(19):1817–25. doi:10.1056/NEJMoa1011923

26. Hoff DDV, Ervin T, Arena FP, Chiorean EG, Infante J, Moore M, et al. Increased Survival in Pancreatic Cancer with nab-Paclitaxel plus Gemcitabine. N Engl J Med. 2013 Oct 31;369(18):1691–703. doi:10.1056/NEJMoa1304369

27. Conroy T, Hammel P, Hebbar M, Abdelghani MB, Wei AC, Raoul JL, et al. FOLFIRINOX or Gemcitabine as Adjuvant Therapy for Pancreatic Cancer. N Engl J Med. 2018 Dec 20;379(25):2395–406. doi:10.1056/NEJMoa1809775

28. Chari ST. Detecting Early Pancreatic Cancer- Problems and Prospects. Semin Oncol. 2007 Aug;34(4):284–94. doi:10.1053/j.seminoncol.2007.05.005 PubMed PMID: 17674956; PubMed Central PMCID: PMC2680914.

29. Stoop TF, Javed AA, Oba A, Koerkamp BG, Seufferlein T, Wilmink JW, et al. Pancreatic cancer. The Lancet. 2025 Apr 5;405(10485):1182–202. doi:10.1016/S0140-6736(25)00261-2

30. Mizrahi JD, Surana R, Valle JW, Shroff RT. Pancreatic cancer. Lancet. 2020 Jun 27;395(10242):2008–20. doi:10.1016/S0140-6736(20)30974-0 PubMed PMID: 32593337.

31. Wangjam T, Zhang Z, Zhou XC, Lyer L, Faisal F, Soares KC, et al. Resected pancreatic ductal adenocarcinomas with recurrence limited in lung have a significantly better prognosis than those with other recurrence patterns. Oncotarget. 2015 Sep 10;6(34):36903–10. doi:10.18632/oncotarget.5054 PubMed PMID: 26372811; PubMed Central PMCID: PMC4742219.

32. Labib PLZ, Russell TB, Denson JL, Puckett MA, Ausania F, Pando E, et al. Patterns, timing and predictors of recurrence following pancreaticoduodenectomy for pancreatic ductal adenocarcinoma: an international multicentre retrospective cohort study. HPB. 2025 Apr 1;27(4):445–60. doi:10.1016/j.hpb.2024.11.015

33. Conroy T, Castan F, Lopez A, Turpin A, Ben Abdelghani M, Wei AC, et al. Five-Year Outcomes of FOLFIRINOX vs Gemcitabine as Adjuvant Therapy for Pancreatic Cancer: A Randomized Clinical Trial. JAMA Oncol. 2022 Nov 1;8(11):1571–8. doi:10.1001/jamaoncol.2022.3829 PubMed PMID: 36048453; PubMed Central PMCID: PMC9437831.

34. Neoptolemos JP, Palmer DH, Ghaneh P, Psarelli EE, Valle JW, Halloran CM, et al. Comparison of adjuvant gemcitabine and capecitabine with gemcitabine monotherapy in patients with resected pancreatic cancer (ESPAC-4): a multicentre, open-label, randomised, phase 3 trial. The Lancet. 2017 Mar 11;389(10073):1011–24. doi:10.1016/S0140-6736(16)32409-6 PubMed PMID: 28129987.

35. Strickler JH, Satake H, George TJ, Yaeger R, Hollebecque A, Garrido-Laguna I, et al. Sotorasib in KRAS p.G12C-Mutated Advanced Pancreatic Cancer. N Engl J Med. 2023 Jan 5;388(1):33–43. doi:10.1056/NEJMoa2208470 PubMed PMID: 36546651; PubMed Central PMCID: PMC10506456.

36. Hallin J, Bowcut V, Calinisan A, Briere DM, Hargis L, Engstrom LD, et al. Anti-tumor efficacy of a potent and selective non-covalent KRASG12D inhibitor. Nat Med. 2022 Oct;28(10):2171–82. doi:10.1038/s41591-022-02007-7 PubMed PMID: 36216931.

37. Wolpin BM, Park W, Garrido-Laguna I, Spira A, Starodub A, Sommerhalder D, et al. Daraxonrasib in Previously Treated Advanced RAS-Mutated Pancreatic Cancer. N Engl J Med. 2026 May 7;394(18):1790–802. doi:10.1056/NEJMoa2505783 PubMed PMID: 42090791.

38. Liaki V, Barrambana S, Kostopoulou M, Lechuga CG, Zamorano-Dominguez E, Acosta D, et al. A targeted combination therapy achieves effective pancreatic cancer regression and prevents tumor resistance. Proc Natl Acad Sci U S A. 122(49):e2523039122.

doi:10.1073/pnas.2523039122 PubMed PMID: 41329731; PubMed Central PMCID: PMC12704802.

39. Turner KM, Delman AM, Vaysburg DM, Kharofa JR, Smith MT, Choe KA, et al. Systemic Therapy for Resected Pancreatic Adenocarcinoma: How Much is Enough? Ann Surg Oncol. 2022 Jun;29(6):3463–72. doi:10.1245/s10434-022-11363-0 PubMed PMID: 35141802.

40. Boubaddi M, Rossi J, Marichez A, Marty M, Amintas S, Laurent C, et al. Preoperative Prognostic Factors in Resectable Pancreatic Cancer: State of the Art and Prospects. Ann Surg Oncol. 2025 Jun;32(6):4117–27. doi:10.1245/s10434-025-17062-w PubMed PMID: 40095311.

41. Conroy T, Pfeiffer P, Vilgrain V, Lamarca A, Seufferlein T, O'Reilly EM, et al. Pancreatic cancer: ESMO Clinical Practice Guideline for diagnosis, treatment and follow-up. Ann Oncol Off J Eur Soc Med Oncol. 2023 Nov;34(11):987–1002. doi:10.1016/j.annonc.2023.08.009 PubMed PMID: 37678671.

42. Boggi U, Kauffmann EF, Napoli N, Barreto SG, Besselink MG, Fusai GK, et al. REDISCOVER guidelines for borderline-resectable and locally advanced pancreatic cancer: management algorithm, unanswered questions, and future perspectives. Updat Surg. 2024 Sep;76(5):1573–91. doi:10.1007/s13304-024-01860-0 PubMed PMID: 38684573; PubMed Central PMCID: PMC11455680.

43. Bachmann J, Heiligensetzer M, Krakowski-Roosen H, Büchler MW, Friess H, Martignoni ME. Cachexia worsens prognosis in patients with resectable pancreatic cancer. J Gastrointest Surg Off J Soc Surg Aliment Tract. 2008 Jul;12(7):1193–201. doi:10.1007/s11605-008-0505-z PubMed PMID: 18347879.

44. Ho WJ, Jaffee EM, Zheng L. The tumour microenvironment in pancreatic cancer — clinical challenges and opportunities. Nat Rev Clin Oncol. 2020 Sep;17(9):527–40. doi:10.1038/s41571-020-0363-5 PubMed PMID: 32398706; PubMed Central PMCID: PMC7442729.

45. Hezel AF, Kimmelman AC, Stanger BZ, Bardeesy N, DePinho RA. Genetics and biology of pancreatic ductal adenocarcinoma. Genes Dev. 2006 May 15;20(10):1218–49. doi:10.1101/gad.1415606 PubMed PMID: 16702400.

46. Provenzano PP, Cuevas C, Chang AE, Goel VK, Von Hoff DD, Hingorani SR. Enzymatic Targeting of the Stroma Ablates Physical Barriers to Treatment of Pancreatic Ductal Adenocarcinoma. Cancer Cell. 2012 Mar 20;21(3):418–29. doi:10.1016/j.ccr.2012.01.007 PubMed PMID: 22439937.

47. Nieskoski MD, Marra K, Gunn JR, Hoopes PJ, Doyley MM, Hasan T, et al. Collagen Complexity Spatially Defines Microregions of Total Tissue Pressure in Pancreatic Cancer. Sci Rep. 2017 Aug 30;7(1):10093. doi:10.1038/s41598-017-10671-w

48. Sivakumar S, Jainarayanan A, Arbe-Barnes E, Sharma PK, Leathlobhair MN, Amin S, et al. Distinct immune cell infiltration patterns in pancreatic ductal adenocarcinoma (PDAC) exhibit divergent immune cell selection and immunosuppressive mechanisms. Nat Commun. 2025 Feb 6;16(1):1397. doi:10.1038/s41467-024-55424-2

49. Joseph AM, Al Aiyan A, Al-Ramadi B, Singh SK, Kishore U. Innate and adaptive immune-directed tumour microenvironment in pancreatic ductal adenocarcinoma. Front Immunol. 2024 Feb 7;15. doi:10.3389/fimmu.2024.1323198

50. Apte MV, Pirola RC, Wilson JS. Pancreatic stellate cells: a starring role in normal and diseased pancreas. Front Physiol. 2012;3:344. doi:10.3389/fphys.2012.00344 PubMed PMID: 22973234; PubMed Central PMCID: PMC3428781.

51. Bachem MG, Schünemann M, Ramadani M, Siech M, Beger H, Buck A, et al. Pancreatic carcinoma cells induce fibrosis by stimulating proliferation and matrix synthesis of stellate cells. Gastroenterology. 2005 Apr 1;128(4):907–21. doi:10.1053/j.gastro.2004.12.036 PubMed PMID: 15825074.

52. Tonini V, Zanni M. Pancreatic cancer in 2025: Have we found a solution? World J Gastroenterol. 2025 Nov 21;31(43):111433. doi:10.3748/wjg.v31.i43.111433 PubMed PMID: 41358172; PubMed Central PMCID: PMC12678954.

53. Feig C, Jones JO, Kraman M, Wells RJB, Deonarine A, Chan DS, et al. Targeting CXCL12 from FAP-expressing carcinoma-associated fibroblasts synergizes with anti–PD-L1 immunotherapy in pancreatic cancer. Proc Natl Acad Sci. 2013 Dec 10;110(50):20212–7. doi:10.1073/pnas.1320318110

54. Öhlund D, Handly-Santana A, Biffi G, Elyada E, Almeida AS, Ponz-Sarvise M, et al. Distinct populations of inflammatory fibroblasts and myofibroblasts in pancreatic cancer. J Exp Med. 2017 Mar 6;214(3):579–96. doi:10.1084/jem.20162024 PubMed PMID: 28232471; PubMed Central PMCID: PMC5339682.

55. Elyada E, Bolisetty M, Laise P, Flynn WF, Courtois ET, Burkhart RA, et al. Cross-Species Single-Cell Analysis of Pancreatic Ductal Adenocarcinoma Reveals Antigen-Presenting Cancer-Associated Fibroblasts. Cancer Discov. 2019 Aug;9(8):1102–23. doi:10.1158/2159-8290.CD-19-0094 PubMed PMID: 31197017; PubMed Central PMCID: PMC6727976.

56. Menezes S, Okail MH, Jalil SMA, Kocher HM, Cameron AJM. Cancer-associated fibroblasts in pancreatic cancer: new subtypes, new markers, new targets. J Pathol. 2022 Jul;257(4):526–44. doi:10.1002/path.5926 PubMed PMID: 35533046; PubMed Central PMCID: PMC9327514.

57. Neuzillet C, Tijeras-Raballand A, Ragulan C, Cros J, Patil Y, Martinet M, et al. Inter- and intra-tumoural heterogeneity in cancer-associated fibroblasts of human pancreatic ductal adenocarcinoma. J Pathol. 2019 May;248(1):51–65. doi:10.1002/path.5224 PubMed PMID: 30575030; PubMed Central PMCID: PMC6492001.

58. Neuzillet C, Nicolle R, Raffenne J, Tijeras-Raballand A, Brunel A, Astorgues-Xerri L, et al. Periostin- and podoplanin-positive cancer-associated fibroblast subtypes cooperate to shape the inflamed tumor microenvironment in aggressive pancreatic adenocarcinoma. J Pathol. 2022 Dec;258(4):408–25. doi:10.1002/path.6011 PubMed PMID: 36102377; PubMed Central PMCID: PMC9828775.

59. Principe DR, Timbers KE, Atia LG, Koch RM, Rana A. TGFβ Signaling in the Pancreatic Tumor Microenvironment. Cancers. 2021 Oct 11;13(20):5086. doi:10.3390/cancers13205086 PubMed PMID: 34680235; PubMed Central PMCID: PMC8533869.

60. Siret C, Collignon A, Silvy F, Robert S, Cheyrol T, André P, et al. Deciphering the Crosstalk Between Myeloid-Derived Suppressor Cells and Regulatory T Cells in Pancreatic Ductal Adenocarcinoma. Front Immunol. 2020 Jan 22;10:3070. doi:10.3389/fimmu.2019.03070 PubMed PMID: 32038621; PubMed Central PMCID: PMC6987391.

61. Clark CE, Hingorani SR, Mick R, Combs C, Tuveson DA, Vonderheide RH. Dynamics of the immune reaction to pancreatic cancer from inception to invasion. Cancer Res. 2007 Oct 1;67(19):9518–27. doi:10.1158/0008-5472.CAN-07-0175 PubMed PMID: 17909062.

62. Pylayeva-Gupta Y, Lee KE, Hajdu CH, Miller G, Bar-Sagi D. Oncogenic Kras-induced GM-CSF production promotes the development of pancreatic neoplasia. Cancer Cell. 2012 Jun 12;21(6):836–47. doi:10.1016/j.ccr.2012.04.024 PubMed PMID: 22698407; PubMed Central PMCID: PMC3721510.

63. Mikucki ME, Fisher DT, Matsuzaki J, Skitzki JJ, Gaulin NB, Muhitch JB, et al. Non-redundant requirement for CXCR3 signalling during tumoricidal T-cell trafficking across tumour vascular checkpoints. Nat Commun. 2015 Nov;6(1):7458. doi:10.1038/ncomms8458

64. Hirai I, Kimura W, Ozawa K, Kudo S, Suto K, Kuzu H, et al. Perineural Invasion in Pancreatic Cancer. Pancreas. 2002 Jan;24(1):15.

65. Ceyhan GO, Demir IE, Altintas B, Rauch U, Thiel G, Müller MW, et al. Neural invasion in pancreatic cancer: A mutual tropism between neurons and cancer cells. Biochem Biophys Res Commun. 2008 Sep 26;374(3):442–7. doi:10.1016/j.bbrc.2008.07.035

66. Cavel O, Shomron O, Shabtay A, Vital J, Trejo-Leider L, Weizman N, et al. Endoneurial Macrophages Induce Perineural Invasion of Pancreatic Cancer Cells by Secretion of GDNF and Activation of RET Tyrosine Kinase Receptor. Cancer Res. 2012 Nov 14;72(22):5733–43. doi:10.1158/0008-5472.CAN-12-0764

67. Begum A, Ewachiw T, Jung C, Huang A, Norberg KJ, Marchionni L, et al. The extracellular matrix and focal adhesion kinase signaling regulate cancer stem cell function in pancreatic ductal adenocarcinoma. PLOS ONE. 2017 Jul 10;12(7):e0180181. doi:10.1371/journal.pone.0180181

68. Rhim AD, Oberstein PE, Thomas DH, Mirek ET, Palermo CF, Sastra SA, et al. Stromal elements act to restrain, rather than support, pancreatic ductal adenocarcinoma. Cancer Cell. 2014 Jun 16;25(6):735–47. doi:10.1016/j.ccr.2014.04.021 PubMed PMID: 24856585; PubMed Central PMCID: PMC4096698.

69. Özdemir BC, Pentcheva-Hoang T, Carstens JL, Zheng X, Wu CC, Simpson TR, et al. Depletion of carcinoma-associated fibroblasts and fibrosis induces immunosuppression and accelerates pancreas cancer with reduced survival. Cancer Cell. 2014 Jun 16;25(6):719–34. doi:10.1016/j.ccr.2014.04.005 PubMed PMID: 24856586; PubMed Central PMCID: PMC4180632.

70. Rojas LA, Sethna Z, Soares KC, Olcese C, Pang N, Patterson E, et al. Personalized RNA neoantigen vaccines stimulate T cells in pancreatic cancer. Nature. 2023 Jun;618(7963):144–50. doi:10.1038/s41586-023-06063-y

71. Cai Z, Li Z, Zhong W, Lin F, Dong X, Ye H, et al. Targeting Mesothelin Enhances Personalized Neoantigen Vaccine Induced Antitumor Immune Response in Orthotopic Pancreatic Cancer Mouse Models. Adv Sci. 2025 Mar;12(12):e2407976. doi:10.1002/advs.202407976 PubMed PMID: 39887656; PubMed Central PMCID: PMC11948035.

72. Wang Y, Huang P, Li C, Tu S, Yang H. Therapeutic cancer vaccines in pancreatic cancer. Front Immunol. 2025 Oct 20;16:1674743. doi:10.3389/fimmu.2025.1674743 PubMed PMID: 41190066; PubMed Central PMCID: PMC12580372.

73. Bever KM, Huff AL, Danilova L, Wetzel M, Tandurella JA, Durham JN, et al. A randomized phase II study: CRS207/GVAX plus anti-PD1 and anti-CTLA4 recruits mesothelin- and mKRAS-specific T cells into PDAC. Cancer Immunol Res. 2026 Mar 4;14(3):411–22. doi:10.1158/2326-6066.CIR-25-0545 PubMed PMID: 41524570; PubMed Central PMCID: PMC12869358.

74. Agarwal P, Guo M, Munjal K, Qi H, Parkinson R, Ferguson A, et al. A Phase II Study of Neoadjuvant GVAX and Cyclophosphamide Combined with Nivolumab and SBRT Followed by Surgery in Borderline Resectable Pancreatic Adenocarcinoma. Clin Cancer Res. 2025 Aug 1;31(15):3205–14. doi:10.1158/1078-0432.CCR-24-3403

75. Le DT, Picozzi VJ, Ko AH, Wainberg ZA, Kindler H, Wang-Gillam A, et al. Results from a Phase IIb, Randomized, Multicenter Study of GVAX Pancreas and CRS-207 Compared with Chemotherapy in Adults with Previously Treated Metastatic Pancreatic Adenocarcinoma

(ECLIPSE Study). Clin Cancer Res Off J Am Assoc Cancer Res. 2019 Sep 15;25(18):5493–502. doi:10.1158/1078-0432.CCR-18-2992 PubMed PMID: 31126960; PubMed Central PMCID: PMC7376746.

76. Wu AA, Bever KM, Ho WJ, Fertig EJ, Niu N, Zheng L, et al. A Phase II Study of Allogeneic GM-CSF–Transfected Pancreatic Tumor Vaccine (GVAX) with Ipilimumab as Maintenance Treatment for Metastatic Pancreatic Cancer. Clin Cancer Res. 2020 Oct 1;26(19):5129–39. doi:10.1158/1078-0432.CCR-20-1025

77. Ho WJ, Jaffee EM, Zheng L. The tumour microenvironment in pancreatic cancer - clinical challenges and opportunities. Nat Rev Clin Oncol. 2020 Sep;17(9):527–40. doi:10.1038/s41571-020-0363-5 PubMed PMID: 32398706; PubMed Central PMCID: PMC7442729.

78. Middleton G, Silcocks P, Cox T, Valle J, Wadsley J, Propper D, et al. Gemcitabine and capecitabine with or without telomerase peptide vaccine GV1001 in patients with locally advanced or metastatic pancreatic cancer (TeloVac): an open-label, randomised, phase 3 trial. Lancet Oncol. 2014 Jul;15(8):829–40. doi:10.1016/S1470-2045(14)70236-0 PubMed PMID: 24954781.

79. Cheng NC, Vonderheide RH. Immune vulnerabilities of mutant KRAS in pancreatic cancer. Trends Cancer. 2023 Nov;9(11):928–36. doi:10.1016/j.trecan.2023.07.004 PubMed PMID: 37524642; PubMed Central PMCID: PMC10592263.

80. Taïeb J, Sayah L, Heinrich K, Kunzmann V, Boileve A, Cirkel G, et al. Efficacy of immune checkpoint inhibitors in microsatellite unstable/mismatch repair-deficient advanced pancreatic adenocarcinoma: an AGEO European Cohort. Eur J Cancer. 2023 Jul;188:90–7. doi:10.1016/j.ejca.2023.04.012 PubMed PMID: 37229836.

81. Beatty GL, Chiorean EG, Fishman MP, Saboury B, Teitelbaum UR, Sun W, et al. CD40 agonists alter tumor stroma and show efficacy against pancreatic carcinoma in mice and humans. Science. 2011 Mar 25;331(6024):1612–6. doi:10.1126/science.1198443 PubMed PMID: 21436454; PubMed Central PMCID: PMC3406187.

82. Vincent J, Mignot G, Chalmin F, Ladoire S, Bruchard M, Chevriaux A, et al. 5-Fluorouracil selectively kills tumor-associated myeloid-derived suppressor cells resulting in enhanced T cell-dependent antitumor immunity. Cancer Res. 2010 Apr 15;70(8):3052–61. doi:10.1158/0008-5472.CAN-09-3690 PubMed PMID: 20388795.

83. Eriksson E, Wenthe J, Irenaeus S, Loskog A, Ullenhag G. Gemcitabine reduces MDSCs, tregs and TGFβ-1 while restoring the teff/treg ratio in patients with pancreatic cancer. J Transl Med. 2016 Sep 29;14(1):282. doi:10.1186/s12967-016-1037-z PubMed PMID: 27687804; PubMed Central PMCID: PMC5041438.

84. Picozzi V, Alseidi A, Winter J, Pishvaian M, Mody K, Glaspy J, et al. Gemcitabine/nab-paclitaxel with pamrevlumab: a novel drug combination and trial design for the treatment of locally advanced pancreatic cancer. ESMO Open. 2020 Aug 19;5(4):e000668. doi:10.1136/esmoopen-2019-000668 PubMed PMID: 32817130; PubMed Central PMCID: PMC7440698.

85. Van Cutsem E, Tempero MA, Sigal D, Oh DY, Fazio N, Macarulla T, et al. Randomized Phase III Trial of Pegvorhyaluronidase Alfa With Nab-Paclitaxel Plus Gemcitabine for Patients With Hyaluronan-High Metastatic Pancreatic Adenocarcinoma. J Clin Oncol Off J Am Soc Clin Oncol. 2020 Sep 20;38(27):3185–94. doi:10.1200/JCO.20.00590 PubMed PMID: 32706635; PubMed Central PMCID: PMC7499614.

86. Wang-Gillam A, Lim KH, McWilliams R, Suresh R, Lockhart AC, Brown A, et al. Defactinib, pembrolizumab, and gemcitabine in patients with advanced treatment refractory pancreatic cancer: A phase I, dose escalation, and expansion study. Clin Cancer Res Off J Am Assoc Cancer

Res. 2022 Dec 15;28(24):5254–62. doi:10.1158/1078-0432.CCR-22-0308 PubMed PMID: 36228156; PubMed Central PMCID: PMC9772237.

87. Rosenberg SA, Packard BS, Aebersold PM, Solomon D, Topalian SL, Toy ST, et al. Use of tumor-infiltrating lymphocytes and interleukin-2 in the immunotherapy of patients with metastatic melanoma. A preliminary report. N Engl J Med. 1988 Dec 22;319(25):1676–80. doi:10.1056/NEJM198812223192527 PubMed PMID: 3264384.

88. June CH, Sadelain M. Chimeric Antigen Receptor Therapy. N Engl J Med. 2018 Jul 5;379(1):64–73. doi:10.1056/NEJMra1706169 PubMed PMID: 29972754; PubMed Central PMCID: PMC7433347.

89. Gross G, Waks T, Eshhar Z. Expression of immunoglobulin-T-cell receptor chimeric molecules as functional receptors with antibody-type specificity. Proc Natl Acad Sci U S A. 1989 Dec;86(24):10024–8. doi:10.1073/pnas.86.24.10024 PubMed PMID: 2513569; PubMed Central PMCID: PMC298636.

90. Kuwana Y, Asakura Y, Utsunomiya N, Nakanishi M, Arata Y, Itoh S, et al. Expression of chimeric receptor composed of immunoglobulin-derived V regions and T-cell receptor-derived C regions. Biochem Biophys Res Commun. 1987 Dec 31;149(3):960–8. doi:10.1016/0006-291x(87)90502-x PubMed PMID: 3122749.

91. Moritz D, Groner B. A spacer region between the single chain antibody- and the CD3 zeta-chain domain of chimeric T cell receptor components is required for efficient ligand binding and signaling activity. Gene Ther. 1995 Oct;2(8):539–46. PubMed PMID: 8593604.

92. Brocker T, Karjalainen K. Signals through T cell receptor-zeta chain alone are insufficient to prime resting T lymphocytes. J Exp Med. 1995 May 1;181(5):1653–9. doi:10.1084/jem.181.5.1653 PubMed PMID: 7722445; PubMed Central PMCID: PMC2192006.

93. Carcopino C, Erdogan E, Henrich M, Kobold S. Armoring chimeric antigen receptor (CAR) T cells as micropharmacies for cancer therapy. Immuno-Oncol Technol. 2024 Sep 25;24:100739. doi:10.1016/j.iotech.2024.100739 PubMed PMID: 39711794.

94. Morris EC, Neelapu SS, Giavridis T, Sadelain M. Cytokine release syndrome and associated neurotoxicity in cancer immunotherapy. Nat Rev Immunol. 2022 Feb;22(2):85–96. doi:10.1038/s41577-021-00547-6

95. Morgan RA, Yang JC, Kitano M, Dudley ME, Laurencot CM, Rosenberg SA. Case report of a serious adverse event following the administration of T cells transduced with a chimeric antigen receptor recognizing ERBB2. Mol Ther J Am Soc Gene Ther. 2010 Apr;18(4):843–51. doi:10.1038/mt.2010.24 PubMed PMID: 20179677; PubMed Central PMCID: PMC2862534.

96. Maude SL, Laetsch TW, Buechner J, Rives S, Boyer M, Bittencourt H, et al. Tisagenlecleucel in Children and Young Adults with B-Cell Lymphoblastic Leukemia. N Engl J Med. 2018 Feb 1;378(5):439–48. doi:10.1056/NEJMoa1709866

97. Neelapu SS, Locke FL, Bartlett NL, Lekakis LJ, Miklos DB, Jacobson CA, et al. Axicabtagene Ciloleucel CAR T-Cell Therapy in Refractory Large B-Cell Lymphoma. N Engl J Med. 2017 Dec 28;377(26):2531–44. doi:10.1056/NEJMoa1707447

98. Lesch S, Blumenberg V, Stoiber S, Gottschlich A, Ogonek J, Cadilha BL, et al. T cells armed with C-X-C chemokine receptor type 6 enhance adoptive cell therapy for pancreatic tumours. Nat Biomed Eng. 2021 Jun 3. doi:10.1038/s41551-021-00737-6

99. Cadilha BL, Benmebarek MR, Dorman K, Oner A, Lorenzini T, Obeck H, et al. Combined tumor-directed recruitment and protection from immune suppression enable CAR T cell efficacy in solid tumors. Sci Adv. 2021 Jun 11;7(24):eabi5781. doi:10.1126/sciadv.abi5781

100. Rataj F, Kraus FBT, Chaloupka M, Grassmann S, Heise C, Cadilha BL, et al. PD1-CD28 Fusion Protein Enables CD4+ T Cell Help for Adoptive T Cell Therapy in Models of Pancreatic Cancer and Non-hodgkin Lymphoma. Front Immunol. 2018 Aug 30;9. doi:10.3389/fimmu.2018.01955

101. Lynn RC, Weber EW, Sotillo E, Gennert D, Xu P, Good Z, et al. c-Jun overexpression in CAR T cells induces exhaustion resistance. Nature. 2019 Dec;576(7786):293–300. doi:10.1038/s41586-019-1805-z

102. Peng L, Sferruzza G, Yang L, Zhou L, Chen S. CAR-T and CAR-NK as cellular cancer immunotherapy for solid tumors. Cell Mol Immunol. 2024 Oct;21(10):1089–108. doi:10.1038/s41423-024-01207-0

103. Klichinsky M, Ruella M, Shestova O, Lu XM, Best A, Zeeman M, et al. Human chimeric antigen receptor macrophages for cancer immunotherapy. Nat Biotechnol. 2020 Aug;38(8):947–53. doi:10.1038/s41587-020-0462-y PubMed PMID: 32361713; PubMed Central PMCID: PMC7883632.

104. Wang LCS, Lo A, Scholler J, Sun J, Majumdar RS, Kapoor V, et al. Targeting fibroblast activation protein in tumor stroma with chimeric antigen receptor T cells can inhibit tumor growth and augment host immunity without severe toxicity. Cancer Immunol Res. 2014 Feb;2(2):154–66. doi:10.1158/2326-6066.CIR-13-0027 PubMed PMID: 24778279; PubMed Central PMCID: PMC4007316.

105. Nicolai CJ, Parker MH, Qin J, Tang W, Ulrich-Lewis JT, Gottschalk RJ, et al. In vivo CAR T-cell generation in nonhuman primates using lentiviral vectors displaying a multidomain fusion ligand. Blood. 2024 Aug 29;144(9):977–87. doi:10.1182/blood.2024024523 PubMed PMID: 38861668; PubMed Central PMCID: PMC11406189.

106. Pfeiffer A, Thalheimer FB, Hartmann S, Frank AM, Bender RR, Danisch S, et al. In vivo generation of human CD19-CAR T cells results in B-cell depletion and signs of cytokine release syndrome. EMBO Mol Med. 2018 Nov;10(11):e9158. doi:10.15252/emmm.201809158 PubMed PMID: 30224381; PubMed Central PMCID: PMC6220327.

107. Frank AM, Braun AH, Scheib L, Agarwal S, Schneider IC, Fusil F, et al. Combining T-cell-specific activation and in vivo gene delivery through CD3-targeted lentiviral vectors. Blood Adv. 2020 Nov 24;4(22):5702–15. doi:10.1182/bloodadvances.2020002229 PubMed PMID: 33216892; PubMed Central PMCID: PMC7686896.

108. Czaplicka A, Lachota M, Pączek L, Zagożdżon R, Kaleta B. Chimeric Antigen Receptor T Cell Therapy for Pancreatic Cancer: A Review of Current Evidence. Cells. 2024 Jan 4;13(1):101. doi:10.3390/cells13010101 PubMed PMID: 38201305; PubMed Central PMCID: PMC10777940.

109. Rodriguez-Garcia A, Palazon A, Noguera-Ortega E, Powell DJ, Guedan S. CAR-T Cells Hit the Tumor Microenvironment: Strategies to Overcome Tumor Escape. Front Immunol. 2020 Jun 17;11:1109. doi:10.3389/fimmu.2020.01109 PubMed PMID: 32625204; PubMed Central PMCID: PMC7311654.

110. Gao TA, Chen YY. Engineering Next-Generation CAR-T Cells: Overcoming Tumor Hypoxia and Metabolism. Annu Rev Chem Biomol Eng. 2022 Jun 10;13:193–216. doi:10.1146/annurev-chembioeng-092120-092914 PubMed PMID: 35700528.

111. Beatty GL, Haas AR, Maus MV, Torigian DA, Soulen MC, Plesa G, et al. Mesothelin-Specific Chimeric Antigen Receptor mRNA-Engineered T Cells Induce Antitumor Activity in Solid Malignancies. Cancer Immunol Res. 2014 Feb 1;2(2):112–20. doi:10.1158/2326-6066.CIR-13-0170

112. Feng K, Liu Y, Guo Y, Qiu J, Wu Z, Dai H, et al. Phase I study of chimeric antigen receptor modified T cells in treating HER2-positive advanced biliary tract cancers and pancreatic cancers. Protein Cell. 2018 Oct;9(10):838–47. doi:10.1007/s13238-017-0440-4 PubMed PMID: 28710747; PubMed Central PMCID: PMC6160389.

113. Qi C, Gong J, Li J, Liu D, Qin Y, Ge S, et al. Claudin18.2-specific CAR T cells in gastrointestinal cancers: phase 1 trial interim results. Nat Med. 2022 Jun;28(6):1189–98. doi:10.1038/s41591-022-01800-8

114. Qi C, Xie T, Zhou J, Wang X, Gong J, Zhang X, et al. CT041 CAR T cell therapy for Claudin18.2-positive metastatic pancreatic cancer. J Hematol OncolJ Hematol Oncol. 2023 Sep 9;16:102. doi:10.1186/s13045-023-01491-9 PubMed PMID: 37689733; PubMed Central PMCID: PMC10492318.

115. Peng J, Sun BF, Chen CY, Zhou JY, Chen YS, Chen H, et al. Single-cell RNA-seq highlights intra-tumoral heterogeneity and malignant progression in pancreatic ductal adenocarcinoma. Cell Res. 2019 Sep;29(9):725–38. doi:10.1038/s41422-019-0195-y

116. Argani P, Iacobuzio-Donahue C, Ryu B, Rosty C, Goggins M, Wilentz RE, et al. Mesothelin Is Overexpressed in the Vast Majority of Ductal Adenocarcinomas of the Pancreas: Identification of a New Pancreatic Cancer Marker by Serial Analysis of Gene Expression (SAGE). Clin Cancer Res. 2001 Dec 1;7(12):3862–8.

117. Hassan R, Bullock S, Premkumar A, Kreitman RJ, Kindler H, Willingham MC, et al. Phase I study of SS1P, a recombinant anti-mesothelin immunotoxin given as a bolus I.V. infusion to patients with mesothelin-expressing mesothelioma, ovarian, and pancreatic cancers. Clin Cancer Res Off J Am Assoc Cancer Res. 2007 Sep 1;13(17):5144–9. doi:10.1158/1078-0432.CCR-07-0869 PubMed PMID: 17785569.

118. Le DT, Wang-Gillam A, Picozzi V, Greten TF, Crocenzi T, Springett G, et al. Safety and survival with GVAX pancreas prime and Listeria Monocytogenes-expressing mesothelin (CRS-207) boost vaccines for metastatic pancreatic cancer. J Clin Oncol Off J Am Soc Clin Oncol. 2015 Apr 20;33(12):1325–33. doi:10.1200/JCO.2014.57.4244 PubMed PMID: 25584002; PubMed Central PMCID: PMC4397277.

119. Beatty GL, O'Hara MH, Lacey SF, Torigian DA, Nazimuddin F, Chen F, et al. Activity of Mesothelin-Specific Chimeric Antigen Receptor T Cells Against Pancreatic Carcinoma Metastases in a Phase 1 Trial. Gastroenterology. 2018 Jul;155(1):29–32. doi:10.1053/j.gastro.2018.03.029 PubMed PMID: 29567081; PubMed Central PMCID: PMC6035088.

120. Simula L, Fumagalli M, Vimeux L, Rajnpreht I, Icard P, Birsen G, et al. Mitochondrial metabolism sustains CD8+ T cell migration for an efficient infiltration into solid tumors. Nat Commun. 2024 Mar 11;15(1):2203. doi:10.1038/s41467-024-46377-7 PubMed PMID: 38467616; PubMed Central PMCID: PMC10928223.

121. Lontos K, Wang Y, Joshi SK, Frisch AT, Watson MJ, Kumar A, et al. Metabolic reprogramming via an engineered PGC-1α improves human chimeric antigen receptor T-cell therapy against solid tumors. J Immunother Cancer. 2023 Mar;11(3):e006522. doi:10.1136/jitc-2022-006522 PubMed PMID: 36914208; PubMed Central PMCID: PMC10016249.

122. Kobold S, Grassmann S, Chaloupka M, Lampert C, Wenk S, Kraus F, et al. Impact of a New Fusion Receptor on PD-1-Mediated Immunosuppression in Adoptive T Cell Therapy. J Natl Cancer Inst. 2015 Aug;107(8):djv146. doi:10.1093/jnci/djv146 PubMed PMID: 26105028; PubMed Central PMCID: PMC4609553.

123. Chmielewski M, Abken H. CAR T Cells Releasing IL-18 Convert to T-Bethigh FoxO1low Effectors that Exhibit Augmented Activity against Advanced Solid Tumors. Cell Rep. 2017 Dec 12;21(11):3205–19. doi:10.1016/j.celrep.2017.11.063 PubMed PMID: 29241547.

124. Zhao R, Cui Y, Zheng Y, Li S, Lv J, Wu Q, et al. Human Hyaluronidase PH20 Potentiates the Antitumor Activities of Mesothelin-Specific CAR-T Cells Against Gastric Cancer. Front Immunol [Internet]. 2021 [cited 2022 Jun 26];12. Available from: https://www.frontiersin.org/article/10.3389/fimmu.2021.660488

125. Wehrli M, Guinn S, Birocchi F, Kuo A, Sun Y, Larson RC, et al. Mesothelin CAR T Cells Secreting Anti-FAP/Anti-CD3 Molecules Efficiently Target Pancreatic Adenocarcinoma and its Stroma. Clin Cancer Res Off J Am Assoc Cancer Res. 2024 May 1;30(9):1859–77. doi:10.1158/1078-0432.CCR-23-3841 PubMed PMID: 38393682; PubMed Central PMCID: PMC11062832.

126. Evgin L, Kottke T, Tonne J, Thompson J, Huff AL, van Vloten J, et al. Oncolytic virus–mediated expansion of dual-specific CAR T cells improves efficacy against solid tumors in mice. Sci Transl Med. 2022 Apr 13;14(640):eabn2231. doi:10.1126/scitranslmed.abn2231

127. Parker CL, Jacobs TM, Huckaby JT, Harit D, Lai SK. Efficient and Highly Specific Gene Transfer Using Mutated Lentiviral Vectors Redirected with Bispecific Antibodies. mBio. 2020 Jan 21;11(1):e02990-19. doi:10.1128/mBio.02990-19 PubMed PMID: 31964730; PubMed Central PMCID: PMC6989108.

128. Alizadeh D, Wong RA, Gholamin S, Maker M, Aftabizadeh M, Yang X, et al. IFNγ Is Critical for CAR T Cell-Mediated Myeloid Activation and Induction of Endogenous Immunity. Cancer Discov. 2021 Sep;11(9):2248–65. doi:10.1158/2159-8290.CD-20-1661 PubMed PMID: 33837065; PubMed Central PMCID: PMC8561746.

129. Watanabe K, Luo Y, Da T, Guedan S, Ruella M, Scholler J, et al. Pancreatic cancer therapy with combined mesothelin-redirected chimeric antigen receptor T cells and cytokine-armed oncolytic adenoviruses. JCI Insight. 2018 Apr 5;3(7). doi:10.1172/jci.insight.99573 PubMed PMID: 0.

130. Henze J, Tacke F, Hardt O, Alves F, Al Rawashdeh W. Enhancing the Efficacy of CAR T Cells in the Tumor Microenvironment of Pancreatic Cancer. Cancers. 2020 May 28;12(6):1389. doi:10.3390/cancers12061389 PubMed PMID: 32481570; PubMed Central PMCID: PMC7353070.

131. Ju Y, Xu D, Liao M miao, Sun Y, Bao W dai, Yao F, et al. Barriers and opportunities in pancreatic cancer immunotherapy. Npj Precis Oncol. 2024 Sep 12;8(1):199. doi:10.1038/s41698-024-00681-z

132. Irving M, Vuillefroy de Silly R, Scholten K, Dilek N, Coukos G. Engineering Chimeric Antigen Receptor T-Cells for Racing in Solid Tumors: Don't Forget the Fuel. Front Immunol. 2017 Apr 3;8. doi:10.3389/fimmu.2017.00267

133. Guirguis DA, Hasan F, Morris N, Alabd A, Tawfik PMS, Pramanik K, et al. Tumor tough, therapy smarter: Rethinking CAR-T for pancreatic cancer. Semin Oncol. 2025 Dec 1;52(6):152411. doi:10.1016/j.seminoncol.2025.152411

134. Jacobetz MA, Chan DS, Neesse A, Bapiro TE, Cook N, Frese KK, et al. Hyaluronan impairs vascular function and drug delivery in a mouse model of pancreatic cancer. Gut. 2013 Jan;62(1):112–20. doi:10.1136/gutjnl-2012-302529 PubMed PMID: 22466618; PubMed Central PMCID: PMC3551211.

135. Ene-Obong A, Clear AJ, Watt J, Wang J, Fatah R, Riches JC, et al. Activated pancreatic stellate cells sequester CD8+ T cells to reduce their infiltration of the juxtatumoral compartment of pancreatic ductal adenocarcinoma. Gastroenterology. 2013 Nov;145(5):1121–32. doi:10.1053/j.gastro.2013.07.025 PubMed PMID: 23891972; PubMed Central PMCID: PMC3896919.

136. Sugiura A, Rathmell JC. Metabolic Barriers to T Cell Function in Tumors. J Immunol Baltim Md 1950. 2018 Jan 15;200(2):400–7. doi:10.4049/jimmunol.1701041 PubMed PMID: 29311381; PubMed Central PMCID: PMC5777533.

137. Nicoletti A, Vitale F, Quero G, Paratore M, Fiorillo C, Negri M, et al. Immunohistochemical Evaluation of the Expression of Specific Membrane Antigens in Patients with Pancreatic Ductal Adenocarcinoma. Cancers. 2023 Jan;15(18):4586. doi:10.3390/cancers15184586

138. Sanford DE, Belt BA, Panni RZ, Mayer A, Deshpande AD, Carpenter D, et al. Inflammatory monocyte mobilization decreases patient survival in pancreatic cancer: a role for targeting the CCL2/CCR2 axis. Clin Cancer Res Off J Am Assoc Cancer Res. 2013 Jul 1;19(13):3404–15. doi:10.1158/1078-0432.CCR-13-0525 PubMed PMID: 23653148; PubMed Central PMCID: PMC3700620.

139. Candido JB, Morton JP, Bailey P, Campbell AD, Karim SA, Jamieson T, et al. CSF1R+ Macrophages Sustain Pancreatic Tumor Growth through T Cell Suppression and Maintenance of Key Gene Programs that Define the Squamous Subtype. Cell Rep. 2018 May 1;23(5):1448–60. doi:10.1016/j.celrep.2018.03.131 PubMed PMID: 29719257; PubMed Central PMCID: PMC5946718.

140. Soares KC, Rucki AA, Kim V, Foley K, Solt S, Wolfgang CL, et al. TGF-β blockade depletes T regulatory cells from metastatic pancreatic tumors in a vaccine dependent manner. Oncotarget. 2015 Oct 15;6(40):43005–15. doi:10.18632/oncotarget.5656 PubMed PMID: 26515728; PubMed Central PMCID: PMC4767487.

141. Mace TA, Shakya R, Pitarresi JR, Swanson B, McQuinn CW, Loftus S, et al. IL-6 and PD-L1 antibody blockade combination therapy reduces tumour progression in murine models of pancreatic cancer. Gut. 2018 Feb;67(2):320–32. doi:10.1136/gutjnl-2016-311585 PubMed PMID: 27797936; PubMed Central PMCID: PMC5406266.

142. Melisi D, Garcia-Carbonero R, Macarulla T, Pezet D, Deplanque G, Fuchs M, et al. Galunisertib plus gemcitabine vs. gemcitabine for first-line treatment of patients with unresectable pancreatic cancer. Br J Cancer. 2018 Nov;119(10):1208–14. doi:10.1038/s41416-018-0246-z

143. Jiang H, Hegde S, Knolhoff BL, Zhu Y, Herndon JM, Meyer MA, et al. Targeting focal adhesion kinase renders pancreatic cancers responsive to checkpoint immunotherapy. Nat Med. 2016 Aug;22(8):851–60. doi:10.1038/nm.4123 PubMed PMID: 27376576; PubMed Central PMCID: PMC4935930.

144. Diop-Frimpong B, Chauhan VP, Krane S, Boucher Y, Jain RK. Losartan inhibits collagen I synthesis and improves the distribution and efficacy of nanotherapeutics in tumors. Proc Natl Acad Sci. 2011 Feb 15;108(7):2909–14. doi:10.1073/pnas.1018892108

145. Murphy JE, Wo JY, Ryan DP, Clark JW, Jiang W, Yeap BY, et al. Total Neoadjuvant Therapy With FOLFIRINOX in Combination With Losartan Followed by Chemoradiotherapy for Locally Advanced Pancreatic Cancer: A Phase 2 Clinical Trial. JAMA Oncol. 2019 Jul 1;5(7):1020–7.

doi:10.1001/jamaoncol.2019.0892 PubMed PMID: 31145418; PubMed Central PMCID: PMC6547247.

146. Liu Y, Guo Y, Wu Z, Feng K, Tong C, Wang Y, et al. Anti-EGFR chimeric antigen receptor-modified T cells in metastatic pancreatic carcinoma: A phase I clinical trial. Cytotherapy. 2020 Oct;22(10):573–80. doi:10.1016/j.jcyt.2020.04.088 PubMed PMID: 32527643.

147. Qi C, Zhang P, Liu C, Zhang J, Zhou J, Yuan J, et al. Safety and Efficacy of CT041 in Patients With Refractory Metastatic Pancreatic Cancer: A Pooled Analysis of Two Early-Phase Trials. J Clin Oncol Off J Am Soc Clin Oncol. 2024 Jul 20;42(21):2565–77. doi:10.1200/JCO.23.02314 PubMed PMID: 38788174.

148. Stein MN, Dumbrava EE, Teply BA, Gergis US, Guiterrez ME, Reshef R, et al. PSCA-targeted BPX-601 CAR T cells with pharmacological activation by rimiducid in metastatic pancreatic and prostate cancer: a phase 1 dose escalation trial. Nat Commun. 2024 Dec 30;15(1):10743. doi:10.1038/s41467-024-53220-6

149. Michaelides S, Obeck H, Kechur D, Endres S, Kobold S. Migratory Engineering of T Cells for Cancer Therapy. Vaccines. 2022 Nov;10(11):1845. doi:10.3390/vaccines10111845

150. Kohli K, Pillarisetty VG, Kim TS. Key chemokines direct migration of immune cells in solid tumors. Cancer Gene Ther. 2022 Jan;29(1):10–21. doi:10.1038/s41417-021-00303-x

151. Tokunaga R, Zhang W, Naseem M, Puccini A, Berger MD, Soni S, et al. CXCL9, CXCL10, CXCL11/CXCR3 axis for immune activation - A target for novel cancer therapy. Cancer Treat Rev. 2018 Feb;63:40–7. doi:10.1016/j.ctrv.2017.11.007 PubMed PMID: 29207310; PubMed Central PMCID: PMC5801162.

152. Romero JM, Grünwald B, Jang GH, Bavi PP, Jhaveri A, Masoomian M, et al. A Four-Chemokine Signature Is Associated with a T-cell–Inflamed Phenotype in Primary and Metastatic Pancreatic Cancer. Clin Cancer Res. 2020 Apr 15;26(8):1997–2010. doi:10.1158/1078-0432.CCR-19-2803

153. Conlon KC, Miljkovic MD, Waldmann TA. Cytokines in the Treatment of Cancer. J Interferon Cytokine Res. 2019 Jan 1;39(1):6–21. doi:10.1089/jir.2018.0019 PubMed PMID: 29889594; PubMed Central PMCID: PMC6350412.

154. Dholakia J, Cohen AC, Leath CA, Evans ET, Alvarez RD, Thaker PH. Development of Delivery Systems for Local Administration of Cytokines/Cytokine Gene-Directed Therapeutics: Modern Oncologic Implications. Curr Oncol Rep. 2022 Apr;24(4):389–97. doi:10.1007/s11912-022-01221-3 PubMed PMID: 35141857; PubMed Central PMCID: PMC10466172.

155. Fu Y, Tang R, Zhao X. Engineering cytokines for cancer immunotherapy: a systematic review. Front Immunol. 2023 Jul 6;14:1218082. doi:10.3389/fimmu.2023.1218082 PubMed PMID: 37483629; PubMed Central PMCID: PMC10357296.

156. Wendel M, Galani IE, Suri-Payer E, Cerwenka A. Natural Killer Cell Accumulation in Tumors Is Dependent on IFN-γ and CXCR3 Ligands. Cancer Res. 2008 Oct 15;68(20):8437–45. doi:10.1158/0008-5472.CAN-08-1440

157. Neill T, Schaefer L, Iozzo RV. Decorin as a multivalent therapeutic agent against cancer. Adv Drug Deliv Rev. 2016 Feb 1;97:174–85. doi:10.1016/j.addr.2015.10.016 PubMed PMID: 26522384; PubMed Central PMCID: PMC4753134.

158. Köninger J, Giese NA, di Mola FF, Berberat P, Giese T, Esposito I, et al. Overexpressed Decorin in Pancreatic Cancer: Potential Tumor Growth Inhibition and Attenuation of

Chemotherapeutic Action. Clin Cancer Res. 2004 Jul 21;10(14):4776–83. doi:10.1158/1078-0432.CCR-1190-03

159. Zhang W, Ge Y, Cheng Q, Zhang Q, Fang L, Zheng J. Decorin is a pivotal effector in the extracellular matrix and tumour microenvironment. Oncotarget. 2018 Jan 3;9(4):5480–91. doi:10.18632/oncotarget.23869 PubMed PMID: 29435195; PubMed Central PMCID: PMC5797066.

160. Buraschi S, Pal N, Tyler-Rubinstein N, Owens RT, Neill T, Iozzo RV. Decorin antagonizes Met receptor activity and down-regulates {beta}-catenin and Myc levels. J Biol Chem. 2010 Dec 31;285(53):42075–85. doi:10.1074/jbc.M110.172841 PubMed PMID: 20974860; PubMed Central PMCID: PMC3009933.

161. Xie C, Mondal DK, Ulas M, Neill T, Iozzo RV. Oncosuppressive roles of decorin through regulation of multiple receptors and diverse signaling pathways. Am J Physiol - Cell Physiol. 2022 Mar 1;322(3):C554–66. doi:10.1152/ajpcell.00016.2022 PubMed PMID: 35171698; PubMed Central PMCID: PMC8917911.

162. Zhang C, Fang L, Wang X, Yuan S, Li W, Tian W, et al. Oncolytic adenovirus-mediated expression of decorin facilitates CAIX-targeting CAR-T therapy against renal cell carcinoma. Mol Ther Oncolytics. 2021 Nov 29;24:14–25. doi:10.1016/j.omto.2021.11.018 PubMed PMID: 34977339; PubMed Central PMCID: PMC8688951.

163. Zheng N, Xiang L, Xu G, Liu Y, Xu C, Zhang L, et al. Decorin facilitates T cell-mediated antitumor immunity and augments the efficacy of anti-PD1 immunotherapy. Cancer Immunol Immunother CII. 2026 Jan 27;75(2):45. doi:10.1007/s00262-025-04290-y PubMed PMID: 41591489.

164. Merline R, Moreth K, Beckmann J, Nastase MV, Zeng-Brouwers J, Tralhão JG, et al. Signaling by the Matrix Proteoglycan Decorin Controls Inflammation and Cancer through PDCD4 and microRNA-21. Sci Signal. 2011 Nov 15;4(199):ra75. doi:10.1126/scisignal.2001868 PubMed PMID: 22087031; PubMed Central PMCID: PMC5029092.

165. Frey H, Schroeder N, Manon-Jensen T, Iozzo RV, Schaefer L. Biological interplay between proteoglycans and their innate immune receptors in inflammation. FEBS J. 2013 May;280(10):2165–79. doi:10.1111/febs.12145 PubMed PMID: 23350913; PubMed Central PMCID: PMC3651745.

166. Massagué J, Sheppard D. TGF-β Signaling in Health and Disease. Cell. 2023 Sep 14;186(19):4007–37. doi:10.1016/j.cell.2023.07.036 PubMed PMID: 37714133; PubMed Central PMCID: PMC10772989.

167. Penn JW, Grobbelaar AO, Rolfe KJ. The role of the TGF-β family in wound healing, burns and scarring: a review. Int J Burns Trauma. 2012 Feb 5;2(1):18–28. PubMed PMID: 22928164; PubMed Central PMCID: PMC3415964.

168. Lacouture ME, Morris JC, Lawrence DP, Tan AR, Olencki TE, Shapiro GI, et al. Cutaneous keratoacanthomas/squamous cell carcinomas associated with neutralization of transforming growth factor β by the monoclonal antibody fresolimumab (GC1008). Cancer Immunol Immunother CII. 2015 Apr;64(4):437–46. doi:10.1007/s00262-015-1653-0 PubMed PMID: 25579378; PubMed Central PMCID: PMC6730642.

169. Lafitte M, Rousseau B, Moranvillier I, Taillepierre M, Peuchant E, Guyonnet-Dupérat V, et al. In vivo gene transfer targeting in pancreatic adenocarcinoma with cell surface antigens. Mol Cancer. 2012 Dec;11(1):81. doi:10.1186/1476-4598-11-81

170. Showalter SL, Huang YH, Witkiewicz A, Costantino CL, Yeo CJ, Green JJ, et al. Nanoparticulate delivery of diphtheria toxin DNA effectively kills Mesothelin expressing pancreatic cancer cells. Cancer Biol Ther. 2008 Oct;7(10):1584–90. doi:10.4161/cbt.7.10.6562 PubMed PMID: 19039293; PubMed Central PMCID: PMC3218426.

171. Zhang WW, Li L, Li D, Liu J, Li X, Li W, et al. The First Approved Gene Therapy Product for Cancer Ad-p53 (Gendicine): 12 Years in the Clinic. Hum Gene Ther. 2018 Feb;29(2):160–79. doi:10.1089/hum.2017.218 PubMed PMID: 29338444.

172. Herman JM, Wild AT, Wang H, Tran PT, Chang KJ, Taylor GE, et al. Randomized phase III multi-institutional study of TNFerade biologic with fluorouracil and radiotherapy for locally advanced pancreatic cancer: final results. J Clin Oncol Off J Am Soc Clin Oncol. 2013 Mar 1;31(7):886–94. doi:10.1200/JCO.2012.44.7516 PubMed PMID: 23341531; PubMed Central PMCID: PMC4820756.

173. Naldini L, Blömer U, Gallay P, Ory D, Mulligan R, Gage FH, et al. In vivo gene delivery and stable transduction of nondividing cells by a lentiviral vector. Science. 1996 Apr 12;272(5259):263–7. doi:10.1126/science.272.5259.263 PubMed PMID: 8602510.

174. Naldini L. Gene therapy returns to centre stage. Nature. 2015 Oct;526(7573):351–60. doi:10.1038/nature15818

175. Cronin J, Zhang XY, Reiser J. Altering the Tropism of Lentiviral Vectors through Pseudotyping. Curr Gene Ther. 2005 Aug;5(4):387–98. doi:10.2174/1566523054546224 PubMed PMID: 16101513; PubMed Central PMCID: PMC1368960.

176. Burns JC, Friedmann T, Driever W, Burrascano M, Yee JK. Vesicular stomatitis virus G glycoprotein pseudotyped retroviral vectors: concentration to very high titer and efficient gene transfer into mammalian and nonmammalian cells. Proc Natl Acad Sci U S A. 1993 Sep 1;90(17):8033–7. doi:10.1073/pnas.90.17.8033 PubMed PMID: 8396259; PubMed Central PMCID: PMC47282.

177. Kneissl S, Abel T, Rasbach A, Brynza J, Schneider-Schaulies J, Buchholz CJ. Measles Virus Glycoprotein-Based Lentiviral Targeting Vectors That Avoid Neutralizing Antibodies. PLoS ONE. 2012 Oct 10;7(10):e46667. doi:10.1371/journal.pone.0046667 PubMed PMID: 23071609; PubMed Central PMCID: PMC3468630.

178. Morizono K, Ku A, Xie Y, Harui A, Kung SKP, Roth MD, et al. Redirecting Lentiviral Vectors Pseudotyped with Sindbis Virus-Derived Envelope Proteins to DC-SIGN by Modification of N-Linked Glycans of Envelope Proteins. J Virol. 2010 Jul 15;84(14):6923–34. doi:10.1128/jvi.00435-10

179. Rossi J, Martinello C, Sorrentino R, Guyonnet-Duperat V, Amintas S, Abrey Recalde MJ, et al. Engineering precision oncology: Targeting tumors and immune cells with lentiviral vectors. Mol Ther Oncol. 2026 Jun 18;34(2):201197. doi:10.1016/j.omton.2026.201197

180. Spizzo G, Fong D, Wurm M, Ensinger C, Obrist P, Hofer C, et al. EpCAM expression in primary tumour tissues and metastases: an immunohistochemical analysis. J Clin Pathol. 2011 May 1;64(5):415–20. doi:10.1136/jcp.2011.090274 PubMed PMID: 21415054.

181. Zhang S, Fang W, Zhou S, Zhu D, Chen R, Gao X, et al. Single cell transcriptomic analyses implicate an immunosuppressive tumor microenvironment in pancreatic cancer liver metastasis. Nat Commun. 2023 Aug 23;14(1):5123. doi:10.1038/s41467-023-40727-7

182. Bird RE, Hardman KD, Jacobson JW, Johnson S, Kaufman BM, Lee SM, et al. Single-chain antigen-binding proteins. Science. 1988 Oct 21;242(4877):423–6. doi:10.1126/science.3140379 PubMed PMID: 3140379.

183. Huston JS, Levinson D, Mudgett-Hunter M, Tai MS, Novotný J, Margolies MN, et al. Protein engineering of antibody binding sites: recovery of specific activity in an anti-digoxin single-chain Fv analogue produced in Escherichia coli. Proc Natl Acad Sci U S A. 1988 Aug;85(16):5879–83. doi:10.1073/pnas.85.16.5879 PubMed PMID: 3045807; PubMed Central PMCID: PMC281868.

184. Situ K, Chua BA, Bae SY, Meyer A, Morizono K. Versatile targeting system for lentiviral vectors involving biotinylated targeting molecules. Virology. 2018 Dec;525:170–81. doi:10.1016/j.virol.2018.09.017 PubMed PMID: 30290312; PubMed Central PMCID: PMC6269213.

185. Zhou Q, Schneider IC, Edes I, Honegger A, Bach P, Schönfeld K, et al. T-cell receptor gene transfer exclusively to human CD8+ cells enhances tumor cell killing. Blood. 2012 Nov 22;120(22):4334–42. doi:10.1182/blood-2012-02-412973

186. Frecha C, Lévy C, Costa C, Nègre D, Amirache F, Buckland R, et al. Measles Virus Glycoprotein-Pseudotyped Lentiviral Vector-Mediated Gene Transfer into Quiescent Lymphocytes Requires Binding to both SLAM and CD46 Entry Receptors. J Virol. 2011 Jun 15;85(12):5975–85. doi:10.1128/jvi.00324-11

187. Bender RR, Muth A, Schneider IC, Friedel T, Hartmann J, Plückthun A, et al. Receptor-Targeted Nipah Virus Glycoproteins Improve Cell-Type Selective Gene Delivery and Reveal a Preference for Membrane-Proximal Cell Attachment. PLoS Pathog. 2016 Jun;12(6):e1005641. doi:10.1371/journal.ppat.1005641 PubMed PMID: 27281338; PubMed Central PMCID: PMC4900575.

188. Ammayappan A, Peng KW, Russell SJ. Characteristics of Oncolytic Vesicular Stomatitis Virus Displaying Tumor-Targeting Ligands. J Virol. 2013 Dec;87(24):13543–55. doi:10.1128/JVI.02240-13 PubMed PMID: 24089573; PubMed Central PMCID: PMC3838279.

189. Harris L, Fondrie WE, Oh S, Noble WS. Evaluating Proteomics Imputation Methods with Improved Criteria. J Proteome Res. 2023 Nov 3;22(11):3427–38. doi:10.1021/acs.jproteome.3c00205

190. Smith SN, Schubert R, Simic B, Brücher D, Schmid M, Kirk N, et al. The SHREAD gene therapy platform for paracrine delivery improves tumor localization and intratumoral effects of a clinical antibody. Proc Natl Acad Sci U S A. 2021 May 25;118(21):e2017925118. doi:10.1073/pnas.2017925118 PubMed PMID: 34001602; PubMed Central PMCID: PMC8166199.

191. Aires Da Silva F, Leite Costa MJ, Corte-Real S, Goncalves J. Cell Type–Specific Targeting with Sindbis Pseudotyped Lentiviral Vectors Displaying Anti-CCR5 Single-Chain Antibodies. Hum Gene Ther. 2005 Feb;16(2):223–34. doi:10.1089/hum.2005.16.223

192. Ibrahim KE, Mears KS, Allen PM, Chinai JM, Avila OI, Muscato AJ, et al. In vivo CAR T cell generation using retargeted and functionalized lentiviral vectors with reduced immunogenicity. Nat Commun. 2026 Apr 6;17(1):4923. doi:10.1038/s41467-026-71395-y

193. Majzner RG, Rietberg SP, Sotillo E, Dong R, Vachharajani VT, Labanieh L, et al. Tuning the Antigen Density Requirement for CAR T-cell Activity. Cancer Discov. 2020 May;10(5):702–23. doi:10.1158/2159-8290.CD-19-0945 PubMed PMID: 32193224; PubMed Central PMCID: PMC7939454.

194. Groom JR, Luster AD. CXCR3 in T cell function. Exp Cell Res. 2011 Mar 10;317(5):620–31. doi:10.1016/j.yexcr.2010.12.017 PubMed PMID: 21376175; PubMed Central PMCID: PMC3065205.

195. Thomas DA, Massagué J. TGF-beta directly targets cytotoxic T cell functions during tumor evasion of immune surveillance. Cancer Cell. 2005 Nov;8(5):369–80. doi:10.1016/j.ccr.2005.10.012 PubMed PMID: 16286245.

196. Mariathasan S, Turley SJ, Nickles D, Castiglioni A, Yuen K, Wang Y, et al. TGFβ attenuates tumour response to PD-L1 blockade by contributing to exclusion of T cells. Nature. 2018 Feb 22;554(7693):544–8. doi:10.1038/nature25501 PubMed PMID: 29443960; PubMed Central PMCID: PMC6028240.

197. Gunderson AJ, Yamazaki T, McCarty K, Fox N, Phillips M, Alice A, et al. TGFβ suppresses CD8+ T cell expression of CXCR3 and tumor trafficking. Nat Commun. 2020 Apr 9;11(1):1749. doi:10.1038/s41467-020-15404-8

198. Olive KP, Jacobetz MA, Davidson CJ, Gopinathan A, McIntyre D, Honess D, et al. Inhibition of Hedgehog signaling enhances delivery of chemotherapy in a mouse model of pancreatic cancer. Science. 2009 Jun 12;324(5933):1457–61. doi:10.1126/science.1171362 PubMed PMID: 19460966; PubMed Central PMCID: PMC2998180.

199. Özdemir BC, Pentcheva-Hoang T, Carstens JL, Zheng X, Wu CC, Simpson T, et al. Depletion of Carcinoma-Associated Fibroblasts and Fibrosis Induces Immunosuppression and Accelerates Pancreas Cancer with Diminished Survival. Cancer Cell. 2014 Jun 16;25(6):719–34. doi:10.1016/j.ccr.2014.04.005 PubMed PMID: 24856586; PubMed Central PMCID: PMC4180632.

200. Elyada E, Bolisetty M, Laise P, Flynn WF, Courtois ET, Burkhart RA, et al. Cross-Species Single-Cell Analysis of Pancreatic Ductal Adenocarcinoma Reveals Antigen-Presenting Cancer-Associated Fibroblasts. Cancer Discov. 2019 Aug;9(8):1102–23. doi:10.1158/2159-8290.CD-19-0094 PubMed PMID: 31197017; PubMed Central PMCID: PMC6727976.

201. Biffi G, Oni TE, Spielman B, Hao Y, Elyada E, Park Y, et al. IL1-Induced JAK/STAT Signaling Is Antagonized by TGFβ to Shape CAF Heterogeneity in Pancreatic Ductal Adenocarcinoma. Cancer Discov. 2019 Feb;9(2):282–301. doi:10.1158/2159-8290.CD-18-0710 PubMed PMID: 30366930; PubMed Central PMCID: PMC6368881.

202. Nicolas-Boluda A, Vaquero J, Vimeux L, Guilbert T, Barrin S, Kantari-Mimoun C, et al. Tumor stiffening reversion through collagen crosslinking inhibition improves T cell migration and anti-PD-1 treatment. Malissen B, Ojala PM, editors. eLife. 2021 Jun 9;10:e58688. doi:10.7554/eLife.58688

203. Xiao Z, Todd L, Huang L, Noguera-Ortega E, Lu Z, Huang L, et al. Desmoplastic stroma restricts T cell extravasation and mediates immune exclusion and immunosuppression in solid tumors. Nat Commun. 2023 Aug 22;14(1):5110. doi:10.1038/s41467-023-40850-5

204. Lunardi S, Jamieson NB, Lim SY, Griffiths KL, Carvalho-Gaspar M, Al-Assar O, et al. IP-10/CXCL10 induction in human pancreatic cancer stroma influences lymphocytes recruitment and correlates with poor survival. Oncotarget. 2014 Nov 25;5(22):11064–80. doi:10.18632/oncotarget.2519 PubMed PMID: 25415223; PubMed Central PMCID: PMC4294325.

205. Chen W, Jin W, Hardegen N, Lei KJ, Li L, Marinos N, et al. Conversion of peripheral CD4+CD25- naive T cells to CD4+CD25+ regulatory T cells by TGF-beta induction of transcription factor Foxp3. J Exp Med. 2003 Dec 15;198(12):1875–86. doi:10.1084/jem.20030152 PubMed PMID: 14676299; PubMed Central PMCID: PMC2194145.

206. Marie JC, Letterio JJ, Gavin M, Rudensky AY. TGF-beta1 maintains suppressor function and Foxp3 expression in CD4+CD25+ regulatory T cells. J Exp Med. 2005 Apr 4;201(7):1061–7. doi:10.1084/jem.20042276 PubMed PMID: 15809351; PubMed Central PMCID: PMC2213134.

207. Schönherr E, Broszat M, Brandan E, Bruckner P, Kresse H. Decorin core protein fragment Leu155-Val260 interacts with TGF-beta but does not compete for decorin binding to type I collagen. Arch Biochem Biophys. 1998 Jul 15;355(2):241–8. doi:10.1006/abbi.1998.0720 PubMed PMID: 9675033.

208. Diehl V, Huber LS, Trebicka J, Wygrecka M, Iozzo RV, Schaefer L. The Role of Decorin and Biglycan Signaling in Tumorigenesis. Front Oncol. 2021 Nov 30;11. doi:10.3389/fonc.2021.801801

209. Gubbiotti MA, Vallet SD, Ricard-Blum S, Iozzo RV. Decorin interacting network: A comprehensive analysis of decorin-binding partners and their versatile functions. Matrix Biol J Int Soc Matrix Biol. 2016 Sep;55:7–21. doi:10.1016/j.matbio.2016.09.009 PubMed PMID: 27693454; PubMed Central PMCID: PMC6938589.

210. Salter AI, Ivey RG, Kennedy JJ, Voillet V, Rajan A, Alderman EJ, et al. Phosphoproteomic analysis of chimeric antigen receptor signaling reveals kinetic and quantitative differences that affect cell function. Sci Signal. 2018 Aug 21;11(544):eaat6753. doi:10.1126/scisignal.aat6753

211. Locard-Paulet M, Voisinne G, Froment C, Goncalves Menoita M, Ounoughene Y, Girard L, et al. LymphoAtlas: a dynamic and integrated phosphoproteomic resource of TCR signaling in primary T cells reveals ITSN2 as a regulator of effector functions. Mol Syst Biol. 2020 Jul 3;16(7):MSB209524. doi:10.15252/msb.20209524

212. Scharping NE, Ge X, Matias MI, Jiang F, Cafferata A, Heeg M, et al. Proteostasis sustains T cell differentiation potential and tumor-infiltrating lymphocyte function. Cell. 2026 May 14;189(10):2857-2874.e31. doi:10.1016/j.cell.2026.02.019 PubMed PMID: 42061400.

213. Griffith AA, Callahan KP, King NG, Xiao Q, Su X, Salomon AR. SILAC phosphoproteomics reveals unique signaling circuits in CAR-T cells and the inhibition of B cell-activating phosphorylation in target cells. J Proteome Res. 2022 Feb 4;21(2):395–409. doi:10.1021/acs.jproteome.1c00735 PubMed PMID: 35014847; PubMed Central PMCID: PMC8830406.

214. Tan H, Yang K, Li Y, Shaw TI, Wang Y, Blanco DB, et al. Integrative proteomics and phosphoproteomics profiling reveals dynamic signaling networks and bioenergetics pathways underlying T cell activation. Immunity. 2017 Mar 21;46(3):488–503. doi:10.1016/j.immuni.2017.02.010 PubMed PMID: 28285833; PubMed Central PMCID: PMC5466820.

215. Stromnes IM, Schmitt TM, Hulbert A, Brockenbrough JS, Nguyen H, Cuevas C, et al. T Cells Engineered against a Native Antigen Can Surmount Immunologic and Physical Barriers to Treat Pancreatic Ductal Adenocarcinoma. Cancer Cell. 2015 Nov 9;28(5):638–52. doi:10.1016/j.ccell.2015.09.022 PubMed PMID: 26525103; PubMed Central PMCID: PMC4724422.

216. Hecht JR, Farrell JJ, Senzer N, Nemunaitis J, Rosemurgy A, Chung T, et al. EUS or percutaneously guided intratumoral TNFerade biologic with 5-fluorouracil and radiotherapy for first-line treatment of locally advanced pancreatic cancer: a phase I/II study. Gastrointest Endosc. 2012 Feb;75(2):332–8. doi:10.1016/j.gie.2011.10.007 PubMed PMID: 22248601; PubMed Central PMCID: PMC4380192.

217. Adusumilli PS, Cherkassky L, Villena-Vargas J, Colovos C, Servais E, Plotkin J, et al. Regional delivery of mesothelin-targeted CAR T cell therapy generates potent and long-lasting CD4-dependent tumor immunity. Sci Transl Med. 2014 Nov 5;6(261):261ra151. doi:10.1126/scitranslmed.3010162 PubMed PMID: 25378643; PubMed Central PMCID: PMC4373413.

218. Zhang S, Fang W, Zhou S, Zhu D, Chen R, Gao X, et al. Single cell transcriptomic analyses implicate an immunosuppressive tumor microenvironment in pancreatic cancer liver metastasis. Nat Commun. 2023 Aug 23;14(1):5123. doi:10.1038/s41467-023-40727-7

Scientific publications

- Boubaddi, M., **Rossi, J**., Marichez, A., Marty, M., Amintas, S., Laurent, C., & Dabernat, S. (2025). Preoperative Prognostic Factors in Resectable Pancreatic Cancer: State of the Art and Prospects. *Annals of surgical oncology*, *32*(6), 4117–4127. https://doi.org/10.1245/s10434-025-17062-w

- **Rossi, J.,** Martinello, C., Sorrentino, R., Guyonnet-Duperat, V., Amintas, S., Abrey Recalde, M. J., Verhoeyen, E., & Dabernat, S. (2026). Engineering precision oncology: Targeting tumors and immune cells with lentiviral vectors. *Molecular therapy. Oncology*, *34*(2), 201197. https://doi.org/10.1016/j.omton.2026.201197

- **J Rossi**, N Richet, C Martinello, S Kobold, …, A Bedel, F Moreau-Gaudry, V Guyonnet-Dupérat, E Verhoeyen, and S Dabernat. Comparative lentiviral pseudotyping identifies Sindbis virus glycoprotein as a versatile platform for highly specific *in vivo* tumor targeting *(Under revision, Molecular Therapy)*

- **J Rossi**, N Richet, S Michaelides, L Mora Charrot, …, A Bedel, F Moreau-Gaudry, V Guyonnet-Dupérat, S Kobold, S Dabernat. Decorin secretion by pancreatic tumor cells enhances T cell therapy by matrix- and TGFβ-associated barrier modulation *(Under preparation)*

Scientific communications

- October 2022: **Talk** at the AFRCP annual meeting, Paris, France

"Pancreatic cancer immuno-permissiveness shaping by gene therapy"

- September 2024: **Talk** at the AFRCP annual meeting, Toulouse, France

"Tumor microenvironment shaping by gene therapy"

- October 2024: **Poster** presentation at the ESGCT Collaborative Congress, Rome, Italy

"Lentivector onco-targeting for solid tumor gene therapy"

- December 2024: **Poster** presentation at the SBM day, Bordeaux, France

"Lentivector onco-targeting for solid tumor gene therapy"

- March 2025: **Talk** at the SFTCG annual meeting, Bordeaux, France

"Lentivector onco-targeting for solid tumor gene therapy"

- September 2025: **Poster** presentation at the ARC - Pancreatic Cancer Symposium, Paris, France

"Lentivector onco-targeting for solid tumor gene therapy"

- October 2025: **Poster** presentation at the 3rd Young Scientist Cancer Congress (YS2C), Berlin, Germany

"Lentivector onco-targeting for solid tumor gene therapy"

- March 2026: **Poster** presentation at the 3D model in oncology seminar, Bordeaux, France

"3D in vitro strategies to assess viral vector gene therapy for enhanced CAR T cell efficacy "

Teaching and supervision

- 2-month internship for a pharmacy student at Ecole Santé Sciences, college Santé,

Université de Bordeaux, May to June 2023

- 10-month internship for a Master 2 student,

University of Milan, Erasmus from January to November 2024

- 3-month internship for a engineering student at École Nationale Supérieure de Technologie des Biomolécules de Bordeaux

ENSTBB - BORDEAUX INP June to September 2024

- 6-month internship for a engineering student at École Nationale Supérieure de Technologie des Biomolécules de Bordeaux

ENSTBB - BORDEAUX INP March to September 2025

- Lecture during the INSERM training course “Lentiviral vectors: tools for gene transfer”, module on lentiviral pseudotyping, envelope glycoprotein modification and cell targeting.

INSERM, Bordeaux, 2025

French and English abstracts

Ingénierie ciblée de la niche tumorale par vecteurs lentiviraux pour améliorer l'efficacité des cellules CAR T dans l'adénocarcinome canalaire pancréatique

Résumé

L'adénocarcinome canalaire pancréatique (PDAC) demeure l'une des tumeurs solides les plus létales, avec des options thérapeutiques limitées et un pronostic défavorable. Bien que les immunothérapies aient transformé la prise en charge de plusieurs cancers, leur efficacité dans le PDAC reste limitée. Parmi ces approches, le transfert adoptif de cellules exprimant un récepteur antigénique chimérique, ou cellules CAR T, présente un fort potentiel cytotoxique. Cependant, son application au PDAC est limitée par une infiltration tumorale insuffisante, des barrières stromales denses et un microenvironnement tumoral immunosuppresseur.

Cette thèse explore l'ingénierie ciblée de la niche tumorale par vecteurs lentiviraux comme stratégie pour remodeler localement le microenvironnement du PDAC et améliorer l'efficacité des cellules CAR T. Puisqu'il n'est pas possible de transduire l'ensemble des cellules tumorales, l'approche proposée repose sur la délivrance sélective de gènes à une fraction de cellules tumorales exprimant des antigènes cibles, afin de les convertir en sources locales de signaux diffusibles immunomodulateurs et capables de remodeler le stroma. Pour permettre une délivrance restreinte à la tumeur, des vecteurs lentiviraux ont été conçus avec des glycoprotéines virales modifiées afin de reconnaître des antigènes de surface associés aux cellules tumorales.

Une analyse comparative de différentes plateformes de pseudotypage a permis d'identifier les glycoprotéines dérivées du virus Sindbis comme un système robuste et polyvalent pour la transduction lentivirale antigène-dépendante de cellules de tumeurs solides. Cette plateforme de délivrance ciblée sera utilisée pour exprimer des transgènes thérapeutiques conçus pour remodeler localement la niche tumorale, notamment des chimiokines afin de favoriser l'attraction des cellules immunitaires, ainsi que la décorine afin de moduler le compartiment stromal et de faciliter l'accès à la tumeur des cellules T cytotoxiques endogènes ou transférées de manière adoptive, incluant les cellules CAR T.

Dans son ensemble, ce travail soutient le concept selon lequel les vecteurs lentiviraux ciblés peuvent être utilisés comme plateformes d'ingénierie locale du microenvironnement tumoral. Cette approche pourrait constituer une stratégie complémentaire pour surmonter les principales barrières limitant l'efficacité des cellules CAR T dans le PDAC et d'autres tumeurs solides.

Mots-clés : thérapie génique, vecteurs lentiviraux ciblés, microenvironnement tumoral, adénocarcinome canalaire pancréatique, cellules CAR T, pseudotypage viral, chimiokines

Targeted lentiviral niche-engineering to enhance CAR T cell efficacy in pancreatic ductal adenocarcinoma

Abstract

Pancreatic ductal adenocarcinoma (PDAC) remains one of the most lethal solid malignancies, with limited therapeutic options and poor clinical outcomes. Although immunotherapies have transformed the treatment of several cancers, their efficacy in PDAC remains limited. Among these approaches, adoptive cell transfer using chimeric antigen receptor CAR T cells offers strong cytotoxic potential, but its application to PDAC is constrained by inefficient tumor infiltration, dense stromal barriers, and an immunosuppressive tumor microenvironment.

This thesis explores targeted lentiviral niche engineering as a strategy to locally remodel the PDAC microenvironment and improve CAR T cell efficacy. As transducing every tumor cell is not possible, the proposed approach relies on selective gene delivery to a fraction of antigen-expressing tumor cells, converting them into local sources of diffusible immunomodulatory and stromal-remodeling signals. To achieve tumor-restricted delivery, lentiviral vectors were engineered with retargeted viral glycoproteins designed to recognize tumor-associated surface antigens.

A comparative analysis of pseudotyping platforms identified Sindbis virus-derived glycoproteins as a robust and versatile system for antigen-dependent lentiviral transduction of solid tumor cells. This targeted delivery platform will be used to express therapeutic payloads designed to locally reshape the tumor niche, including chemokines to promote immune-cell attraction and decorin to modulate the stromal compartment and facilitate tumor access of endogenous and adoptively transferred cytotoxic T cells, including CAR T cells.

Overall, this work supports the concept that targeted lentiviral vectors can be used as local tumor microenvironment engineering platforms. This approach may provide a complementary strategy to overcome key barriers limiting CAR T cell efficacy in PDAC and other solid tumors.

Keywords: gene therapy, targeted lentiviral vectors, tumor microenvironment, pancreatic ductal adenocarcinoma, CAR T cells, Sindbis virus pseudotyping, chemokines

Unité de recherche

U1312- BRIC - Bordeaux Institute of Oncology - Inserm

Campus Carreire - Bâtiment BBS

2, Rue du Dr Hoffmann Martinot 33000 Bordeaux